MOTION PREDICTION AND DYNAMIC STABILITY ANALYSIS OF HUMAN WALKING: THE EFFECT OF LEG PROPERTY

A thesis submitted to The University of Manchester for the degree of

Doctor of Philosophy

in the Faculty of Engineering and Physical Science

2013

Amaraporn Boonpratatong

School of Mechanical, Aerospace and Civil Engineering

70,237 words

List of Table

Page

Chapter 3

Chapter 4

Chapter 5

Chapter 6

List of Figures

Page

Chapter 1

Chapter 2

Chapter 3

Chapter 4

Chapter 5

Chapter 7

Nomenclature

Chapter 3

CoM	center of mass
CoP	center of pressure
$\vec{r}$	location
$\vec{v}$	velocity
$\vec{r}_i^{cm}$	position vector of CoM location of i^{th} body segment
m_i^r	mass of i^{th}body segment
m	whole-body mass
F^x	vertical ground reaction force
F^y	horizontal ground reaction force
v^x	horizontal velocity of the whole-body centre of mass
v^y	vertical velocity of the whole-body centre of mass
u_0^x	initial horizontal velocity of the whole-body centre of mass
u_0^y	initial vertical velocity of the whole-body centre of mass
r_0^x	initial horizontal position of the whole-body centre of mass
r_0^y	initial vertical position of the whole-body centre of mass
t^{stance}	stance time

x^{CoP}	centre of pressure

Chapter 4

l	virtual leg length
θ	leg angle
$\theta^{contact}$	contact angle
k^n	axial stiffness
k^t	tangential stiffness
F^n	axial force
F^t	tangential force
F^g	total ground reaction force
CoP	centre of pressure
CoM	centre of mass
a	coefficient of nonlinear stiffness
l_0	rest length
k^n_{lin}	linear axial stiffness
k^n_{nln}	nonlinear stiffness
b	exponential power of nonlinear coefficient
θ_0	force-free leg angle

F^t	projection of the total ground reaction force onto the perpendicular line of the virtual leg
F^n	projection of the total ground reaction force onto the virtual leg axis
k_{lin}^t	linear tangential stiffness
θ^{td}	leg angle at touchdown
θ_1^{re}	leg angle at the first peak of the tangential force
θ_2^{re}	leg angle at the second peak of the tangential force
θ_0^F	leg angle when the total ground reaction force applies through the leg axis
θ^{to}	leg angle at take-off
k_1, k_2, k_3, k_4	tangential leg properties comprising four of tangential stiffness
a_n , b_n	Fourier coefficients for the fluctuation of tangential force
z	total stiffness or mechanical impedance
RMSE	root-mean-square error
GRF	ground reaction force
a_m , b_m	Fourier coefficients
$\overline{\boldsymbol{F}}_{\boldsymbol{fixed}}^{\boldsymbol{n}}$	fixed contact axial force
BW	body weight

$\bar{\boldsymbol{l}}_{\boldsymbol{fixed}}$	fixed contact leg length
$\boldsymbol{l^{st}}$	leg length obtained during still standing
$\boldsymbol{\nabla}$	Touchdown
Δ	take-off
$\bar{\boldsymbol{k}}^{\boldsymbol{n}}_{\boldsymbol{lin}}$	normalised linear axial stiffness
z^{n}_{lin}	total axial stiffness
$z^{n,fixed}_{nln}$	non-linear elasticity
$l^{fixed}_{0,nln}$	corresponding rest length
$\bar{z}^{n,fixed}_{nln}$	normalised total stiffness of nonliner axial stiffness in fixed contact condition
$\bar{l}^{fixed}_{0,nln}$	rest length of nonlinear elacticity in fixed contact condition
$\bar{F}^{n}_{move}$	moving contact axial force
$\bar{l}_{\ move}$	moving contact leg length
$z^{n,move}_{nln}$	moving contact non-linar elasticity
$\bar{z}^{n,move}_{nln}$	normalised total stiffness of nonliner axial stiffness in moving contact condition
$\bar{F}^{t}_{fixed}$	tangential leg force
$\theta_{\ fixed}$	fixed contact leg angle

z_{lin}^{t}	total tangential stiffness
$\theta_{0,lin}$	corresponding force-free leg angle
$\bar{F}_{move}^{t}$	moving contact tangential leg force
$\bar{F}_{fixed}^{t}$	fixed contact tangential leg force
z^{n}	total axial stiffness
z^{t}	total tangential stiffness
$(l_0 - l)$	leg deflection

Chapter 5

θ Ipsilateral leg angle

θ_0^F	mid-stance force-free leg angle
θ^{td}	Ipsilateral leg angle at touchdown
θ^{to}	Ipsilateral leg angle at take-off
q	Posture index
F_q^n	axial force due to posture-dependent elasticity of the virtual leg
$k_{q,lin}^{n}$	linear axial stiffness
$l_{0,q}^{fixed}$	posture-dependent force-free leg length in fixed contact condition
l^{td}	rest length varies around the touchdown

l^{to}	take-off leg length
d^{l}	excursion length
$f_0(q)$	finite Fourier series
a_m^n , b_m^n	Fourier coefficients
$l_{0,q}$	posture-dependent force-free leg length
$l_{0,q}^{move}$	moving contact condition
d^{θ}	additional nonlinear term of force-free leg length in moving contact condition
A^{θ}	peak amplitude of leg angle
A^{l}	peak amplitude of leg length
$A_0^{l,fixed}$	peak amplitude of force-free leg length in fixed contact condition
$A_0^{l,move}$	peak amplitude of force-free leg length in moving contact condition
l_0^l	force-free leg length
A_0^l	peak amplitude
$t^{contact}$	moving contact condition during the foot-ground contact
F_q^t	tangential leg force based on posture-dependent elasticity of the virtual leg
$\theta_{0,q}$	mid-stance force-free leg angle

$k_q^t(q)$	posture-dependent tangential stiffness in terms of finite Fourier series constraining tangential stiffness to zero at touchdown and take-off regardless of the touchdown and take-off angle value
a_m^t , b_m^t	Fourier coefficients of posture-dependent tangential stiffness
$\theta - \theta^{td}$	leg posture
$\theta_{0,q} - \theta$	leg angular deflection
z	total stiffness
$z_{q,hard}^t$	total tangential stiffness for hard nonlinear stiffness
$z_{q,soft}^t$	total tangential stiffness for soft nonlinear stiffness
θ_{max}	maximum leg angle
$k_{q,lin}^{n,fixed}$	Linear axial stiffness
$A_0^{l,fixed}$	force-free leg length
$\bar{k}_{q,lin}^{n,fixed}$	normalised linear axial stiffness in fixed contact condition
$\bar{A}_0^{l,fixed}$	amplitude of force-free leg length in fixed contact condition
l^{st}	leg length obtained during still standing
$\bar{l}_{fixed}$	fixed contact leg length
$\bar{F}_{fixed}^n$	fixed contact axial force
BW	body weight

$\bar{F}_{move}^{n}$	moving contact axial force
l_{move}	moving contact leg length
$A_0^{l,move}$	corresponding peak amplitude of variation of the force-free leg length
$\bar{A}_0^{l,move}$	amplitude of force-free leg length in moving contact condition
$\bar{F}_{fixed}^{t}$	fixed contact tangential force
θ_{fixed}	fixed contact Leg angle
∇	touchdown
Δ	take-off
$z_{q,hard}^{t,fixed}$	total tangential stiffness for hard nonlinear stiffness
$z_{q,soft}^{t,fixed}$	total tangential stiffness for soft nonlinear stiffness
$\bar{z}_{q,hard}^{t,fixed}$	total tangential stiffness for soft nonlinear stiffness of posture-dependent property in fixed contact condition
$\bar{z}_{q,soft}^{t,fixed}$	total tangential stiffness for hard nonlinear stiffness of posture-dependent property in fixed contact condition
$\theta_{0,q}^{fixed}$	corresponding force-free leg angle
$\bar{z}_{q}^{t,fixed}$	total tangential stiffness for posture-dependent property in fixed contact condition

$\theta_{0,q}^{fixed}$	force-free leg angle for posture-dependent property in fixed contact condition
F_{move}^{t}	moving contact tangential leg force
θ_{move}	moving contact tangential leg angle
$z_{q,hard}^{t,move}$	total tangential stiffness for hard nonlinear stiffness
$z_{q,soft}^{t,move}$	total tangential stiffness for soft nonlinear stiffness
$\theta_{0,q}^{move}$	force-free leg angle
CoM	centre of mass
$\bar{z}_{q}^{t,move}$	total tangential stiffness for posture-dependent property in moving contact condition

Chapter 6

$\theta_{td}^{contact}$	initial contact angle
k^{n}	axial leg stiffness
$\theta_{td}^{contact}$	touchdown leg angle
v_{0}^{x}	initial horizontal speed
k^{n}	axial stiffness
CoM	centre of mass

θ_0	force-free leg angle
k^t	tangential stiffness
l_0	rest length
θ^{td}	touchdown leg angle
$\ddot{x}$, $\ddot{y}$	horizontal and vertical acceleretion
x , y	horizontal and vertical displacement
g	gravitation
d	step length
k^{n*}	changeable axial stiffness
l^{trail}	trailing leg length
l^{lead}	leading leg length
Δx	horizontal distance between the CoM and the contact point
VLO	vertical leg orientation
i	step number
$\theta^{cont,td}$	touchdown contact angle
s	state variables
θ_0^v	velocity angle
$y_0, \dot{x}_0$	measured initial condition

y_0	initial condition comprising the height
$\dot{x}_0$	horizontal velocity
a, b	coefficients
z^n	axial elasticity
θ_0^{cont}	force-free contact angle
GRF	ground reaction force
l	leg length
θ	leg angle
F^x	vertical ground reaction force
F^y	horizontal ground reaction force
N	Newton
t	contact time
s	second
m	meter
F^t	tangential force
F^n	axial force
$s_{i,j}$	state variable number j for step i
j^{th}	state variable number

i^{th}	step number
s_j^*	fixed point of state variable
k^r	stiffness ratio
rad	leg length is in radian
$k^n_{nln,\, F^n_{max}}$	stiffness at the maximum
$k^n_{nln,\, F^n_0}$	minimum axial force

Chapter 7

$k^n_{q,lin}$	linear axial stiffness
l_0^*	variable force-free leg length
k_q^t	variable tangential stiffness
θ_0^*	force-free leg angle
m	whole-body mass
g	gravity
θ^{trail}	trialing leg angle
θ^{lead}	leading leg angle
l	leg length
θ	leg angle

i	step number
l_0	rest length
$\theta_{td}^{contact}$	touchdown contact angle
CoM	centre of mass
VLO	vertical leg orientation
Δx	horizontal distance between the CoM and the contact point
y_0	CoM height
θ_0^v	velocity angle
s	state variables
E^s	system potential energy
E^k	kinetic potential energy
E^g	gravitational potential energy
E^e	elastic potential energy
m	meter
A_0^l	peak amplitude of force –free leg length variation
l^{td}	touchdown leg length
d^l	Excursion length
$z_{q,hard}^{t,fixed}$	Total dynamic stiffness on hardening elastic profile

$z_{q,soft}^{t,fixed}$	Total dynamic stiffness on softening elastic profile
θ^{td}	touchdown contact angle
F^x	vertical ground reaction force
F^y	horizontal ground reaction force
N	Newton
t	contact time
s	second
F^t	tangential force
F^n	axial force

The University of Manchester, Miss Amaraporn Boonpratatong

Degree: Doctor of Philosophy (PhD)

Title: Human Motion Prediction and Dynamic Stability Analysis of Human Walking: the Effect of Leg Properties

Date: October 13th, 2013

Abstract

The objective of this thesis is to develop and validate a computational framework based on mathematical models for the motion prediction and dynamic stability quantification of human walking, which can differentiate the dynamic stability of human walking with different mechanical properties of the leg.

Firstly, a large measurement database of human walking motion was created. It contains walking measurement data of 8 subjects on 3 self-selected walking speeds, which 10 trials were recorded at each walking speed. The motion of whole-body centre of mass and the leg were calculated from the kinetic-kinematic measurement data.

The fundamentals of leg property have been presented, and the parameters of leg property were extracted from the measurement data of human walking where the effects of walking speed and condition of foot-ground contact were investigated. Three different leg property definitions comprising linear axial elastic leg property, nonlinear axial elastic leg property and linear axial-tangential elastic leg property were used to extracted leg property parameters. The concept of posture-dependent leg property has been proposed, and the leg property parameters were extracted from the measurement data of human walking motion where the effects of walking speed and condition of foot-ground contact were also investigated.

The compliant leg model with axial elastic property (CAE) was used for the dynamic stability analysis of human walking with linear and nonlinear axial elastic leg property. The compliant leg model with axial and tangential elastic property (CATE) was used for that with linear axial-tangential elastic leg property. The posture - dependent elastic leg model (PDE) was used for that with posture-dependent leg property.

It was found that, with linear axial elastic leg property, the global stability of human walking improves with the bigger touchdown contact angle. The average leg property obtained from the measurement data of all participants allows the maximum global stability of human walking. With nonlinear axial elastic leg property, the global stability decreases with the stronger nonlinearity of leg stiffness. The incorporation of the tangential elasticity improves the global stability and shifts the stable walking velocity close to that of human walking at self-selected low speed (1.1-1.25 m/s).

By the PDE model, the human walking motions were better predicted than by the CATE model. The effective range of walking prediction was enlarged to 1.12 – 1.8 m/s. However, represented by PDE model, only 1-2 walking steps can be achieved. In addition, the profiles of mechanical energies represented by the PDE model are different from that of the orbital stable walking represented by CATE model.

Finally, the minimal requirements of the human walking measurements and the flexibility of simple walking models with deliberate leg property definitions allow the computational framework to be applicable in the dynamic stability analysis of the walking motion with a wide variety of mechanical property of the leg.

CANDIDATE DECLARATION

Amaraporn Boonpratatong

Faculty of Engineering and Physical Sciences

MOTION PREDICTION AND DYNAMIC STABILITY ANALYSIS OF HUMAN WALKING: THE EFFECT OF LEG PROPERTY

I declare that no portion of the work referred to this thesis has been submitted in support of an application for another degree or qualification of this or any other university or other institute of learning.

Signed_____ **Date**_____

COPYRIGHT STATEMENT

Acknowledgements

I would like to express my sincere gratitude to those who have made significant contributions to the completion of this thesis.

I owe my greatest gratitude to my thesis supervisor, Dr. Lei Ren. Without his patience and infinite supervision, this thesis would not have been possible. This work contains a number of improvements based on comments provided by Dr. Tianjian Ji and Dr. Thrishantha Nanayakkara. It is my pleasure to express my sincere thanks to them for their throughout examination and suggestion.

I am indebted to the research collaborator in Structure and Motion Lab, the Royal Veterinary College, London who supported the venue and equipments for the measurement in this research work. I would like to thank all of the staffs in the Office of Educational Affair (OEA), London, the Education and Training Abroad Centre, the Office of Civil Service Commission (OCSC) and colleagues in the faculty of Engineering, Srinakarinwirot University for their support and encouragement. I extend my sincere thanks to the Royal-Thai government for granting me the scholarship, which made my doctoral study possible. I would also like to thank my teachers and friends who took part in my study life for their coaching and friendship.

I am extremely grateful for the love and support given to me by my big family and my dedicated husband and finally, for all the difficulties, which guided me to put for the life-long study. To them, I dedicate all contributions arising from this thesis.

Original publications arising from this thesis work

1. Amaraporn Boonpratatong, Lei Ren. The mechanical property of human leg during normal walking I: linearity and non-linearity. Journal of Experimental Biology (To be submitted)

2. Amaraporn Boonpratatong, Lei Ren. The mechanical property of human leg during normal walking II: a posture-dependent hypothesis. Journal of Experimental Biology (To be submitted)

3. Amaraporn Boonpratatong, Lei Ren. A dynamic stability analysis of human walking: the effect of tangential leg force. PLoS ONE (To be submitted)

4. Amaraporn Boonpratatong, Lei Ren. Human walking motion prediction based on a posture-dependent hypothesis. Journal of Biomechanics (To be submitted)

5. Boonpratatong, A. & Ren, L. The non-linear nature of virtual human leg property during level walking. XXIIrd Congress of International Society of Biomechanics, Belgium, 2011.

6. Boonpratatong, A. & Ren, L. The non-linear mechanical property of human leg during level walking. 6th North West Biomechanics Research Day. Manchester, UK: Institute for Biomedical Research into Human Movement & Health, 2011.

7. Boonpratatong, A. & Ren, L. The human ankle-foot complex as a multi-configurable mechanism during the stance phase of walking. Journal of Bionic Engineering, 7, 2010, 211-218.

8. Amaraporn Boonpratatong, Lei Ren. Couple kinematic chain in the human head-spine-pelvis complex. 6th World Congress on Biomechanics, Singapore, 2010.

Chapter 1 Introduction

1.1 Background

Walking has been reported as one of the top activities that people does in daily life (Simpson et al., 2003; Eyler et al., 2003). Quantified by a wide variety of methodology, the walking stability was found to be maintained in healthy adults, and decline after the age range of 60-70 (Lockhart et al., 2003; Tinetti et al., 1995; Kallin et al., 2004; Moreland et al., 2004). In addition to the aging, other factors i.e. pregnancy and the deficiency in the somatosensory system can also effect on the walking stability. The increase of fall risk with the introduction of these factors is well known. However, other fall risks that have not been fully investigated are the slips and trips of healthy human walking. According to a survey conducted by Health and Safety Executive, slips and trips were the most common cause of major injuries to employees (Health and Safety Executive, 2012). In addition, the compensation claims of injury due to the slips and trips on unexpected walking surface without involvement of walking pathology has grown rapidly over the past couple of years. These claims approached 0.5 billion pounds per year (National Accident Helpline Limited, 2013). This evidence reflexes that, not only the fall risk guidance for pathological walking, but also that for healthy human walking (Kang and Dingwell, 2008) is also required.

Similar to other activities, walking motion is performed by the interactions between neural and motion system based on both instinct and learning (Rose and Gamble, 2006). These complex interactions make individuals walk and response to perturbation differently. The dynamic stability of human walking may be quantified by the response

to external perturbation. However, since human locomotion adapts to situations (Kurz et al., 2010; Bruijn, 2010), a method for isolating such effect from the human locomotion measurements are required. Up until now, the accepted method for such isolation has not been identified (Bruijn, 2010). More importantly, the experiment of perturbed human motion needs to be conducted carefully to maintain the ethics of human experiment. All of these limitations make the measures of human locomotion in response to perturbation an open question.

Despite the introduction of disturbance, the inherent variations emerging from complex neuro-musculoskeletal interactions during human walking can be treated as a small perturbation in the examinations for the rate of convergence to the steady walking motion (Steven, 1994), and the rate of divergence from nearby trajectory (Rosenstein et al., 1993). These examinations have been widely used to quantify local stability of the human locomotion based on the relatively small size of perturbations (Hurmuzlu and Basdogan, 1994; Dingwell and Kang, 2007; Dingwell et al., 2007;Bruijn et al., 2009; Kang and Dingwell, 2009).

With the incorporation of human locomotion models, the global stability can be a reasonable prediction of fall possibility. Since the global stability is defined by the maximum perturbation before the occurrence of fall (Shub, 1987; Hsu, 1987; Guckenheimer and Holmes, 1983). This stability quantification is applicable only when a model is used to simulate human walking. Global stability can be estimated by many techniques i.e. maximum allowable disturbance (Karssen and Wisse, 2011) and basin of attraction (Schwab and Wisse, 2001). The area of basin of attraction is used to quantify global stability in term of robustness. This area was widely used to compare between

the dynamic stability of bipedal locomotion with the wide variety of mechanical property (Schwab and Wisse, 2001; Rummel et al., 2010).

Despite the wide variety of stability indices, one may question that, based on a particular quantification method, how well can the individual locomotion stability be differentiated from others. As individuals have different walking motions, do they have the same level of walking stability and if not, what makes the difference? Human locomotion models may be able to response to these questions as they can provide insights into different levels of complexity of the whole-body motion system. The complexity level can range from minimum level of leg and joint complexity (Geyer et al., 2006; Lipfert et al., 2012; Seyfarth et al., 2001; Gunther and Blickhan, 2002) to the interactions between motion and neural system during locomotion (Hase and Yamazaki, 1998; Yamazaki et al., 1996; Ogihara and Yamazaki, 2001). However, due to the model complexity and limited knowledge of neuron inputs, the application of neuro-musculoskeletal model in dynamic stability quantification may be not suitable.

With the incorporation of human locomotion models, the human walking motion can be predicted, and the fall possibility can be examined. However, one of the challenges is how to ensure that walking motion is predicted from the human parameter range and how to extract such human mechanical property from the measurement data. Elastic leg property has been implemented into the compliant leg model with axial elastic property (CAE) to examine the validity of predict human locomotion (Lipfert et al., 2012). This examination suggested that more complicated leg definition may be required to represent the foot-ground contact and the change of leg property during the gait. This suggestion supports the robot leg design inspired by the stabilising mechanisms in insect running legs (Schmitt and Clark, 2009). The actuated rest length incorporating

with the variation of touchdown angle has been found as stabilising mechanisms in running with perturbations. Such natural variation of leg property has never been investigated in human walking.

The combination between the locomotion modelling, mechanical property and dynamic stability quantification technique is crucial to the reliability of dynamic stability analysis. On the wide variety of mechanical properties, the human locomotion may be predicted by human locomotion model and the global stability can be quantified. With the mechanical property being extracted from the human walking measurement date, this scheme for the dynamic stability analysis of healthy human walking may be able to provide insight into the difference between the dynamic stability of individuals.

1.2 Aim and objectives

The objective of the work presented in this thesis was to develop and validate a computational methodology for dynamic stability analysis of the human walking motion, and to use this methodology to examine the effects of leg property on the dynamic stability of human walking. This work is aimed to provide a computational framework for dynamic stability analysis of human walking, which requires minimum measurement data, is flexible to a wide variety of mechanical property of human leg, and can predict accurate walking motion and dynamic stability of individuals. The primary objective was completed by following secondary objectives.

- To obtain the mechanical property of human leg during walking motion and validate the human walking prediction, a large measurement database of human

walking motion was created. The measurement of human walking at different speeds was conducted.

- To provide insight into a wide variety of human leg property, the definitions of mechanical property of human leg during walking motion were presented. Fundamentals of leg property were defined for the extraction of crucial leg parameters from the measurement data. The crucial leg parameters are the minimum numbers of leg parameter required to identify human walking motion. Then, based on the fundamentals of leg property, the wide variety of leg property definition were presented, and used to extract the leg property from the measurement data.

- To predict the accurate human walking motion from the wide variety of leg property. Simple models of human walking were developed to accommodate the wide variety of human leg property, and were used to predict walking motion. The simple walking models with different configurations and operating principles were developed to predict the effect of different leg property on the walking motion.

- To differentiate the level of dynamic stability by the leg property, the dynamic stability of human walking with different leg property was analysed. The global stability was used to quantify the dynamic stability on the human walking prediction. The leg property requirements for stable walking motion were also identified.

1.3 Thesis overview

The thesis is divided into eight chapters. This first chapter briefly reviews the current state of the analysis of human walking stability with the effects of dynamic leg properties, introduces the objectives of the research work of this thesis, and proposed the methodology adopted. The remaining seven chapters include: a chapter reviewing the literature on human locomotion modelling and dynamic stability quantifications, five chapters describing the core work of the thesis (see Figure 1.1), and a concluding chapter that summarises the work presented in the thesis as a whole and proposes an experimental and computational framework for dynamic stability quantification of human walking based on a wide variety of dynamic leg properties.

The chapters describing the core work begin with a brief introduction that outlines the objectives of the work to be presented in that chapter and end with a short conclusion or discussion that summarises the major points from that chapter. Below is a breakdown of the thesis, previewing the content of each of the constituent chapters.

In Chapter 2, a literature review of the relevant research for the analysis of human walking stability is presented, this being the basis of the proposed methodology for dynamic stability quantification of human walking motion. Firstly, the human locomotion modelling is introduced in a sequence of model complexity from minimum to maximum complexity. Secondly, the mechanical property of the leg during locomotion are introduced which include the leg property in human, animals and biped robots for the locomotion on different terrains. Finally, the methods to quantify the

walking stability are classified. In the conclusion, the best possible combination of human locomotion models, dynamic leg property and quantification methods for dynamic stability are proposed.

In Chapter 3, the limitations of the use of three-dimensional whole-body walking measurement in dynamic stability analysis was raised. The three-dimensional whole-body walking measurement for the development and validation of human walking model for dynamic stability analysis was introduced. The experimental protocol and process for three-dimensional whole-body walking measurement was presented. A carefully designed experimental protocol, together with a set of specially designed plastic plates carrying reflective marker clusters, were adopted to capture the motion of all the major body segments. Anatomical landmarks and local coordinate systems were used to reconstruct position and orientations of each body segment. The software GMAS (General Motion Analysis Software) is used to analyse three-dimensional kinematic and kinetic data. The data needed for leg property identification was calculated thereafter. The Chapter ends with some measurement results obtained.

The fundamentals of leg property are described in Chapter 4. This includes the leg property definitions and a methodology for leg property extraction from human walking measurements. The fundamental leg properties of different walking speeds, in different contact conditions and with different elastic properties are presented.

In Chapter 5, the posture-dependent leg property is proposed for the study of the leg property variation throughout the gait cycle. The posture-dependent leg properties of different walking speeds, in different contact conditions and also the advantages over the fundamental leg properties are investigated. The potential applications in human walking prediction are analysed.

In Chapter 6, the fundamental leg property is implemented into two simple walking models. The first model accommodates only the axial component of the fundamental leg property (CAE model). The second model accommodates both of the axial and tangential components of the fundamental leg property (CATE model). The constant system energy is assumed. The validity regions of human walking prediction by using CAE and CATE model with fundamental leg properties are presented. The human walking predictions provided by fundamental leg properties at different walking speeds, in different contact conditions and with different elastic functions are analysed. The dynamic stability of the predicted walking motions is quantified. The effects of elastic properties and the introduction of the tangential leg property on the dynamic stability of human walking are investigated.

In Chapter 7, a posture-dependent elastic leg model operating with variable system energy is proposed. Human walking motions were predicted by the posture-dependent leg properties. The effect of posture-dependent leg property on the prediction accuracy of periodic walking motion is investigated. The limitations of posture-dependent elastic leg model in dynamic stability quantification are discussed.

Finally, Chapter 8 reviews the work of each constituent chapter by summarising the main points and drawing general conclusions. Integrating the methodologies employed in this thesis, an experimental and computational framework for dynamic stability quantification of human walking motion has been proposed, which may also provide guidance for the dynamic stability in clinical applications. Finally, some suggestions for future work are given.

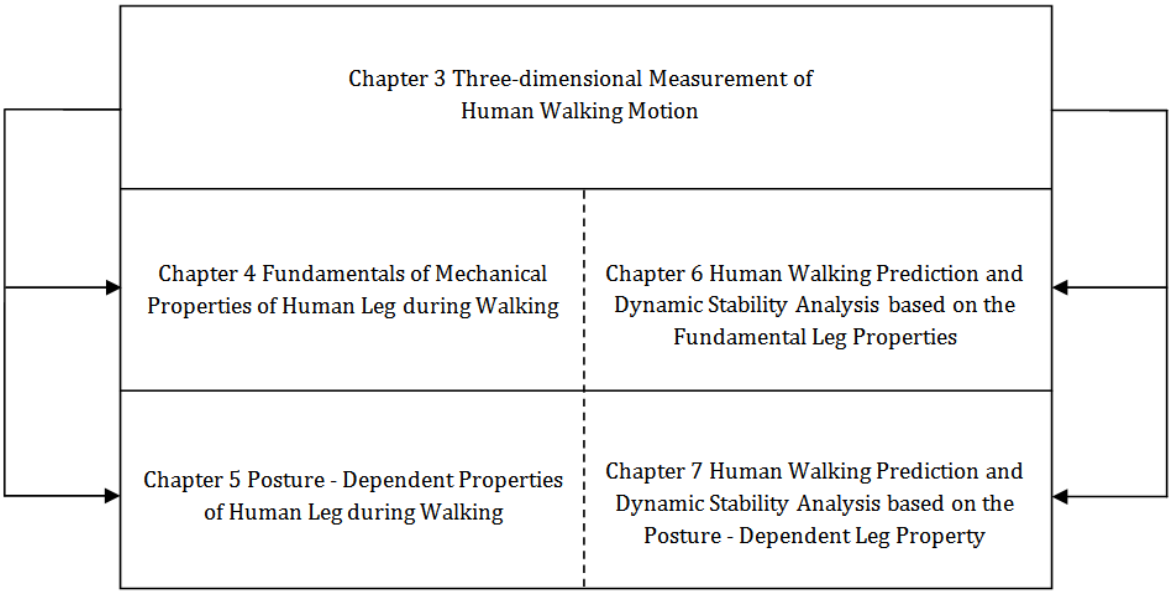

Figure 1.1 The relationship between the main chapters of the thesis. The measurement data in Chapter 3 is used to extract the leg properties in Chapter 4 and Chapter 5 and also to validate the human walking prediction in Chapter 6 and Chapter 7. Chapter 4 and Chapter 6 are based on the fundamental leg property definition. Chapter 5 and Chapter 7 are based on the posture-dependent leg property definition. The dynamic stability analysis was presented in Chapter 6 and Chapter 7 based on fundamental and posture-dependent leg property, respectively.

Chapter 2 Literature Review

2.1 Introduction

This chapter presents a review of previous works related to the human locomotion modelling, leg properties during locomotion and techniques for dynamic stability quantification of human walking, which are the basic of the methodology proposed in this thesis for dynamic stability quantification of human walking motion. The review is divided into three key areas: 1). Bipedal locomotion modelling, 2). Mechanical properties of legs during locomotion and 3).Dynamic stability quantifications of bipedal locomotion. In the conclusions, the relationships between the three key areas, their roles in dynamic stability analysis and the applications in this thesis work will be discussed.

2.2 Bipedal locomotion modelling

The sequence of processes for human locomotion may be summarized as followings: neuron actions from central to peripheral nervous system; contraction of muscles that develop tension; generation of forces at, and moments across, synovial joints; coordination of rigid skeletal segments based on their anthropometry movement; and generation of ground reaction forces. The whole-sequence proceeds along with the real-time interaction between sensory and motor system (Vaughan, 1999; Vaughan et al., 1999). Human gait model that tries to underline the most of this sequence is called the forward dynamic neuro-musculoskeletal model in which the model inputs are derived from different bases of neuro-excitation. Despite being represented by the

highest level of complexity, the human gait can be minimally represented by compass legs and a point mass representing the centre of mass motion. It depends on the ultimate applications that define which parts in the locomotion process to be included in a gait model. The development of human gait model is primarily involved in two research fields: the design of legged robotics and biomechanics of animal and human locomotion. Both fields accept all levels of system complexity and involvement in stability prediction, which will be reviewed together in this sub-section in a sequence of system complexity.

2.2.1 Inverted pendulum model

Inverted pendulum model is widely used as a simplest model operated by the net effect of forces and torques or moments applied on a point or lump mass representing whole-body mass. The simplicity and analytical solution allow the fundamental studies such as static and dynamic stability, performance and effect of mechanical properties on locomotion.

Rigid leg inverted pendulum model

The early study of biped walking mechanism used a rigid leg inverted pendulum model to express the ideal energy exchange during the curvilinear body motion over the foot-ground contact point. (Cavagna et al., 1963; Cavagna et al., 1976; Cavagna et al., 1977) studied the mechanism of the body-ground interaction of biped locomotion by means of mechanical work done estimated by the measured ground reaction force and whole-body kinematics. The external mechanical work done in elevation and forward

acceleration of the CoM during one-step walking and running were investigated when the net momentum of body-segment was considered as a constant. It was found that, the inverted pendulum being equivalent to rolling egg model provides exceptional quality explanations of the kinetic-gravitational energy exchange in intermediate speed walking. However, the energy storage and recovery performed by some sort of elastic mechanism better explained running motion. The complete energy exchange was found in inverted pendulum model with the rear foot pushing upward during the late stance (Cavagna et al., 1977).

Afterwards, the interest was changed from mechanical energy to balance and stability of the locomotion, one of which is the study of balance stepping which was simplified by the motion of rigid leg inverted pendulum. Townsend (1985), Millard et al. (2009) and Wight et al. (2008) studied the foot placement, the location the foot needs to be placed to restore balance in biped walking. For lateral balance restoration, Townsend (1985) found the lateral foot placements as a linear function of the whole-body centre of mass position and velocity at the time of touchdown. Afterwards, Wight et al. (2008) focused on walking in the sagittal plane and derived the stable walking region based on the stability "in-the-sense of Lyapunov" by examining the initial tilting angle and angular velocity, energy balance and friction force. This stable walking region was used to quantify, the dynamic stability of the given initial walking condition. The foot placement estimator (FPE) was derived by the foot placement on a given initial condition, which can maintain the stable state variables and conservative angular momentum prior and after the touchdown impact (see Figure 2.1). The validation with human walking measurement data showed moderate stability prediction using foot placement

estimator. More details can be found in sub-section 2.4.3. Millard et al. (2012) extended the foot placement for balance restoration to 3D walking system by introducing an Euler pendulum, a rigid-leg monopod with disc-shaped foot. The rolling resistance and spin friction were included with the assumption of conserved angular momentum. The stable regions of walking were defined in the sense of Lyapunov by examining the initial tilting angle, angular velocity, energy balance, rolling resistance and spinning friction of Euler pendulum. An additional foot placement named capture point (CAP), a foot placement location to restore balance for a linear-inverted-pendulum was recalled (Pratt et al., 2006). The human foot placement location was bounded by the CAP and the FPE location since the human legs have been found to be stiffer than the nonlinear spring of the linear-inverted-pendulum model and more compliant than that the rigid leg FPE. The validation with human walking measurement showed considerable correspondence of 3DFPE to human foot placement (HFP).

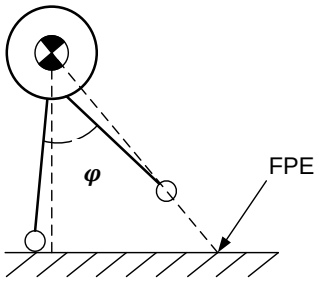

Figure 2.1 The FPE location derived from the projection of the angle φ from the CoM to the walking surface (Wight et al., 2008).

The inverted pendulum model with variable leg length

The inverted pendulum model with variable leg length has been developed especially for the conceptual analysis of CoM motion control during biped locomotion. Inman (1966) was one of the first investigators who suggested the idea of effective leg length

or virtual leg length for the analysis of centre of mass motion. This virtual leg was defined by the line connecting the whole-body centre of mass (CoM) and foot–ground contact point, the length of which varies during locomotion. He and his colleagues found that foot and ankle mechanisms are involved in the compression of the virtual leg length during mid-stance, which results in the lesser fluctuation the CoM trajectory. This concept renders in the gait control of machine walkers in that the constant CoM height is the only remaining control to achieve for the biped locomotion synthesis. Thereafter, the complexity level of IPM control for biped walking synthesis has been reduced to the minimal control on minimal joint actuation for examples, ankle and hip actuation that generate virtual leg length fluctuation to maintain the horizontal of CoM trajectory. Such system was called linear-inverted pendulum model (Saunders et al., 1953; Inman, 1966; Inman et al., 1994). Later on, Kajita and Tani (1991) proposed two telescopic legs with a 2-DoF actuator on the leg tops generating the horizontal motion of CoM on the constant CoM height assumption. The gait pattern was determined by minimal ankle torque around the contact point. The 3D version (Kajita et al., 2001; Kajita et al., 2002) has row and pitch actuation at the contact point of the inverted pendulum to generate the flat CoM motion on a horizontal plane on single and double leg support.

Lee and Farley (1998) studied the compression, touchdown angle and swept angle of the stance-limb for the prediction of CoM trajectory during walking and running. The stance-limb compression was defined as the difference between the leg length at heel-strike and that at each instant during the stance phase. An inverted pendulum model with compressible stance-limb and a spring-mass model were used in predicting the actual CoM motion during walking and running, respectively. The touchdown angle and the timing of maximum compression of virtual stance-limb were found dependent and

responsible to the trajectory of the centre of mass during walking and running. The translation of the foot-ground contact point was found to decrease the stance-limb touchdown angle (with respect to vertical) and flatten the CoM trajectory.

Srinivasan and Ruina (2006) used inverted pendulum model with fluctuating leg length to study human gait on minimal energy cost. It is a conceptual model with an assumption that the cost of transport is proportional to muscle work. The legs were assumed to be massless and can be oriented, lengthen and shorten with no energy cost. The fluctuated leg length l(t) was formed by telescopic axial actuator in representing flexion of hip, knee and ankle and generating compressive time-varying force F= F(t) without elastic energy storage (see Figure 2.2). Potential-kinetic energy exchange regulated by leg length fluctuation was the key of this model. Only single support phase of the gait was addressed to examine mechanical work done during the locomotion. The optimal energy results showed that the stiff-leg, pendular running and impulsive contact are the less exhausted mechanics of moderate speed walking, walk-to-run transition and running, respectively.

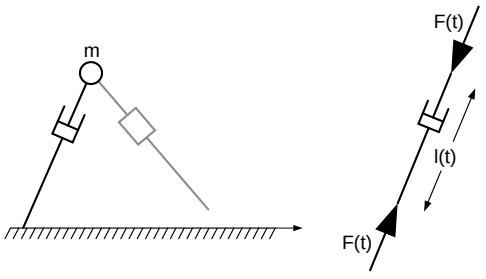

Figure 2.2 Inverted pendulum model with fluctuated leg length (Srinivasan and Ruina 2006)

Inverted pendulum model with rotating mass

By McGhee and Kuhner (1969), angular momentum has been introduced to a system of planar inverted pendulum as locomotion stabiliser. Actuated by moment (M), a rotating mass was simply included in the leg mechanisms for the locomotion stabilisation (see Figure 2.3). The equations of motion were linearised and solved for static stability, periodic motion and locomotion. The stable region was found to be enlarged by foot-like extension. By defining the relationship between leg angle (φ_1) and trunk angle (φ_2), the periodic motion was achieved by body torque control and extended to the locomotion by the planning sequence of two mass-less legs.

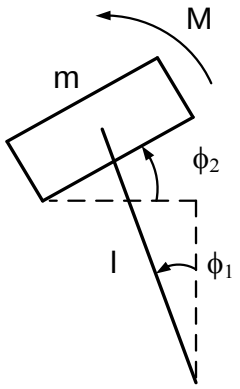

Figure 2.3 The inverted pendulum with rotating mass (McGhee and Kuhner, 1969)

Frank (1970) proposed an inverted pendulum model with six-degree of freedom in which the whole-body angular inertia is taken into account. This inverted pendulum model demonstrates the trade-off between the energy cost, body stability, body path stability and gait stability. The dynamic stability was founded with the sacrifice of minimum energy. Despite the nonlinear leg fluctuation minimizing the vertical displacements of the centre of mass (Saunders et al., 1953; Inman, 1966), a stiff-legged

gait permitting curvilinear motion of centre of mass was found to render as gait stabilisation.

As a stability improvement version of the linear-inverted pendulum model, a two-mass inverted pendulum has been introduced by Park and Kim (1998) with one mass being assumed to concentrate at the foot of the swing leg and another mass being distributed over the rest of the body. The constrained motion of the swing leg was assumed to have no inertia effect. It was found that the locomotion formulated by this gravity-compensated inverted pendulum model (GCIPM) is more stable than that of the simple inverted pendulum model.

Albert and Gerth (2003) extended Park and Kim (1998)'s model to the multiple mass inverted pendulum model (MMIPM) without a trunk based on the control principle for zero moment around contact point (ZMP). This model allows leg trajectories to be responsible for the whole-body motion and gait stability. It was found that the dynamics of the swing leg i.e. rotational inertia facilitates the ZMP control such that the 3D gait pattern generator can regulate the ZMP to locate in the middle of the foot. With the ZMP at the maximum stability margin, the MMIP model was as one of the most stable inverted pendulum models. More details on ZMP and stability margin can be found in sub-section 2.4.3.

On the same basis of ZMP control, the angular-momentum-inducing inverted pendulum (AMIP) was introduced by Kudoh and Komura (2003). By introducing the angular

momentum around the CoM, it was found that the controls for CoM motion in the sagittal and frontal plane can be achieved separately. The modified version by Ha and Choi (2007) introduced a virtual height (VHIM) adjustment depending on walking speed and mass distribution of the inverted pendulum. Since the ZMP trajectory is mainly determined by the CoM trajectory, the simple adjustment of the CoM height in this inverted pendulum was shown to improve the ZMP control.

The linear-inverted pendulum has been used widely and successfully in biped locomotion synthesis because it helps to simplify the control of joint actuation and the body momentum. However, it was found that the additional angular momentum was introduced to every modified version of the linear-inverted pendulum. This is possibly the substitution to the absence of angular momentum of curvilinear motion of the CoM, which supports Frank (1970)'s suggestion in that the CoM vaulting over the contact point is fundamental to the stability of biped locomotion. This underlines a drawback of flat CoM trajectory on locomotion stability, which is also supported by the fact that the flat CoM trajectory has never been found in human locomotion.

By using the rigid leg inverted pendulum model, a decent quality prediction of human walking has been found at medium walking speed when the gravitational energy almost entirely exchanges with kinetic energy. A better prediction of hi-speed walking and running was found in the compressible leg inverted pendulum model. In these inverted pendulum models, different CoM trajectories of walking and running were represented by different touchdown angle and energy storage. The double support phase of walking

has not been considered deliberately. In addition, based only on the net effect of force and moment, the IPM may not render as an accurate prediction of the energy cost. For example, the leg fluctuation representing joint flexions during the gait may lead to incorrect interpretations of muscle work and energy cost of the expedition, as has been demonstrated in Heglund and Cavagna (1985) that the metabolic energy is used only when a muscle is activated and develops tension, does not matter the created mechanical work. Thus, in the fluctuating leg length - inverted pendulum model, the less mechanical cost of transport is not necessarily corresponding to either the less muscle work or the less exhausted condition in human walking. Apart from the energy prediction, the IPM can render in a simple description, prediction and design for the global mechanics of human locomotion and stabilisation.

2.2.2 Spring loaded inverted pendulum model (SLIP)

The gravitational potential energy and kinetic energy are not entirely exchanged in one stride of human walking. The mechanical energy stored as elastic energy and recovered as kinetic and gravitational energy have been found as energy transfer between stride (Cavagna et al., 1977). This mechanism can be represented by compliant mechanisms, which permit energy storage -release and the leg compression to represent more accurate dynamics of locomotion.

Simple spring-mass model

A simple spring-mass model was one of the first compliant mechanism models introduced by (Siegler et al., 1982). It was a simplified version of the inverted pendulum

model introduced by (Frank, 1970) in which the body was regarded as a point mass rather than a rigid body. The mass is supported by two linear visco-elastic legs representing the mechanical properties of the musculoskeletal system, which explain the generation of the ground reaction force during single and double support phase. Other two versions of this model are the three-dimensional model and the two-dimensional model with foot being perpendicular to the leg. The stance phase of human gait was simulated by solving the initial value problem in which the initial motion and model's parameters were obtained from human gait measurement. The gait characteristics simulated by using these three models are in close agreement with published measurement data. However, despite a good quality prediction of gait characteristics, the models are too complex to render as gait analysis in wide biological parameter space.

By Blickhan (1989), a simpler spring-mass model was introduced to address the mechanics of human running and hopping as an extension of animal bouncing gait. Human running was modelled as a hopping forward with a spring angle at landing. The simulations showed that the CoM motion is uniquely characterised by leg stiffness, the velocity vector and spring length at landing. McMahon and Cheng (1990) used a similar hopping forward model justified by previously published experimental data of ground reaction force during running to study the coupling between leg-spring stiffness, gravity and forward speed. A steady running was achieved by a set of input parameters comprising the leg length and CoM velocity at landing which leads to a repetitive running motion. For a combination of leg stiffness and vertical velocity, the model

predicts relative stride length and initial angle in good agreement with experimental data. At high forward speed, leg stiffness is a nearly linear coupling with velocity vector.

Alexander (1992) proposed a model of bipedal locomotion on compliant legs as an extension of his inverted pendulum model for quadrupeds (Alexander, 1980). The two-dimensional model consists of a rigid trunk and two legs in which the centre of mass is located at the hip. Each leg has a telescopic actuator that can be lengthen and shorten and exert force, which represent the length change due to the flexion and extension of the knee and ankle joints. A spring aligned with the long axis of the leg represents the leg compliance. There is also a torque actuator at the hip representing the flexion and extension of human hip joint. The leg mass was assumed to be concentrate at a point located at a constant distance from the hip joint. The model walks or runs with constant touching down intervals. Each foot is alternately on and off the ground for stance phase and swing phase, respectively. Model parameters such as anatomical parameters and compliant properties were obtained from previous published data. The forward dynamic problem was solved by the optimisation of expenditure cost based on the assumption that the cost of transport is a proportion of muscle work. The results showed indistinct work requirement between walking and running which are different from the conducted metabolic cost measurement. The muscle performance estimated by metabolic cost, perfect elasticity and constant elastic compliance assumption were found as three factors resulting in inaccurate prediction of walking-running energy cost. As mentioned earlier in the previous sub-section, the metabolic energy is used only when a muscle is activated and develops tension, does not matter the created mechanical work (Heglund and Cavagna, 1985). Thus, the changes in leg length for

optimal mechanical energy are not necessarily related to optimal metabolic energy. This may be one of the sources for the inaccurate prediction.

The modified version of Alexander (1992)'s model took account of the extra cost of the knee extensor muscles which increases the moments acting about the knee in the hi-speed gait (Minetti and Alexander, 1997). The telescopic actuator was replaced by torque actuator at the knee joint. This torque actuator was introduced to balance the moment of a given ground force. By assuming the direct relationships between metabolic costs, muscle work and mechanical work done by the knee and hip torque, the walking simulation showed less expenditure energy than that of running at low speeds. However, since the relationship between the cost function, muscle work and mechanical work done by the model's actuators is still ambiguous, the expenditure energy of human locomotion may be not best estimated by compliant leg model with axial elastic property.

Afterward, the spring loaded inverted pendulum model was widely used to study the effect of leg mechanics on the locomotion stability. Running stability was the major topic at the early development as demonstrated in Raibert(1986), Schwind (1998), Seyfarth et al.,(2002) and Geyer et al (2005). Seyfarth et al. (2002) studied a criterion of stable running motion in terms of spring-like leg adjustments. The linear spring-mass model with designed attack angle was developed and justified by experimental tendon stress-strain relationships published in Alexander et al. (1986). The simulation started at the apex of flight phase with nominal leg length. The designed model parameters are

the body mass, leg stiffness, the nominal leg length and the angle of attack. Spring loaded inverted pendulum predicted periodic running motion within a certain range of leg stiffness (k_{leg})and angle of attack (α) in which the empirical relationship was found as

$$k_{leg}(\alpha) = \frac{c}{1-\sin\alpha} \tag{2.1}$$

when c is a constant. The periodic running motion remains within a small range of leg stiffness and angle of attack. The stability of the periodic running motion was analysed by using the return map of the height and horizontal velocity at the apex of CoM trajectory. Limit cycles were identified using a stride number analysis and a stride-to-stride analysis. The fixed point of limit cycle was examined if its gradient around the neighbourhood is within [-1, 1]. In stable running region, it was found that the adaptations of leg stiffness with the chosen angle of attack results in almost constant maximum leg force. The spring-mass model validation with experimental data of running animal and human showed the self-stabilised running motion as a proper adjustment of leg stiffness, angle of attack at running speed above 3.5 m/s (Farley et al., 1993). Ghigliazz et al., (2003) used a similar model to derive an explicit expression of the return map of spring-loaded inverted pendulum for running motion by neglecting gravity during stance. Geyer (2005) extended from stable region of running in Seyfarth (2002) to the closed-form approximation of stable running by assuming small spring angles during stance to redirect the gravitational force vector to the spring axis. With less computational intense, the simple closed-form solution of stable running was

suggested as a tool for gait stability analysis in large biological parameter space. However, as the operating region of locomotion speed is above the region of human walking speed, this simple spring-mass model was recognised as a human running template.

Afterwards, Geyer et al. (2006) proposed a bipedal spring-mass model with more deliberate properties of spring leg to represent both walking and running. For walking simulation, the double support phase was described by the motion between swing leg touchdown and stand leg take-off. A kinematic touchdown condition of the swing leg was defined by the leg striking the ground with rest length at fixed leg orientation with respect to gravity. The stand leg take-off condition was defined to occur when the spring leg reaches its rest length. The model parameters were justified by human measurement data. The simulations were started at the apex, or when the CoM trajectory is at the highest point during single support phase. The initial value problem was solved to obtain the periodic motion of apex-to-apex walking and running. The gait characteristics such as ground reaction force pattern, CoM trajectory and phase of mechanical energies were used to establish the region of spring leg stiffness and touchdown angle for human-like walking and running motion. The gait stability was examined by using apex return map and the Eigenvalues of the Jacobian matrix. The stable region of walking and running were distinguished by the angle of attack, spring stiffness, system energy and the present of double support phase. Despite the complete energy exchange ruled by rigid-leg inverted pendulum, this model suggested that walking efficiency depends on how much the stride energy can be stored elastically when redirecting the CoM during double support phase.

Some additional efficiencies i.e. performance and robustness have been studied deliberately for the design of stable walking machine (Iida et al., 2007; Rummel et al., 2010). One of which is the derivation of stable motion range of symmetric and asymmetric walking motion by identifying the leg stiffness that provides stable walking. The robustness against small perturbation was examined by the calculation of the area of the basin of attraction (Rummel et al., 2010). The results showed a wide range of angle of attack in the stable region of walking permitting the flexibility of attack angle to prepare for leg touchdown. The walking with higher linear stiffness has relatively small area of the basin of attraction indicating poor robustness against perturbations. To improve the robustness, non-linear leg functions with decreased slope of force-length relationship were suggested.

Although the SLIP can predict the motion and dynamic stability of human walking and running, it underestimates the horizontal displacement of CoM and overestimates the vertical displacement of CoM and magnitude of ground reaction force. To predict the precise walking motion in human range, Lipfert et al. (2012) determined the realistic parameter range for human gait by the linear least square fitting on the data plot between the total ground reaction force and leg length obtained from human walking and running measurement. The mechanical parameters i.e. leg stiffness and rest length extracted by the fitting were directly fed into the SLIP model with the initial condition obtained from gait measurement. Preliminarily, none of the periodic motion for walking and running was found but, with compromises between leg property and initial condition, the solutions were finally found in a range of walking and running. The

limited range of solution is most likely caused by two reasons; the first one is the overestimation of extracted leg stiffness due to the leg force definition in which the total ground reaction force was transmitted to apply along the leg to the CoM. In fact, the total ground reaction force of each leg does not always apply along the leg and, therefore, the decomposition of the total GRF is required for the accurate estimation of the leg force-length relationship. The second one is the controversy between the model configuration and the initial condition used in the model. The human gait is, in fact, asymmetrical about the mid-stance, and therefore, feeding the measured initial condition into the symmetrical SLIP model would not likely to reproduce periodic motion. Although the deliberate selection of experimental data is required to validate the prediction range of the simple model of human locomotion, the flexibility of the model parameters allows the examination in a wide range of human locomotion parameters and thus can provide insight into the different mechanical properties of human locomotion i.e. leg stiffness and rest length.

The spring-mass model with variable leg properties

Schwind (1998) was one of the first investigators who proposed the nonlinear spring-mass model of which the leg stiffness changes were operated by adaptive controller during the gait. The non-linear spring leg model was developed to solve for the analytical solution of periodic motion of human running. Only symmetrical stance phase was found to reproduce the periodic motion. Later on, based on the conservation of mechanical energy, another non-linear spring leg model for the design of running machine was proposed by Karssen and Wisse (2011). The optimal non-linear leg stiffness for maximum tolerance to small disturbance so called disturbance rejection

(Hobbelen and Wisse, 2007) was determined. The soft nonlinear stiffness was found to increase the disturbance rejection which is consistent with the results of those in segmented leg running model (Rummel and Seyfarth, 2008). However, these results are in contrast to those in passive dynamic running model with nonlinear spring leg (Owaki and Ishiguro, 2007). Based on orbital stability quantification using maximum Floquet multipliers, the optimal stability was found in a certain design of hard nonlinear spring leg. More details for disturbance rejection and minimum Floquet multipliers can be found in sub-section 2.4.1.

Despite the conservative system energy as a facility for the orbital stable locomotion, the energy variation found in animal self-stabilised mechanisms (Dudek and Full, 2006; Daley and Biewener, 2006; Daley et al., 2007; Sponberg and Full, 2008) has been applied to the SLIP model such that the storage-release, dissipation and production of energy can be managed by changes in leg properties. The self-stabilised locomotion in horizontal and sagittal plane was found as a result of clock-driven energy variations (Seyfarth et al., 2003; Seipel and Holmes, 2007; Kukillaya and Holmes, 2007). Schmitt and Clark (2009) introduced the variable force-free leg length during stance phase and changes in leg touchdown angle between strides to address the energy variation. The actuation of the force-free leg length modulates the spring force such that the energy stored in the spring does not equal the work done by the spring deflection and, therefore, non-conservative leg force-length relationship was established. It was adapted from a net effect of muscle-tendon coordination, which cyclically absorbs and produces energy during the first and the second half of the stance phase, respectively. A gait with variable force-free leg length is asymmetrical around mid-stance and requires

cooperation from leg angle variation or swing-leg retraction (Seyfarth et al., 2003) to regulate the CoM momentum around the contact point. In conjunction with either leg angle control or swing-leg retraction, the predetermined actuation of the force-free leg length during stance was found as a self-stabilised mechanism for the orbital stability of the SLIP model with the introduction of energetic perturbation. Such response to energetic perturbation is the advantage of the SLIP model with leg property variation over that with constant leg properties as the steady state of walking motion predicted by SLIP with constant leg properties will shift to a new steady state or simply fall when come across energetic perturbation (Seyfarth et al., 2002). On the similar basis of energy variation, the modified version of SLIP with instantaneous change of force-free leg length and leg stiffness called ESLIP has been introduced in Ludwig et al. (2012). These changes of leg properties were proposed to trace the CoM motion during human running. The multi-value of force-free leg length and leg stiffness were used to predict the precise human running motion.

The spring-mass model with angular momentum of the body parts

The angular momentum of the body parts has been introduced to the SLIP model to further study the propulsion mechanics, CoP trajectory on the foot and upper body tilting for walking stability. The roller feet were included in the simple mass-spring model developed by Geyer et al. (2006) to the CoP progression (Whittington and Thelen, 2009). It was found that, with the assumption of the total ground reaction force pointing towards the CoM, the horizontal distance between the CoP and CoM can be reduced by the forward progression of the CoP which results in the smaller magnitude of the A-P and vertical ground reaction force compared to that of the conventional

simple spring-mass model. Another application of the spring mass model with roller feet included a damper to the spring leg to study the propulsion mechanic during human walking (Kim and Park, 2011). To simulate one-step walking at different speeds, the model parameters and initial condition were adjusted with human walking measurements. The results showed that the propulsion energy is increased by the speed-dependent increment of leg stiffness, which underlines the relationship between elastic and propulsion energy. The damping coefficient was remarkably small and slightly increased with speed. The major drawback of these roller feet models is the statically unstable motion on the arc-shaped base, which have never been presented in human locomotion (Wisse et al., 2006).

The effect of upper body angular momentum on the human locomotion stability has been studied. The experimental studies of primate locomotion have advised that the total ground reaction force pointing above the CoM as a result of the upright body posture may be an advantage of human locomotion over that of other primates (Thorpe et al., 2007; Kivell and Schmitt, 2009;Lovejoy et al., 2009). Maus et al (2010) proposed a SLIP model with a lumped mass hanged on the compass leg by a pin hip joint to study the effect of upright trunk on biped locomotion. A hip torque was introduced at the pin joint in order to tilt the trunk such that the total ground reaction forces point towards a certain point on a trunk so called virtual pivot point (VPP) (see Figure 2.4). Such mechanism was introduced to turn the inverted pendulum into regular pendulum mechanism termed virtual pendulum (VP), which inherits better self-stabilisation. The initial value problem with the assumption of constant transferred angular momentum was solved to achieve periodic motion solution. The system of trunk oscillation as the

redirection of net resultant force toward the virtual pivot point (VPP) was found to stabilise the walking after small perturbations. The most stable walking motion was found at the VPP heights of approximately 1-25 cm. The predicted hip torque and ground reaction force patterns are close to those observed in human walking motion.

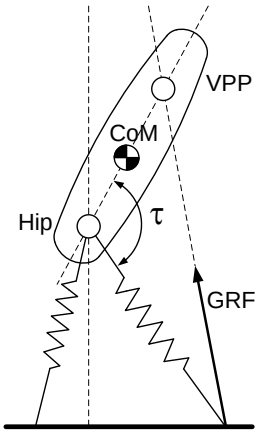

Figure 2.4 The VPP model with VPP point being above the CoM. The hip torque (τ) redirects the ground reaction force (GRF) to point toward the VPP point.

The spring-mass model provides insight into the elasticity of the human gait such as the energy storage and release by changes in leg length. With the proper combination of system parameters and the initial and touchdown condition, the locomotion predicted by SLIP model on the conserved system energy may inherit orbital stability. Such system can tolerate for small perturbation and converge to steady state but will shift to a new steady state or simply fall if comes across large perturbation. The SLIP operated on energy variation can facilitate the self-stability against energetic perturbation. Being accompanied with mechanical energy variation, the changes in leg properties have been found as a mechanical energy adjustment to perturbations. The coordination between the variation of leg properties and touchdown angle plays a crucial role in the self-

stability of SLIP against energetic perturbation. One of the drawbacks of the SLIP is on the study of muscle and metabolic energy. As in human locomotion, the actions corresponding to changes in leg length does not always require muscle activation, the elasticity represented by SLIP model has no direct relationship with either muscle or metabolic energy. Another drawback is the absence of touchdown impact. As the compliant leg is assumed to be massless and the touchdown is always presented as part of the storage of mechanical energy, the touchdown impact is neglected or never presented. The loss at impact may be introduced by considering a small rigid foot with mass, however, touchdown at high velocity may result as a bouncing foot after a strike, and the biped will lose the ground.

2.2.3 Passive dynamic walking model

Passive dynamic walking model has been derived from ballistic walking in which the gait is induced by gravitation and zero actuation at the joints. This passive locomotion was proposed by McGeer (1990) based on the evidence from muscle activities during human walking motion which is remarkably low during swing phase and relatively high during double support phase (McMahon, 1984). Such activities were applied to the unpowered compass leg structure for the down-slope walking by the gravity–induced motion. The biped structure has a point mass at the hip with two links on each leg connected by the knee joint, and the distal link mounted rigidly with the roller feet. The knee is passively locked and unlocked at the determined sequence, which maintains the biped to be upright and progress forward. The sequence also regulates the stance leg and swing leg. The prototypes performed a stable walk down the slope. Over a decade, the nonlinear equations of ballistic walking were further studied to establish the

numerical solutions and the region of validity (Goswami et al., 1996; Goswami et al., 1997; Goswami et al., 1998; Garcia et al., 1998). More studies were on the derivation of a natural and simple gait pattern for biped robotics (Rostami and Bessonnet, 2001a; Rostami and Bessonnet, 2001b). Later on it was used in biomechanical study as a simple gait description and the fundamentals of gait stability such as lateral balance (Bauby and Kuo, 2000), foot placement estimation (Millard et al., 2009; Wight et al., 2008) and walking stability (van der Kooij, 2001; Kooij, 2001; Dingwell and Kang, 2007; Verdaasdonk et al., 2009). The 3D version accounted for the coupling between lateral rocking and forward swinging motion. The curved feet with compliant heels and mechanically constrained arms were added to provide harmonious coordination for stable gait. (Collins et al., 2001; Wisse et al., 2004). Despite the improvement of dynamic stability, the statically unstable motion or unbalance stance on the roller feet was one of limitations for the study of gait stability. Such an unbalance state was overcome by the dynamics of flat feet with ankle spring (see Figure 2.5). The flat feet model with equivalent dynamic stability to the roller feet version was proposed to represent the balance and dynamic stability of human walking (Wisse et al., 2006). It also has been found that an actuated bipedal robot based on passive dynamic walking principle can maintain dynamic stability on walking on rough terrain (Byl and Tadrake, 2008)

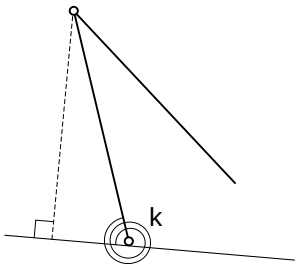

Figure 2.5 The passive dynamic model with flat feet mounted on the ankle with spring (*k*)

The major drawback of the PDW model is the horizontal speed limits. Such natural motion has restricted speed region for stable walking motion due to the zero actuation.

2.2.4 Multi-body model

The multi-body model is used to represent the human whole-body as the articulation of the series segments, where the limbs are not telescopic, and elasticity is localised at the joint level. Multi-body model enables the study of joint torques and muscle contributions at the joint level and thus the prediction of body segment coordination during locomotion. Also, by the mean backwards, the body segment coordination obtained from the gait measurements can be used to predict the coordination of joint torques and muscle contributions. The availability of input resources and final application of the results define which solving technique is to be used.

The forward dynamic determination of the multi-body models for human locomotion study is scarce, due to the limited resources of input parameters. Alexander (1995) used segmented leg model driven by extensor musculature to study the effect of muscle properties, mass distribution of segment, number of leg segment and the leg geometry on standing jump. This multi-segment model with deliberate muscle insertion showed that the maximum shortening speeds, series compliances of leg muscles and the overall leg mass are the keys for high jumping. The leg geometry facilitates the jumping at different speeds by the changes of muscle moment arms. Such a model driven by deliberate joint dynamics was then developed especially for the posture balance prediction (Gunther et al., 2004). The forward dynamic determination on the multi-body models has been found in the study of gait synthesis for stable biped robot. The

nonlinear joint stiffness and the gentle touchdown impact were found to improve the stability of biped running robot(Rummel and Seyfarth, 2008; Hutter et al., 2010). Despite the challenges of forward dynamic determination, a multi-body model with revolute joints was developed for the inverse dynamic problem in which the kinematic and kinetic measurement is the only requirement to solve for joint torques performing locomotion. The results primarily promote the understanding of joint coordination during locomotion. For example, the coupling between joint elasticity in the knee and ankle has been found as one of the joint properties playing a crucial role to stabilise the human locomotion and biped robot (Seyfarth et al., 2001; Gunther and Blickhan, 2002) . More details on forward and inverse dynamic determination can be found in sub-section 2.2.5.

2.2.5 Musculoskeletal model

The whole-body musculoskeletal model incorporates the whole-system of the human body structure to determine as a result of the movement or motion, the joint torques and muscle forces. The direct measurement of muscle forces is generally not feasible in the clinical setting. For example, the most advance EMG can measure only the muscle activation signals, which rather indicates the timing than the magnitude of the force.

The relationships between the forces applied to the body and the resulting motion of the body segments regardless of whether the skeleton is in two or three dimension can be expressed in the form

$$\mathrm{M}(\underline{q})\ddot{\underline{q}} + C\left(\underline{q}\right)\dot{\underline{q}}^2 + \underline{G}\left(\underline{q}\right) + R\left(\underline{q}\right)F^{MT} + \underline{E}\left(\underline{q},\dot{\underline{q}}\right) = \underline{0}, \tag{2.2}$$

Where $\underline{q}$, $\underline{\dot{q}}$, $\underline{\ddot{q}}$ are vectors of the generalized coordinates, velocities, and accerelations, respectively; M($\underline{q}$) is the system mass matrix and M($\underline{q}$)$\underline{\ddot{q}}$ is a vector of inertial forces and torques; $C\left(\underline{q}\right)\underline{\dot{q}}^2$ is a vector of centrifugal and Coriolis forces and torques; $\underline{G}\left(\underline{q}\right)$ is a vector of gravitational forces and torques; $R\left(\underline{q}\right)$ is the matrix of muscle moment arms; F^{MT} is a vector of musculotendon forces and $R\left(\underline{q}\right)F^{MT}$ a vector of musculotendon torques; and $\underline{E}\left(\underline{q},\underline{\dot{q}}\right)$ is a vector of external forces and torques applied to the body by the environment. The contact between the body and environment is one of the most challenging parts in this model. This interaction has been dealing in many different but simple ways. For example, the heel contact is treated as an impact transition in the simplest models. The foot-ground interaction also can be simulated efficiently using compliance components such as damped springs in which the vertical force applied by the springs varies exponentially with the height of the foot above the ground (Pandy and Anderson, 2000; Pandy and Andriacchi, 2010; Pandy, 2001).

Motion problems expressed by such an equation of motion can be categorised in two types, forward and inverse dynamics. The forward dynamic involves the calculation of body segment motion given the muscle forces acting on the body segment. The initial value of the muscle forces in this problem is critical and primarily effects in computational time and the accuracy of body motion estimation. The muscle forces may be estimated from the available force-length-velocity-activation relationships obtained from the recorded electromyography signals during the movement. The optimisation technique helps to determine the optimal muscle forces, through the integration of the equation of motion that satisfies given cost function corresponding to the tasks i.e.

minimum expenditure energy (Pandy and Berme, 1988b; Pandy and Berme, 1988a; Pandy et al., 1992; Pandy and Anderson, 2000; Anderson and Pandy, 2001). One of the challenges in this scheme is the determination of the muscle-tendon moment arms and lines of action as the small errors in these geometries can lead to large errors in muscle forces.

The inverse dynamics determines the muscle forces by tracing the measured kinematic and kinetic of the body i.e. position and external forces acting on the body. The optimisation technique is also required to solve the redundant muscle forces subjecting the cost function (Crowninshield and Brand, 1981; Glitsch and Baumann, 1997). This scheme is computationally efficient as it does not require the system differential equation to be numerical integrated. In addition, the initial values of optimization parameters can be set without the need of measurement data. However, one of limitations is that the accuracy of joint moment calculation highly depends on the measurement of mass and inertia of each body segment. The estimation of inertia using scaling rules may be a major source of errors. In addition, only the equation of motion of multi-segment model for the open- chained link during the single support phase can be solved. Therefore, most of the original models of inverse dynamics only considered running motion and the walking motion with an instantaneous double support phase. An alternative gait prediction model has offered a new determination during double support phase. This method combined inverse dynamic solving and optimization method based on minimum energy and task constraints. It requires only few gait parameters and the assumption of force transfer ratio to define the task constraints (Ren et al., 2005). Another model has been proposed with the assumption of a smooth

transition to the double support phase (Ren et al., 2007). The model required the measured kinematic data of all major body segments. The calculation sequence started with the determination of GRF from the measured data allows the determination on various activities. However, a shortcoming of this method is that the accuracy of gait prediction is highly sensitive to the measurement quality. Both forward and inverse dynamic scheme have been used to predict joint coordination facilitating in the stable locomotion (Zajac et al., 2002; Zajac et al., 2003). However, the comparison between the prediction and the relevant human locomotion measurement remains a challenge for the musculoskeletal model validations.

2.2.6 Integrated neuro-musculoskeletal models

The most complicated model for human locomotion incorporates nervous system control within a musculoskeletal model. The major aim of this model is to estimate or predict muscle forces, joint moments and/or joint kinematics from neural signals. The dynamics of the whole system including neural commands, muscles and body segments currently can be implemented only in forward dynamics form. In inverse dynamics scheme, since the internal counterbalances between flexion and extension muscle to muscle activation remains unknown, the net values of the joint reaction forces and moments are the only ultimate prediction (Buchanan and Shreeve, 1996; Herzog and Leonard, 1991). In forward dynamics approach, the input is the neural command which specifies the magnitude of muscle activation. Such input can be taken from electromyograms (EMGs) or estimated by the optimization or neural network models. The muscle contraction dynamics was created on the dynamics of neural command. This muscle contraction dynamics designs the transformations from muscle activations

into muscle forces. Most models created the muscle contraction dynamics based on Hill's muscle model (Hill, 1938) or other more complex biophysical model of Huxley (Huxley, 1957;Huxley and Simmons, 1971). Then the musculoskeletal geometry is used to transform muscle forces to joint moments. Finally, by solving the equations of dynamic system, the joint movement is predicted.

The use of such interaction between multi-body dynamics and neuron mechanism for the study of biped locomotion has grown over the previous decade (Taga et al., 1991; Taga, 1994; Taga, 1995a; Taga, 1995b; Hase and Yamazaki, 1998; Yamazaki et al., 1996; Ogihara and Yamazaki, 2001). Currently, in clinical biomechanics, the EMG driven models of varying complexity have been used to estimate joint moments i.e. knee and low back muscle moment (Lloyd and Besier, 2003; Lloyd and Buchanan, 1996; McGill and Norman, 1986; Thelen et al., 1994). However, this forward dynamic determination is time-consuming, and verification of the central pattern generator (CPG), the cyclical generation of neural signals for human motor control is still an open question.

The high variability of in EMG is a major drawback limiting the neuro-musculoskeletal models to represent the precise human locomotion. The optimisation methods may be used to predict muscle force directly, however, the proper cost function incorporating substantial neural actions has not been recognised. The neuro-musculoskeletal models in robotics considered the gait stability as a necessary condition to proceed the locomotion (Taga et al., 1991; Taga, 1994; Hase and Yamazaki, 1998). With the extreme level of complexity and highly limited information of muscle activation inputs, the whole-body neuro-musculoskeletal models for human locomotion are still under

investigation (Taga, 1995a; Taga, 1995b; Yamazaki et al., 1996; Ogihara and Yamazaki, 2001). The applications in dynamic stability quantification have not been recognised.

2.3 Mechanical properties of legs during locomotion

As mentioned earlier in the previous section, the spring-mass model precisely predicts human running because the spring leg is an appropriate mechanism performing the elastic-kinetic-gravitational energy transfer which is a crucial energy flow in human running. However, the strategic functions of whole-body muscle-tendon structure do not rely only on the single valued force-length relationship of such perfect elastic mechanism (Wainwright et al., 1976). For example, not only to return the energy stored previously, the leg also needs to produce energy to accelerate and elevate the CoM especially during late stance (Alexander, 1988). The complex functions of the human leg during the various types of locomotion may be briefly categorised into three classes; energy conservation, power attenuation and power amplification (Roberts and Azizi, 2011). The combination of these functions performs sophisticated locomotion that a human does in daily-life without thinking. This may be a consequence of the design of structural organisms in the legs and other body parts which was adapted from generation to generation for certain functions (Wainwright et al., 1976). For the human leg, one of the most important functions may be the management between energy cost and dynamic stability during locomotion (Blickhan et al., 2007; Srinivasan and Ruina, 2006). Previous studies on the relationships between leg properties and its function during locomotion mainly concentrated on insect and robotic legs. Very few of which provide insight into human leg properties during locomotion possibly due to the experimental limitations and complexity of musculoskeletal structure. In this section,

the review is divided into two parts, each part concerned with different leg structural property: 1). Compliant leg properties 2). Variable leg properties

2.3.1 Compliant leg properties

Complaint legged machines operated on the conservation of system energy have been found to inherit the self-stability (Blickhan et al., 2007;Seyfarth et al., 2002 and 2006; Geyer et al. 2005 and 2006; Rummel et al., 2010). In a certain energy range, the well-tuned combinations of linear elastic leg properties and touchdown timing defined by leg angle and leg length at touchdown instant are required to carry out periodic motion of walking and running. It was found that the orbital stability of the gait decays with higher leg stiffness (Geyer et al., 2005, 2006; Rummel et al., 2010). Similar results have been found in the study of leg parameters and elasticity during insect locomotion. The common combination of dimensionless leg parameters in the population of cockroach B. Discoidalis i.e. leg stiffness, leg angle and leg length, was found to stabilise the running over the rough terrain. It was suggested as a dimensionless design of leg properties for stable locomotion (Schmitt et al., 2002).

The mechanical properties of the human leg during the gait were estimated by the linear elastic leg function (Lipfert et al., 2012). A linear axial force - leg deflection relationship were used to extract the elastic property and angle of attack of the leg. The dimensionless leg stiffness of 29- 45 and 21-23 and the attack angle ranging from 68 – 85 and 73-88 degree were found during human walking and running, respectively. By feeding the leg properties into the simulation of walking and running by using spring-mass model, it was found that the proper combination of leg properties and leg

positioning is required to carry on the periodic motion of walking and running. This underlines the relationship between the properties and elastic function of the leg during locomotion. With the proper combination of leg properties and leg positioning i.e. leg angle and leg length at touchdown instant and the elastic leg function can facilitate the periodic motion and stability of locomotion.

Five different mathematical models for the estimation of leg stiffness during braking phase of running have been compared (Coleman et al., 2012). One of which requires kinetic-kinematic recordings with leg length being defined as the distance from the CoP of the foot to the greater trochanter. The leg force was calculated from the net resultant force being decomposed into the direction of leg compression. The other four models are conventional which require only force platform-derived data and anthropometric measure to calculate the leg stiffness. The estimations of peak vertical force and the leg length compression are the key for leg stiffness extraction. The peak vertical forces were mainly estimated as the functions of body weight and the duration of flight and ground contact. The leg length compressions were estimated as functions of the leg length during still standing, average horizontal velocity and vertical displacement of the CoM (Morin et al., 2005; Morin et al., 2011; Blum et al., 2009; Farley et al., 1993; Farley and Gonzalez, 1996). Each model predicted significantly different leg stiffness from the others. However, the leg stiffness values predicted by kinetic-kinematic model and nonlinear estimation of peak vertical force and leg length compression are close. The two models share the stiffness range of 10.22 - 16.14 kN/m with the average body weight of 67 kg. Based on relatively small coefficients of variation, the direct kinematic-kinetic measurement was suggested for the precise quantification of leg stiffness. The

nonlinear estimation of peak vertical force and leg length compression (Morin et al 2005) was suggested as an alternative when kinematic measurement is unavailable.

This underlines the importance of leg definition on the study of properties and function of legs during locomotion. Depending on the availability of locomotion measurements, the mechanical properties of the human leg can be estimated on different knowledge of leg functions.

2.3.2 The variable leg properties

As an advantage over the linear elastic leg properties, the effect of the non-linear spring in straight and segmented leg on the disturbance resistance during running has been studied. It has been found that the biped running simulation with soft nonlinear spring leg has fall region further away from the stable limit cycle than that with linear spring leg (Karssen and Wisse, 2011; Rummel and Seyfarth, 2008). However, with energy dissipation at the leg touchdown, the hard nonlinear stiffness was found to improve the orbital stability of passive dynamic running (Owaki et al., 2006). The variation of leg stiffness during the gait is likely another mechanical property facilitating in negotiation with small perturbation.

Many examinations on arthropod leg properties showed the roles of elastic and damping property in energy management and locomotion stabilisation (Alexander, 1988; Cavagna et al., 1977; Kubow and Full, 1999; Full and Koditschek, 1999; Schmitt and Holmes, 2000a; Schmitt and Holmes, 2000b; Schmitt and Holmes, 2003). The passive mechanical properties of rapid running cockroach leg have been examined for

roles in self-stabilisation (Dudek and Full, 2006). With a very short time to react to perturbations, the energy management by rapid running cockroach leg could be assumed as feed-forward type. Energy absorption was found with leg resilience properties being ranged from 60 to 75%. It was found that, extracted from the leg force-displacement data of individual cockroach leg over a wide range of leg frequencies, the elasticity and hysteretic damping (Nashif et al., 1985) are equivalent to that estimated for a single leg of human hopping on damped surfaces (Moritz and Farley, 2003). The frequency independence of hysteretic damping was suggested as embedded dynamics in running leg playing a crucial role as energy absorber handling the disturbance without sensing.

A number of legged machine designs have utilised the leg property variation corresponding to the energy variation found in stable insect running to provide insight into the leg properties for stable biped locomotion (Raibert, 1986; Seyfarth et al., 2003; Schmitt, 2006). To introduce the different leg length at touchdown and leave-off, the elastic leg properties with variable force-free leg length (Schmitt and Clark, 2009) has been studied. A non-conservative force-length relationship was introduced to prescribe the increased or decreased duration of leg extension during the late stance which results in the increase and decrease of CoM velocity at the end of stance phase, respectively. It was found that such variations of force-free leg length allow the variations of CoM velocity to recover from energetic perturbation. However, with its non-conservative energy, the combination of variable force-free leg length and fixed leg touchdown angle yields unstable velocity heading angle or unstable angle between horizontal and net velocity of the CoM. The coupling between the variation in leg length

and leg angle at touchdown was introduced as feed-forward regulation against the change in CoM momentum and, therefore, stabilise the velocity heading angle by leading to steady velocity heading (Seyfarth et al., 2003; Schmitt and Clark, 2009).

The relationship between the change of leg properties and the instantaneous changes in the mechanical energy during the gait has been studied (Carver et al., 2009; Riese and Seyfarth, 2012). In Carver et al. (2009), the spring force was constrained at the instant of the lowest CoM position during running to permit variation of the leg stiffness and force-free leg length, and the instantaneous change of the mechanical energy. It was found that such constraints permitting mechanical energy variation stabilise the gait pattern of biped machine running. Such instantaneous change of leg properties during human running were studied (Ludwig et al., 2012). By fitting such spring force-length relationship onto the measurement data of three-consecutive running steps, the dimensionless leg stiffness was found in the range of 18.7 and 21.2, which is close to the linear leg stiffness calculated by Coleman's model (Coleman et al., 2012).

A hip torque driven by cyclical prescription of rotational stiffness has been introduced to the SLIP model to improve the orbital stability (Seipel and Holmes, 2007). The model assumes that the total leg force exerts to the CoM, therefore, the body has no rotation. It was found that, in a range of axial and rotational stiffness, this modified SLIP model can recover from large perturbation (100% of its fixed point value). However, the orbital stability is highly sensitive to the leg angle and leg length at touchdown and lift-off. The

rotational actuation was found to resist the motion and manage mechanical energy exchange during the gait which is necessary for recovery from large perturbation.

Despite their benefits on the stabilisation of running insects and biped robot after large perturbation, the variable leg properties during human gait and their effect on dynamic stability have not been fully explored. Similarly, the motion resistance and mechanical energy exchange managed by hip torque during human locomotion has never been studied. In addition, the coordination between axial and rotational actuation found to enhance perturbation resistance in biped robot simulation has never been investigated in human locomotion. Such leg properties and axial and rotational actuation may be obtainable from human locomotion measurement. It depends on the ultimate applications that define which part of leg mechanics to be included in the studies.

2.4 Dynamic stability quantifications of biped locomotion

The common purpose of dynamic stability quantification on biped locomotion may be to identify the ability to maintain steady motion after the destabilised situation i.e. the present of external perturbation and the inherent variation of the motion (Wisse, 2004; Rose and Gamble, 2006). In this section, the review of dynamic stability quantification is divided into three categories based on the outcome of the quantification: 1). Quantifications of the tendency to regain steady state after perturbations, 2). Quantifications of sensitivity to variation and 3). Criteria for stability maintenance.

2.4.1 Quantifications of the tendency to regain steady state after perturbations

Largest Floquet multiplier

Floquet multipliers quantify at a certain moment of each motion cycle, the tendency of the system's state to return to steady state, so called "limit cycle orbit", after small perturbations.

The relationship between the initial system's state (s) and the resulting system's state after one step $P(s)$ defines a return map of which the collection is called Poincare map (see figure 2.6). The ideal initial state (s) holding a return map to it expressed by $P(s) = s$ is called the fixed point. However, the system starting away from the fixed point can also converge to it. The conventional examination of this convergence introduces the deviation from the fixed point as a small disturbance. The gradient of which toward the fixed point, so called Jacobian matrix is calculated to identify whether the system has a return tendency and if so to measure at what rate. Such gradient values or Eigenvalues of Jacobian matrix so called Floquet multiplier lies within a unit circle for the convergence to steady state, the smaller magnitude indicates the faster rate of convergence. For the motion system with multiple state variables, one of which providing the largest Floquet multiplier implies the worst case of orbital stability (Steven, 1994; Hasan, 1995). More details can be found in chapter 5. The largest Floquet multiplier has been widely used with legged robot and simulations of biped walking (Hurmuzlu and Moskowitz, 1986; McGeer, 1990; Garcia et al., 1998; Seyfarth et al. 2002; Geyer et al., 2005; Geyer et al., 2006; Seyfarth et al., 2002). It was adapted to use with human locomotion with a periodic motion assumption. The orbital stability of human walking was determined by having the mean of return map during steady state walking to represent the limit cycle. The natural variation of human walking motion was treated as a perturbation (Hurmuzlu and Basdogan, 1994; Dingwell and Kang, 2007; Dingwell et

al., 2007; Schablowski and Gerner, 2006; Bruijn et al., 2009; Kang and Dingwell, 2009; Granata and Lockhart, 2008). Healthy human walking over ground and on treadmill at different speeds showed orbital stability(Bruijn et al., 2009; Kang and Dingwell, 2009). However, its correlation with the risk of falling was unclear as very few studies can include the possibility of falls on such ethical measurement. One of which showed the higher value of maximum Floquet multiplier in fall-prone elderly compared to that in healthy elderly This study relates the decay of orbital stability with the higher risk of falling (Granata and Lockhart, 2008). Despite the difficulty to relate the orbital stability to the risk of falls during human walking, some simple walking models with falling inductions such as changes of floor height were introduced for the quantification of orbital stability on the fall-prone walking situations. However, the correlations between them still cannot be established(Su and Dingwell, 2007; Hobbelen and Wisse, 2007; Bruijn et al., 2011). From all of the above evidences, this orbital stability can be the best in quantifying the inherent stability of the gait pattern when coming across small perturbations.

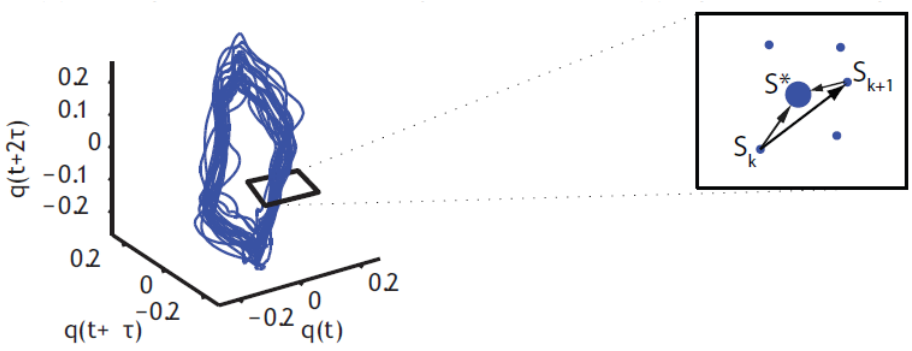

Figure 2.6 The time-history of system's state ($q(t)$) and the Pointcare map captured on Pointcare section in perpendicular to the flow of system's state (left). The close up of Pointcare section (right) shows return map (s_k) and limit cycle (s^*) (Bruijn 2010).

Basin of attraction

The entire collection of the initial states leading the walking motion to steady-state is called the basin of attraction (BoA). The walking is orbital stable if it holds some basin of attraction, the size of which indicates the reliability so called the “robustness” of walking motion to changes in the initial condition. In other words, the large size of the basin of attraction possesses the high number of initial states leading the system to steady-state walking. The basin of attraction can be used to quantify the global stability in term of robustness. A couple of methods were used to draw the region of the basin of attraction (Guckenheimer and Holmes, 1983; Parker and Chua, 1989; Schwab and Wisse, 2001). More details can be found in chapter 5. It is widely used to compare the orbital stability between different designs or configurations of walking robot (Rummel et al., 2010; Wisse, 2004). The distance from the limit cycle to the border of the BoA is potentially equivalent to the biggest size of perturbation the walking motion can handle without falls (Wisse, 2004). However, such quantification would need to bring the subject near to fall if the global stability of human walking were to be defined. Above all, the BoA is a comparative quantification as it is not the actual area but a region contains all possible initial conditions. Therefore, the two basins of attraction need to be collected at the same sampling resolution for that their collections can be compared.

Gait sensitivity norm

As a practical extension from Floquet multipliers, a new measure called Gait sensitivity norm was introduced (Hobbelen and Wisse, 2007). In this measure, the rate of convergence to the limit cycle was applied to the gait indicators such as step width and step time. The dynamic response of which to perturbations is more easily to be

visualised compared to that of state variables. As a linearised response of gait indicators g to a single disturbance e_0, the Gait sensitivity norm (GSN) was defined as

$$\left\|\frac{\partial g}{\partial e}\right\|_2 = \frac{1}{|e_0|}\sqrt{\sum_{i=1}^{q}\sum_{k=0}^{\infty}(g_k(i) - g^*(i))^2} \quad (2.3)$$

,in which $g_k(i)$ is the value of the ith gait indicator at kth step after disturbance and q is the number of gait indicators. The nominal value of gait indicators $g^*(i)$ is calculated from the mean value of gait indicators during steady-state walking. The Gait sensitivity norm being less than 1 indicates stable walking. A pilot study of the GSN in human walking selected the CoM position (with respect to the foot) as a gait indicator on a finite number of strides after it was perturbed by a side way pull (Bruijn, 2010). The variance of the CoM motion in perturbed walking was normalised to the variance of which in unperturbed walking to account for differences in natural variability. The GSN of the CoM position predicted that the walking pattern is more stable in the fast walk than in the normal walking. In general calculation of the GSN, the response to the actual disturbance and the variation of gait parameters are combined to capture all relevant consequences of the perturbation. However, based on the linearisation, it quantifies only the local stability of the gait pattern. In addition, it was found that the Gait sensitivity norm is highly sensitive to the selection of disturbances e_0 and gait indicator g (Karssen and Wisse, 2011; Hobbelen and Wisse, 2007; Bruijn, 2010).

Maximum allowable external perturbation

The largest deterministic disturbance quantifies the maximal disturbance a motion can handle, but does not take into account the convergence rate after a disturbance

(McGeer, 1990; Pratt et al., 2001; Wisse et al., 2005). To determine the maximal disturbance, the different sizes of single perturbation, for example, a floor height and push disturbance were introduced until the motion system fails to produce periodic motion.

To quantify the maximal disturbance capability of the motion system, some random multiple disturbances were introduced, and the rate of convergence to the steady state was quantified until motion system fails to produce periodic motion. The random multiple disturbances that result in a failure of periodic motion are called largest allowable random disturbance (Hobbelen and Wisse, 2007; Pavol et al., 2002; Pijnappels et al., 2008).

Based on the examination of the responses to actual perturbations, these maximum allowable perturbations directly reflex the probability that the biped locomotion will fall. However, these global stability quantifications are hypothetical for human walking and thus, purely used in legged robot, which can bear with a very long experiment on falling situation.

Metastable limit cycle analysis

When the discrete impact events were taken into account, the dynamics of walking systems may be considered by using the discrete, closed-loop return-map dynamics. In such dynamic walking systems, the stochastic perturbation is introduced and the dynamic stability of the transient state of the dynamic system is quantified. The behaviour of this stochastic dynamic system may be steady for a long period, however, the occurrence of fall mode is guaranteed. These types of system cannot be classified as

stable, but it is also unsubstantiated to classify it as unstable (Talkner et al., 1987; Bovier et al., 2000; Maas et al., 2004; Weber et al., 2006). The dynamic stability of the stochastic dynamic system may be quantified based on a discrete-time, continuous-state Markov process in which the the convergence to the absorbing state (fall mode) can be quantified by using an eigenmode analysis (Bovier et al., 2000; Maas et al., 2004; Weber et al., 2006;Byl and Tedrake, 2009). This type of dynamic stability analysis has been applied to the passive walking model to improve the mechanical designs for dynamic stability of (Byl and Tedrake, 2009). The application in the dynamic stability analysis of human walking motion has not been recognised.

2.4.2 Quantifications of the sensitivity to natural variation

Maximum finite time Lyapunov exponent

Maximum finite time Lyapunov exponent (λ) is a continuous capture of short (λ_s) and long term (λ_l) response to a very small perturbation. The neighbouring trajectories of state variable(s), are traced to calculate the average logarithmic rate of separation so called “the rate of divergence”. The short (λ_s)and long term (λ_l) responses are estimated during the first stride and between fourth and tenth stride, respectively. The negative rate of divergence (λ) indicates that the neighbouring trajectories move closer together, which represents stable response to small perturbation. The positive rate indicates that the neighbouring trajectories move away, which represents instability in the sense of “chaos”. The higher value of the finite time Lyapunov exponents (λ) indicates less stable motion system (Rosenstein et al., 1993; Kantz, 2004). With a perceptive mathematical foundation, maximum finite time Lyapunov exponent (λ) has

been widely used to assess and compare the local stability in various walking situations (Dingwell 2000; Dingwell 2000; Buzzi 2003; Manor 2008; Dingwell 2006; Bruijn 2009). More studies designed fall-prone situations to establish the correlation between the sensitivity to natural variation quantified by maximum finite time Lyapunov exponent and the probability of falling. The experimental results from subjects with reported balance problems, simple passive dynamic model walking on slope variation and powered walking robot with disturbed movement control showed similar correlation between the rate of separation and the probability of falls (Lockhart and Liu, 2008; Su and Dingwell, 2007; Garcia et al., 1998; Roos and Dingwell, 2011). It was found that the short term response (λ_s) is highly related to probability of falls while the relationship between the long term response(λ_l) and probability of falls was still unclear. A validation of such relationships simulated the fall-prone situation by changes in morphology, the difference in mechanical properties, the introduction of perturbations and the combination of all situations with the extended version of passive walking model with arched feet and a hip spring (Hobbelen and Wisse, 2007). It confirms the established correlation between the short term response (λ_s) and probability of falling, which is consistent with the global stability quantified by maximum allowable perturbation (Bruijn et al., 2012). However, the explicit relationship between the maximum finite time Lyapunov exponent, the possibility of falls and the global stability remains an open question.

Similar to the largest Floquet multiplier, the maximum finite time Lyapunov exponent does not require the external perturbation during walking. The finite time Lyapunov exponent and the Floquet multipliers are defined by the rate of divergence and the rate of convergence, respectively, in response to the natural variation. The difference is the

reference for the calculation. For the Floquet multipliers, the motion is considered as periodic motion and each trajectory of a state variable is compared to the steady-state trajectory. However, for the finite time Lyapunov exponents, the motion is considered as aperiodic motion and each state variable is compared to the nearest neighbour. This indicates that the two indices quantify the different dynamics stability. The response to small perturbation is the only similarity, which groups them into local stability quantification.

Variability measures

Kinematic variability during the gait has been studied over decades based on some knowledge of the relationships between the nature of variations and control strategies during human movement (Haken et al., 1985; Hausdorff, 2005; Brach et al., 2005; Brach et al., 2007). Although such relationships have not been fully established, the measures of variability have been progressively developed in various gait conditions. The statistics of the variation such as the variance, standard deviation, median absolute deviation and coefficient of variation were used to quantify the variability of gait variables that may be in relationship with falls. The gait variables such as stride time - stride width, the double-support duration and trunk movement have been widely used in variability measures (Su and Dingwell, 2007); Roos and Dingwell, 2011). Despite the wide variety of available quantification, very few of the which have been found to be capable to establish the relationship between the natural variation of the gait variables and the dynamic stability of the locomotion (Maki, 1997; van Emmerik and van Wegen, 2002). In a simulation of a rimless wheel motion on the slope with the stochastic changes of leg length, initial condition and external perturbation, it has been found that

the dynamic stability of bipedal walking motion is highly dependent on such stochastic variability (Thrishantha, et. al, 2012).

In addition, even though such relationship can be established, the kinematic variability still have no relationship with the recovery from perturbation and, therefore, does not necessarily indicate the probability of falls (Bruijn et al., 2011). Since the direct relationship between kinematic variability and probability of falls is still unclear, some assumptions or constraints, for example, an assumption that the stiff or rigid movement is less adaptable to perturbation, are crucial to correlate between the kinematic variability and probability of falls (Stergiou and Decker, 2011).

Criteria for stability maintenance

Criteria for balance and dynamic stability maintenance based on inverted pendulum model

A well-known criterion of static stability states that the vertical projection of the centre of mass (CoM) must be located within the base of support (BoS) to maintain static stability of the centre of mass. An extension of this rule was proposed for dynamic stability quantification base on a simple inverted pendulum model. This extension called extrapolated centre of mass position (XcoM) was calculated as

$$XCoM = CoM + \frac{v}{\omega_0}, \tag{2.4}$$

where CoM, v and ω are location and velocity of the CoM and the pendulum eigenfrequency expressed by

$$\omega_0 = \sqrt{\frac{g}{l}} \tag{2.5}$$

where g and l represent gravitational force and the CoM height at upright standing. The margin of stability (b) is defined by the distance between the location of $XCoM$ and the edge of the base of support (Hof et al., 2005). The biped locomotion is defined to be dynamically stable, if the margin of stability (b) is above zero. In human walking, it was assumed to be coincident with the centre of pressure location (CoP)(Hof et al., 2007;Morasso and Schieppati, 1999). Despite the perceptive foundation of the criterion, it has not been widely used in stability analysis during human walking as it is only applicable in the medio-lateral stability. The stability margin was used to differentiate between the dynamic stability of the walking motion of the above knee amputee and healthy subject. It was found that the stability margin is extended in the walking motion of the above knee amputee (Hof et al., 2007). Another study used stability margin to investigate the effect of compliant surface on the dynamic stability of human walking, and found that the stability margin is extended in the human walking on the compliant surface (MacLellan and Patla, 2006). Those studies underline the extension of stability margin in the fall induced situation, which may then be used to discriminate the fall-prone walking from the normal one. However, this dynamic stability index may need some verification to establish the relationship with the response to perturbation and probability of falls.

A foot placement estimator has been derived on the assumption of conservative angular momentum during the walking motion to estimate the location that the foot should be

placed on to maintain dynamic stability (Mile 1985; Wight 2008). It was found that an inverted pendulum model representing human walking motion is asymptotically stable when a foot is placed right on the estimated point so called the foot placement estimator (FPE). The experimental validation showed that the healthy human walking manages to place the centre of pressure (CoP) slightly ahead the FPE. From those results, it was suggested that placing the CoP slightly behind and ahead the FPE may help to regulate the angular momentum in response to the destabilised situation, and may reduce the possibility of falls (Wight 2009). The 3D version includes the medio-lateral foot placement estimation (Milard 2012) and the capture point (CAP) (Pratt, 2006) adopted from a linear-inverted-pendulum design of biped robot. The 3D-FPE defines a boundary in which the human foot placement should never leave in order to optimise between dynamic stability and energy cost. A further study on the relationship between the FPE-CoP distance and recovery from perturbation may be required to establish the relation with probability of falls.

Criteria dynamic stability maintenance based on multi-body model

Legged robotics have used the zero moment point (ZMP), foot rotation indicator (FRI) and centroidal moment pivot (CMP) as ground reference points to maintain the dynamic stability of the walking machine. The ZMP was defined as a point of resulting reaction force at the contact surface between the leg and the ground (Vukobrat.M and Juricic, 1969). It was used to trace the walking stability while the foot is flat on the ground. The FRI is the point of application of the total ground reaction force due to the body motion and the foot angular momentum. The CMP is a point where the ground reaction force should apply to keep the horizontal component of the whole-body angular momentum constant (Popovic et al., 2005). The experimental validation in

healthy human walking supports the use of the ZMP and CMP to trace CoP and whole-body angular momentum of human walking, respectively, to maintain dynamic stability of bipedal robot walking. As the human foot is light compared to the whole-body, it provides relatively small angular momentum. The ZMP and the FRI during human walking was found at nearly the same location. From such result, it was suggested that the incorporation of the foot angular momentum during the foot-ground interface is crucial in biped robot but has never found in human (Popovic et al., 2005). However, the application of the ZMP and CMP in human walking with pathological problem showed that CoP location does not follow the ZMP and the minimal whole-body angular momentum is not maintained (Brach et al., 2005; Brach et al., 2007). Above all, all of the three ground reference points is primarily a necessary condition for stable walking in which perturbation is not involved. That is, with the present of perturbations, this necessary condition may have no roles in recovery to steady walking.

2.5 Conclusions

Dynamic stability analysis of human locomotion involves the measurement of human locomotion and the quantitative method for dynamic stability. To quantify the dynamic stability, a long history of motion data is required such that the ability to return to steady motion or recover from perturbation can be examined. The human gait models can render in the simulation of repeat gait when the long track or long duration for gait measurement is not applicable (Hartmut, 2005; Geyer, 2005). In addition, the dynamic stability analysis of human locomotion may require gait models to simulate different

gait dynamics and perturbation to the locomotion (Gunther and Blickhan, 2002, Geyer, 2005, Hobbelen and Wisse, 2007).

To serve on different purposes of study, the gait models of different levels of complexity have been used in dynamic stability analysis of animal, biped robot and human locomotion. The minimal model i.e. inverted pendulum, spring-loaded inverted pendulum and passive dynamic walking model were widely used to study the CoM motion and the effect of leg mechanics (Seyfarth et al., 2002; Geyer et al., 2006; Owaki et al., 2006; Lipfert et al., 2012). In the multi-body models, the effect of joint properties i.e. the effect of joint stiffness on the locomotion stability can be examined (Seyfarth et al., 2001; Gunther and Blickhan, 2002). More deliberate joint contributions can be examined by using the gait models with higher level of complexity i.e. musculoskeletal and neuro-musculoskeletal model (Zajac et al., 2002; Zajac et al., 2003). However, in such high level of complexity, the estimations of the joint contributions i.e. joint moment are highly sensitive to measurement quality and the objective function used to solve the motion problem (Ren et al., 2005). Thus, the applications of the complex model of bipedal locomotion in the dynamic stability analysis are limited to the stability of running and walking robots in which the interaction between the mechanical and control system is known and thus, the measurement data and objective function do not play a significant role in the estimation of joint contribution.

In addition to the dynamics of leg and joints, the operation or the function corresponding to the mechanical property is another key factor in dynamic stability of bipedal locomotion. It has been found that leg elasticity facilitates in the stability of gait

pattern in running and walking robots (Lida et al., 2007, Rummel et al., 2010, Seyfarth et al., 2006). The disturbance absorption and angular momentum adjustment have been found to accompany with dynamic properties of the animal, insect and robot leg during locomotion (Raibert, 1986; Seyfarth et al. 2003; Schmitt, 2006). These functions play crucial roles for that the heavy control, and intensive energy are not required to maintain locomotion stability (Wainwright et al., 1976). Such functions of the human leg have not been fully investigated as it is limited by the measurement of the force and displacement of the muscles and tendons, which would be required to estimate the elastic energy during locomotion. The invasive measurement of these quantities is impractical while the available technology for non-invasive one still cannot provide accurate estimation of such force-length relationship (Buchanan et al., 2004). Adopted from the measurement in robot and insect leg (Dudek and Full, 2006; Rummel et al., 2010), the entire of the human leg may be considered as a spring and the elastic energy can be defined by the relationships between the leg length, leg angle and resultant leg forces. The better understanding of the human leg functions can improve the dynamic stability analysis in human locomotion. For example, in daily-life, people always come across stability challenges and individual human gait seems to possess different ability to get over them (Rose and Gamble, 2006). The dynamic stability quantification on different function and mechanical properties of the human leg can provide insight into the dynamic stability of individual human gait. This can be alternative stability guidance to that from the comparison between the gait pattern stability in healthy and faller population.

In dynamic stability quantification, the rate of recovery from perturbation, for example, the rate of convergence to steady state (Floquet multipliers) and the rate of divergence due to the natural variation (finite Lyapunov exponents) were calculated from the motion of the centre of mass (CoM). Some gait characteristics i.e. stride time-stride width and double support duration were used to calculated the variability of the locomotion, but the role in recovery from perturbation has not been recognised. Thus, it is sufficient to use the simple models of human gait, which primarily represent the CoM motion, to simulate the human gait for dynamic stability quantification. The major advantage of the simple models is that it can accommodate the wide variety of the operation and mechanical property of the human leg, which can benefit in the analysis of dynamic stability on the effect of function and mechanical property of the leg.

The wide variety of available quantification methods serves on different purposes of quantification of the dynamic stability during human locomotion. The inherent variations emerging from complex neuro-musculoskeletal interaction during human locomotion can be treated as a small perturbation in the examinations of convergence to the steady locomotion. These examinations quantify local stability of the human locomotion based on the relatively small size of perturbations. The maximum Floquet multiplier was widely used to quantify the orbital stability or stability of gait pattern of the human and biped robot locomotion. It was found to be able to differentiate between the stable and unstable gait pattern (Hobbelen and Wisse, 2007; and Granata and Lockhart 2008). The finite time Lyapunov exponents were used to quantify the sensitivity of the locomotion to the perturbation due to natural variation of human locomotion. It was found to predict instability in healthy human locomotion and higher

instability in the locomotion of fallers (Dingwell and Cusumano, 2000; Dingwell et al., 2000). The statistic calculations of the inherent variation of the gait characteristics i.e. coefficient of variation of the stride time-stride width has not been found to be in relationship with recovery from perturbation(Dingwell and Marin, 2006). The similar limitation was found in the validation of zero moment point (ZMP), centroidal moment pivot (CMP) and foot rotation indicator (FRI) with human locomotion measurements (Brach et al., 2005; Brach et al., 2007). For the foot placement estimator (FPE), although it was found that the returning to steady state locomotion can be achieved by placing the foot slightly ahead or behind the FPE (Wight 2008; Wight 2009; Milard 2012), the validation of such recovery in human locomotion may be required.

Defined by the maximum perturbation before the occurrence of fall, the global stability has been found to predict good quality of fall possibility (Shub, 1987; Hsu, 1987; Guckenheimer and Holmes, 1983). Global stability in term of robustness quantified by the basin of attraction was used to compare dynamic stability of the bipedal locomotion on different structural properties (Rummel et al., 2010; Wisse, 2004). Although, this global stability quantification is computationally intensive, its relationship with the local stability (gait pattern stability) can reduce the computational time in searching the area of the basin of attraction (Parker and Chua, 1989; Schwab and Wisse, 2001). The maximum allowable external perturbation was also used in the similar dynamic stability analysis, but it requires higher intensive computation compared to that of the basin of attraction (Hobbelen and Wisse, 2007; Pavol et al., 2002; Pijnappels et al., 2008). With the incorporation of gait model, the global stability can be included in the

dynamic stability analysis in which large deviations from the steady locomotion are addressed.

In this thesis, the dynamic stability of human walking on the effect of leg properties has been analysed with the incorporation of simple models of human walking. A simple model was adopted from a previous study (Geyer et al., 2006) and two simple models were developed in the thesis work. Different models were used to represent the centre of mass motion on different leg functions in corresponding to mechanical property of the human leg during walking motion. The global stability of human walking motion on different mechanical properties of the leg was quantified. The analysis of the dynamic stability of human walking on the wide variety of leg properties can provide insight into the difference dynamic stability between individual human walking motions. This can be an alternative to the comparison of walking stability between healthy and faller population.

Chapter 3 Three-dimensional Measurement of Human Walking Motion

3.1 Introduction

In Chapter 2, it was suggested by the previous studies that the dynamic stability analysis of human gait may require both measurement data and mathematical model to provide insight into the structural and dynamic properties in corresponding to the dynamic stability of human gait (Gunther and Blickhan, 2002, Hartmut, 2005; Geyer, 2005, Hobbelen and Wisse, 2007). The measurement data of the CoM motion during human walking alone may be sufficient for the dynamic stability quantification (Bruijn et al., 2009; Kang and Dingwell, 2009; Granata and Lockhart, 2008). However, the incorporation of mathematical model may be required to provide insight into the effect of mechanical property on the dynamic stability of the walking motion. In such a deliberate study, both of the kinetic and kinematic measurement of human walking can play crucial roles in the development and validation of the human walking model, which can then improve the reliability of dynamic stability analysis.

In this research work, the three-dimensional whole-body walking measurement was conducted to facilitate and validate the human walking model, which is aimed to improve the accuracy of human walking prediction and the reliability of dynamic stability analysis. In previous studies, the walking and running motion have been predicted by simple gait models (Gunther and Blickhan, 2002; Geyer et al., 2006; Maus et al., 2010). However, very few of which used the human gait measurement data to support and validate the predictions (Lipfert et al., 2012; Ludwig et al., 2012). The

integration of human walking measurement data and the simple walking model can ensure that the walking motion is predicted from the human parameter range. In addition, the flexibility of the simple model parameter allows a wide range of human parameter to be examined for the walking prediction and the corresponding dynamic stability. In this way, the accuracy of the human walking prediction and the reliability of dynamic stability analysis can be improved.

In this chapter, the experimental protocol and process for three-dimensional whole-body walking measurement were presented. The measurements have been conducted using a multi-camera motion analysis system and a force plate array. Eight subjects participated in the measurement at three self-selected walking speeds. A set of specially designed reflective marker clusters were used to capture the three-dimensional motions of all major body segment. The orientations and positions of each body segment were defined based on a set of anatomical landmarks. A software package GMAS (General Motion Analysis Software) (Ren et al., 2005) was used to process the three-dimensional kinematic and kinetic data of the whole-body walking motions which was then used in the calculation of the whole-body CoM motion, CoP location and the ground reaction forces and moments.

3.2 3D whole-body walking measurement

Three-dimensional walking measurements were conducted to capture the whole-body walking motion at different walking speeds. Eight healthy male subjects participated in the measurement and were asked to walk at self-selected speed for slow, normal and fast walking. Prior to the participation, the subjects provided informed consent in accordance with the policies of Institutional Review Board Committee. Subjects were

asked to walking ten times at each self-selected speed. Motion data were recorded at 150 Hz using an eight-camera motion analysis system (Qualisys, Sweden). Six force plates (Kistler, Switzerland) mounted flushed with the surface of the walking way were used (see Figure 3.1) to record ground reaction forces and moments at 1000 Hz. The array force plate and a long walking path allow the measurement at self-selected walking speed.

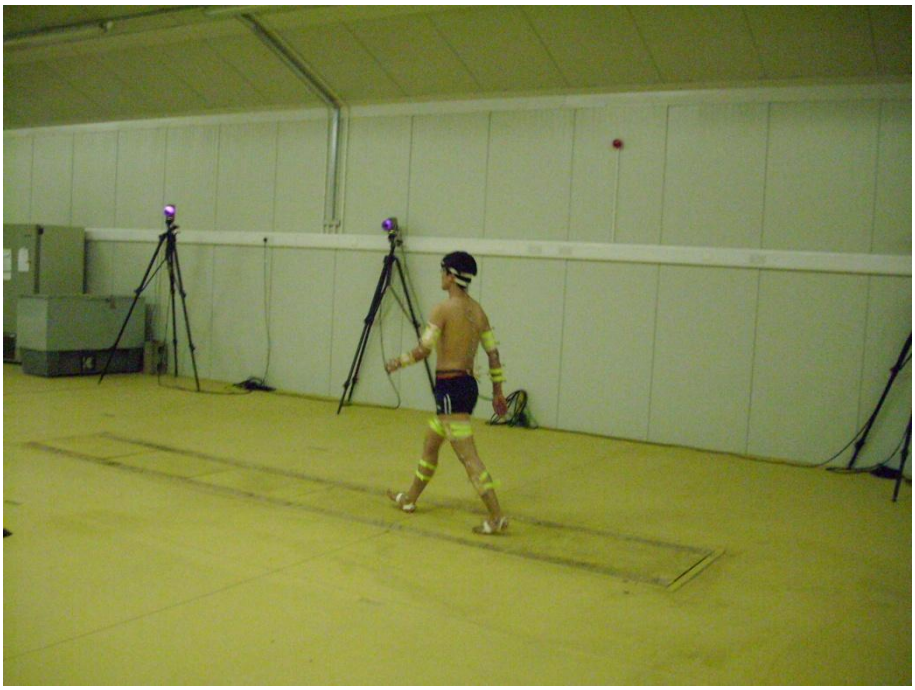

Figure3.2 The measurement system comprising multi-camera motion analysis system (Qualisys, Sweden) and six force plates (Kistler, Switzerland) mounted flushed with the surface of the walking way. Measurement venue: Structure and Motion Lab, the Royal Veterinary College, London.

3.2.1 Experimental protocol

For each subject, the movement of 13 major body segments (the head, torso, pelvis, right and left humerus, right and left forearms, and both legs comprising thighs, shanks and feet) were recorded (see Figure 3.2). A set of specially designed thermoplastic

plates, each carrying a cluster of four reflective markers, were attached to each body segment (Ren et al., 2005, Ren et al., 2008) . A head band was used to carry the four markers on the head. An elastic hip belt was used to firmly locate the plastic plate carrying the four markers on the pelvis. In total, 52 reflective markers were used to capture whole-body motion during the walking trials (see Figure 3.2). The use of plastic plates eliminates the relative motion between the markers on a segment, thus increasing the accuracy of the recorded motion data (Ren et al., 2008).

To describe the segment positions and orientations in a standardised way, anatomical landmarks and bone-embedded anatomical reference system are defined for each major segment. These landmarks and reference frames are based mainly on the recommendations of (Cappozzo et al., 1995) and (Vanderhelm and Pronk, 1995) with small adaptations as presented in (Ren et al., 2008). A detailed description of the anatomical coordinate system for each major body segment is described in Appendix A. Before the walking trials, a set of static calibration procedures were undertaken to locate the anatomical landmarks based on the CAST technique (Calibrated Anatomical System Technique)(Cappozzo et al., 1995). A wand with two reflective markers was used to determine the spatial positions of the anatomical landmarks that are not conveniently determined by reflective markers. This applies to landmarks: VERT, RASIS, LASIS, RPSIS and LPSIS (defined in Appendix A). Other anatomical landmarks were determined directly using reflective markers. Before the walking trials, the calibration markers were removed according to the CAST technique.

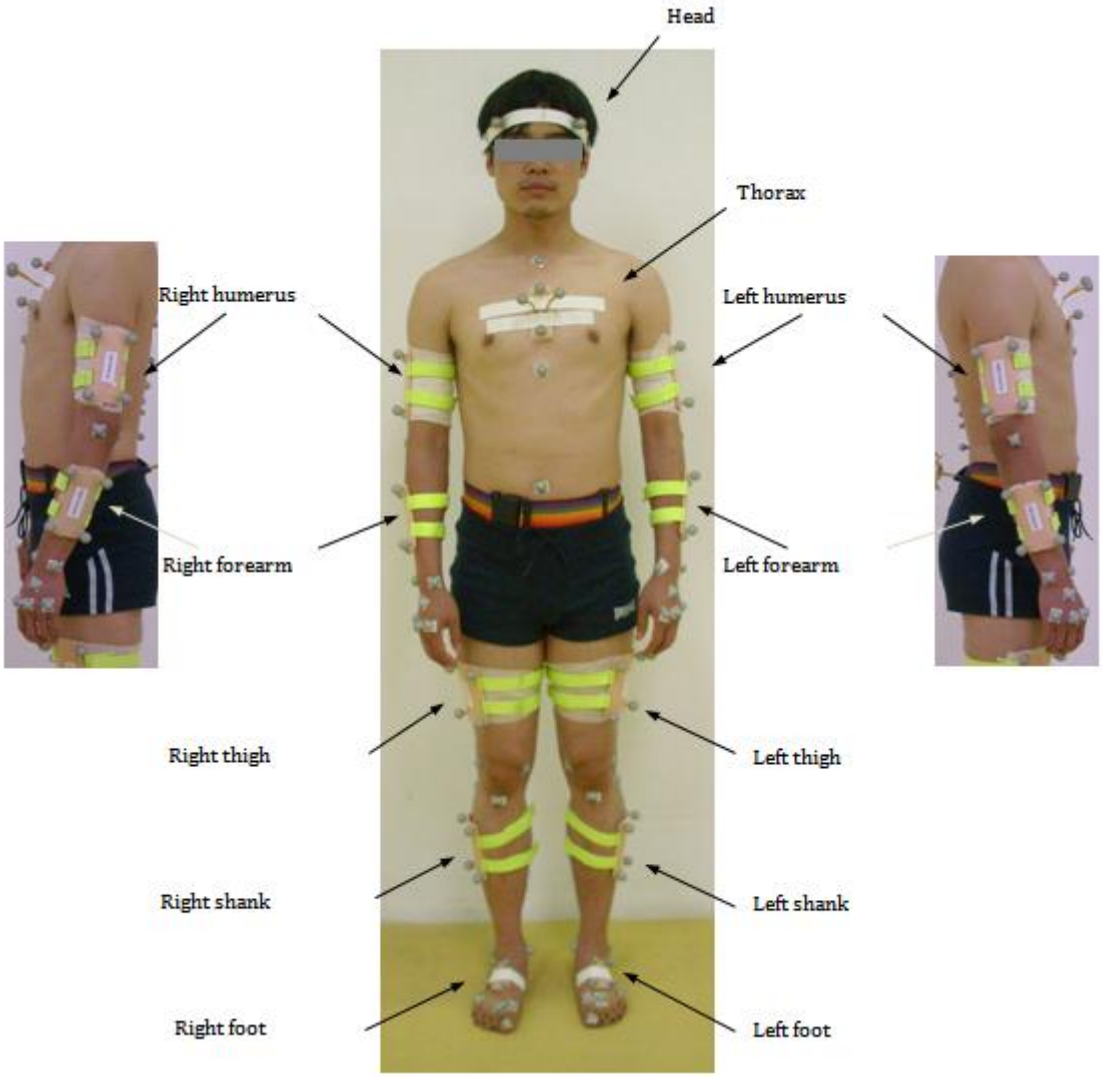

Figure 3.2 The marker clusters used to capture three-dimensional whole body motions including 13 major body segments: head, thorax, pelvis, right and left humerus, right and left forearms, and both legs comprising thighs, shanks and feet

Also before the walking trials, the functional joint trials were conducted to determine the local coordinate of the major joints of the whole-body comprising shoulders, elbows, hips, knees and ankles. The shoulder joint centre is defined to be the functional humerothoracic joint centre which is the effective centre of rotation between the upper arm and the torso. As shoulder movement involves compound motions of the humerus, scapula and clavicle, it is unlikely that the centre of rotation is located at the centre of

the humeral head. The functional approach (Cappozzo, 1984); (Leardini et al., 1999) has been used to establish the humerothoracic joint centre as well as the hip joint centre, both of which are assumed to be ideal ball-and-socket joints. The subjects were asked to move the relevant segment (thigh or humerus) with respect to its proximal segment (pelvis or trunk) through a continuous sequence of motions including flexion, extension, abduction, adduction and circumduction at a self-selected velocity. A closed-form algorithm is employed to estimate the joint's centre of rotation (Gamage and Lasenby, 2002) in which the manual adjustment of optimisation parameters is not required. The positions of the other joint centres were determined directly from bony anatomical landmarks, for example, the knee joint centre coincides with the midpoint between the lateral epicondyle and medial epicondyle. The anatomical joint involved in the whole-body walking measurements and the relevant anatomical landmarks used to estimate the joint centre positions are listed in Table 3.1.

In walking trials, the technical marker clusters were used to capture the body segment motions. The marker data from walking trials functional joint trials and static calibration trials were processed by using GMAS software to provide 3D segmental positions and orientations for each sampled instant of time.

Since the ground reaction forces are recorded in local coordinate system of the force plate. Thus, an additional force plate location trial is needed to determine the force plate position in the global reference frame. A set of technical markers were attached on each corner of the force plates to define the local coordinate. The coordinate transformation was conducted in the GMAS software to obtain the ground reaction forces in the global reference frame.

Table 3.1 Determination of the joint centre position (see Appendix A for anatomical landmark definitions)

Joint	Joint centre position
Neck	Projection of C7 on the y-axis of the head local coordinate system
Waist	Projection of the midpoint between RASIS & LASIS on the y-axis of the trunk local coordinate system
Right shoulder	Functional humerothoracic rotation centre
Left shoulder	Functional humerothoracic rotation centre
Right elbow	Midpoint between RMHU & RLHU
Left elbow	Midpoint between LMHU & LLHU
Right hip	Functional rotational centre
Left hip	Functional rotational centre
Right knee	Midpoint between RLEP & RMEP
Left knee	Midpoint between LLEP & LMEP
Right ankle	Midpoint between RMML & RLML
Left ankle	Midpoint between LMML & LLML

3.2.2 Data analysis (GMAS, General Motion Analysis Software) (Ren et. al., 2008)

In the GMAS software, all trials with more than 10 consecutive missing frames were discarded. After fill-gap processing, the data were filtered using a low pass zero lag fourth-order Butterworth digital filter with a cut-off frequency of 6.0 Hz. The segment positions and orientations were defined in an anatomically significant way. From the static calibration data, the relative positions of the anatomical landmarks with respect to the technical markers were obtained. For some anatomical landmarks i.e. shoulders and hips, the reconstruction based on dynamic calibration trials (functional method) was used. As the joint centre positions were described in local coordinate system of the adjacent segment, the transformation from local to global coordinate system was

employed. Thereafter, given the derived anatomical landmark position, the poses of the anatomical coordinate systems were obtained for each sampled instant of time.

Given the poses of the anatomical coordinate systems, the location of segment mass centre was determined from the relevant anatomical landmarks, where some three-dimensional anthropometric data was used (de Leva, 1996). The linear velocities and accelerations of the segment mass centre were then calculated using the finite difference methods (Bedford and Fowler, 1996 ; Hibbeler, 1997). For the ground reaction forces and moments, the transformation matrix from the force plate local coordinate system to the global reference coordinate system was derived and then used to transform the ground reaction forces and moments to the global reference frame. The location of the centre of pressure (CoP) was then determined by the application point of the ground reaction force in global reference frame.

3.3 The calculation of motions of the centre of mass and the leg

After the centre of mass motion of major body segments at each sampled instant of time was calculated by the GMAS software. The location ($\vec{r}$) and velocity ($\vec{v}$) of the whole-body centre of mass in three-dimensional space can be calculated as given below.

$$\vec{r} = \frac{1}{m}\sum_{i=1}^{13} m_i \vec{r}_i^{cm} \tag{3.1}$$

$$\vec{v} = \frac{d\vec{r}}{dt} \tag{3.2}$$

$\vec{r}_i^{cm}$ is the position vector of CoM location of i^{th} body segment. m_i is the mass of i^{th}body segment. m is whole-body mass. The location ($\vec{r}$) and velocity ($\vec{v}$) of the whole-body CoM in Equation 3.1-3.2 were used as initial condition to calculate the whole-body CoM motion (x, y, v^x, v^y) by integrating ground reaction forces (Cavagna et al., 1983, Cavagna, 1975; Tesio et al., 2010) given by.

$$\int F^x dt = mv^x + v_0^x \tag{3.3}$$

$$\int (F^y - mg) dt = mv^y + v_0^y \tag{3.4}$$

$$\int v^x dt = x + x_0 \tag{3.5}$$

$$\int v^y dt = y + y_0 \tag{3.6}$$

F^x and F^y are the recorded horizontal and vertical ground reaction force obtained from the force plates. v^x and v^y are the horizontal and vertical velocities of the whole-body centre of mass. v_0^x and v_0^y are initial horizontal and vertical velocities of the whole-body centre of mass obtained from Equation 3.2 at the touchdown instant. x and y are the horizontal and vertical positions of the whole-body centre of mass. x_0 and y_0 are initial horizontal and vertical position of the whole-body centre of mass obtained from Equation 3.1 at the touchdown instant (td).

Gait cycles are marked by two subsequence heel-strike or the touchdown (td) events of the same foot. The heel-strike is defined as the instant when the foot-ground contact initially occurs without exerted force. In the measurement, the GRF is initially detected when it is above zero. The numerical extrapolation (Bedford and Fowler, 1996 ;

Hibbeler, 1997) was applied to the GRF records to estimate the instance and CoP location at the zero GRF. Accordingly, the toe-off or the take-off (to) is defined as the final instant of the foot-ground contact when the GRF reduces to zero. A similar numerical extrapolation technique is used to estimate the instant and CoP location for the take-off (to). The leg length and leg angle were then calculated between the heel-strike and toe-off of the same leg.

3.4 Some measurement results

The general information of individual subject is shown in Table 3.2. The distance between the whole-body CoM and the foot-ground contact point during still standing calculated from the measurement data is also shown. The 3D motion data of major body segments and the ground reaction forces processed in the GMAS software is shown in Figure 3.3 -3.15 and 3.17-3.18, respectively. The whole-body CoM motion obtained from kinetic-kinematic measurement data is shown in Figure 3.16. The whole-body CoM motion in sagittal plane calculated by using equation 3.1-3.2 is shown in Figure 3.19. The leg lengths and leg angles calculated in the fixed and moving contact conditions are shown in Figure 3.20.

Table 3.2 General information (age-weight-height) and the still-standing leg length (l^{st}) of individual subject.

Subject	Age(year)	Weight(kg)	Height(cm)	l^{st} (mm)
No.1	26	67	177	895.17
No.2	24	69	179	913.93
No.3	31	53.5	165	839.81
No.4	25	71	181	917.59
No.5	22	79	180	931.66
No.6	21	65.5	178	926.18
No.7	22	72	183	919.08
No.8	26	68	175	896.23

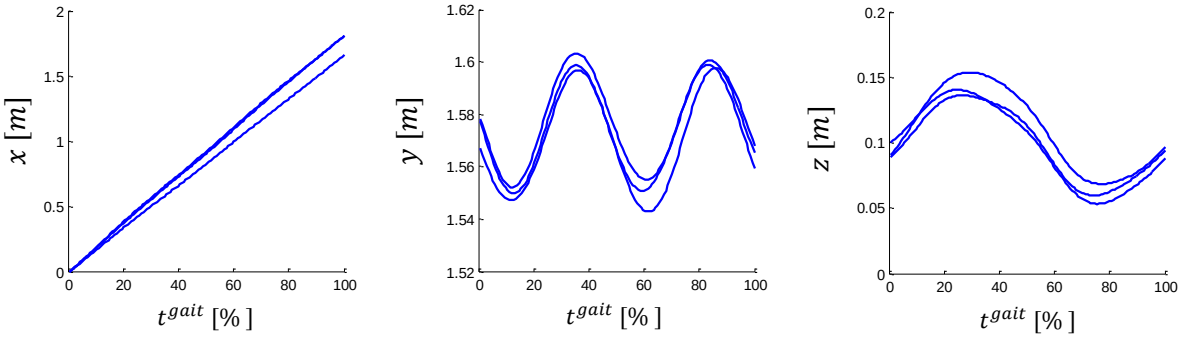

Figure 3.3 Trajectories of the head's centre of mass in fore-aft (x), vertical (y) and lateral (z) coordinate during a gait cycle (between the consecutive heel–strikes of the same leg). The data set is obtained from three good trials of the walking measurements of subject no.2 at self-selected normal walking speed.

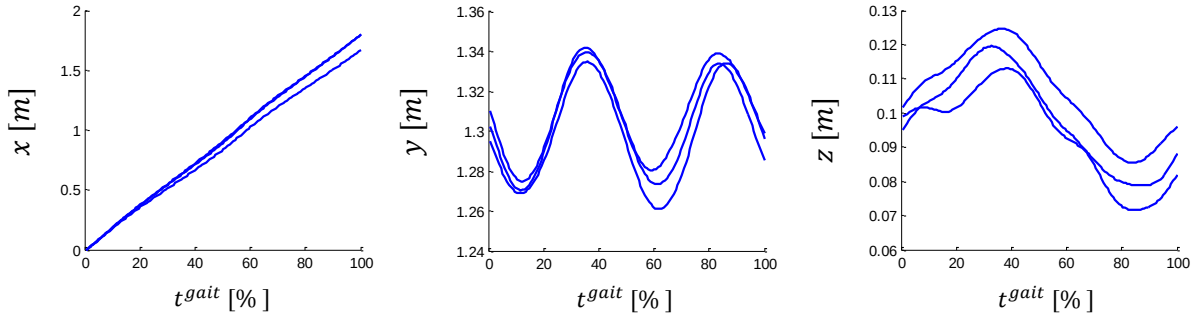

Figure 3.4 Trajectories of the torso's centre of mass in fore-aft (x), vertical (y) and lateral (z) coordinate during a gait cycle (between the consecutive heel–strikes of the same leg). The data set is obtained from three good trials of the walking measurements of subject no.2 at self-selected normal walking speed.

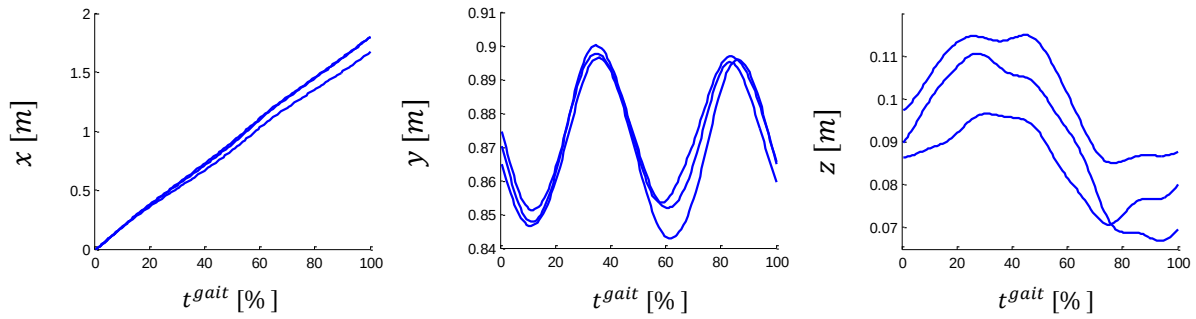

Figure 3.5 Trajectories of the pelvis's centre of mass in fore-aft (x), vertical (y) and lateral (z) coordinate during a gait cycle (between the consecutive heel–strikes of the same leg). The data set is obtained from three good trials of the walking measurements of subject no.2 at self-selected normal walking speed.

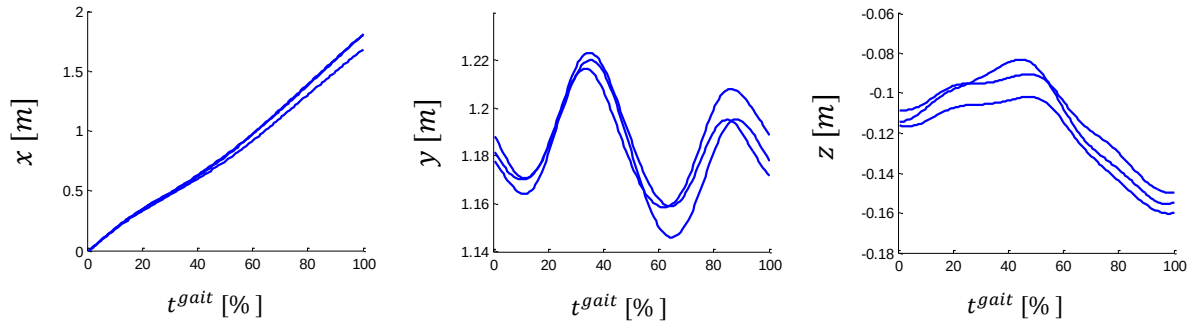

Figure 3.6 Trajectories of the right upper arm's centre of mass in fore-aft (x), vertical (y) and lateral (z) coordinate during a gait cycle (between the consecutive heel–strikes of the same leg). The data set is obtained from three good trials of the walking measurements of subject no.2 at self-selected normal walking speed.

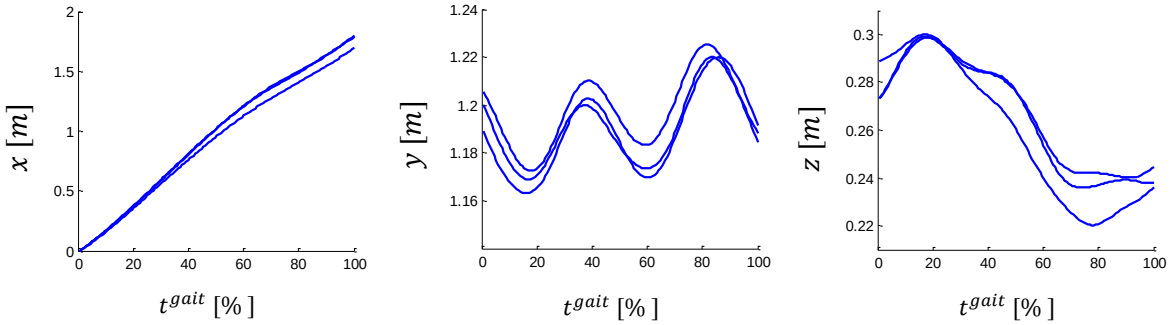

Figure 3.7 Trajectories of the left upper arm's centre of mass in fore-aft (x), vertical (y) and lateral (z) coordinate during a gait cycle (between the consecutive heel–strikes of the same leg). The data set is obtained from three good trials of the walking measurements of subject no.2 at self-selected normal walking speed.

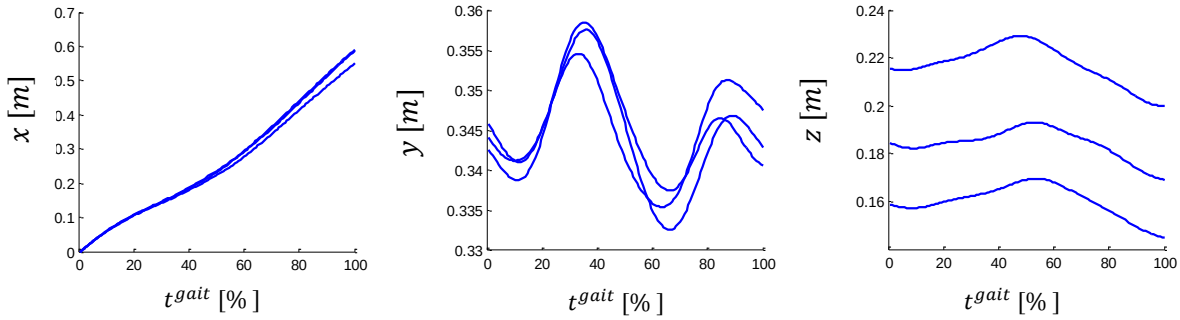

Figure 3.8Trajectories of the right lower arm's centre of mass in fore-aft (x), vertical (y) and lateral (z) coordinate during a gait cycle (between the consecutive heel–strikes of the same leg). The data set is obtained from three good trials of the walking measurements of subject no.2 at self-selected normal walking speed.

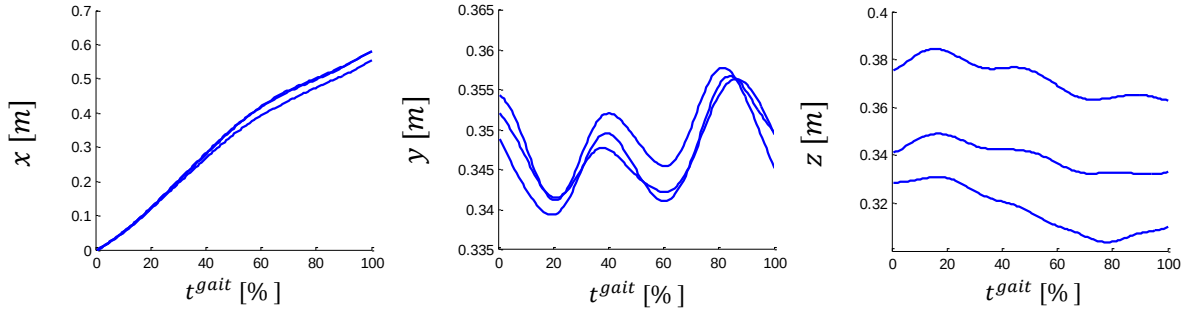

Figure 3.9 Trajectories of the left lower arm's centre of mass in fore-aft (x), vertical (y) and lateral (z) coordinate during a gait cycle (between the consecutive heel–strikes of the same leg). The data set is obtained from three good trials of the walking measurements of subject no.2 at self-selected normal walking speed.

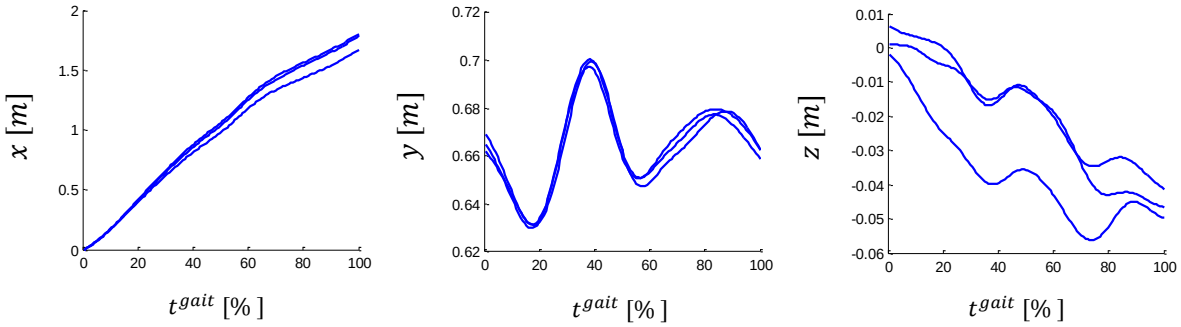

Figure 3.10 Trajectories of the right thigh's centre of mass in fore-aft (x), vertical (y) and lateral (z) coordinate during a gait cycle (between the consecutive heel–strikes of the same leg). The data set is obtained from three good trials of the walking measurements of subject no.2 at self-selected normal walking speed.

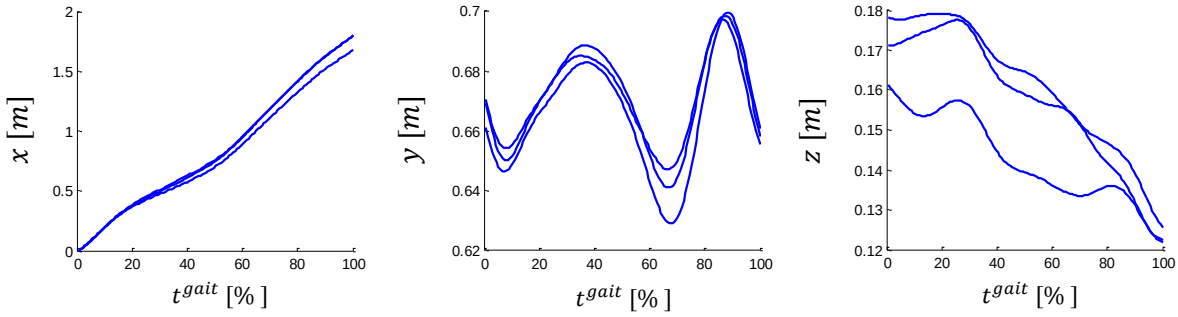

Figure 3.11 Trajectories of the left thigh's centre of mass in fore-aft (x), vertical (y) and lateral (z) coordinate during a gait cycle (between the consecutive heel–strikes of the same leg). The data set is obtained from three good trials of the walking measurements of subject no.2 at self-selected normal walking speed.

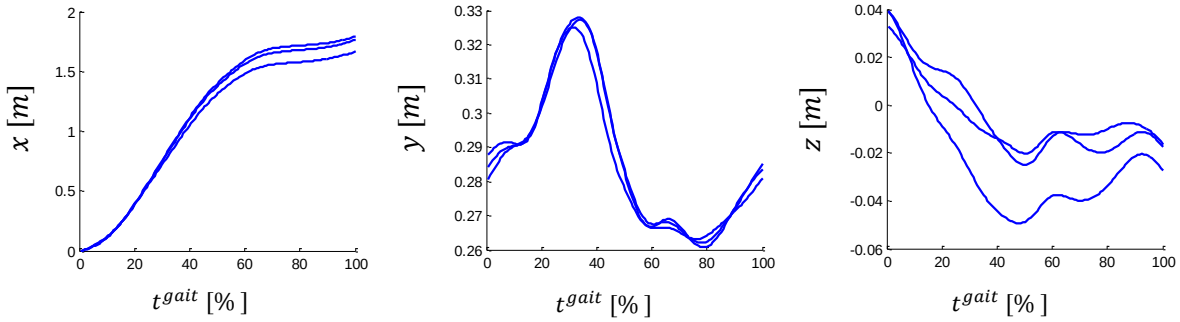

Figure 3.12 Trajectories of the right shank's centre of mass in fore-aft (x), vertical (y) and lateral (z) coordinate during a gait cycle (between the consecutive heel–strikes of the same leg). The data set is obtained from three good trials of the walking measurements of subject no.2 at self-selected normal walking speed.

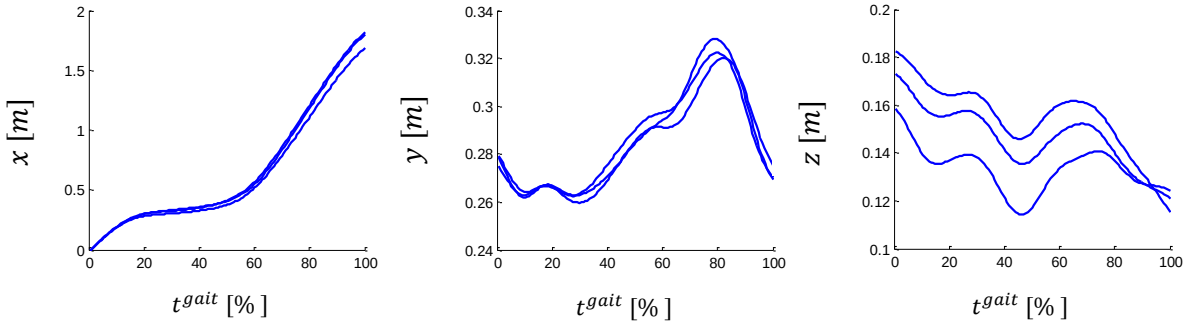

Figure 3.13 Trajectories of the left shank's centre of mass in fore-aft (x), vertical (y) and lateral (z) coordinate during a gait cycle(between the consecutive heel–strikes of the same leg). The data set is obtained from three good trials of the walking measurements of subject no.2 at self-selected normal walking speed.

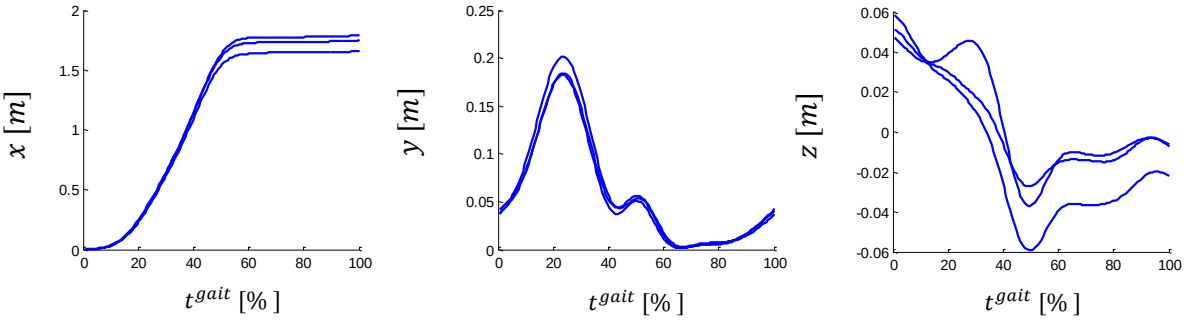

Figure 3.14 Trajectories of the right foot's centre of mass in fore-aft (x), vertical (y) and lateral (z) coordinate during a gait cycle (between the consecutive heel–strikes of the same leg). The data set is obtained from three good trials of the walking measurements of subject no.2 at self-selected normal walking speed.

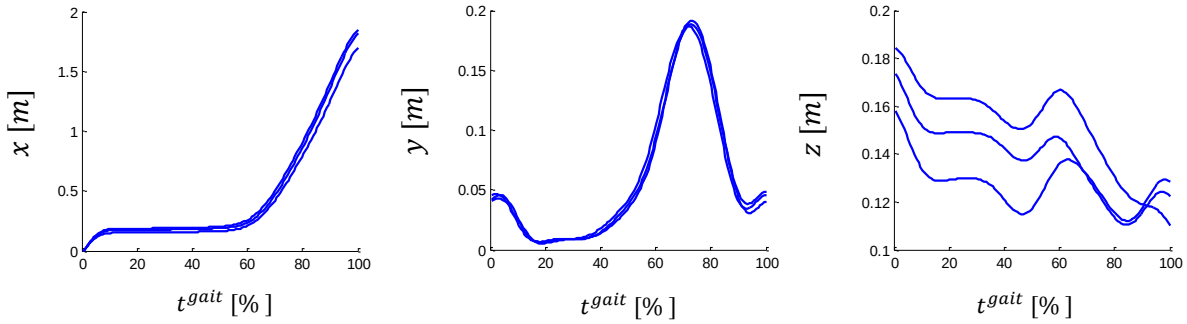

Figure 3.15 Trajectories of the left foot's centre of mass in fore-aft (x), vertical (y) and lateral (z) coordinate during a gait cycle (between the consecutive heel–strikes of the same leg). The data set is obtained from three good trials of the walking measurements of subject no.2 at self-selected normal walking speed.

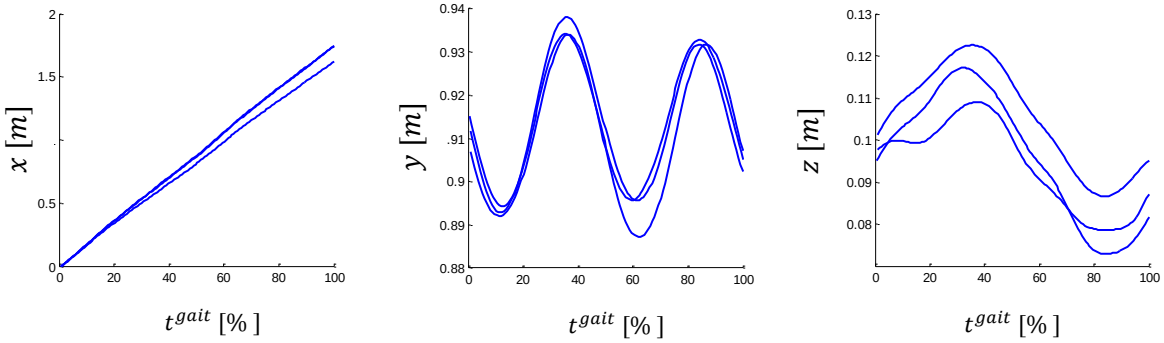

Figure 3.16 Trajectories of the whole-body centre of mass in fore-aft (x), vertical (y) and lateral (z) coordinate during a gait cycle (between the consecutive heel–strikes of the same leg). The data set is obtained from three good trials of the walking measurements of subject no.2 at self-selected normal walking speed.

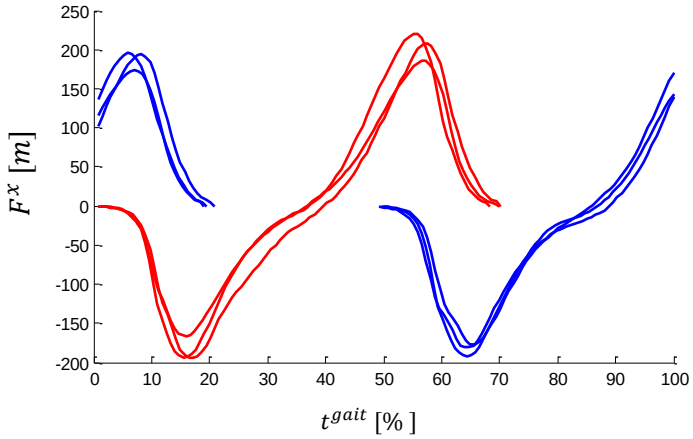

Figure 3.17 Fore-aft ground reaction forces (F^x) for leading (red) and trailing (blue) foot during a gait cycle (between the consecutive heel–strikes of the same leg). The data set is obtained from three good trials of the walking measurements of subject no.2 at self-selected normal walking speed.

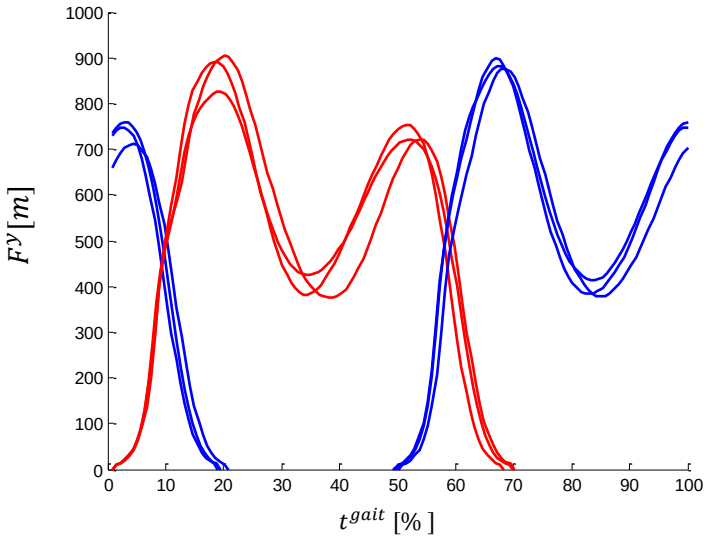

Figure 3.18 Vertical ground reaction forces (F^y) for leading (red) and trailing (blue) foot during a gait cycle (between the consecutive heel–strikes of the same leg). The data set is obtained from three good trials of the walking measurements of subject no.2 at self-selected normal walking speed.

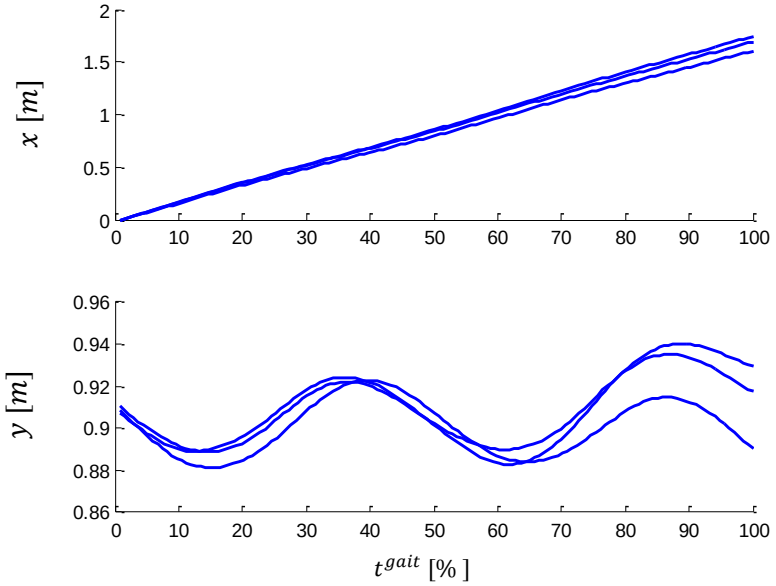

Figure 3.19 Calculated displacement of whole-body centre of mass in fore-aft (x) and vertical (y) coordinate during a gait cycle (between the consecutive heel–strikes of the same leg). The data set from three good trials of the walking measurements of subject no.2 at self-selected normal walking speed is used for the calculations.

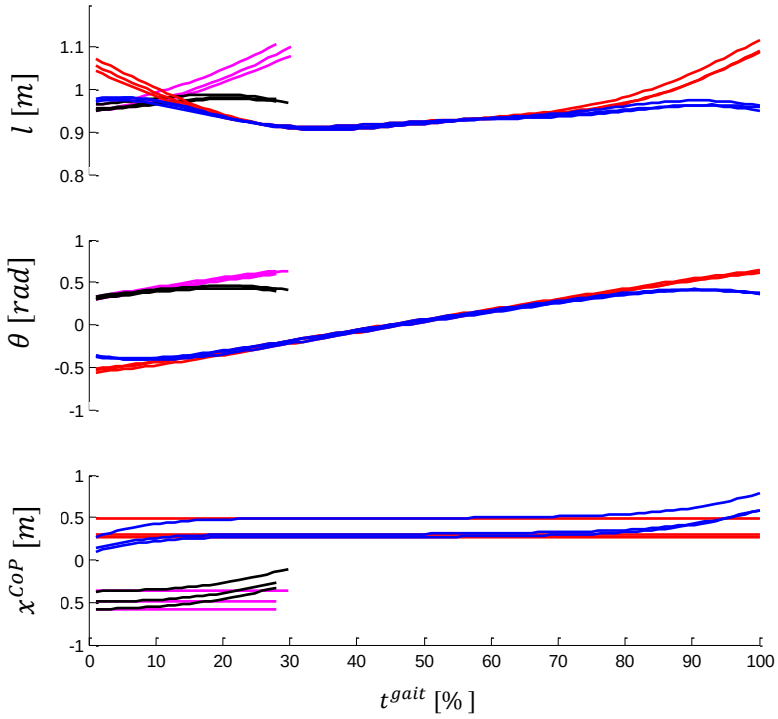

Figure 3.20 Calculated leg lengths and leg angles for leading (blue and red) and trailing (black and magenta) leg and calculated centre of pressures for leading (blue and red) and trailing (black and magenta) foot in fixed (red and magenta) and moving contact (blue and black) conditions during a gait cycle (between the consecutive heel–strikes of the same leg). The data set from three good trials of the walking measurements of subject no.2 at self-selected normal walking speed is used for the calculations.

Chapter 4 The Fundamentals of Mechanical Properties of Human Leg during Walking

This chapter presents the mechanical properties of the human leg on the linearity and non-linearity of axial and tangential elasticity during human walking motion. The fundamentals of mechanical leg properties during human walking motion are proposed. The mechanical leg properties are extracted from human walking measurements at different self-selected walking speeds and on fixed and moving condition of foot-ground contact.

4.1 Background

Leg elasticity has involved in the broad study of human locomotion ranging from basic mechanical energy to the motion prediction by using spring-mass model. In the study of basic mechanical work, the leg elasticity is a crucial mechanical function for the proper exchanges between mechanical energies during the gait cycle (Cavagna et al., 1976; Cavagna et al., 1977). In human locomotion prediction, the spring stiffness is a crucial elastic leg property transforming the change in leg length to that in leg force and vice versa. This basic leg property aims to address the global elasticity of the whole-body structure as a consequence of joint elasticity (Alexander, 1988a; Alexander, 1988b; Hof, 1990). In the prediction of human running, it was found that the spring stiffness is dependent on the running speed. For human walking prediction, the speed dependent of spring stiffness limits the prediction to the averaged walking speed of 1.5 m/s.

The studies of leg stiffness during the human locomotion have been based on the change in leg length and the total ground reaction force considered to apply along the leg axis (McMahon and Cheng, 1990; Lee and Farley, 1998; Morin et al., 2005; Morin et al., 2011; Blum et al., 2009; Lipfert et al., 2012). In fact, the total ground reaction force during the gait does not always apply along the leg axis. In joint level, when the human body is considered as a multi-segment system, it has been found that the coordination of joint elasticity and the geometry of multi-segment body during locomotion results in the centre of mass motion in parallel and perpendicular direction to the leg axis (Alexander, 1988a; Alexander, 1988b; Hof, 1990; Gunther and Blickhan, 2002). Thus, the projection of the resultant force onto both directions needs to be addressed carefully to account for all corresponding mechanical properties of the human leg during locomotion.

The rotational elasticity in human walking has been studied by using spring-mass model with hip joint and torso (Maus et al., 2010). This model addresses the relationship between the components of total ground reaction force, the axial and rotational elasticity during human walking. The nonlinear relationships between ground reaction force components, the axial and rotational elasticity were found. Although, the predicted ground reaction force and hip torque profile are slightly different from that from human walking experiments, the relationship between ground reaction force components and the axial and rotational elasticity were found to facilitate in human walking stabilisation (Maus et al., 2010).

Most of the study of leg properties during the human locomotion primarily focused on linear elasticity, until it has been found recently that the changes in leg stiffness and rest length during the gait improve the human running prediction of the spring-loaded-inverted pendulum model (Ludwig et al., 2012). This supports the previous findings

that the nonlinear elasticity can stabilise the spring leg robot after perturbation and touchdown impact. The soft nonlinear elasticity was found to stabilise the spring leg running after perturbation (Karssen and Wisse, 2011) while the hard nonlinear elasticity was found to stabilise the gait pattern after touchdown impact (Owaki et al., 2006)

Leg positioning i.e. leg angle at heel-strike and take-off has been found as one of the crucial adjustments for the contact duration and phase transition in animal and biped robot locomotion (Farley and Gonzalez, 1996; Geyer et al., 2005; Dudek and Full, 2006; Daley and Biewener, 2006). Predicted by the spring-mass model, the change of touchdown angle with the change in leg stiffness was found to regulate the energy transfers during the gait cycle (Blickhan, 1989; McMahon and Cheng, 1990; Farley and Gonzalez, 1996; Geyer et al., 2005; Geyer et al., 2006). However, such adjustment during human locomotion has not been fully investigated.

In brief, the elastic properties and the leg positioning have been found as crucial mechanical properties of the human leg during locomotion. The proper combination of the axial and rotational or tangential stiffness, rest length and the leg positioning are required to predict the precise walking motion and phase transition. Depending on available human walking measurements and purpose of study, these leg properties during the walking motion can be estimated by different leg property definitions. In this chapter, the single valued force- displacement relationships are used to simplify the mechanical properties extraction on linear and nonlinear elasticity of human leg during walking motion.

4.2 The fundamentals of mechanical properties of the human walking leg

Fundamental leg properties comprising leg stiffness, rest leg length and three force-free leg angles are proposed to express leg elasticity and phase transition, which are necessary mechanical properties to representation the human walking. In this section, the fundamentals of mechanical properties of the human leg are defined and extracted from the measurement data by a technique of minimum root-mean-squares error fitting.

4.2.1 Axial stiffness and rest length

In this study, the virtual leg is defined as a straight leg represented by a line connecting the centre of mass (CoM) and the foot-ground contact point (Figure 4.1). The foot-ground contact point is defined in two conditions (Figure 4.2). The first condition considers the moving contact calculated from the fore-aft position of the centre of pressure (CoP) for each foot. The second condition considers the fixed contact defined by the centre of pressure (CoP) where the virtual leg on moving contact reaches vertical leg orientation.

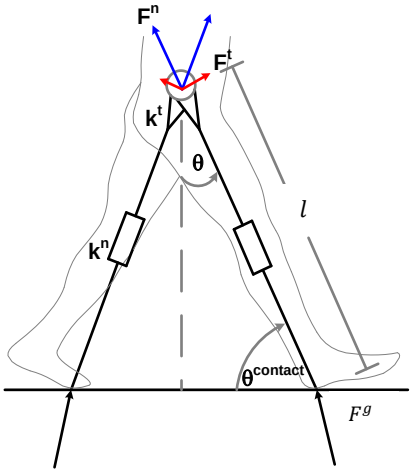

Figure 4.1 The mechanical system of human walking represented by leg length (l), leg angle (θ), contact angle ($\theta^{contact}$), axial (k^n) and tangential (k^t) stiffness and axial(F^n) and tangential (F^t) force (as the projections of the total ground reaction force (F^g)).

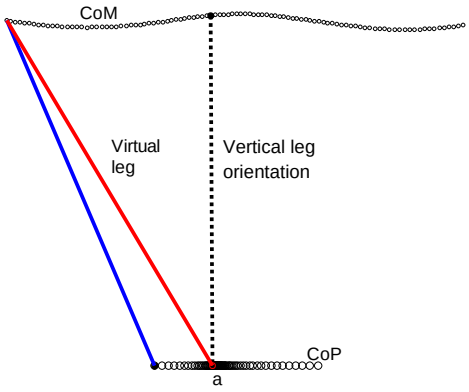

Figure 4.2 The virtual leg in moving contact condition (blue) is defined by a straight line connecting between the centre of mass (CoM) and the moving contact. The moving contact is defined by the location of the centre of pressure (CoP). The virtual leg in fixed contact condition (red) is defined by a straight line connecting between the centre of mass (CoM) and the fixed contact. The fixed contact (a) is defined by the location of the centre of pressure (CoP) at which the virtual leg on moving contact reaches the vertical leg orientation (dash).

The leg stiffness comprises axial and tangential stiffness. The axial stiffness is derived from the leg compression-extension, the rest leg length and the projection of the total ground reaction force onto the virtual leg so called axial force. The axial stiffness (k^n) and rest length (l_0) will be extracted from the axial force-leg length relationship on both

linear and nonlinear elasticity of the virtual leg. For the linear elasticity, the axial force-leg length relationship is defined as

$$F^n = k_{lin}^n(l_0 - l) \tag{4.1}$$

where F^n is the projection of the total ground reaction force onto the virtual leg axis, l is the virtual leg length, k_{lin}^n is the linear axial stiffness and l_0 is the rest length which is the force-free leg length at initial and terminal contact. The force-free leg length (l_0) is the leg length when the ground reaction force is zero during the ground contact (see Fig 4.3).

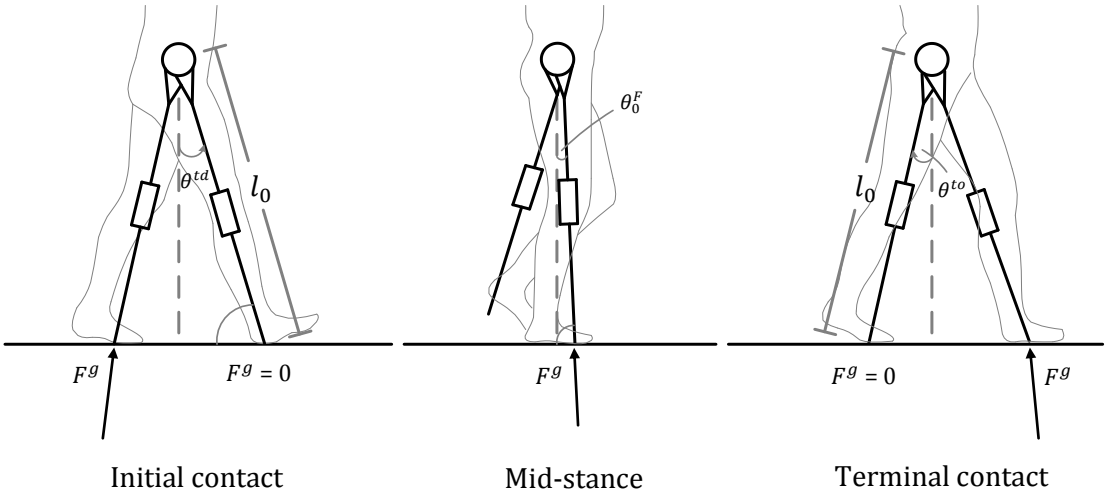

Figure 4.3 The illustration of force-free leg length (l_0) at initial and terminal contact when the ground reaction force (F^g) is zero and force-free leg angle (θ_0) at initial contact ($\theta_0 = \theta^{td}$), mid-stance ($\theta_0 = \theta_0^F$) and terminal contact ($\theta_0 = \theta^{td}$).

To represent the nonlinear elasticity, the axial force- leg length relationship is defined as

$$F^n = k^n_{nln}(l_0 - l) \tag{4.2}$$

$$k^n_{nln} = k^n_{lin,b}(1 + a\, e^b(l_0 - l)) \tag{4.3}$$

where k^n_{nln} is the nonlinear stiffness as a quadratic function of leg deflection $(l_0 - l)$. $k^n_{lin,b}$ is basic linear stiffness. a is a coefficient of nonlinear stiffness. b is exponential power of nonlinear coefficient . The square of axial deflection $(l_0 - l)$expresses the moderate strength of non-linearity. This exponential-quadratic form requires only two parameters to fit the axial-force leg length relationship. The preliminary examination on other nonlinear forms such as Fourier series, pure exponential and pure quadratic functions showed that more parameters are required while the RMSE is not significantly reduced.

4.2.2 Tangential stiffness and force-free leg angles

The tangential stiffness is derived from the angular deflection of the virtual leg and the projection of the total ground reaction force onto the perpendicular line of the virtual leg. The leg angle is defined as the angle between the virtual leg and the vertical. The angle made by virtual leg and the horizontal is defined as contact angle.

The tangential stiffness (k^t) and force-free leg angle (θ_0) will be extracted from the relationships between tangential force and leg angle. Both linear and nonlinear elasticity will be examined. The tangential force- leg angle relationship for linear elasticity is defined as

$$F^t = \frac{k_{lin}^t}{l}(\theta_0 - \theta) \tag{4.4}$$

$$k_{lin}^t = \begin{cases} -k_1 & if\ \theta^{td} \le \theta \le \theta_1^{re} \\ k_2 & if\ \theta_1^{re} < \theta \le \theta_0^F \\ k_3 & if\ \theta_0^F < \theta \le \theta_2^{re} \\ -k_4 & if\ \theta_2^{re} < \theta \le \theta^{to} \end{cases} \tag{4.5}$$

$$\theta_0 = \begin{cases} \theta^{td} & if\ \theta^{td} \le \theta \le \theta_1^{re} \\ \theta_0^F & if\ \theta_1^{re} < \theta \le \theta_2^{re} \\ \theta^{to} & if\ \theta_2^{re} < \theta \le \theta^{to} \end{cases} \tag{4.6}$$

where F^t is the projection of the total ground reaction force onto the perpendicular line of the virtual leg, θ is the leg angle, l is the virtual leg length and k_{lin}^t is the linear tangential stiffness and. $\theta^{td}$is the leg angle at touchdown, θ_1^{re} and θ_2^{re} are the leg angle at the first and second peak of the tangential force, respectively. θ_0^F is the leg angle when the total ground reaction force applies through the leg axis and thus, the tangential force becomes zero. θ^{to} is the leg angle at take-off. θ_0 is the rest angle or the force-free leg angle at initial contact (td), mid-stance and terminal contact (to). The force-free leg angle is the leg angle at which the tangential force is zero (see Fig 4.3).

The illustrations of tangential leg properties are shown in Figure 4.4. The force-free leg angles were assumed to change discretely according to the change of tangential force.

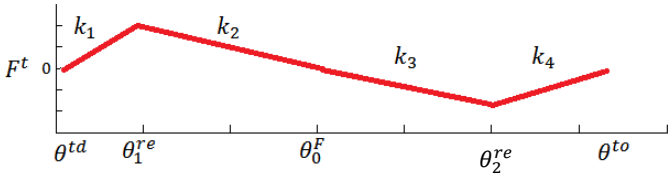

Figure 4.4 The illustrations of tangential leg properties comprising four of tangential stiffness ($k_1 - k_4$), three of force-free leg angles ($\theta^{td}, \theta_0^F and\ \theta^{to}$) and leg angle at first and second force peak ($\theta_1^{re} and\ \theta_2^{re}$)

For the nonlinear elasticity, the tangential force – leg angle relationship is defined by

$$F^t = \frac{\sum_{n=1}^{2}\left(a_n(\cos\frac{n\pi\theta^*}{p}-1)+b_n\sin\frac{n\pi\theta^*}{p}\right)}{l} \tag{4.6}$$

$$\theta^* = \theta - \theta^{td} \tag{4.7}$$

$$p = \frac{\theta^{to}-\theta^{td}}{2} \tag{4.8}$$

where a_n and $b_n$are the Fourier coefficients for the fluctuation of tangential force. The Fourier series were selected from the nonlinear functions including exponential and polynomial function that can give minimum RMS error by using minimum number of parameter. The preliminary examination on Fourier series in higher order showed that the RMSE is not significantly reduced.

In order to compare between the linear and nonlinear elasticity, the stiffness on maximum force and displacement so called total stiffness (z) (Wainwright et al., 1976) is used, which can be given by

$$z^n = \frac{(max(F^n)-min(F^n))}{(l_{min}-l_0)} \tag{4.9}$$

for the axial stiffness and

$$z^t = \frac{(max(F^t)-min(F^t))}{(\theta_{min}-\theta_0)} \tag{4.10}$$

for the tangential stiffness.

4.2.3 Leg property extraction

To estimate the axial stiffness (k^n) and the rest length (l_0), the minimisation of root-mean-square error (RMSE) is used to fit the force equations onto the axial force – leg length data sets obtained from the walking measurement. The data set of the virtual leg length is fed into Equation 4.1 to estimate the linear axial stiffness (k^n) and the rest length (l_0) that minimizes the difference between the measured force and calculated force quantified by root-mean-square error (RMSE). The minimization of the RMSE is operated by using optimisation function fmincon in MATLAB version 2010. With the similar scheme, Equation 4.2 and 4.3 are used to estimate the nonlinear axial stiffness (k^n) and the corresponding rest length (l_0).

The linear tangential stiffness (k^t) and force-free leg angle (θ_0) are estimated by feeding the data set of the leg angle and the leg length into Equation 4.4 and 4.5 and following the similar optimisation scheme. For the nonlinear elasticity of the tangential force, the Fourier coefficients (a_m , b_m), the leg angle at touchdown (θ^{td}) and take-off (θ^{to}) are estimated by feeding the measurement data of the leg angle and the leg length into Equation 4.6-4.8 and following the similar optimisation scheme. After the equation parameters were determined by the minimum RMSE fitting, the force equations are substituted into Equation 4.9 and Equation 4.10 to calculate the total stiffness or mechanical impedance (z) for axial and tangential stiffness, respectively. The total stiffness (z) is used to compare the linear and nonlinear elasticity. This extraction procedure is different from those in other studies in which the linear least squares method was used to find the axial stiffness and rest length that minimise the square

error regardless the violation of perfect elasticity (Lipfert et al., 2012; Coleman et al., 2012).

For each subject, the axial force – leg length and tangential force – leg angle relationships in fixed and moving contact conditions are calculated from measurement data of the CoM, CoP and ground reaction force at each self-selected walking speed (see section 3.3-3.4 Chapter 3). The leg properties for linear and nonlinear elasticity of the virtual leg are extracted. The diagram for the leg property extraction is shown in Figure 4.5.

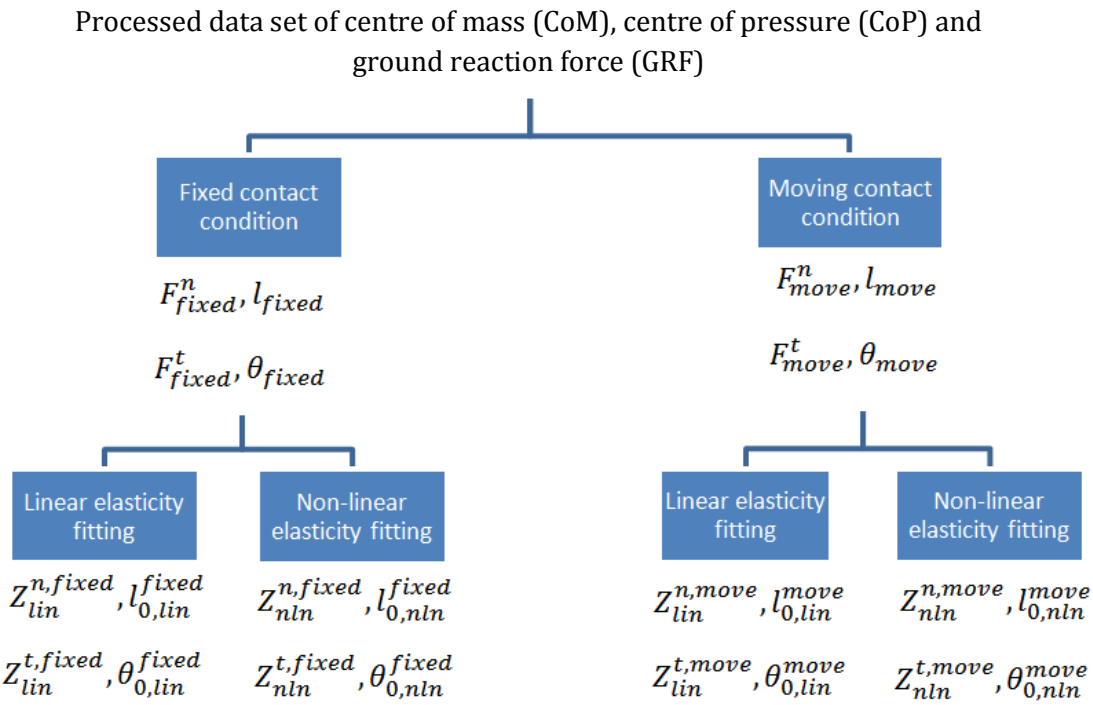

Figure 4.5 Extraction process for the axial stiffness (k^n), rest length (l_0), tangential stiffness (k^t) and force-free leg angles (θ_0)

4.3 The results of mechanical properties of human walking leg

This section presents the fundamental leg properties of a representative subject (Subject No. 2) and the average from all subjects. The fundamental leg properties for linear and nonlinear elasticity of the virtual leg in fixed and moving contact condition

were extracted from the walking measurements at self-selected slow, normal and fast speed.

4.3.1 Linear axial stiffness and rest length

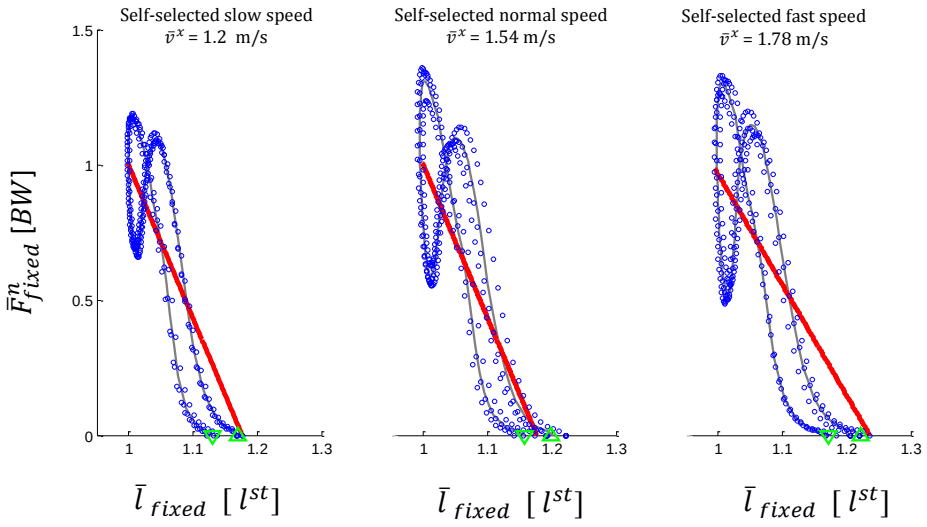

$\bar{z}^{n,fixed}_{lin} = \bar{k}^{n,fixed}_{lin}\left[\frac{BW}{l^{st}}\right]$	5.6	4.4	4.1
$\bar{l}^{l,fixed}_0[l^{st}]$	1.17	1.22	1.24

Figure 4.6 The fixed contact axial force – length data set (blue) at self-selected slow, normal and fast walking speed and linear elastic fits (red)from a representative subject (subject no.2) are shown. Axial force ($\bar{F}^n_{fixed}$) is normalised by body weight (BW), leg length ($\bar{l}_{fixed}$) is normalised by the leg length obtained during still standing (l^{st}). Touchdown(td) and take-off are denoted by ∇ (td) and Δ (to). Linear axial stiffness(k^n_{lin}) and the corresponding rest length (l_0)determined by the RMS fit are given for each walking speed. $\bar{k}^n_{lin}$ is normalised by BW and l^{st} . $\bar{l}_0$ is normalised by l^{st}. The data set is obtained from three good trials of the walking measurements of subject no.2 at each self-selected walking speed. For the linear elasticity, $\bar{z}^n_{lin} = \bar{k}^n_{lin}$.

Figure 4.6 shows that for all walking speeds, the measured leg length at touchdown is shorter than that at take-off, the measured leg length at maximum shortening is close to that during still standing (l^{st}) and the linear elastic fitting underestimates the axial force at maximum leg shortening.

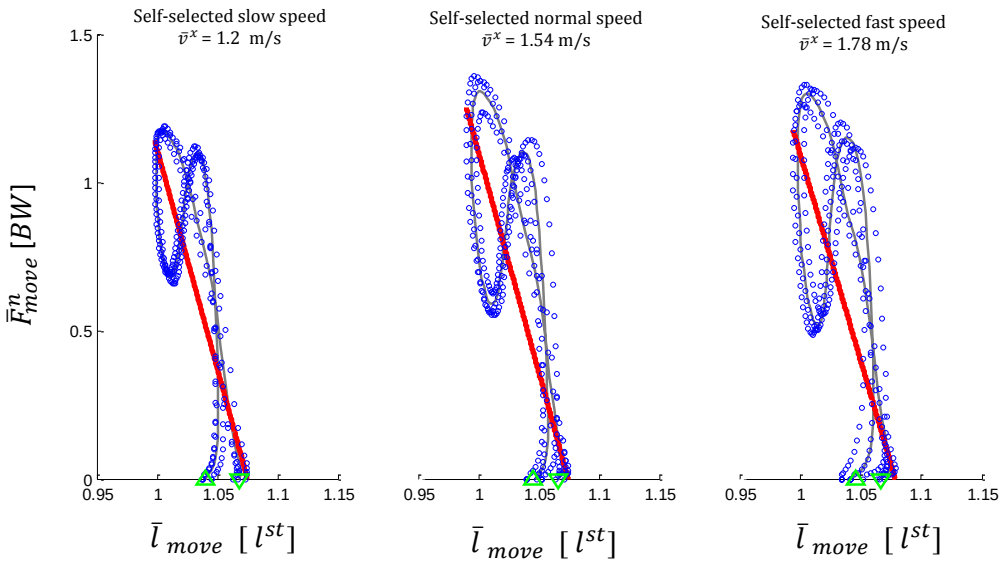

$\bar{z}^{n,move}_{lin} = \bar{k}^{n,move}_{lin}\left[\frac{BW}{l^{st}}\right]$	14.8	13.2	13.9
$\bar{l}^{l,move}_0[l^{st}]$	1.072	1.074	1.078

Figure 4.7 The moving contact axial force – length data set (blue) at self-selected slow, normal and fast walking speed and linear fits (red)from a representative subject (subject no.2) are shown. Axial force ($\bar{F}^n_{move}$) is normalised by body weight (BW), leg length ($\bar{l}_{move}$) is normalised by the leg length obtained during quite standing (l^{st}). Touchdown(td) and take-off are denoted by ∇ (td) and Δ (to). Axial linear stiffness(k^n_{lin}) and the corresponding rest length (l_0)determined by the RMS fit are given for each walking speed. $\bar{k}^n_{lin}$ is normalised by BW and l^{st} . $\bar{l}_0$ is normalised by l^{st}. The data set is obtained from three good trials of the walking measurements of subject no.2 at each self-selected walking speed. For the linear elasticity, $\bar{z}^n_{lin} = \bar{k}^n_{lin}$.

Figure 4.7 shows that for all walking speeds, the measured leg length at touchdown is longer than that at take-off. Similar to the fixed contact condition, the measured leg length at maximum shortening is close to that during still standing (l^{st}). Compared with the linear elastic leg properties on fixed contact at the same speed, the linear elastic leg properties on moving contact have shorter rest length (l_0) and higher total axial stiffness (z^n_{lin}).

4.3.2 Nonlinear axial stiffness and rest length

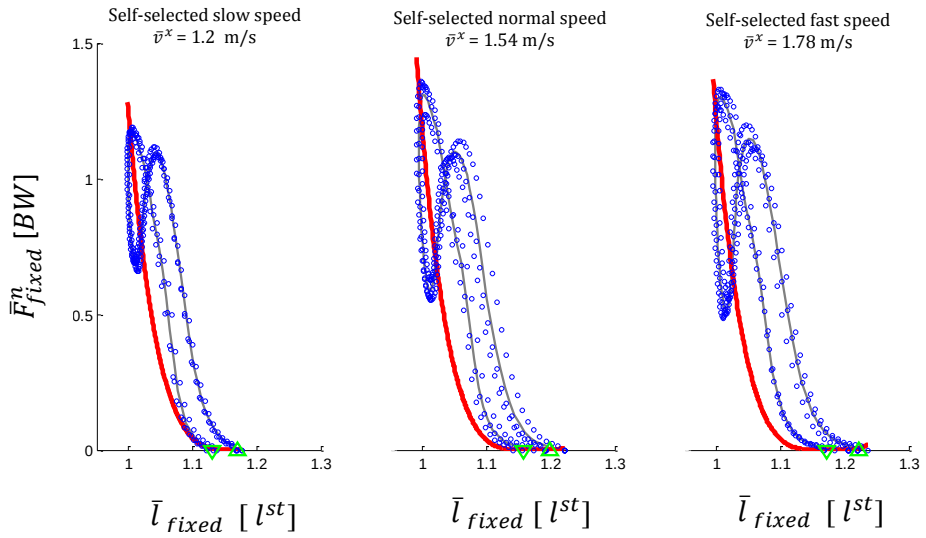

$\bar{z}^{n,fixed}_{nln}\left[\frac{BW}{l^{st}}\right]$	8.7	7.2	8.1
$\bar{l}^{l,fixed}_{0,nln}[l^{st}]$	1.18	1.16	1.17

Figure 4.8 The fixed contact axial force – length data set (blue) at self-selected slow, normal and fast walking speed and nonlinear fits (red)from a representative subject (subject no.2) are shown. Axial force ($\bar{F}^n_{fixed}$) is normalised by body weight (BW), leg length ($\bar{l}_{fixed}$) is normalised by the leg length obtained during still standing (l^{st}). Touchdown(td) and take-off are denoted by ∇ (td) and Δ (to). Total axial stiffness based on non-linar elasticity($z^{n,fixed}_{nln}$) and the corresponding rest length ($l^{fixed}_{0,nln}$)determined by the rms fit are given for each walking speed. $\bar{z}^{n,fixed}_{nln}$ is normalised by BW and l^{st} . $\bar{l}^{fixed}_{0,nln}$ is normalised by l^{st}. The data set is obtained from three good trials of the walking measurements of subject no.2 at each self-selected walking speed.

Figure 4.8 shows that the nonlinear elastic fitting overestimates the axial force around maximum leg shortening for slow and normal walking. Compared with the linear elastic leg properties on the same contact condition at same walking speed, the nonlinear elastic leg properties have higher total axial stiffness (z^n_{nln}) and generally shorter rest length (l_0).

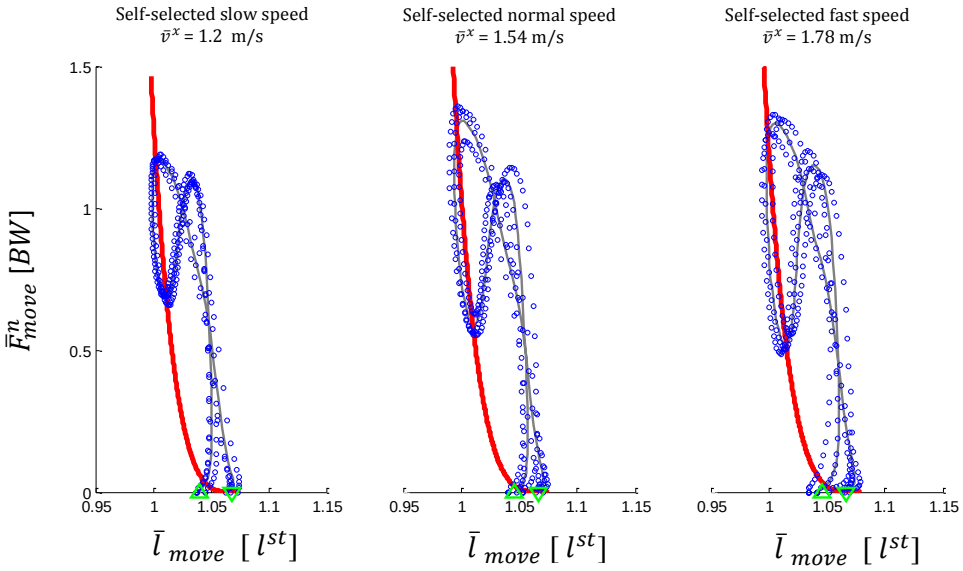

$\bar{z}^{n,move}_{nln}\left[\frac{BW}{l^{st}}\right]$	24.2	22.5	25.2
$\bar{l}^{l,move}_{0,nln}[l^{st}]$	1.074	1.076	1.079

Figure 4.9 The moving contact axial force – length data set (blue)at self-selected slow, normal and fast walking speed and linear fits (red)from a representative subject (subject no.2) are shown. Axial force ($\bar{F}^n_{move}$) is normalised by body weight (BW), leg length ($\bar{l}_{move}$) is normalised by the leg length obtained during still standing (l^{st}). Touchdown(td) and take-off are denoted by ∇ (td) and Δ (to). Total axial stiffness based on non-linar elasticity($z^{n,move}_{nln}$) and the corresponding rest length ($l^{move}_{0,nln}$)determined by the RMS fit are given for each walking speed. $\bar{z}^{n,move}_{nln}$ is normalised by BW and l^{st} . $\bar{l}^{move}_{0,nln}$ is normalised by l^{st}. The data set is obtained from three good trials of the walking measurements of subject no.2 at each self-selected walking speed.

Figure 4.9 shows that, for all walking speeds given here, the nonlinear elastic fitting overestimates the axial force when the leg is at the maximum leg shortening. Compared to the linear elastic leg properties in the same contact condition at the same walking speed, the nonlinear elastic leg properties have higher total axial stiffness (z^n_{nln}) and nearly the same rest length (l_0). Compared to the nonlinear elastic leg properties in fixed contact condition at same walking speed, the nonlinear elastic leg properties on moving contact condition have higher total axial stiffness (z^n_{nln}) and shorter rest length (l_0).

4.3.3 Linear tangential stiffness and force-free leg angles

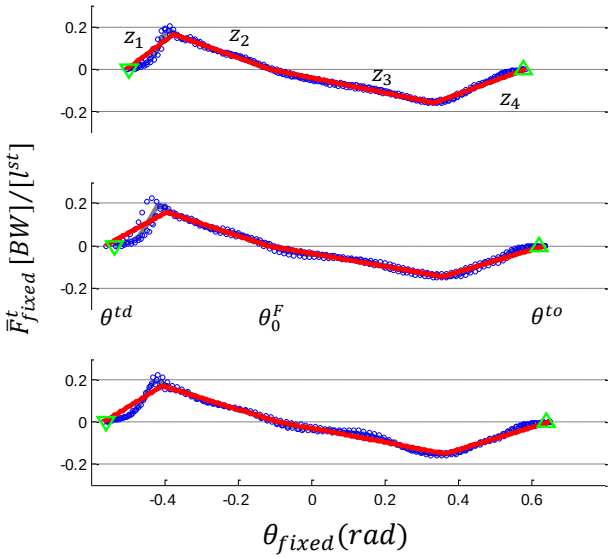

		$1(td)$	$2(F0)$	$3(t0)$	4
Self-selected slow speed $\bar{v}^x$ = 1.2 m/s	$\bar{z}^{t,fixed}_{lin}$	1.5	0.58	0.36	0.64
	$\theta^{t,fixed}_{lin}$	-0.5	-0.11	0.58	
Self-selected normal speed $\bar{v}^x$ = 1.54 m/s	$\bar{z}^{t,fixed}_{lin}$	1.14	0.46	0.30	0.56
	$\theta^{t,fixed}_{lin}$	-0.56	-0.1	0.64	
Self-selected fast speed $\bar{v}^x$ = 1.78 m/s	$\bar{z}^{t,fixed}_{lin}$	1.22	0.52	0.33	0.51
	$\theta^{t,fixed}_{lin}$	-0.56	-0.1	0.65	

Figure 4.10 The fixed contact tangential force – leg angle data set (blue) at self-selected slow, normal and fast walking speed and linear fits (red)from a representative subject (subject no.2) are shown. Tangential leg force ($\bar{F}^t_{fixed}$) is normalised by body weight (BW) and the leg length obtained during still standing (l^{st}). Leg angle (θ_{fixed}) is in radian. Touchdown(td) and take-off are denoted by ∇ (td) and Δ (to). Total tangential stiffness(z^t_{lin}) and the corresponding force-free leg angle ($\theta_{0,lin}$)determined by the RMS fit are given for each walking speed. $\bar{z}^t_{lin}$ is normalised by BW and l^{st} or $[BW \cdot l^{st}]$. $\theta_{0,lin}$ is in radian. For the linear elasticity, $z^t_{lin} = k^t_{lin}$. The data set is obtained from three good trials of the walking measurements of subject no.2 at each self-selected walking speed.

Figure 4.10 shows that in the fixed contact condition at all walking speeds, the absolute value of force-free leg angle at touchdown (θ^{td}) is smaller than that at take-off (θ^{to}). The total tangential stiffness (z^t_{lin}) is highest at the early stance. The force-free leg angle at mid stance (θ^F_0) hardly changes with walking speed.

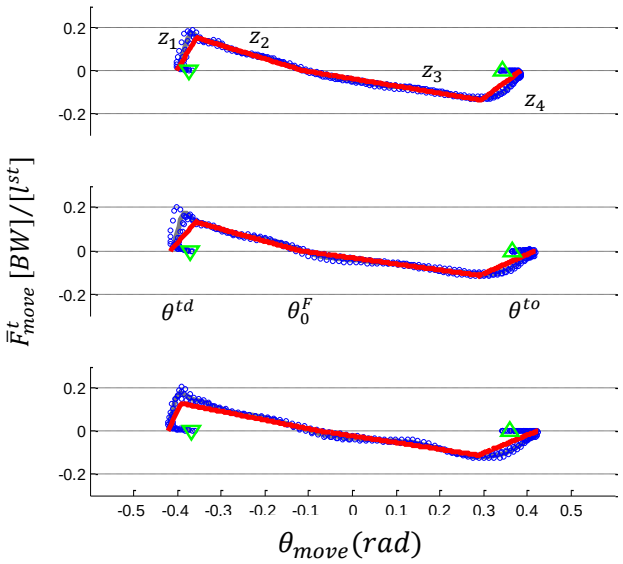

		1(td)	2($F0$)	3($t0$)	4
Self-selected slow speed $\bar{v}^x$ = 1.2 m/s	$\bar{z}^{t,move}_{lin}$	0.51	0.38	0.24	0.64
	$\theta^{t,move}_{lin}$	-0.44	-0.16	0.44	
Self-selected normal speed $\bar{v}^x$ = 1.54 m/s	$\bar{z}^{t,move}_{lin}$	0.76	0.63	0.28	0.74
	$\theta^{t,move}_{lin}$	-0.42	-0.12	0.42	
Self-selected fast speed $\bar{v}^x$ = 1.78 m/s	$\bar{z}^{t,move}_{lin}$	0.77	0.65	0.28	0.74
	$\theta^{t,move}_{lin}$	-0.42	-0.11	0.42	

Figure 4.11 The moving contact tangential force – leg angle data set (blue) at self-selected slow, normal and fast walking speed and linear fits (red)from a representative subject (subject no.2) are shown. Tangential leg force ($\bar{F}^t_{move}$) is normalised by body weight (BW) and the leg length obtained during still standing (l^{st}). Leg angle (θ_{fixed}) is in radian. Touchdown(td) and take-off are denoted by ∇ (td) and Δ (to). Total tangential stiffness(z^t_{lin}) and the corresponding force-free leg angle ($\theta_{0,lin}$)determined by the RMS fit are given for each walking speed. $\bar{z}^t_{lin}$ is normalised by BW and l^{st} or $[BW \cdot l^{st}]$. $\theta_{0,lin}$ is in radian. For the linear elasticity, $z^t_{lin} = k^t_{lin}$. The data set is obtained from three good trials of the walking measurements of subject no.2 at each self-selected walking speed.

Figure 4.11 shows that in moving contact condition, the absolute value of force-free leg angles at touchdown (θ^{td}) and take-off (θ^{to}) at each walking speed are nearly equivalent. Similar to that in fixed contact condition, the total tangential stiffness (z^t_{lin}) is highest at the early stance for all walking speeds. For linear elasticity, the total tangential stiffness (z^t_{lin}) in moving contact condition is higher than that in fixed contact condition at the same speed.

4.3.4 Nonlinear tangential stiffness and force-free leg angles

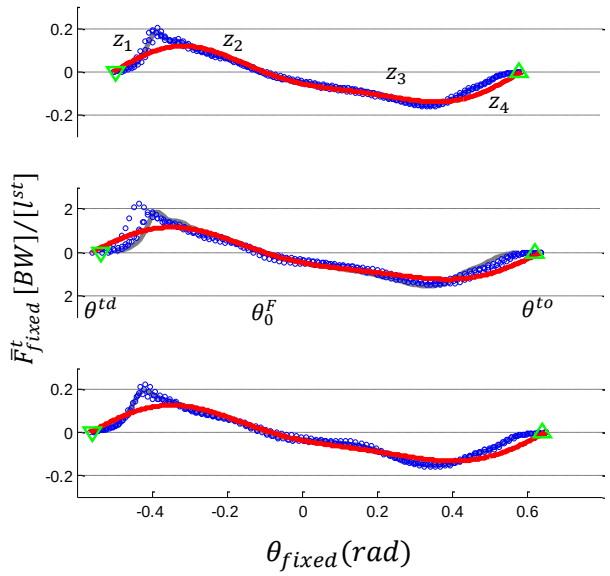

		$1(td)$	$2(F0)$	$3(t0)$	4
Self-selected slow speed $\bar{v}^x$ = 1.2 m/s	$\bar{z}^{t,fixed}_{nln}$	0.65	0.56	0.30	0.60
	$\theta^{t,fixed}_{nln}$	-0.5	-0.10	0.58	
Self-selected normal speed $\bar{v}^x$ = 1.54 m/s	$\bar{z}^{t,fixed}_{nln}$	1.14	0.46	0.30	0.56
	$\theta^{t,fixed}_{nln}$	-0.56	-0.1	0.64	
Self-selected fast speed $\bar{v}^x$ = 1.78 m/s	$\bar{z}^{t,fixed}_{nln}$	1.22	0.52	0.33	0.51
	$\theta^{t,fixed}_{nln}$	-0.56	-0.1	0.65	

Figure 4.12 The fixed contact tangential force – leg angle data set (blue) at self-selected slow, normal and fast walking speed and nonlinearfits (red)from a representative subject (subject no.2)are shown. Tangential leg force ($\bar{F}^t_{fixed}$) is normalised by body weight (BW) and the leg length obtained during still standing (l^{st}). Leg angle (θ_{fixed}) is in radian. Touchdown(td) and take-off are denoted by ∇ (td) and Δ (to). The total tangential stiffness(z^t_{nln}) and the corresponding force-free leg angle ($\theta_{0,nln}$)determined by the RMS fit are given for each walking speed. $\bar{z}^t_{nln}$ is normalised by BW and l^{st}or $[BW \cdot l^{st}]$. $\theta_{0,nln}$ is in radian. The data set is obtained from three good trials of the walking measurements of subject no.2 at each self-selected walking speed.

Figure 4.12 shows that in fixed contact condition for all walking speeds given here, the nonlinear elastic fitting underestimates the first peak of tangential force. In the same contact condition and at the same walking speed, total tangential stiffness (z^t_{nln}) of the nonlinear elasticity is lower than that of linear elasticity.

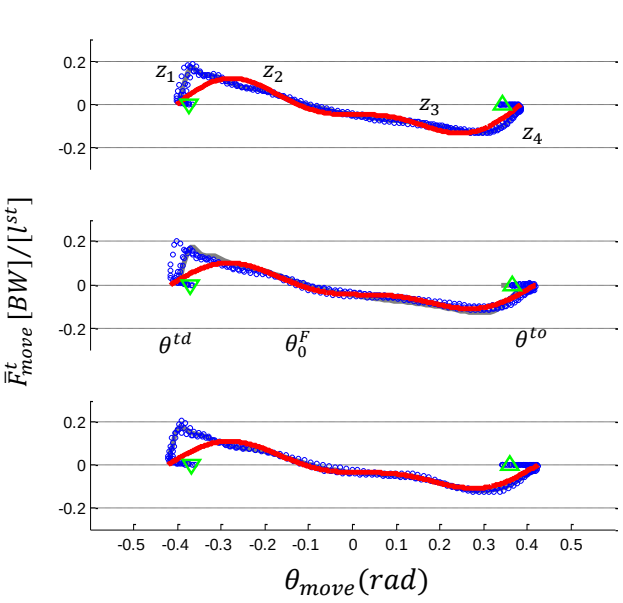

		$1(td)$	$2(F0)$	$3(t0)$	4
Self-selected slow speed $\bar{v}^x$ = 1.2 m/s	$\bar{z}^{t,move}_{nln}$	0.51	0.38	0.24	0.64
	$\theta^{t,move}_{nln}$	-0.44	-0.16	0.44	
Self-selected normal speed $\bar{v}^x$ = 1.54 m/s	$\bar{z}^{t,move}_{nln}$	0.76	0.63	0.28	0.74
	$\theta^{t,move}_{nln}$	-0.42	-0.12	0.42	
Self-selected fast speed $\bar{v}^x$ = 1.78 m/s	$\bar{z}^{t,move}_{nln}$	0.77	0.65	0.28	0.74
	$\theta^{t,move}_{nln}$	-0.42	-0.11	0.42	

Figure 4.13 The moving contact tangential force – leg angle data set (blue) at self-selected slow, normal and fast walking speed and nonlinearfits (red)from a representative subject (subject no.2)are shown. Tangential leg force ($\bar{F}^t_{move}$) is normalised by body weight (BW) and the leg length obtained during still standing (l^{st}). Leg angle (θ_{fixed}) is in radian. Touchdown(td) and take-off are denoted by ∇ (td) and Δ (to). The total tangential stiffness(z^t_{nln}) and the corresponding force-free leg angle ($\theta_{0,nln}$)determined by the RMS fit are given for each walking speed. $\bar{z}^t_{nln}$ is normalised by BW and l^{st}or $[BW \cdot l^{st}]$. $\theta_{0,nln}$ is in radian. The data set is obtained from three good trials of the walking measurements of subject no.2 at each self-selected walking speed.

Figure 4.13 shows that in moving contact condition at all walking speeds given here, the nonlinear elastic fitting underestimate the first peak of tangential force. In the same contact condition and at the same walking speed, the total tangential stiffness (z^t_{nln}) of nonlinear elasticity is lower than that of linear elasticity. However, this total tangential stiffness (z^t_{nln}) of nonlinear elasticity in moving contact condition is higher than that in fixed contact condition.

4.3.5 Summative results for all subjects

The actual and normalised values of the axial and tangential properties from the measurement data for all three walking speeds and all the participants are processed.

The summative values for both fixed and moving contact condition are list in Table 4.1-4.2.

Table 4.1 Axial properties during walking ($mean \pm SD$)

Axial properties			Slow (1.12-1.31 m/s)		Normal(1.35-1.54 m/s)		Fast (1.58–1.8 m/s)	
			moving CoP	fixed CoP	moving CoP	fixed CoP	moving CoP	fixed CoP
Total dynamic stiffness (z^n)	Linear	Actual, (kN/m)	12 ± 2.5	4.2 ± 0.8	11 ± 1.7	3.6 ± 0.9	11.2 ± 2.5	4 .0± 1.3
		Normalised	16.5 ± 2.0	5.7 ± 0.6	15.2 ± 1.8	5.0 ± 0.7	15.3 ± 2.2	5.4 ± 1.2
	Non-linear	Actual, (kN/m)	16.6 ± 4.1	5.8 ± 0.8	15.5 ± 3.5	5.2 ± 0.8	16 ± 3.5	5.6 ± 0.7
		Normalised	22.6 ± 3.9	8.0 ± 0.6	21.3 ± 3.5	7.1 ± 0.9	22.0 ± 3.1	7.7 ± 0.5
Rest length (l_0)	Linear	Actual, (m)	0.960 ± 0.034	1.043 ± 0.033	0.962 ± 0.040	1.076 ± 0.041	0.964 ± 0.038	1.075 ± 0.049
		Normalised	1.062 ± 0.017	1.155 ± 0.033	1.064 ± 0.018	1.191 ± 0.033	1.066 ± 0.017	1.189 ± 0.043
	Non-linear	Actual, (m)	0.957 ± 0.030	1.045 ± 0.026	0.960 ± 0.037	1.048 ± 0.022	0.963 ± 0.034	1.045 ± 0.017
		Normalised	1.059 ± 0.018	1.157 ± 0.026	1.062 ± 0.018	1.161 ± 0.041	1.065 ± 0.016	1.157 ± 0.039

Table 4.1 shows the axial properties comprising total axial stiffness (z^n) and rest length (l_0) during walking at self-selected slow, normal and fast speed. These are the averaged values for all participants. The total axial stiffness (z^n) is normalised by body weight (BW) and leg length during still standing (l^{st}). The rest length is normalised by leg length during still standing (l^{st}).

Due to the smaller leg deflection ($l_0 - l$), the axial stiffness in the moving contact condition is higher than that in fixed contact condition, which can be seen in Figure 4.7 and 4.9. The total dynamic stiffness of nonlinear elasticity is higher than that of the linear elasticity in both contact conditions at all walking speeds. From both elasticity fittings in both contact conditions, the total axial stiffness (z^n) and rest length (l_0) are independent of walking speeds.

Table 4.2 Tangential properties during walking extracted from measurement data ($mean \pm SD$)

Tangential properties			Slow(1.12-1.31 m/s)		Normal(1.35-1.54 m/s)		Fast(1.58–1.8 m/s)	
			moving CoP	fixed CoP	moving CoP	fixed CoP	moving CoP	fixed CoP
Total dynamic stiffness (z^t)	Linear	Actual ($kN \cdot m/rad$)	2.18 ± 0.70	0.76 ± 0.19	1.68 ± 0.48	0.73 ± 0.29	2.5 ± 0.81	0.68 ± 0.15
			0.39 ± 0.06	0.34 ± 0.13	0.33 ± 0.07	0.29 ± 0.07	0.29 ± 0.05	0.17 ± 0.31
			0.21 ± 0.05	0.24 ± 0.06	0.20 ± 0.04	0.22 ± 0.04	0.20± 0.04	0.12 ± 0.20
			0.93 ± 0.33	0.46 ± 0.13	0.85 ± 0.21	0.40 ± 0.06	0.90 ± 0.35	0.40 ± 0.08
		Normalised	3.24 ± 0.74	1.17 ± 0.19	2.52 ± 0.43	1.12 ± 0.30	3.72 ± 0.94	0.96 ± 0.15
			0.59± 0.04	0.52 ± 0.13	0.49 ± 0.06	0.44 ± 0.07	0.44± 0.05	0.26 ± 0.31
			0.32± 0.04	0.36 ± 0.06	0.30 ± 0.05	0.34 ± 0.04	0.31 ± 0.03	0.19 ± 0.20
			1.38± 0.40	0.71 ± 0.13	1.32 ± 0.40	0.63 ± 0.06	1.39 ± 0.55	0.54 ± 0.08
	Non-linear	Actual ($kN \cdot m/rad$)	1.26 ±0.12	0.57± 0.08	1.37 ± 0.142	0.55± 0.09	1.35 ± 0.20	0.50± 0.1
			0.29 ± 0.03	0.23 ± 0.08	0.35 ± 0.12	0.25 ± 0.07	0.30 ± 0.07	0.26 ± 0.08
			0.20 ± 0.05	0.21 ± 0.05	0.22 ± 0.04	0.2 ± 0.03	0.23 ± 0.14	0.21 ± 0.05
			0.52 ± 0.16	0.44 ± 0.10	0.59 ± 0.12	0.37 ± 0.06	0.62 ± 0.18	0.41 ± 0.10
		Normalised	1.71 ± 0.12	0.91 ± 0.10	2.01 ± 0.16	0.89 ± 0.12	1.86 ± 0.25	0.82 ± 0.14
			0.40 ± .0.03	0.32 ± 0.10	0.49 ± 0.14	0.35 ± 0.08	0.43 ± 0.10	0.36 ± 0.10
			0.27 ± 0.05	0.29 ± 0.06	0.30 ± 0.04	0.27 ± 0.036	0.31 ± 0.19	0.29 ± 0.05
			0.70 ± 0.17	0.6 ± 0.13	0.82 ± 0.13	0.52 ± 0.08	0.85 ± 0.20	0.56 ± 0.11
Contact angel ($\theta^{contact}$) or ($90^\circ + \theta$)	Linear	θ^{td}, (deg)	66.5 ± 1.1	60.8 ± 0.8	66.0 ± 0.5	58.9 ± 0.8	65.6 ± 1.0	57.8 ± 0.5
		θ_1^{re}, (deg)	69.1 ± 0.9	66.9 ± 0.9	68.8 ± 0.6	65.7 ± 0.9	67.6 ± 1.0	64.7 ± 1.2
		θ_0^F, (deg)	82.2 ± 2.3	82.3 ± 1.4	82.6 ± 1.4	82.3 ± 1.9	83.9 ± 1.9	81.8 ± 1.8
		θ_2^{re}, (deg)	-73.1 ± 0.2	-70.6 ± 2.0	-71.9 ± 1.5	-68.9 ± 1.0	-72.3 ± 1.3	-68.7± 1.3
		θ^{to}, (deg)	-66.7 ± 2.3	-56.2 ± 2.4	-65.8 ± 0.8	-53.3 ± 1.5	-65.7 ± 0.9	-53.4 ± 1.3
	Non-linear	θ^{td}, (deg)	66.2 ± 1.3	60.8 ± 0.7	65.8 ± 0.4	59.0 ± 0.7	65.1 ± 1.07	57.9 ± 0.6
		θ_1^{re}, (deg)	78.2 ± 0.7	70.0 ± 1.1	72.6 ± 0.6	69.1 ± 0.8	72.3 ± 1.07	68.0 ± 1.4
		θ_0^F, (deg)	79.8± 1.6	82.9 ± 1.6	81.1 ± 1.6	82.6 ± 1.6	82.4 ± 1.5	82.2 ± 2.1
		θ_2^{re}, (deg)	-75.4 ± 1.2	-69.8 ±1.6	-74.3 ± 0.6	-68.3 ± 1.2	-74.2 ± 0.3	-67.3 ± 0.9
		θ^{to}, (deg)	-66 ± 2.2	-56.2 ± 2.3	-65.3 ± 0.8	-53.3 ± 1.6	-65.2 ± 0.9	-53.4 ± 1.2

Table 4.2 shows the tangential properties comprising total tangential stiffness (z^t) and contact angle ($\theta^{contact}$) during walking at self-selected slow, normal and fast speed. These are the averaged values for all participants. The total tangential stiffness (z^t) is

normalised by body weight (BW) and leg length during still standing (l^{st}). The contact angle is the angle between the virtual leg and horizontal or $\theta^{contact} = 90^{\circ} + \theta$ as shown in Figure 4.1. It comprises five different angles to address the changes in magnitude and direction of the tangential leg force during the contact as can be seen in Figure 4.3-4.4. $\theta^{td}$is the force-free leg angle at touchdown, θ_1^{re} and θ_2^{re} are the leg angle at the first and second peak of the tangential force, respectively. θ_0^F is the force-free leg angle at mid-stance when the total ground reaction force applies along the leg axis. θ^{to} is the force-free leg angle at take-off. The tangential stiffness is normalised by body weight (BW) and leg length during still standing (l^{st}).

The total tangential stiffness (z^t) change according to the changes in magnitude and direction of the tangential force during the gait as can be seen in Figure 4.10-4.13. This total tangential stiffness (z^t) in fixed contact condition is lower than that in moving contact condition. Similarly, the absolute value of contact angle at touchdown and take-off in fixed contact condition is smaller than that in moving contact condition. The total stiffness of the nonlinear elasticity is lower than that of linear elasticity as the non-liner elastic fitting using second-order Fourier series in Equation 4.6-4.8 cannot capture the peak of the tangential force.

In fixed contact condition, for both linear and nonlinear elasticity, the tangential stiffness and the absolute value of contact angle at touchdown and take-off decrease as the walking speed increases. However, in moving contact condition, the tangential stiffness and the absolute value of those contact angles are independent of the walking speed. Regardless of the walking speed, elasticity fitting and contact condition, the force-free contact angle at mid-stance (θ_0^F) is maintained at around 82.3 degree with respect to horizontal.

4.4 Discussion and conclusions

In this chapter, the fundamentals of mechanical properties of human leg during walking have been proposed, which represent the minimal leg properties that are necessary to identify human leg mechanics during walking motion. The axial and tangential properties were extracted from the axial force-leg length and tangential force- leg angle relationships on the virtual leg during human walking. The effects of walking speed and foot-ground contact condition were investigated.

The combination of the extracted linear axial stiffness (k_{lin}^{n}) and touchdown contact angle (θ^{td}) on the moving contact condition falls within the stable range of the leg parameters in the compliant leg model with axial elastic property developed by (Geyer et al., 2006). Their compliant leg model with axial elastic property was operated by axial leg force alone, which predicted that the axial stiffness is dependent on walking speed. Although, the changes of axial stiffness and contact angle in Table 4.1 and 4.2 are speed-independent, it falls within the parameter range of (Geyer et al., 2006)'s compliant leg model, which can reproduce the stable walking motion at speed 1.0- 1.5 m/s.

The speed independence of the linear axial properties in our study is consistent with that in (Lipfert et al., 2012); however, their normalised axial stiffness and contact angle are much higher. In their study, the total ground reaction force obtained from the walking and running measurement was considered to apply along the virtual leg. Such scheme provides the normalised axial stiffness between 31.7 to 45.8 for walking speed between 2.07 to 1.04 m/s. The periodic walking simulation was found only with the axial stiffness being 33.1 and contact angle being 74.8 degree at walking speed of 1.04 m/s. On the same leg property definition, (Lipfert et al., 2012)'s axial stiffness during running is also higher than that of (Coleman et al., 2012) which used similar force

projection technique as our study to extract axial stiffness from human running measurement.

For the nonlinear axial properties, the speed independence is also found. Only the hard nonlinear elasticity can achieve the minimum RMSE fits on the axial force- leg length data. Compared with the linear elastic fittings in the fixed contact condition, the nonlinear elastic fittings better fits the axial force- leg length data in early and mid stance; however, it overestimates the axial force when the leg is at the maximum leg shortening.

There are no previous studies on the tangential leg properties from the walking measurement extraction. Only the hip torque profile during the gait cycle has been introduced in Maus et al. (2010). Such torque profile to stabilise the human upright walking agrees with our tangential force – leg angle relationship in Figure 4.10-4.13. The speed dependence is found in the tangential properties for linear and nonlinear elasticity on the fixed contact condition. However, the nonlinear fittings by using second order Fourier series on the tangential force- leg angle data underestimate the tangential stiffness in early and late stance.

On the effects of foot- ground contact condition, the higher axial and tangential stiffness of the moving contact condition than that of the fixed contact condition are consistent with previous studies in (Bullimore and Burn, 2006;Whittington and Thelen, 2009). As the foot-ground contact moves forward during the stance, the shortening - lengthening ($l_0 - l$) and angular deflection ($\theta_0 - \theta$) of the virtual leg are reduced and thus, increase the total axial and tangential stiffness.

The effects of linear and nonlinear elasticity, foot-ground contact condition and ground reaction force decomposition underline the influence of leg property definition on the extracted leg properties. In fact, there is only a short period during the mid-stance that the direction of total ground reaction force coincides with the leg axis. By projecting the total ground reaction force onto the parallel and perpendicular line of the virtual leg, the axial and tangential stiffness can be estimated from the more realistic force-displacement relationships. Compared to the linear elasticity, the nonlinear elasticity better fits on the axial force – leg length relationship of fixed contact condition. The different conditions of foot-ground contact lead to different force-displacement relationships and thus, the different leg properties as a result of leg property extraction on different leg definition. The implementation of these mechanical leg properties in human walking model is required to validate the leg property region in human walking prediction.

In addition to the fitting, other calculations may also affect on leg properties extraction. One of which is the calculation for centre of mass motion. In our study, the centre of mass motion at the touchdown instant during walking is used as the initial motion for the integration of ground reaction force. Other studies prevented the signal drifts by starting the integration from the still standing (Blum et al., 2009; Lipfert et al., 2012). However, to study human walking at self-selected speed, the latter technique requires a long walking track or a measurement conducted on treadmill. It has been found that the variation of CoM velocity during the over-ground and treadmill walking are fundamentally different (White et al., 1998; Dingwell et al., 2001; Dierick et al., 2004; Schablowski and Gerner, 2006; AlGheshyan, 2012). This may lead to different estimations of CoM motion and thus different force-displacement relationships. In

(Lipfert et al., 2012), extracted from walking measurements on treadmill, it has been found that the rest length is shorter than the leg length at still standing. Such leg properties limit the implementation in compliant leg model with axial elastic property and thus some adjustments were required to validate those leg properties with human walking measurements.

The speed independence of the extracted mechanical leg properties can be interpreted in many different ways. It may imply that the leg elasticity during human walking does not change with walking speed. More implication may be from the fitting function. The single valued force – displacement relationships used in all fittings has some limitations to extract the mechanical leg properties during human walking. As can be seen in Figure 4.5-4.8, the measured axial force- leg length relationships in both contact conditions are non-conservative around the maximum leg shortening. By fitting the single valued force –length function onto such non-conservative relationship, the rest length is stretched to the maximum length to satisfy the spring leg equation (see Figure 4.6-4.9) and may affect on the extracted axial stiffness (see Equation 4.1- 4.3). Similarly, for the tangential properties on the moving contact condition, single valued force – angle function overestimates the absolute leg angle at touchdown and take-off (see Figure 4.10-4.13) and may affect on the extracted tangential stiffness (see Equation 4.4- 4.6). In such cases, the parametric equations may be required to express the multi-valued force–angle and force-length functions for the extraction of axial and tangential leg properties from the force-displacement relationships during human walking.

Chapter 5 Posture - Dependent Properties of Human Leg during Walking

This chapter presents the mechanical properties of human leg on the posture-dependent variation of axial and tangential elasticity during human walking motion. The posture-dependent leg properties during human walking motion are proposed. These mechanical leg properties are extracted from human walking measurements at different self-selected walking speeds on fixed and moving condition of foot-ground contact.

5.1 Background

In Chapter 4, it was found that, obtained from the walking measurements, the relationships of axial force-leg length and tangential force-leg angle change after maximum leg shortening and mid-stance force-free leg angle (θ_0^F), respectively. These non-conservative force-displacement relationships reflex the different mechanical properties of human walking leg during the first and the second half of stance. In addition, it indicates the non-conservative mechanical energy in which the energy stored by leg shortening and first half of leg rotation is unbalance with the energy released during the leg lengthening and the second half of leg rotation. To predict the accurate human walking motion and dynamic stability, the mechanical properties of human walking leg in corresponding to such non-conservative mechanical energy need to be studied.

The variety coordination of complex muscle-tendon structure producing negative and positive work have been found in leg operation during human locomotion (Pollock and Shadwick, 1994; Lindstedt et al., 2002; Purslow, 2002; Roberts and Azizi, 2011). Such coordination may results in the dissipation, production and conservation of mechanical energy depending on the leg function performed during locomotion (Roberts and Azizi, 2011). However, most of the explicit leg functions proposed for the human locomotion were based on the perfect elasticity (Morin et al., 2011; Blum et al., 2009; Lipfert et al., 2012; Coleman et al., 2012) in which only the complete exchanges of mechanical energies are presented. The function and property of the leg permitting the mechanical energy dissipation and production remains an open question in human locomotion study.

The explicit forms of energy dissipation have been developed in human walking modelling and insect locomotion study. In a study of the propulsion of human walking, a viscous-damped compliant leg model with curved feet predicted that the energy dissipation in visco-elastic element is hardly dependent on walking velocity (Kim and Park, 2011). An earlier study on insect running leg suggested a structural damping to represent the independence of energy dissipation on the leg oscillation frequency. This structural damping so called hysteretic damping was adopted from the vibration damping (Nashif et al., 1985; Fung, 1993) to study the energy dissipation embedded with stiffness and positioning of the leg. This frequency-independent energy dissipation was found as a part of self-stabilisation for small perturbation during insect running (Dudek and Full, 2006). However, this structural damping in biped locomotion has not

been recognised. This may be explained by the fact that insect locomotion has much wider range of leg rotational frequency compared to that of bipedal locomotion. Above all, the variety coordination of complex muscle-tendon structure makes the explicit forms of energy dissipation in the human leg during locomotion a remaining open question.

Instead of the explicit sources of energy dissipation and production, some studies on the human and robotic leg properties based on non-linear elasticity with implicit form of energy dissipation may provide some clues for the changes of mechanical property of the human leg during locomotion. To represent energy dissipation, a study of human running motion estimated the leg properties by both linear and non-linear stiffness where the rest length was allowed to vary linearly with time. It suggested that the non-linearity of leg stiffness and variation of rest length may be a general consequence of segmental geometry and non-linear elasticity of the leg joints, whereas the linearity of which requires the proper adjustment of both local properties (Gunther and Blickhan, 2002). This is supported by the theoretical predictions of leg properties from the joint properties in segmented leg robots and running simulation (Raibert, 1986; Seyfarth, 2000; Rummel and Seyfarth, 2008). These results of nonlinear leg properties imply the variation of leg properties due to the change of multi-segment geometry and joint properties.

In the study of the stability of bipedal robot running with perturbation, the energy variation managed by leg property variation in arthropod running (Schmitt and Holmes,

2000a; Schmitt and Holmes, 2000b; Schmitt et al., 2002; Schmitt and Holmes, 2003) has been adopted in spring-loaded inverted pendulum model. The energy dissipation and production during the leg operation was represented by the prescribed force-free leg length as a sinusoidal function of time. The variation of force-free leg length allows the unbalance between elastic energy storage and the work done by spring relaxation. This results in the difference of force-free leg length at touchdown and take-off which adjusts the CoM velocity during late stance of walking as anticipation to external perturbation. This posture-dependent actuation of force-free leg length in conjunction with the proper change in touchdown leg angle from one to the next step (Seyfarth et al., 2003) corresponding to the mechanical energy variation was found to stabilise the biped running against large perturbation (Schmitt and Clark, 2009). As the implicit sources of the energy dissipation and production, such variation of force-free leg length and leg positioning may be utilised to study the walking motion and dynamic stability on non-conservative system energy.

5.2 Posture-dependent leg properties

In this chapter, the variation of leg properties regulated by leg posture so called posture index are proposed to represent the posture-dependent elasticity of the virtual leg. The leg positioning, variable leg stiffness and variable force-free leg length are used as leg properties to facilitate non-conservative mechanical energy during human walking. In this section, the posture- dependent leg properties are defined and then extracted from the measurement data by data fitting.

5.2.1 Posture index

Posture index is the proportion of leg posture change and the swept angle over the duration of foot-ground contact. The leg posture is determined by the difference between the instantaneous leg angle during the contact and leg angle at touchdown instant. Only the angle of ipsilateral leg, the leg that starts the considered walking step, is used to calculate the posture index.

The leg angle during foot- ground contact in fixed contact condition is injective single-valued function (Bartle, 1976); that is the leg angle changes with contact time and never returns to the same angle value (see Figure 5.1a). However, the leg angle in moving contact condition is different as some angle values are repeated after some contact times. As a result, the posture index at each contact instant in moving contact condition is not unique and cannot be used to regulate the leg property variation.

In such a case, the posture index of moving contact condition has to be calculated from the leg angle on fixed contact. This contact condition has foot-ground contact point fixed at the CoP location where the leg angle on moving contact condition reaches vertical leg orientation. The leg angle on this fixed contact can always be obtained from the available data on moving contact (see Figure 4.2 in Chapter 4). Thus, the posture index for both fixed and moving contact can be written as

$$q = \frac{\theta - \theta^{td}}{\theta^{to} - \theta^{td}} \tag{5.1}$$

where θ, θ^{td} and θ^{to} are the angle of ipsilateral leg on fixed contact condition during the stance, at touchdown and at take-off, respectively. The posture index begins with 0 at the touchdown and terminates with 1 at the take-off (see Figure 5.1b).

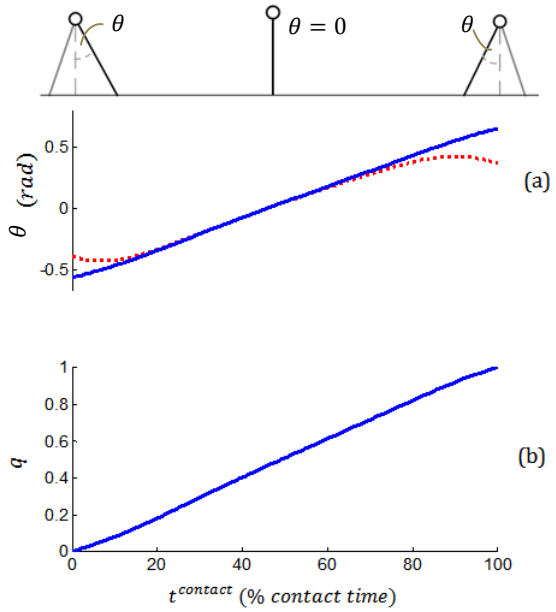

Figure 5.1 (a) Ipsilateral leg angle (θ) in radian during the foot- ground contact for fixed (solid) and moving contact (dash). (b) Posture index (q) for both fixed and moving contact. The walking picture from left to right illustrates the ipsilateral leg (black) at touchdown, vertical leg orientation and take-off. The leg angle and posture index are calculated from the mean of measurement data of subject no.2 on self-selected normal walking.

5.2.2 Posture-dependent axial properties

Posture-dependent axial properties are defined by the axial stiffness and force-free leg length. The linear axial stiffness and the variation of force-free leg length regulated by posture index are used to capture the differences of axial force – leg length relationship during first and second half of stance. The variable force-free leg length managed by leg posture is also used to represent the energy variation during the gait. The posture-dependent axial force – leg length equation for the fixed contact can be written as

$$F_q^n = k_{q,lin}^n (l_{0,q} - l) \tag{5.2}$$

$$l_{0,q}^{fixed} = l^{td} + d^l (q + f_0(q)) \tag{5.3}$$

$$d^l = l^{td} - l^{to} \tag{5.4}$$

$$f_0(q) = \sum_{m=1}^{5} (a_m^n (\cos(2m\pi q) - 1) + b_m^n \sin(2m\pi q)) \tag{5.5}$$

where F_q^n is the axial force due to posture-dependent elasticity of the virtual leg , l is the virtual leg length, $k_{q,lin}^n$ is the linear axial stiffness and $l_{0,q}^{fixed}$ is the posture-dependent force-free leg length in fixed contact condition. This variable force-free leg length ($l_{0,q}^{fixed}$) is a nonlinear function of posture index (q). In other words, this rest length varies around the touchdown (l^{td}) and take-off leg length (l^{to}) (see Figure 5.2) with some deviation in proportional to excursion length (d^l). The finite Fourier series ($f_0(q)$) represents the rest length fluctuation constrained to zero at initial and terminal contact. a_m^n and b_m^n are Fourier coefficients. The fifth-order of Fourier series is selected from the optimal number of Fourier coefficient that minimise the root-mean-square error. The preliminary examination on higher-order of Fourier series showed that the RMSE is not significantly reduced with the more number of Fourier coefficient.

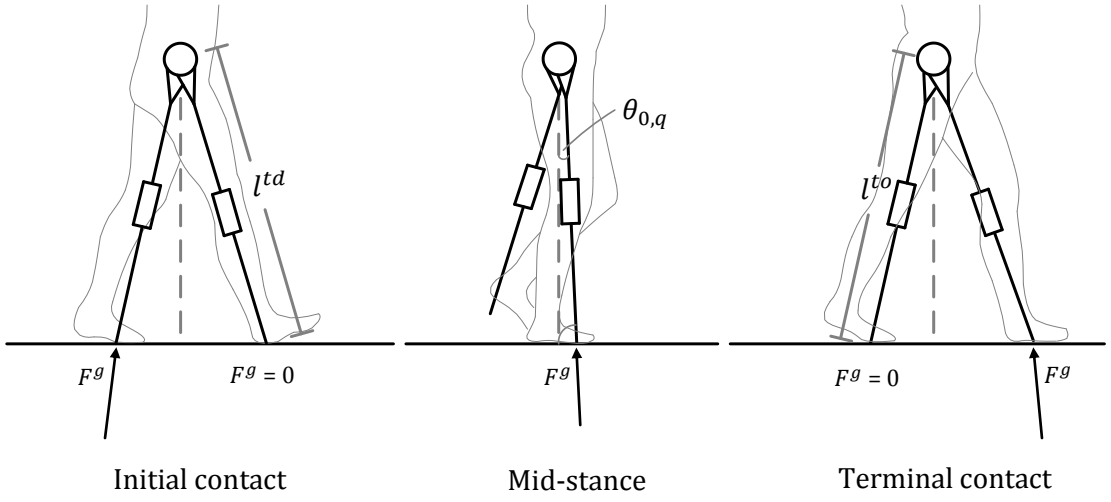

Figure 5.2 The illustration of force-free leg length at initial contact ($l_{0,q} = l^{td}$) and terminal contact ($l_{0,q} = l^{to}$) and force-free leg angle ($\theta_{0,q}$) at mid-stance when the direction of the total ground reaction force (F^g) is coincident with leg axis and, thus the tangential force is zero.

The posture-dependent force-free leg length ($l_{0,q}$) requires additional term to represent the variation of force-free leg length on moving contact. This variable force-free leg length in moving contact condition ($l_{0,q}^{move}$) can be written as

$$l_{0,q}^{move} = l^{td} + d^l\left(q + f_0(q)\right) + d^\theta \tag{5.6}$$

$$d^\theta = \frac{|q(\theta^{to} - \theta^{td}) + \theta^{td}|}{A^\theta} A^l \sin \pi q \tag{5.7}$$

where d^θ represents the additional nonlinear term of force-free leg length in moving contact condition. A^θ and A^l are the peak amplitude from the measurement data of leg angle and leg length, respectively (see Figure 5.3).

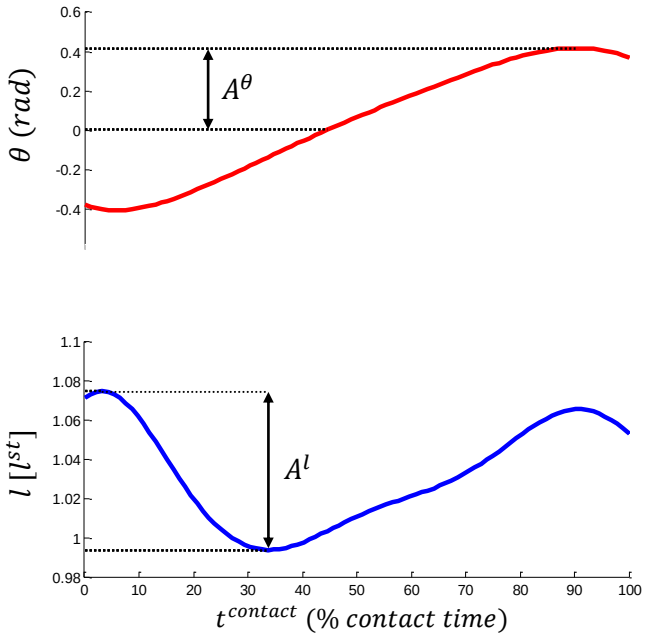

Figure 5.3 Peak amplitude of leg angle (A^{θ}) and leg length (A^{l}) in moving contact condition obtained from the mean of measurement data of subject no.2 on self-selected normal walking.

In order to compare the variation of force-free leg length in fixed and moving contact condition, the peak amplitude of force-free leg length is calculated by

$$A_0^{l,fixed} = max\ (d^l(f_0(q))) \tag{5.8}$$

for the fixed contact and

$$A_0^{l,move} = max\ (d^l(\ f_0(q)) + d^{\theta}) \tag{5.9}$$

for moving contact (see Figure 5.3).

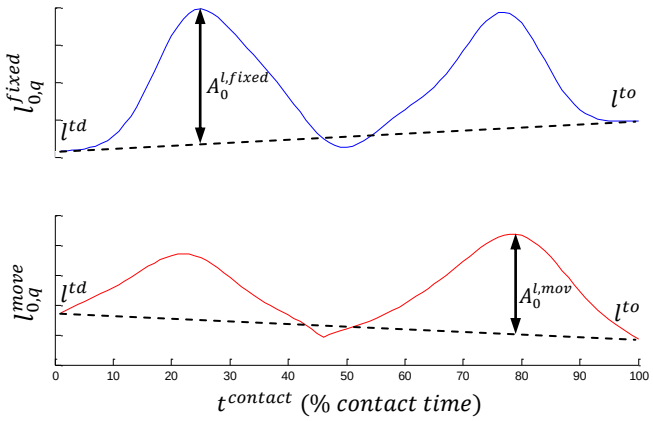

Figure 5.4 The force-free leg length (l_0^l) and the peak amplitude (A_0^l) in fixed and moving contact condition during the foot-ground contact ($t^{contact}$) extracted from the mean of measurement data of subject no.2 on self-selected normal walking speed. l^{td} and l^{to} are the force-free leg length at touchdown and take-off instant, respectively.

5.2.3 Posture-dependent tangential properties

Despite the instantaneous change as presented in Chapter 4, the tangential dynamic leg properties in this chapter are defined by posture-dependent tangential stiffness and a force-free leg angle. A fixed force-free leg angle and variation of tangential stiffness regulated by posture index are utilised to represent the posture-dependent tangential elasticity as a consequence of nonlinear joint stiffness (Raibert, 1986; Seyfarth, 2000; Gunther and Blickhan, 2002; Rummel and Seyfarth, 2008). This force-free leg angle is defined by force-free leg angle occur at the mid-stance when the total ground reaction force applies along the leg and thus, the tangential force becomes zero, which is equivalent to the force-free leg angle at mid-stance (θ_0^F) in Chapter 4 (see Figure 3.10-3.13). The posture-dependent force- angle equation for both contact conditions can be written as

$$F_q^t = \frac{k_q^t(q)}{l}(\theta_{0,q} - \theta) \tag{5.10}$$

$$k_q^t(q) = \sum_{m=1}^{5}(a_m^t\,(\cos(2m\pi q) - 1) + b_m^t \sin(2m\pi q)\,) \tag{5.11}$$

where F_q^t is the tangential leg force based on posture-dependent elasticity of the virtual leg , $\theta_{0,q}$ is the mid-stance force-free leg angle (see Figure 5.2). $k_q^t(q)$ is the posture-dependent tangential stiffness in terms of finite Fourier series constraining tangential stiffness to zero at touchdown and take-off regardless of the touchdown and take-off angle value. a_m^t and b_m^t are Fourier coefficients of posture-dependent tangential stiffness.

The variation of tangential stiffness is divided by the force-free leg angle into two phases. The first phase corresponds to the hard nonlinear elasticity in which the tangential stiffness increases from zero at the touchdown to the maximum value. The second phase corresponds to soft nonlinear elasticity in which the tangential stiffness decreases from the maximum value to zero at the take-off (see Figure 5.5). That is, this tangential stiffness is dependent on leg posture ($\theta - \theta^{td}$) instead of the leg angular deflection ($\theta_{0,q} - \theta$).

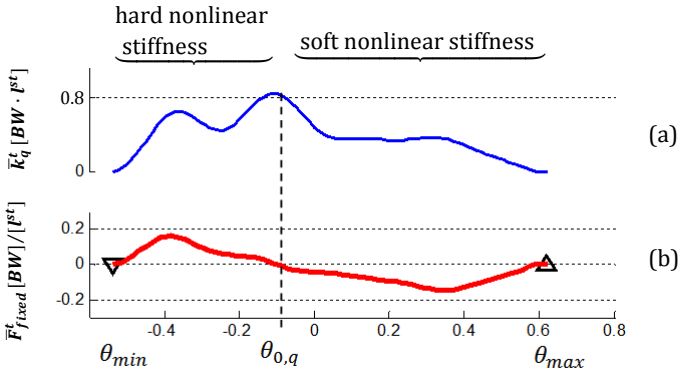

Figure 5.5 An example of two-phases nonlinear stiffness (a) divided by the force-free leg angle ($\theta_{0,q}$) extracted from the mean of measurement data of subject no.2 on self-selected normal walking. The corresponding tangential force (b) is shown with the touchdown (td) and take-off being denoted by ∇ (td) and Δ(to). $\bar{k}_q^{t,move}$ is normalised to body weight (BW) and leg length obtained during still standing (l^{st}) or $[BW \cdot l^{st}]$. ($\bar{F}_{fixed}^t$) is normalised by $[BW]/[l^{st}]$.

The total stiffness (z) is used to compare the tangential stiffness on different nonlinear elasticity. This total stiffness is calculated by

$$z_{q,hard}^t = \frac{max(F_q^t)}{(\theta_{min} - \theta_{0,q})} \tag{5.12}$$

for hard nonlinear elasticity and

$$z_{q,soft}^t = \frac{|min(F_q^t)|}{(\theta_{max} - \theta_{0,q})} \tag{5.13}$$

for soft nonlinear elasticity.

5.2.4 Fitting procedure

For the axial leg properties, the similar fitting method as in Chapter 4 is used. The only difference is that the mean value of measurement data set of axial force- leg length and

tangential force- leg angle at each self-selected walking speed are calculated to allow minimum root-mean-squares fitting on posture-dependent elasticity. The calculated mean value of measurement data set of leg length and leg angle including the peak amplitude of leg length (A^l) and leg angle (A^θ) are fed into Equation 5.1- 5.7 to extract the linear axial stiffness and posture-dependent force-free leg length for fixed and moving contact conditions. The search of leg parameters of the axial force-length equations is operated using the optimisation function fmincon in MATLAB version 2010 to minimise the root-mean-square error. An additional constraint is introduced to the search problem to ensure that the fluctuation of force-free leg length does not dominate the axial property extraction (see Equation 5.2).

$$A^l \geq A_0^l \tag{5.14}$$

The Equation 5.14 constrains the peak amplitude of force-free leg length (A_0^l) to be below the measured peak amplitude of leg length (A^l) to ensure that the variation of force-free leg length will not override the extracted values of other axial properties.

By solving the constrained optimisation problem for minimum RMSE, the eleven axial leg parameters comprising linear leg stiffness ($k_{q,lin}^n$) and Fourier coefficients of variable force-free leg length (a_m^n, b_m^n) are determined. From the optimal solution, the peak amplitude of force-free leg length fluctuation (A_0^l) is calculated by Equation 5.8 and 5.9.

The posture-dependent tangential leg stiffness $k_q^t(q)$ and a force-free leg angle ($\theta_{0,q}$) are estimated by feeding the measurement data set of the leg angle and leg length into Equation 5.1, 5.10 and 5.11. The eleven tangential leg parameters comprising a force-free leg angle ($\theta_{0,q}$) and Fourier coefficients of variable tangential stiffness (a_m^t, b_m^t) are determined. Then, the tangential force equations are substituted into Equation 5.12 and Equation 5.13 to calculate the total stiffness (z) for hard and soft nonlinear elasticity, respectively. This total stiffness (z) is used to compare between different nonlinear elasticity. The diagram for the extraction procedure is shown in Figure 5.6.

The walking measurement and data processing allow for simultaneous analysis of kinetic-kinematic data during single walking step. This is sufficient to obtain the force-displacement relationships of the virtual leg, however, limits the capture of touchdown angle variation from one to the next step. In this chapter, the variation of touchdown leg angle is considered between different walking trials on the same walking speed.

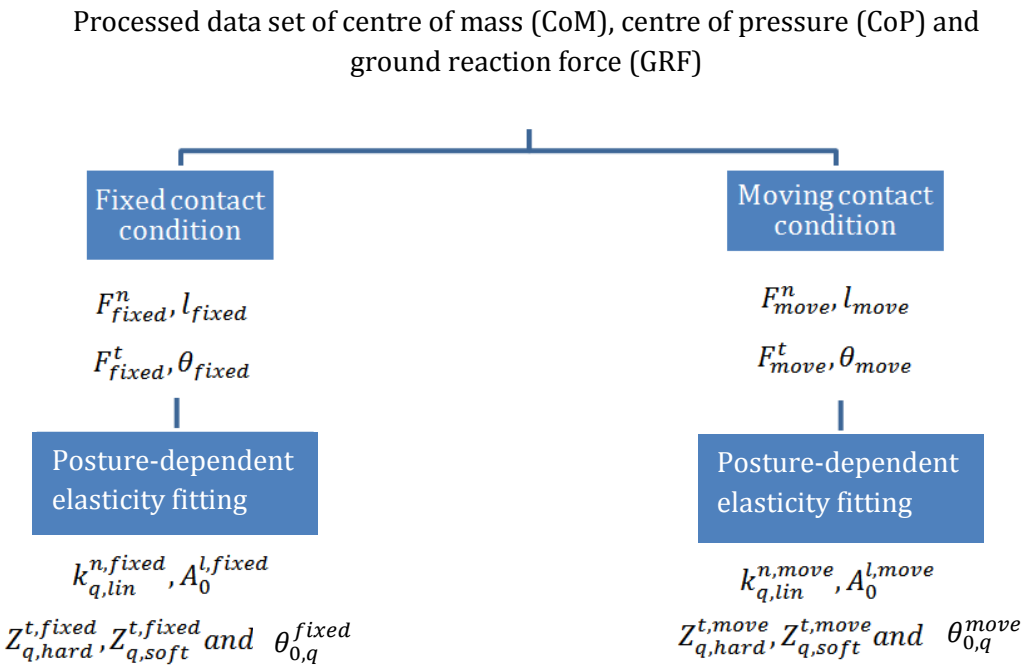

Figure 5.6 Extraction process for the axial stiffness ($k^n_{q,lin}$), peak amplitude of posture-dependent force-free leg length (A^l_0), posture-dependent tangential stiffness ($Z^t_{q,hard}$, $Z^t_{q,soft}$) and force-free leg angle ($\theta_{0,q}$).

5.3 Some fitting results

For each subject, the measurement data of the CoM, CoP and GRF at each self-selected walking speed was processed in two contact conditions namely fixed and moving contact. The variations of leg properties are utilised to represent the posture-dependent elasticity of axial and tangential element of virtual leg to fit the force-displacement relationship of the virtual leg operation on non-conservative mechanical energy. The peak amplitude of variation of the posture-dependent force-free leg length and the total tangential stiffness are calculated.

5.3.1 Linear axial stiffness ($k_{q,lin}^{n,fixed}$) and peak amplitude of variation of the force-free leg length ($A_0^{l,fixed}$)

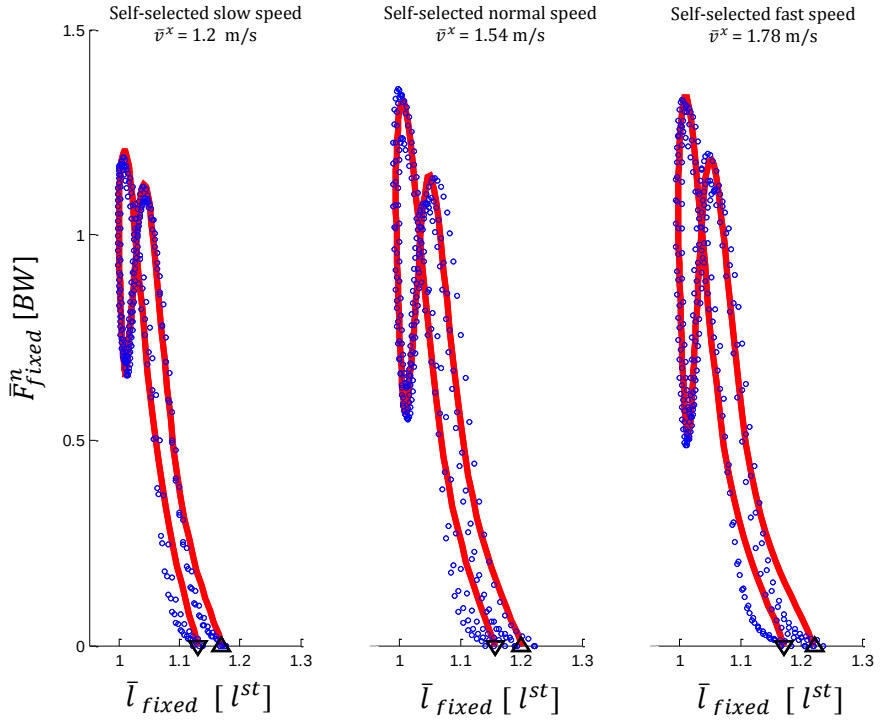

Figure 5.7 The fixed contact axial force – length data set (blue) at self-selected slow, normal and fast walking speed and posture-dependent elasticity fits (red) from a representative subject (subject no.2) are shown. Axial force ($\bar{F}_{fixed}^{n}$) is normalised by body weight (BW), leg length ($\bar{l}_{fixed}$) is normalised by the leg length obtained during still standing (l^{st}). Touchdown(td) and take-off are denoted by ∇ (td) and Δ (to). Linear axial stiffness($k_{q,lin}^{n,fixed}$) and the corresponding peak amplitude of variation of the force-free leg length ($A_0^{l,fixed}$)determined by the RMS fit are given for each walking speed. $\bar{k}_{q,lin}^{n,fixed}$ is normalised by BW and l^{st} . $\bar{A}_0^{l,fixed}$is normalised by l^{st}. The data set is obtained from three good trials of the walking measurements of subject no.2 at each self-selected walking speed.

In Figure 5.7 for the fixed contact condition, the linear stiffness for the posture-dependent elasticity of axial element of the virtual leg at different walking speeds is consistent with that for the linear elasticity except for the fast walking speed in which the posture-dependent elasticity fitting gives higher linear stiffness. Unlike the linear elasticity fitting, the posture-dependent elasticity fitting gives different leg length at

touchdown and take-off. For the representative subject shown here, the peak amplitude of force-free leg length variation is speed-dependent.

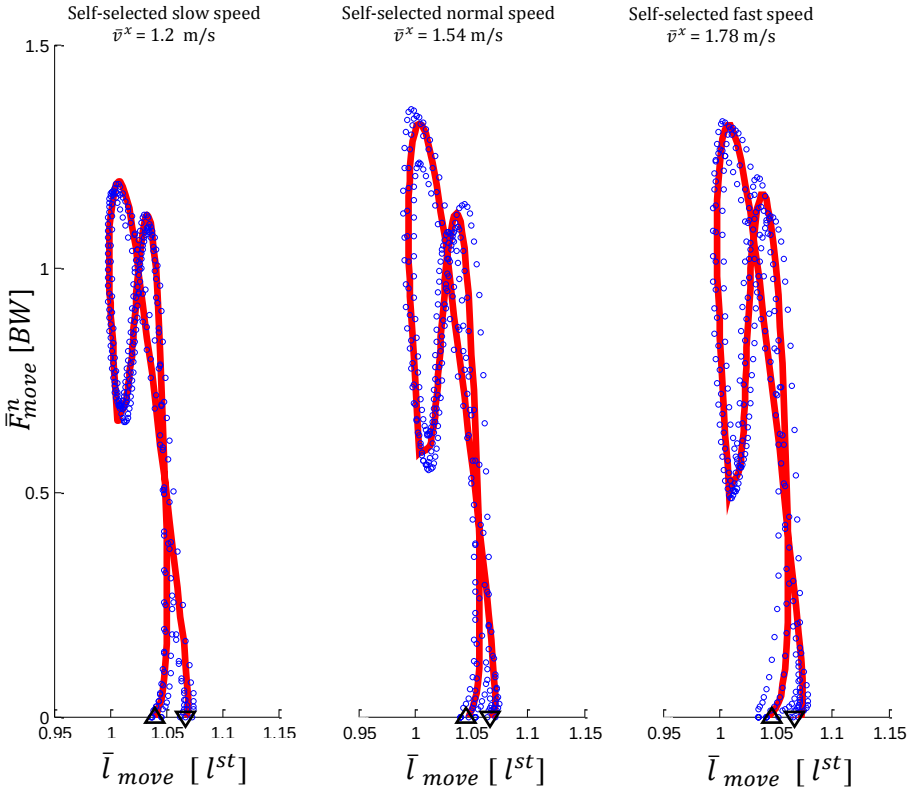

$\bar{k}^{n,move}_{q,lin}\left[\frac{BW}{l^{st}}\right]$	15.7	13.8	17.8
$\bar{A}^{l,move}_0[l^{st}]$	0.054	0.047	0.045

Figure 5.8 The moving contact axial force – length data set (blue) at self-selected slow, normal and fast walking speed and posture-dependent elasticity fits (red)from a representative subject (subject no.2) are shown. Axial force ($\bar{F}^n_{move}$) is normalised by body weight (BW), leg length (l_{move}) is normalised by the leg length obtained during still standing (l^{st}). Touchdown(td) and take-off are denoted by ∇ (td) and Δ (to). The axial linear stiffness($k^n_{q,lin}$) and the corresponding peak amplitude of variation of the force-free leg length ($A^{l,move}_0$) determined by the RMS fit are given for each walking speed. $\bar{k}^n_{q,lin}$ is normalised to , l^{st} . $\bar{A}^{l,move}_0$ is normalised to l^{st}. The data set is obtained from three good trials of the walking measurements of subject no.2 at each self-selected walking speed.

In Figure 5.8 for the moving contact condition, the linear stiffness for the posture-dependent elasticity of axial element of the virtual leg on different walking speeds is consistent with that for the linear elasticity except for the fast walking speed in which

posture-dependent elasticity fitting provides higher linear stiffness. The variation of force-free leg length allows the different leg length at touchdown and take-off. In contrast to the fixed contact, the peak amplitude of variation of force-free leg length decreases with increased walking speed.

5.3.2 Total tangential stiffness and force-free leg angle

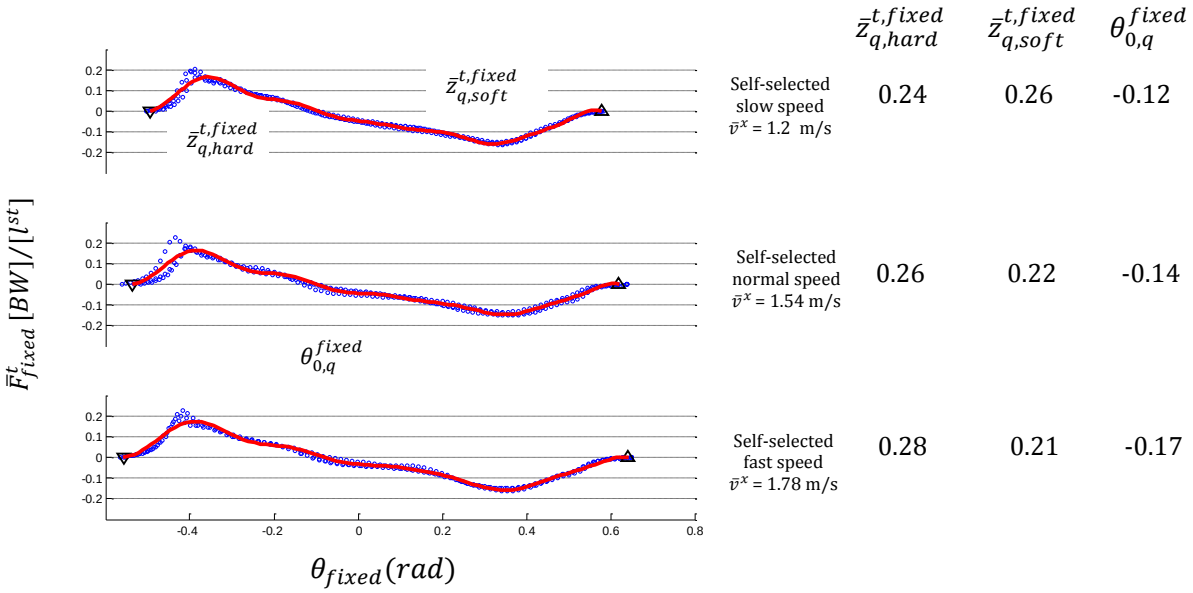

	$\bar{z}_{q,hard}^{t,fixed}$	$\bar{z}_{q,soft}^{t,fixed}$	$\theta_{0,q}^{fixed}$
Self-selected slow speed $\bar{v}^x$ = 1.2 m/s	0.24	0.26	-0.12
Self-selected normal speed $\bar{v}^x$ = 1.54 m/s	0.26	0.22	-0.14
Self-selected fast speed $\bar{v}^x$ = 1.78 m/s	0.28	0.21	-0.17

Figure 5.9 The fixed contact tangential force – leg angle data set (blue) at self-selected slow, normal and fast walking speed and posture-dependent elasticity fits (red)from a representative subject (subject no.2) are shown. Tangential leg force ($\bar{F}_{fixed}^{t}$) is normalised by body weight (BW) and the leg length obtained during quiet standing (l^{st}). Leg angle (θ_{fixed}) is in radian. Touchdown(td) and take-off are denoted by ∇ (td) and Δ (to). The total tangential stiffness for hard ($z_{q,hard}^{t,fixed}$) and soft ($z_{q,soft}^{t,fixed}$) nonlinear stiffness and the corresponding force-free leg angle ($\theta_{0,q}^{fixed}$) determined by the RMS fit are given for each walking speed. $\bar{z}_{q}^{t,fixed}$ is normalised by , l^{st} or $[BW \cdot l^{st}]$. $\theta_{0,q}^{fixed}$ is in radian. The data set is obtained from three good trials of the walking measurements of subject no.2 at each self-selected walking speed.

Despite the instantaneous changes of linear tangential stiffness extracted by linear elasticity fitting as in Chapter 4, the posture-dependent tangential stiffness allows the stiffness variation from hard to soft nonlinear stiffness across the force-free leg angle ($\theta_{0,q}^{fixed}$). The total value of the posture-dependent tangential stiffness is distinct from

that of the linear tangential stiffness in Chapter 4. This is because their leg deflections correspond to different basic of force-free leg angle. However, the force-free leg angle ($\theta_{0,q}^{fixed}$) extracted by the posture-dependent elasticity fittings is consistent to the force-free leg angle during mid-stance (θ_0^F) extracted by linear elasticity fittings. The results from Figure 5.9 shows that the total tangential stiffness for hard nonlinear stiffness ($\bar{z}_{q,hard}^{t,fixed}$) increases whereas that for soft nonlinear stiffness ($\bar{z}_{q,soft}^{t,fixed}$) decreases with increased walking speed.

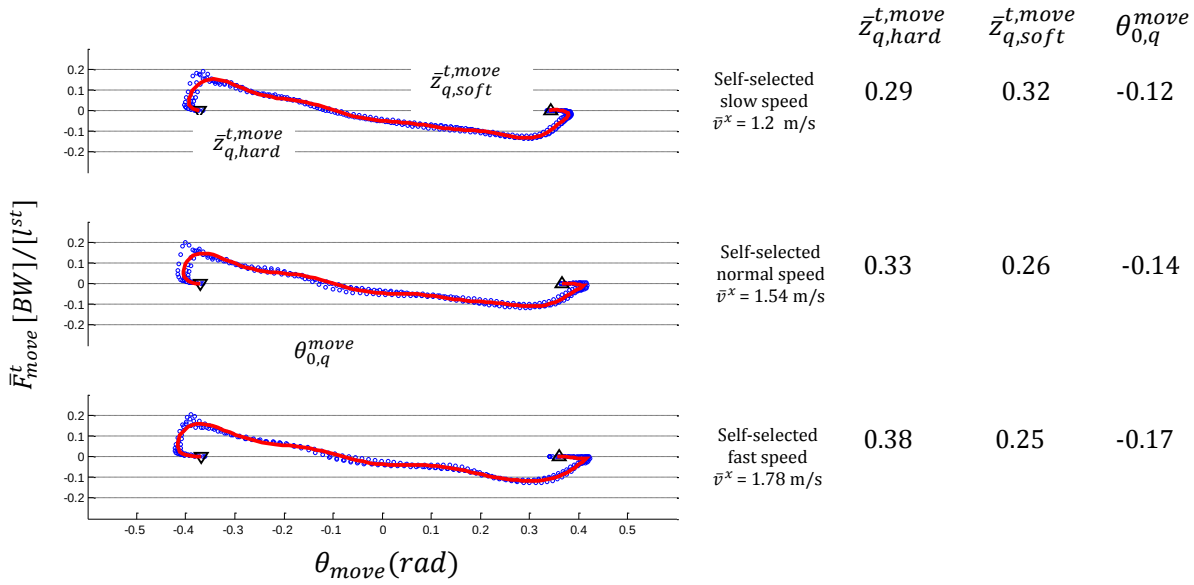

Figure 5.10 The moving contact tangential force – leg angle data set (blue) at self-selected slow, normal and fast walking speed and posture-dependent elasticity fits (red)from a representative subject (subject no.2) are shown. Tangential leg force (F_{move}^{t}) is normalised by body weight (BW) and the leg length obtained during still standing (l^{st}). Leg angle (θ_{move}) is in radian. Touchdown(td) and take-off are denoted by ∇ (td) and Δ (to). The total tangential stiffness for hard ($z_{q,hard}^{t,move}$) and soft nonlinear stiffness ($z_{q,soft}^{t,move}$) and the corresponding force-free leg angle ($\theta_{0,q}^{move}$) determined by the RMS fit are given for each walking speed. $\bar{z}_q^{t,move}$ is normalised to BW , l^{st} or $[BW \cdot l^{st}]$. $\theta_{0,q}^{move}$ is in radian. The data set is obtained from three good trials of the walking measurements of subject no.2 at each self-selected walking speed.

In Figure 5.10 for the moving contact condition, the total tangential stiffness for hard nonlinear stiffness ($z_{q,hard}^{t,move}$) increases whereas the one for soft nonlinear stiffness ($z_{q,soft}^{t,move}$) decreases with walking speed. The force-free leg angle ($\theta_{0,q}^{move}$) is consistent to

that in the fixed contact condition. The tangential force-leg angle relationship is precisely fitted during early and late stance compared with the results obtained in the same contact condition by the linear elastic fitting.

5.3.3 Summative results for all subjects

The actual and normalised values of the posture-dependent leg properties extracted from the measurement data for all three walking speeds and all the participants is processed. The summative values for both fixed and moving contact condition are list in Table 5.1-5.2.

Table 5.1 Posture-dependent axial properties during walking ($mean \pm SD$)

Axial properties		Slow(1.12-1.31 m/s)		Normal(1.35-1.54 m/s)		Fast(1.58–1.8 m/s)	
		Moving CoP	Fixed CoP	Moving CoP	Fixed CoP	Moving CoP	Fixed CoP
Linear stiffness ($k^n_{q,lin}$)	Actual (kN/m)	11.06 ± 1.68	4.54 ± 0.99	9.83 ± 1.20	4.05 ± 1.28	12.00 ± 0.884	4.65 ± 1.37
	Normalised	15.24 ±1.60	6.21 ± 0.77	13.55 ± 1.16	5.50 ± 0.86	16.66 ± 1.45	6.31 ± 1.25
Peak amplitude of force –free leg length variation (A^l_0)	Actual (m)	0.050 ± 0.011	0.071 ± 0.008	0.046 ± 0.010	0.096 ± 0.019	0.042 ± 0.016	0.101 ± 0.017
	Normalised	0.056 ± 0.011	0.078 ± 0.010	0.050 ± 0.010	0.106 ± 0.024	0.046 ± 0.016	0.112 ± 0.020
Touchdown leg length (l^{td})	Actual (m)	0.949 ± 0.030	1.015 ± 0.046	0.953 ± 0.035	1.030 ± 0.052	0.954 ± 0.038	1.046 ± 0.047
	Normalised	1.050 ± 0.017	1.123 ±0.018	1.054 ± 0.017	1.139 ± 0.027	1.056 ± 0.014	1.157 ± 0.019
Excursion length (lf-l0) or (d^l)	Actual (m)	-0.026 ± 0.008	0.037 ± 0.006	-0.018 ± 0.009	0.048 ± 0.014	-0.025 ± 0.011	0.047 ± 0.011
	Normalised	-0.029 ± 0.009	0.041 ± 0.007	-0.020 ± 0.010	0.054 ± 0.017	-0.028 ± 0.011	0.053 ± 0.015

Table 5.1 shows the axial leg properties comprising linear axial leg stiffness ($k^n_{q,lin}$), peak amplitude of force-free leg length variation (A^l_0), touchdown (l^{td}) and excursion leg length (d^l) during walking at self-selected slow, normal and fast speed. These are the averaged values for all participants. The linear axial stiffness is normalised by the body weight (BW) and the leg length during quiet standing (l^{st}). The peak amplitude of

force-free leg length variation (A_0^l) is normalised by leg length during quiet standing (l^{st}). The touchdown (l^{td}) and excursion leg length (d^l) are axial properties obtained from the mean value of the measurement data which were used directly in Equation 5.3 to extract other axial properties.

The change in linear axial stiffness of the posture-dependent leg properties ($k_{q,lin}^n$) is speed-independent and the axial stiffness extracted from walking at self-selected normal speed in both contact conditions is lowest compared to those extracted from walking at lower and higher self-selected speed. The peak amplitude of force-free leg length variation (A_0^l) are speed-dependent for both contact conditions. A_0^l on the fixed contact increases while that on the moving contact decreased as the walking speed increases.

The touchdown leg length (l^{td}) slightly increases with the increased walking speed for both contact conditions. The inter-subject variation of the touchdown leg length (l^{td}) at each walking speed is relatively low and less than 2.4% of the mean value. The excursion leg length (d^l) representing the difference of force-free leg length at touchdown and take-off is hardly dependent of walking speed for both contact conditions. This excursion leg length (d^l) is around 50% smaller than the peak amplitude of force-free leg length variation (A_0^l) for all walking speed indicating that, the posture-dependent variation of force-free leg length is much greater than difference of force-free leg length at touchdown and take-off.

Table 5.2 Posture-dependent tangential leg properties during walking ($mean \pm SD$)

Tangential properties		Slow(1.12-1.31 m/s)		Normal(1.35-1.54 m/s)		Fast(1.58–1.8 m/s)	
		moving CoP	fixed CoP	moving CoP	fixed CoP	moving CoP	fixed CoP
Total dynamic stiffness on hardening elastic profile ($z_{q,hard}^{t,fixed}$)	Actual (kN·m/rad)	0.243 ± 0.065	0.240 ± 0.069	0.256 ± 0.064	0.233 ± 0.059	0.279 ± 0.073	0.220 ± 0.038
	Normalised	0.368 ± 0.068	0.361 ± 0.074	0.386 ± 0.055	0.350 ± 0.055	0.423 ± 0.075	0.334 ± 0.029
Total dynamic stiffness on softening elastic profile ($z_{q,soft}^{t,fixed}$)	Actual (kN·m/rad)	0.204 ± 0.064	0.135 ± 0.026	0.187 ± 0.056	0.134 ± 0.035	0.179 ± 0.062	0.145 ± 0.036
	Normalised	0.306 ± 0.070	0.207 ± 0.035	0.283 ± 0.065	0.207 ± 0.058	0.269 ± 0.069	0.220 ± 0.044
Force-free contact angle $90^{\circ}+(\boldsymbol{\theta_{0,q}})$	(deg)	83.50 ± 3.38	82.43 ± 1.60	82.66 ± 1.50	82.43 ± 1.50	81.74 ± 2.06	81.92 ± 1.95
Touchdown contact angle $90^{\circ}+(\theta^{td})$	(deg)	67.0 ± 1.1	61.0 ± 0.8	66.5 ± 0.5	59.0 ± 0.8	66.0± 1.0	58.0 ± 0.5
Peak amplitude of leg angle (A^{θ})	(deg)	23.32 ± 0.92	29.41 ± 4.01	24.36 ± 0.63	31.93 ± 4.75	24.991 ± 1.26	33.02 ± 5.27

Table 5.2 shows the tangential leg properties including the total stiffness on hard ($z_{q,hard}^{t}$) and soft nonlinear elasticity ($z_{q,soft}^{t}$) and force-free contact angle ($90^{\circ}+\theta_{0,q}$) during walking at each self-selected walking speed. These values are the average of the extracted posture-dependent leg properties from the posture-dependent elastic fitting of the tangential force-leg angle data of all participants. The total dynamic stiffness is normalised by the body weight (BW) and the leg length during quiet standing (l^{st}). The touchdown (θ^{td}) and peak amplitude (A^{θ}) of leg angle are tangential properties obtained from the mean value of the measurement data which were used directly in Equation 5.1 and 5.7 to extract other tangential properties.

The total stiffness of both hard and soft nonlinear elasticity is speed-dependent. The total dynamic stiffness of the hard nonlinear elasticity ($z_{q,hard}^{t}$) for fixed contact decreases while that for moving contact increases with walking speed. In the contrary,

the total stiffness of the soft nonlinear elasticity ($z^t_{q,soft}$) for fixed contact increases while that for moving contact decreases with increased walking speed. The force-free contact angle during mid-stance ($90^\circ + \theta_{0,q}$) for both contact conditions slightly decreases with the increased walking speed. In addition, this is consistent with the results obtained from linear elastic fitting in which the force-free contact leg angle in mid-stance ($90^\circ + \theta_0^F$) in different contact conditions hardly changes with increased walking speed. The touchdown contact angle ($90^\circ + \theta^{td}$) in both contact conditions also slightly decreases with walking speed. The inter-subject variation of this touchdown contact angle ($90^\circ + \theta^{td}$) at each walking speed is relatively low or less than 2% of the mean value implying the common adjustment of touchdown leg angle with walking speed found in the participants of this study. The peak amplitude of leg angle (A^θ) increases with increased walking speed indicating that the maximum leg angle increases with increased walking speed.

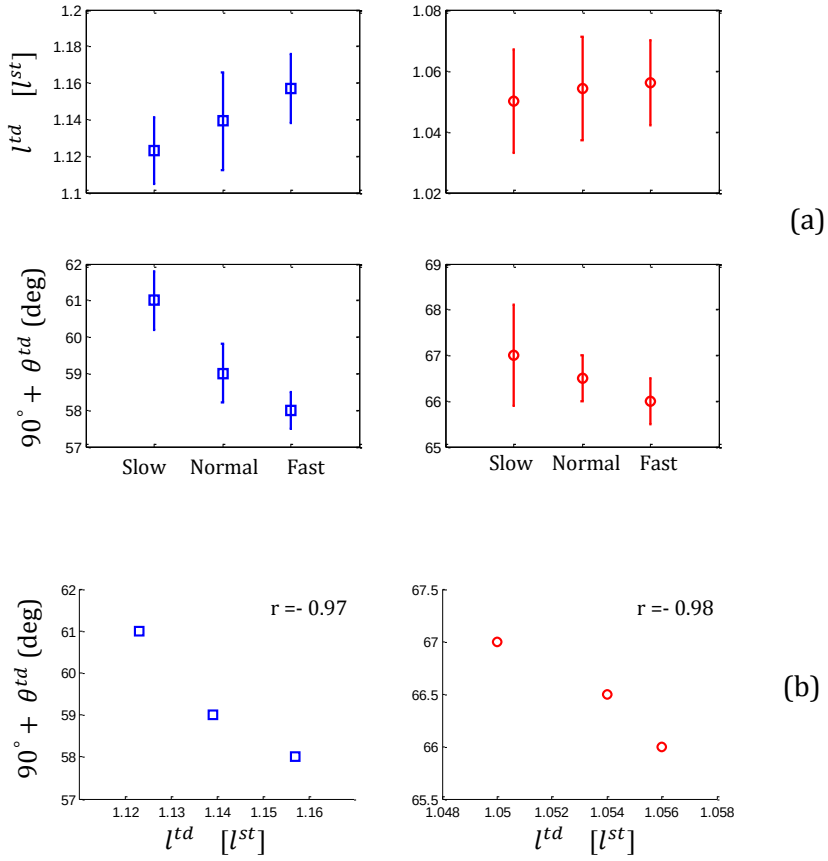

Figure 5.11 The relationship between touchdown leg length (l^{td}) and contact angle ($90^\circ + \theta^{td}$) for fixed contact (square) and moving contact (circle) represented by correlation coefficient (r) are shown. The mean value with standard deviation of touchdown leg length (l^{td}) and contact angle ($90^\circ + \theta^{td}$) at different walking speed (a) as listed in Table 5.1 and 5.2 is shown. The relationship between the mean values of touchdown leg length and contact angle on different walking speeds (b) and correlation coefficients (r) calculated for each contact condition are shown.

Indicated by correlation coefficients, the coupling between touchdown leg length (l^{td}) and contact angle ($90^\circ + \theta^{td}$) exists in both contact conditions. Since, the combination of touchdown leg length and contact angle directly indicates the touchdown height of the CoM. The increase of touchdown leg length with smaller touchdown contact angle along with the increased walking speed indicates the adjustment of touchdown height of the CoM. The correlation coefficients being close to one indicates the strong coordination between touchdown leg length and touchdown contact angle to adjust the touchdown height with walking speed.

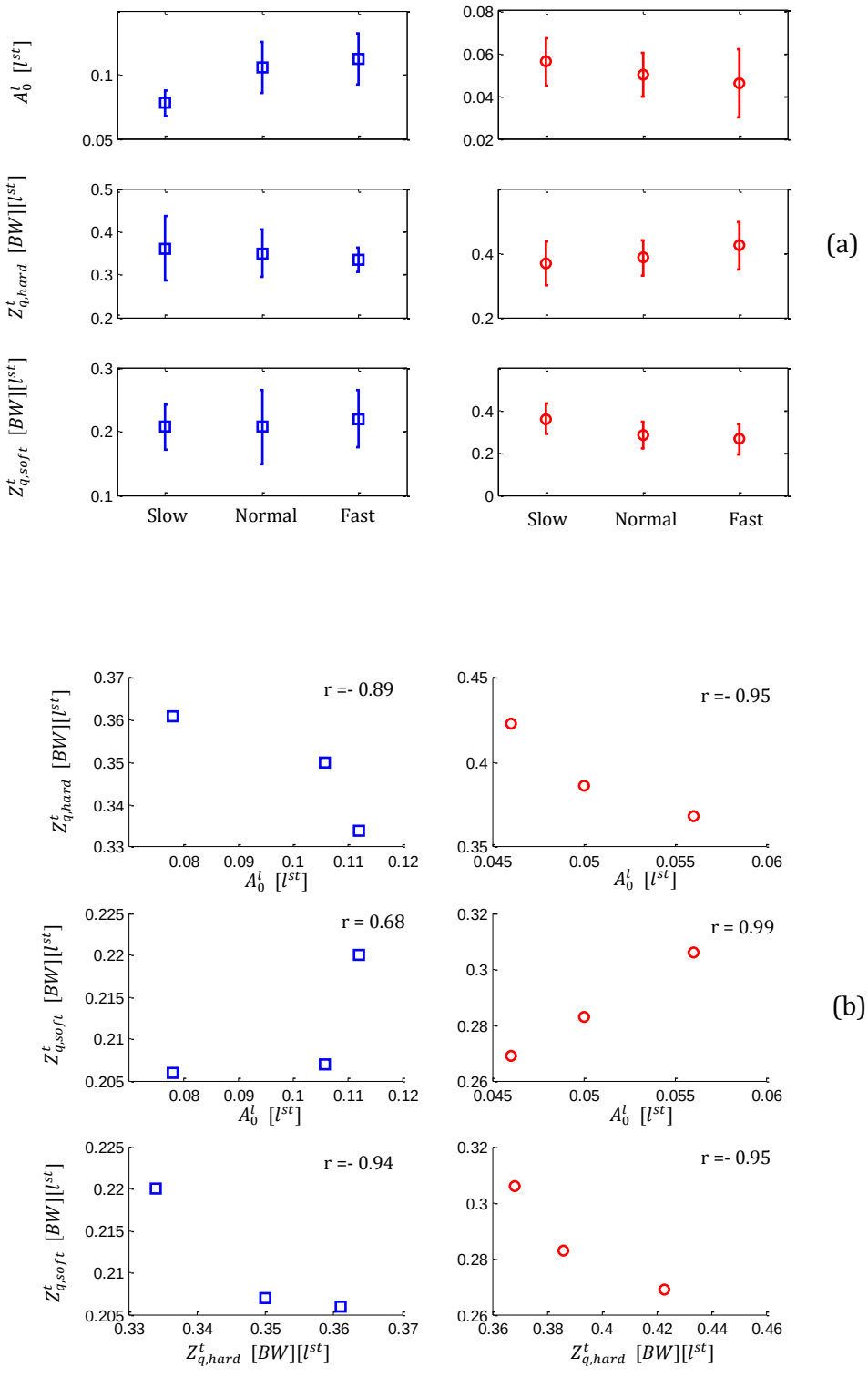

Figure 5.12 The relationship between peak amplitude of force-free leg length variation (A_0^l), total tangential stiffness of hard ($Z_{q,hard}^t$) and soft nonlinear stiffness ($Z_{q,soft}^t$) for fixed (square) and moving contact (circle) represented by correlation coefficient (r) is shown. The mean values with standard deviations of peak amplitude of force-free leg length variation (A_0^l), total tangential stiffness of hard ($Z_{q,hard}^t$) and soft nonlinear stiffness ($Z_{q,soft}^t$) at different walking speed (a) as listed in Table 5.1 and 5.2 are shown. The relationship between the mean values of each combination on different walking speeds (b) and correlation coefficients (r) calculated for each contact condition are shown.

Indicated by correlation coefficients, the coupling between peak amplitude of force-free leg length variation (A_0^l), total tangential stiffness of hard ($Z_{q,hard}^t$) and soft nonlinear stiffness ($Z_{q,soft}^t$) is found for both contact conditions. The three leg properties extracted in moving contact condition have stronger relationship than that extracted in fixed contact condition.

Extracted by posture-dependent leg property definition, the change in linear axial stiffness of the posture-dependent leg properties ($k_{q,lin}^n$) is consistent with that extracted by the linear elasticity property definition in which the change in axial stiffness is speed-independent and the axial stiffness extracted from walking at self-selected normal speed in both contact conditions is lowest compared to those extracted from walking at lower and higher self-selected speed (see Table 5.3 and Figure 5.13).

Table 5.3 The comparison between linear stiffness extracted by linear elastic and posture-dependent leg property definitions

Axial properties		Slow(1.12-1.31 m/s)		Normal(1.35-1.54 m/s)		Fast(1.58–1.8 m/s)	
		moving CoP	fixed CoP	moving CoP	fixed CoP	moving CoP	fixed CoP
Linear stiffness (k_{lin}^n) (linear elastic)	Actual (kN/m)	11.06 ± 1.68	4.54 ± 0.99	9.83 ± 1.20	4.05 ± 1.28	12.00 ± 0.88	4.65 ± 1.37
	Normalised	15.24 ±1.60	6.21 ± 0.77	13.55 ± 1.16	5.50 ± 0.86	16.66 ± 1.45	6.31 ± 1.25
Linear stiffness ($k_{q,lin}^n$) (Posture-dependent)	Actual (kN/m)	12 ± 2.5	4.2 ± 0.8	11 ± 1.7	3.6 ± 0.9	11.2 ± 2.5	4 .0± 1.3
	Normalised	16.5 ± 2.0	5.7 ± 0.6	15.2 ± 1.8	5.0 ± 0.7	15.3 ± 2.2	5.4 ± 1.2

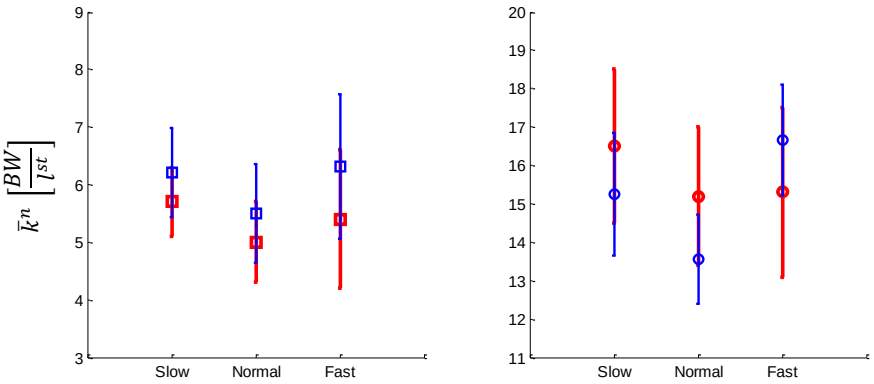

Figure 5.13 The comparison between normalised axial stiffness ($\bar{k}^n$) extracted by linear elastic and posture-dependent leg property definitions. The normalised axial stiffness extracted by linear elastic leg property definition (red) in fixed (□) and moving (○) contact condition are shown in comparison to the normalised axial stiffness extracted posture-dependent leg property definition (blue) in fixed (□) and moving (○) contact condition at each self-selected walking speed.

5.4 Discussions and conclusion

In this chapter, the posture-dependent leg properties during human walking motion have been proposed. These mechanical leg properties were extracted from human walking measurements at different self-selected walking speeds in fixed and moving condition of foot-ground contact. The passive property is represented in terms of linear axial leg stiffness. The non-conservative axial force – leg length relationship is represented by the linear axial leg stiffness and the variation of force-free leg length during the foot-ground contact. The non-conservative tangential force – leg angle relationship is represented by the mid-stance force-free leg angle and the variation of tangential stiffness during the foot-ground contact.

Extracted by posture-dependent property definition, the changes in posture-dependent force-free leg length and tangential stiffness are speed-dependent. However, the change in linear axial leg stiffness are speed-independent, which is consistent to those extracted by linear elasticity definition in Chapter 4 and a previous study (Lipfert et al., 2012).

Indicated by the correlation coefficients, the couplings between the axial and tangential properties on the different walking speeds are found. The adjustment of touchdown height of the CoM is found as a results of the coupling between touchdown leg length (l^{td}) and contact angle ($90^{\circ} + \theta^{td}$). The coupling between peak amplitude of force-free leg length variation (A_0^l), total tangential stiffness of hard ($Z_{q,hard}^t$) and soft nonlinear elasticity ($Z_{q,soft}^t$) in the moving contact condition is stronger than that in fixed contact condition. The coupling between the touchdown leg length and touchdown contact angle of posture-dependent leg properties are consistent to the results from the studies on running animals in which the adjustment of touchdown contact angle and touchdown leg length were found instead of leg stiffness (Farley et al., 1993, Blickhan et al., 2007). Those results suggested that no adjustment of leg stiffness may be required to increase or decrease running speed. This is in contrast to the linear elastic properties in the spring-mass walking model (Geyer et al., 2006) in which the change of the touchdown contact angle ($90^{\circ} + \theta^{td}$) with the change in axial leg stiffness ($k_{q,lin}^n$) along with change of walking speed was found.

The couplings between posture-dependent properties in relations to the management of elastic energy are investigated. The adjustment of touchdown leg length (l^{td}) and contact angle ($90^{\circ} + \theta^{td}$) indicates the adjustment of leg positioning which is known as the management of mechanical energy exchanges between phase transitions (Farley and Gonzalez, 1996; Geyer et al., 2005; Daley and Biewener, 2006). The coupling between the peak amplitude of force-free leg length variation (A_0^l), total tangential stiffness of hard ($Z_{q,hard}^t$) and soft nonlinear elasticity ($Z_{q,soft}^t$) potentially indicates the systematic storage- release, dissipation and production of mechanical energy managed by non-conservative force-displacement relationships of the posture-dependent axial

and tangential elasticity. This is supported by the running simulation results of the spring-loaded inverted pendulum (SLIP) model with clock-driven variation of force-free leg length (Schmitt and Clark, 2009). In this SLIP model, the mechanical energy fluctuation was managed by the proper combination of axial stiffness, the sinusoidal variation of force-free leg length and leg positioning comprising leg angle at touchdown and take-off. The fluctuation of force-free leg length on stance duration produces positive and negative work to facilitate the non-conservative leg function, which adjust the system momentum to get over external perturbation during running. The speed-dependence of axial stiffness and the fluctuation of force-free leg length were found in stable running. More supporting evidence is found in the stable running of two-segmented leg model with rotational elasticity at the knee joint (Rummel and Seyfarth, 2008). The variation of force-free leg length with the two-segmented leg geometry was introduced to represent the nonlinear force-length relationship. Such variation of force-free leg length was found to predict stable region closer to the parameter region of human running. In insects and biped animal i.e. guinea flaw, the variation of force-free leg length has been found as a feed-forward adjustment of mechanical energy against external perturbation (Dudek and Full, 2006; Daley and Biewener, 2006; Daley et al., 2007). Although, such variation of force-free leg length as the anticipation to external perturbation has never been investigated in human walking, the different force-free leg length at heel-strike and take-off can be simply observed from the human walking measurements. To support such observed evidence, the implementation of the posture-dependent free-force leg length in human walking model is performed in Chapter7.

The posture-dependent properties have many advantages over the linear and nonlinear elastic leg properties in Chapter 4 and the conventional passive leg properties in previous studies (Geyer et al., 2006; Seyfarth et al., 2006; Lipfert et al., 2012). The major advantage is the introduction of variable leg property to represent the change of axial force- leg length relationship after maximum leg compression and the change of tangential force- leg angle relationship after mid-stance force-free leg length. This allows the representation of the non-conservative force-displacement relationships of the human leg, which can facilitate in the study of the non-conserve system energy during the gait and the effect on human walking stability. In addition, the finding of the speed-dependence and the coupling between the posture-dependent properties indicates the coordination of leg mechanics to represent human walking at different speeds. This deliberate definition of the posture-dependent leg properties may render to provide insight into subject-specific property of the human leg.

Chapter 6 Human Walking Prediction and Dynamic Stability Quantification based on Fundamental Leg Properties

6.1 Introduction

In Chapter4, the fundamental leg properties extracted from the measured axial force-leg length relationship during human walking motion was found to locate within the parameter region of stable walking motion predicted by a compliant leg walking template (Geyer et al., 2006; Rummel et al., 2010). Those extracted from the measured tangential force-leg angle relationship also reproduces the tangential force in a similar profile as the predicted hip torque for the stable walking motion by spring –mass model with hip joint and torso(Maus et al., 2010). These fundamental leg properties have shown preliminarily the potential use as a fundamental template to represent the mechanical properties of the leg during human walking motion.

To provide insight into the effect of fundamental leg properties on the human walking stability, the validity region of which in human walking prediction needs to be examined. In this chapter, the compliant leg walking template (Geyer et al., 2006) is adopted to use for the dynamic stability analysis of human walking based on the axial elastic leg property. A compliant leg model with axial and tangential elastic property (CATE) is proposed to take account of the rotational dynamics corresponding to tangential elasticity of the virtual leg and, therefore, allow the dynamic stability analysis of human walking based on axial and tangential elastic leg property.

6.2 Background

The bipedal walking model based on compliant leg has been used to predict the human walking motion by using the minimal inputs of elastic leg properties comprising axial leg properties and initial contact angle ($\theta_{td}^{contact}$). In a particular range of walking motion, the proper combinations of axial leg stiffness (k^n) and touchdown leg angle ($\theta_{td}^{contact}$) are required to produce periodic walking motion. However, this production is rather sensitive to the initial condition of the walking motion especially the initial forward speed (v_0^x) which regulates the forward rotation of CoM with respect to the contact point. The proper horizontal speed allows sufficient duration for the upright CoM, which allows the proper energy transfer among potential, strain and kinetic energy. As a result, the proper oscillation of the CoM on the compliant leg is created, which regulates the initiation and termination of double support phase and forward progression the CoM to complete the walking step. In this model, the CoM oscillation increases with increased walking speed. The CoM becomes airborne and fails to complete walking cycle when the walking speed exceeds 1.5 m/s (Geyer et al., 2006). This walking speed limit of the compliant leg walking template restricts the human walking prediction based on the axial elastic leg properties to the moderate walking speed.

Depending on the axial leg properties alone, the CoM motion predicted by compliant leg walking model is regulated by the touchdown contact angle ($\theta_{td}^{contact}$), axial stiffness (k^n) and the initial condition of the CoM motion. The incorporation of the tangential component of the leg force or the rotational elasticity of the virtual leg may render to extend the walking speed range predicted by compliant leg walking model.

In this chapter, to examine the validity region for human walking prediction, the axial and tangential leg properties obtained from the human walking measurement in chapter 3 are fed into the simple walking models. Then, the prediction results are used to quantify the dynamic stability of human walking. The interrelation between the human walking motion predicted by the compliant leg model with axial elastic leg property (CAE) and that predicted by the compliant leg model with axial and tangential elastic leg property (CATE) is investigated. Using the CATE model, the effect of the rotational elasticity of the virtual leg on the dynamic stability of human walking is investigated. The assumption of energy conservation during human walking motion is used on both simple walking models.

6.3 Human walking prediction based on fundamental leg properties

Based on the best fits on the measurement data, the combinations of the fundamental leg property, for example, axial stiffness (k^n) and force-free leg angle (θ_0) may not reproduce human walking motion. The examination for the validity region of this leg property for human walking prediction is required.

For the validity region in predicting human walking motion, the fundamental leg property parameters comprising axial (k^n) and tangential stiffness (k^t), rest length (l_0) and force-free angle (θ_0) are examined. The compliant leg model with axial elastic property (CAE) is used to examine the validity region of axial elastic leg property parameters comprising axial stiffness (k^n), rest length (l_0) and touchdown leg angle (θ^{td}). To examine the validity region of fundamental leg property parameters comprising axial (k^n) and tangential stiffness (k^t), rest length (l_0) and force-free leg

angle (θ_0), the compliant leg model with axial and tangential elastic leg property (CATE) is proposed. The asymmetrical walking motion on the conservation of system energy is illustrated by the operation of axial-tangential elastic leg. The comparison between the human walking motion predicted by conventional and proposed model is presented.

6.3.1 A simple model of human walking based on minimal leg properties

For the minimal model such as compliant leg model with axial elastic property (CAE), a previous study using dynamic leg property parameters extracted from human walking measurement showed the successful prediction of human walking only at the slow walking or at speed of 1.04 m/s (Lipfert et al., 2012). This may be affected by the speed limitation of the compliant leg model with axial elastic property (CAE) and the definition of the dynamic leg property used in the extraction from human walking measurement. The accuracy and the validity region of the human walking prediction may be improved by a careful selection of the input parameters and the utilisation in the nature of the model.

Despite the walking speed limit, the compliant leg model with axial elastic property (CAE) can be utilised as a human walking template based on minimal leg properties in which only the axial stiffness (k^n) and the rest length (l_0) are the required leg parameters. In order to utilise that minimal requirement, the input parameters in terms of initial motion and dynamic leg properties need to be selected and extracted carefully from human walking measurement. The prediction of the human walking motion may not be produced by directly feeding the measured inputs into the minimal model. The nature of the compliant leg model with axial elastic property (CAE), for examples, the

fixed rest length throughout walking cycle and the coupling between the walking speed and leg stiffness needs to be maintained such that the axial elasticity can be the only required leg mechanics to operate the walking model. Thus, some alteration in the input parameters, which are obtained from walking measurement, is required to allow some proper axial elasticity for the leg operation in this minimal walking model. In this way, the actual validity region of human walking prediction based on the axial elastic leg properties can be analysed.

The prediction of human walking motion based on the axial elasticity of the virtual leg requires the input parameters comprising the initial condition of the CoM and axial properties namely, the axial leg stiffness (k^n), rest length (l_0) and the touchdown contact angle ($\theta_{td}^{contact}$). In this minimal model, the symmetrical walking is assumed, and no influence of the swing leg is taken into account. The equations of motion of the CoM during a walking step can be given by

$$m\ddot{x} = P^* x \tag{6.1}$$

$$m\ddot{y} = P^* y - mg \tag{6.2}$$

for the initial single support phase,

$$m\ddot{x} = P^* x - Q^*(d - x) \tag{6.3}$$

$$m\ddot{y} = P^* y + Q^* y - mg \tag{6.4}$$

for the double support phase and

$$m\ddot{x} = -Q^*(d - x) \tag{6.5}$$

$$m\ddot{y} = Q^* y - mg \tag{6.6}$$

for the final single support phase, where

$$P^* = k^{n*}\frac{(l_0 - l^{trail})}{l^{trail}} \tag{6.7}$$

$$Q^* = k^{n*}\frac{(l_0 - l^{lead})}{l^{lead}} \tag{6.8}$$

The leg length (l) during the walking motion can be determined by

$$l^{trail} = \sqrt{x^2 + y^2} \tag{6.9}$$

$$l^{lead} = \sqrt{(d - x)^2 + y^2} \tag{6.10}$$

The forward dynamics model begins at the vertical leg orientation (VLO) with the initial condition given by

$$\begin{aligned} x(0) &= x, \quad \dot{x}(0) = \dot{x}_i, \\ y(0) &= y_i, \quad \dot{y}(0) = 0. \end{aligned} \tag{6.11}$$

The transition from single to double support occurs when

$$y = l_0\, sin(\theta_{td}^{contact}). \tag{6.12}$$

The transition from double to single support occurs when

$$l^{trail} = l_0. \tag{6.13}$$

The leg stiffness (k^{n*}) can be either a linear (k_{lin}^{n}) or non-linear stiffness (Equation 4.3) depending on the elasticity condition used in the extraction. x is the horizontal distance between the CoM and the contact point. i is the step number. l_0 is the rest length. The touchdown contact angle ($\theta_{td}^{contact}$) is the angle between horizontal and the virtual leg at touchdown instant. m is the whole-body mass, g is gravity and d is the step length defined by the distance between the contact point of leading and trailing leg (see Figure 6.1). The force equations of this model can be found in Appendix B.

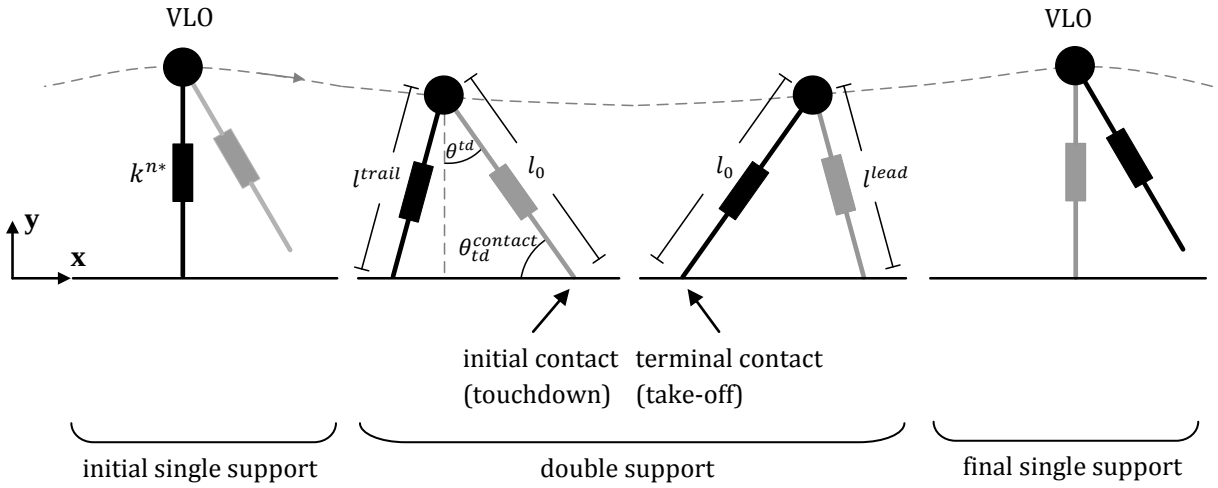

Figure 6.1 The minimal model of human walking based on axial elastic leg properties adopted from (Geyer et al., 2006) is shown. A walking step simulation begins with the initial single support at vertical leg orientation (VLO) of the trailing leg, enters the double support phase at the touchdown instant of the leading leg and then, enters the final single support at the take-off instant of the trailing leg before terminating the termination step at the consecutive vertical leg orientation (VLO).

The equations of motion are numerically solved by using the numerical integrator (ode113) in MATLAB (R 2010a) with an integration step size of 0.001s and an absolute error tolerance of 0.001 metre. The input parameters comprising subject's body mass (m), the initial condition (Equation 6.11), linear (k_{lin}^{n}) or non-linear leg stiffness

(Equation 4.3) and touchdown contact angle ($\theta^{cont,td}$) as presented in Chapter 4 are required.

Due to the walking symmetry, it suffices to obtain a periodic walking motion from the 100 repetition of a single step defined by two subsequent vertical leg orientations. At vertical leg orientation (VLO), the CoM motion reaches the apex or $x = \dot{y}(0) = 0$ and thus, the initial motion can be reduced to $\dot{x}(0) = \dot{x}_i$, $y(0) = y_i$. The height (y_i) and horizontal velocity ($\dot{x}_i$) of the CoM at the instant of vertical leg orientation are considered as state variables (s) or s_i= [$y_i, \dot{x}_i$] and the periodic gait pattern is identified when the difference between the initial and consequent state after one walking step is smaller than absolute error tolerance or $\sum_{j=1}^{2}|s_{i+1,j} - s_{i,j}| < 0.001$ when i = step number and j = state variable number.

6.3.2 A simple model of human walking based on the fundamental leg properties

The fundamental leg properties as presented in Chapter 3 require a compliant leg model with both of the axial and rotational elasticity during human walking. A compliant leg model with axial and tangential elastic property (CATE) is proposed in this section to take account of the rotational dynamics generated by the tangential elasticity of the virtual leg. An additional parameter, velocity angle (θ_0^v), the angle between the total and horizontal velocity of the CoM at vertical leg orientation is introduced to allow for the prediction of asymmetrical walking motion. The initial condition of the CoM motion and the fundamental leg properties comprising axial (k^n) and tangential leg stiffness (k^t), rest length (l_0) and the three of force-free leg angles (θ_0) (see Equation 4.1, 4.4 and 4.5

in Chapter 3) are required in the examination of the validity region of human walking prediction. The equations of motion of the CoM during a walking step can be given by

$$m\ddot{x} = Px + Ry \tag{6.14}$$

$$m\ddot{y} = Py - Rx - mg \tag{6.15}$$

for the initial single support phase,

$$m\ddot{x} = Px - Q(d - x) + (R + S)y \tag{6.16}$$

$$m\ddot{y} = (P + Q)y - Rx + S(d - x) - mg \tag{6.17}$$

for the double support phase and

$$m\ddot{x} = -Q(d - x) + Sy \tag{6.18}$$

$$m\ddot{y} = Qy + S(d - x) - mg \tag{6.19}$$

for the final single support phase, where

$$P = k_{lin}^{n} \frac{(l_0 - l^{trail})}{l^{trial}} \tag{6.20}$$

$$Q = k_{lin}^{n} \frac{(l_0 - l^{lead})}{l^{lead}} \tag{6.21}$$

$$R = k_{lin}^{t} \frac{(\theta_0 - \theta^{trail})}{(l^{trail})^2} \tag{6.22}$$

$$S = k_{lin}^{t} \frac{(\theta_0 - \theta^{lead})}{(l^{lead})^2} \tag{6.23}$$

$$\theta^{trail} = tan^{-1} \frac{x}{y} \tag{6.24}$$

$$\theta^{lead} = tan^{-1}\frac{d-x}{y} \tag{6.25}$$

The linear axial (k_{lin}^{n}) and tangential stiffness (k_{lin}^{t}) and the force-free leg angle (θ_0) presented in Chapter 4 are used in Equation 6.20-6.23. The force equations for CATE model can be found in Appendix B. The same criteria used for the transitions between single and double support in the compliant leg model with axial elastic leg property (CAE) (see Equation 6.12 and 6.13) are adopted here.

This forward dynamic model begins with the initial condition capable of representing both symmetrical and asymmetrical walking motion given by

$$\begin{aligned} x(0) = x, \quad \dot{x}(0) = \dot{x}_i, \\ y(0) = y_i, \quad \dot{y}(0) = \dot{x}_i\, tan(\theta_0^v). \end{aligned} \tag{6.26}$$

The velocity angle (θ_0^v) is introduced to represent the horizontal and vertical velocity of the CoM at the vertical leg orientation (see Figure 6.2). In this model, the vertical leg orientation (VLO)can occur before or after the apex of the CoM motion and possesses both vertical and horizontal velocity in which $tan^{-1}(\frac{\dot{y}_i}{\dot{x}_i}) = \theta_0^v$ represents the direction of the total velocity of the CoM (see Figure 6.2). The initial condition can be expressed by the CoM height (y_0), the horizontal ($\dot{x}_0$) and vertical velocity ($\dot{y}_0$) for both symmetrical and asymmetrical walking motion. Hence, the state variables (s) can be expressed by s_i= $[y_i, \theta_i^v]$ when θ_0^v is the velocity angle introduced earlier in terms of horizontal ($\dot{x}_0$)

and vertical velocity ($\dot{y}_0$) and i = step number. The periodic motion is identified by the similar criterion as used in the axial elastic leg model.

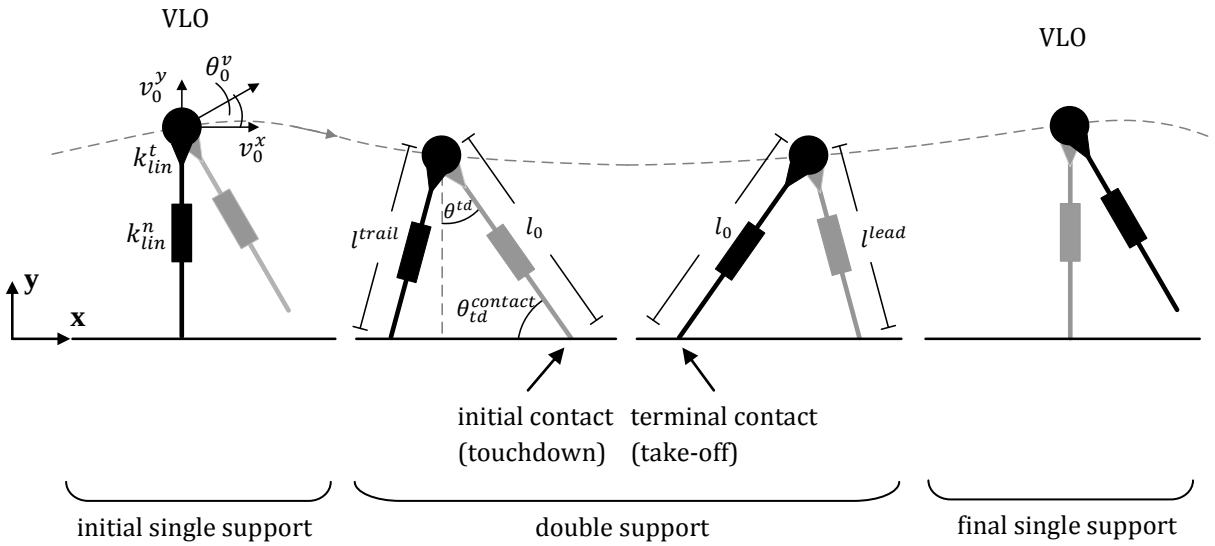

Figure 6.2 A Simple model of human walking based on axial-tangential elastic leg properties is shown. A walking step simulation begins with the initial single support at vertical leg orientation (VLO) of the trailing leg, enters the double support phase at the touchdown instant of the leading leg and then, enters the final single support phase at the take-off instant of the trailing leg before terminating the simulation step at the consecutive vertical leg orientation (VLO). It should be noted that the apex motion of the CoM does not occur at the vertical leg orientation.

6.3.3 Human walking simulation

For each individual subject, the extracted leg properties and the initial condition of CoM motion are fed into the simple walking models. The normalised value is not used in the simulation as in the compliant leg model the leg length at still standing (l^{st}) is not a constant. This leg length varies with axial stiffness (k^n) and, thus, should not be used in normalisation of the leg properties. In this case, the simulation results will be normalised by the rest length (l_0).

Provided by the minimum RMSE fitting of the measurement data, none of the leg property combination extracted can lead the simple walking models to the periodic walking motion. We hypothesize that by given the extracted leg stiffness, the measured initial condition generates too low potential energy change between vertical leg orientation (VLO) and touchdown (td) to transfer to other forms of mechanical energies. Based on the conservation of the walking system energy, the proper energy exchanges among the potential, strain and kinetic energy are required to achieve a walking cycle simulation (Geyer et al., 2006; Rummel et al., 2010). The unsuccessful reproduction of periodic walking motion implies that the combination of measured initial condition ($y_0, \dot{x}_0$), the extracted leg stiffness (k^n), rest length (l_0) and touchdown contact angle ($\theta_{td}^{contact}$) cannot produce the proper works to satisfy such energy transfer requirement. Thus, to examine the validity region of human walking prediction based on the extracted axial stiffness, we allow the combination of the rest length (l_0), touchdown contact angle ($\theta_{td}^{contact}$) and the initial condition comprising the height (y_0) and horizontal velocity ($\dot{x}_0$) of the CoM to vary around 80-120 % of the mean of measured values; while the linear axial stiffness (k_{lin}^n) is maintained at the extracted value. For the non-linear stiffness (k_{nln}^n), the basic linear stiffness ($k_{lin,b}^n$) in Equation 4.3, Chapter 4 is maintained while the coefficients (a, b) and other model parameters are allowed to penetrat within the defined allowance. Despite the absence of soft nonlinear stiffness from the minimum RMSE fitting as presented in Chapter 4, the validity region of soft nonlinear stiffness in human walking prediction can be examined at a similar energy level as that of the hard nonlinear stiffness.

The leg property parameter search was conducted to find the nearest values to that of extracted leg property parameters, which can reproduce periodic walking motion. Each

parameter is examined at 1% increment above and below the extracted value, respectively. The search gives priority to the tangential stiffness (k^t), rest length (l_0), velocity angle, initial horizontal ($\dot{x}_0$) and vertical velocity of the CoM ($\dot{y}_0$), respectively.

For the compliant leg model with axial and tangential elastic property (CATE), the similar allowance as in the compliant leg model with axial elastic property (CAE) is applied to the axial leg property. To examine the validity region of fundamental leg property in predicting the human walking motion, the tangential leg property are also allowed to vary around 80-120% of the extracted value while the velocity angle (θ_0^v) is maintained at the mean of measured value.

6.3.4 Prediction results

To provide insight into the individual walking motion, the measured initial condition and the extracted leg properties of a representative subject were investigated. Among the periodic walking motions predicted by the CAE and CATE models, the leg properties and initial conditions with smallest deviation from the extracted values and the mean of measured values were selected to show in Table 6.1. The total stiffness of the axial elasticity (z^n) (see Equation 4.9) was calculated to compare between the linear, hard nonlinear and soft nonlinear stiffness. For the CATE model (see sub-section 4.3.2, Chapter 4,), in addition to the axial elastic properties (see Equation 4.1-4.3), the four linear tangential stiffness (k^t) and three force-free leg angles (θ_0) (see Equation 4.4 - 4.6) are used in the prediction of periodic human walking motion. The total stiffness of the tangential elasticity (z^t) (see Equation 4.10) was also calculated.

Predicted by the CAE model using the extracted linear axial stiffness (k_{lin}^{n}), the rest length (l_0) and initial condition being within 8% above the extracted value and the means of measured values were found to produce a periodic motion of human walking at the walking speed of 1.18 m/s. With the hard nonlinear stiffness, the periodic walking solution is found with the total stiffness (z^n) and initial condition being within 20% below the extracted value and means of measured values. Both of linear and nonlinear axial stiffness underestimates the walking speed and rest length (l_0) obtained from human walking measurement.

Predicted by the CATE model using the extracted velocity angle (θ_0^v) and linear axial stiffness (k_{lin}^{n}), the other leg properties and initial condition being within 5% below and above the extracted and mean values produced a periodic motion of human walking at the walking speed of 1.25 m/s. Similar to the prediction by the compliant leg model with axial elastic property (CAE), this model underestimates the walking speed and rest length (l_0) while overestimates the CoM height at vertical leg orientation (y_0).

Within the given allowance, the leg properties on fixed contact fail to reproduce even a single cycle human walking. The proper combination of the leg properties and the initial condition of the CoM motion is required to reproduce the periodic motion of human walking by using simple walking models.

The ground reaction force (GRF), CoM displacement (x, y), leg length (l) and leg angle (θ) during a walking step of the periodic motion predicted by CAE model with linear and nonlinear stiffness and the CATE model with linear stiffness as shown in Table 6.1 are compared and analysed (see Figure 6.3 -6.7).

Table6.1 The mechanical properties and initial conditions leading the periodic walking motion predicted by compliant leg model with axial elastic property (CAE) and compliant leg model axial and tangential elastic property (CATE) are shown. The parameter set is based on the walking measurements of subject no.2 at each self-selected walking speed.

		Linear axial		Nonlinear axial(hard)		Nonlinear axial(soft)		Linear axial and tangential	
		model	Fitted	model	fitted	model	fitted	model	fitted
z^n	(kN/m)	10.98	10.98	11.08	17.94	13.3	-	10.98	10.98
k^t	$(kN.m/rad)$	-	-	-	-	-	-	2.23	2.23
								0.45	0.43
								0.21	0.23
								1.07	1
l_0	(m)	0.968	0.982	0.972	0.986	0.972	-	0.972	0.982
$\theta_0^{contact}$	(deg)	70	67.5	69.5	67.5	69.5	-	69.5	67.5
								85.4	83.5
								-68.2	-67.8
m	(kg)	69	69	69	69	69	-	69	69
$\dot{x}_0$	(m/s)	1.1	1.2	0.98	1.2	1.04	-	1.15	1.2
y_0	(m)	0.921	0.921	0.935	0.921	0.935	-	0.936	0.921
θ_0^v	(deg)	-	-	-	-	-	-	7	7

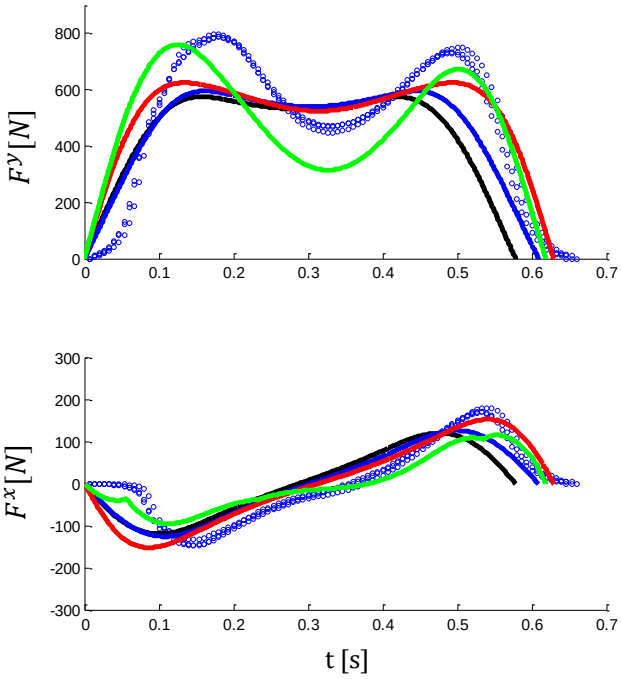

RMSE	Linear axial	Nonlinear axial (hard)	Nonlinear axial (soft)	Linear axial and tangential
$F^y[N]$	124	88.4	60.2	46.4
$F^x[N]$	41.6	33.6	23.8	30.4

Figure 6.3 The predicted vertical (a) and horizontal (b) ground reaction force by CAE model with linear (black), hard nonlinear (blue) and soft nonlinear (red) axial stiffness and by CATE model with linear axial-tangential stiffness (green) as shown in Table 6.1 compared to the measured ground reaction force at self-selected low waling speed (dot). The data set is obtained from three good trials of the walking measurements of subject no.2 at self-selected low walking speed.

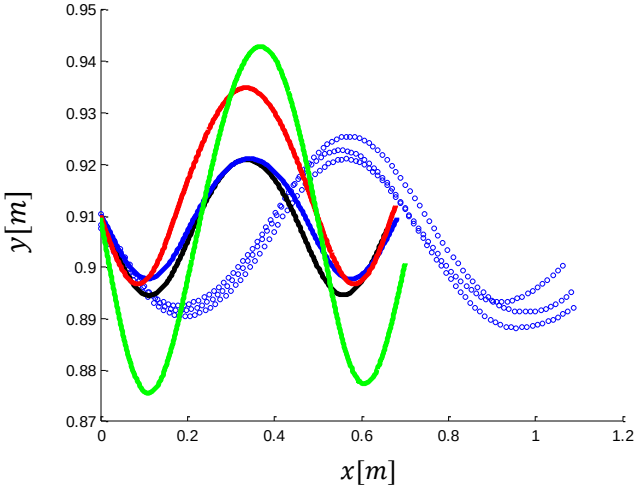

RMSE	Linear axial	Nonlinear axial (hard)	Nonlinear axial (soft)	Linear axial and tangential
$x[m]$	0.52	0.48	0.44	0.40
$y[m]$	0.03	0.024	0.028	0.038

Figure 6.4 The predicted CoM displacement (x, y) by CAE model with linear (black), hard nonlinear (blue) and soft nonlinear (red) axial stiffness and by CATE model with linear axial-tangential stiffness (green)as shown in Table 6.1 compared to the measured CoM displacement (x, y) at self-selected low walking speed (dot). The data set is obtained from three good trials of the walking measurements of subject no.2 at self-selected low walking speed.

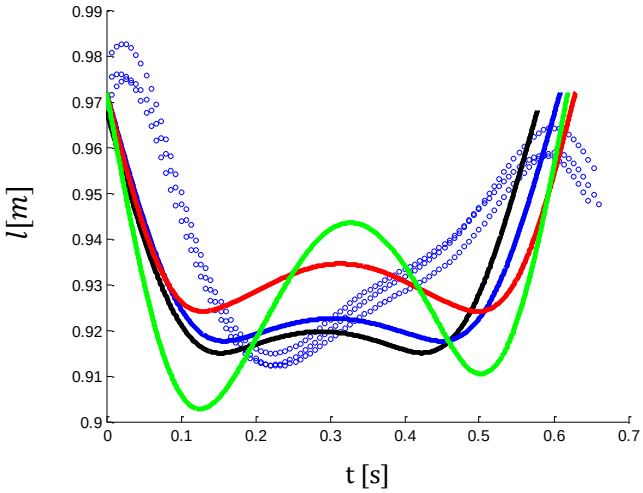

RMSE	Linear axial	Nonlinear axial (hard)	Nonlinear axial (soft)	Linear axial and tangential
$l[m]$	0.098	0.088	0.072	0.116

Figure 6.5 The predicted leg length (l) by CAE model with linear (black), hard nonlinear (blue) and soft nonlinear (red) axial stiffness and by CATE model with linear axial-tangential stiffness (green) as shown in Table 6.1 in compared to the measured leg length at self-selected low speed (dot). The data set is obtained from three good trials of the walking measurements of subject no.2 at self-selected low walking speed.

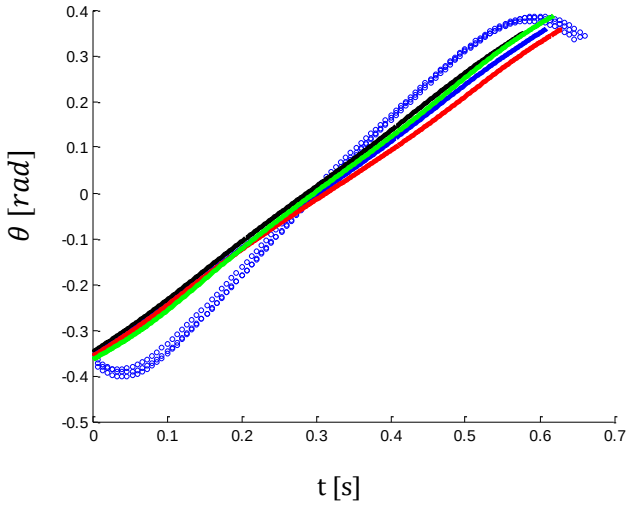

RMSE	Linear axial	Nonlinear axial (hard)	Nonlinear axial (soft)	Linear axial and tangential
$\theta[rad]$	0.1	0.06	0.08	0.1

Figure 6.6 The predicted leg angle (θ) by CAE model with linear (black), hard nonlinear (blue) and soft nonlinear(red) axial stiffness and by CATE model with linear axial-tangential stiffness (green) as shown in Table 6.1 compared to the measured leg angle at self-selected low walking speed (dot). The data set is obtained from three good trials of the walking measurements of subject no.2 at self-selected low walking speed.

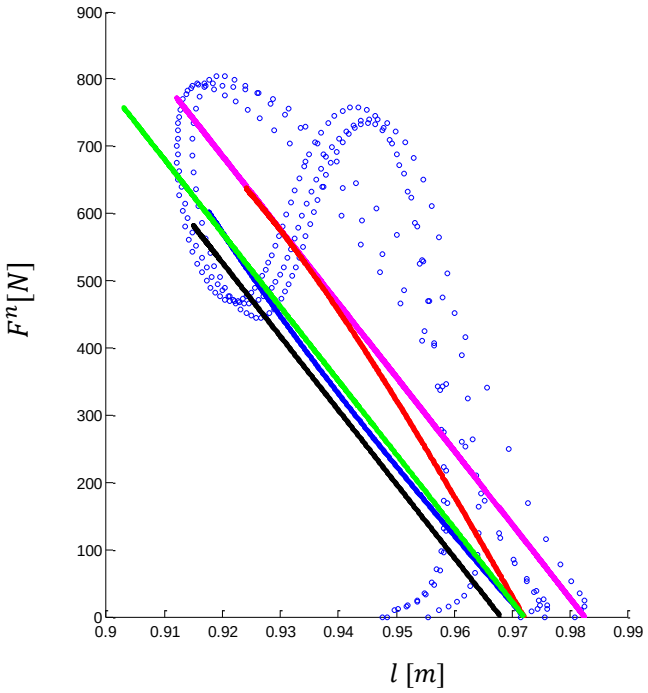

RMSE	Linear axial	Nonlinear axial (hard)	Nonlinear axial (soft)	Linear axial and tangential	Linear fitting
$F^n[N]$	131.1	121.5	98.5	86.3	84.6
$l[m]$	0.098	0.088	0.072	0.116	-

Figure 6.7 The predicted axial force-leg length relationship by CAE model with linear (black), hard nonlinear (blue) and soft nonlinear (red) axial stiffness and the linear axial-tangential stiffness (green) as shown in Table 6.1 compared to the axial force-leg length relationship obtained from linear elastic fitting (magenta) and three good trials of the walking measurements of subject no.2 at self-selected low walking speed (dot).

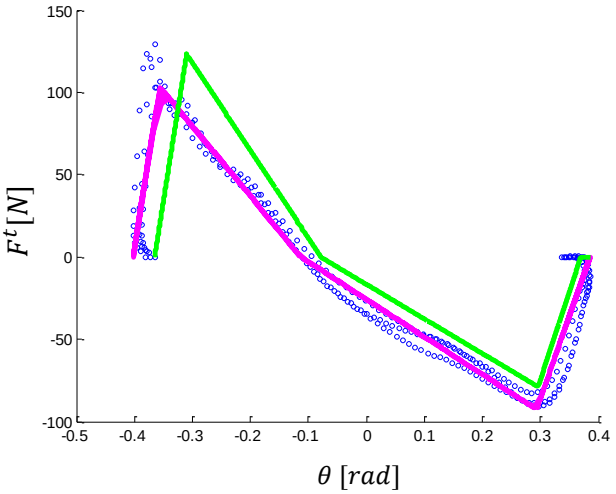

RMSE	Linear axial and tangential	Linear fitting
$F^t[N]$	38.5	30.6
$\theta[rad]$	0.1	-

Figure 6.8 The predicted tangential force-leg angle relationship by CATE model with linear axial-tangential stiffness (green) as shown in Table 6.1 compared to the tangential force-leg angle relationship obtained from linear elastic fitting (magenta) and three good trials of the walking measurements of subject no.2 at self-selected low walking speed (dot).

In Figure 6.3, predicted by the compliant leg model with axial stiffness alone, the horizontal ground reaction force (F^x) is well estimated while the vertical ground reaction force (F^y) is generally underestimated. The peak magnitude of both vertical and horizontal ground reaction force is better predicted by using hard and soft nonlinear stiffness. These two types of nonlinear stiffness also prolong the contact duration compared to that predicted by using linear axial stiffness. The incorporation of linear tangential stiffness provides the best prediction of the peak magnitude of vertical ground reaction force but underestimates that of the horizontal ground reaction force. The linear tangential stiffness also prolongs the contact duration compared to that predicted by compliant leg model with linear axial stiffness alone. The asymmetry of the vertical and horizontal ground reaction force is well predicted by the compliant model with axial and tangential elastic leg property (CATE).

In Figure 6.4, all conditions of the leg stiffness underestimate the horizontal displacement of the CoM. The vertical displacement of the CoM is well predicted by the linear and hard nonlinear axial stiffness, while it is overestimated by the soft nonlinear axial stiffness and the incorporation of linear tangential stiffness.

In Figure 6.5, obtained from the measurement, the non-conservative leg length after the mid-stance cannot be predicted by any compliant leg models. The maximum leg shortening in the early stance is well predicted by CAE model with linear and hard nonlinear stiffness. However, the leg shortening after the mid-stance predicted by both compliant leg models cannot be found in the leg length obtained from the measurement.

In Figure 6.6, the nonlinearity of leg angle obtained from the human walking measurement cannot be predicted by any compliant leg models. However, the instant of vertical leg orientation is well predicted by both compliant leg models.

In Figure 6.7, primarily due to the difference in rest lengths, the axial force-leg length relationships leading to the periodic walking motion shifts away from that provided by minimum RMSE fitting. Based on the compliant leg model with axial stiffness alone, the maximum axial force and maximum leg shortening are underestimated. However, by incorporating the linear tangential stiffness, the maximum leg shortening is overestimated and results in higher maximum axial force.

In Figure 6.8, mainly due to the difference in force-free leg angles, the tangential force-leg angle relationship leading to the periodic walking motion shifts away from that provided by minimum RMSE fitting. The CATE model using linear axial-tangential stiffness overestimates the leg angle (θ) during early stance while underestimates the tangential force during late stance.

The periodic walking motion predicted by CAE model well reproduces the vertical displacement of the CoM (y) (RMSEs are 0.03, 0.024 and 0.028 m for linear, hard nonlinear and soft nonlinear axial elasticity, respectively), but underestimates the vertical ground reaction force (F^y) (RMSEs are 124, 88.4 and 60.2 N for linear, hard nonlinear and soft nonlinear axial elasticity, respectively). It also well reproduces the maximum leg shortening (RMSEs of the leg length are 0.098, 0.088 and 0.072 m for linear, hard nonlinear and soft nonlinear axial elasticity, respectively) but underestimates the maximum axial force (RMSEs of the axial force are 131.1, 121.5 and 98.5 N for linear, hard nonlinear and soft nonlinear axial elasticity, respectively).

For periodic walking motion predicted by CATE model, the asymmetrical ground reaction forces are well reproduced (RMSEs are 46.4 and 30.4 N for vertical and horizontal ground reaction force, respectively). The vertical ground reaction force (F^y) is well reproduced (RMSE = 46.4 N) while the vertical displacement (y) is overestimated (RMSE = 0.038 m). The maximum axial and tangential force is well reproduced (RMSEs are 86.3 and 38.5 N for the linear axial and tangential force, respectively) while the maximum leg shortening and the leg angle during the early stance are overestimated (RMSEs are 0.116 and 0.1 m for leg length and leg angle, respectively).

Predicted by both compliant leg models, the horizontal displacements of the CoM (x) are underestimated (RMSEs are 0.52, 0.48, 0.44 and 0.40 m for linear axial, hard nonlinear axial, soft nonlinear axial and linear axial-tangential elasticity, respectively). The leg lengths are underestimated during the late stance. The nonlinear leg angle obtained from the walking measurement cannot be reproduced.

It is found in this chapter that different components of leg property affect on the predictions of different gait dynamics. The CAE model using linear axial stiffness is proficient in predicting the vertical displacement of the CoM. The nonlinearity of axial stiffness in CAE model and the incorporation of tangential elasticity in CATE model prolong the stance duration to the linear axial stiffness in CAE model. The incorporation of tangential elasticity improves the prediction of vertical ground reaction force while overestimates the vertical displacement. It is interesting that the leg property component, which improves the prediction of vertical displacement, does not improve that of vertical ground reaction force and vice versa.

In addition, none of the dynamic leg properties can predict the leg lengthening obtained from the late stance of human walking, which may be a major source of the underestimation of the horizontal displacement of the CoM. The leg shortening after the mid- stance predicted by both compliant leg models reproduces the second peak of the vertical ground reaction force while attenuates the forward progression of the CoM. On one hand, this re-shortening of the virtual leg is crucial for the elastic leg operation in carrying on the periodic walking motion, but on the other hand it is one of the major drawbacks in the prediction of the leg length and horizontal displacement of the CoM.

6.4 Dynamic stability analysis of human walking motion

In section 6.3, a periodic walking motion is identified when the absolute error of the state variables is smaller than the defined tolerance or $\sum_{j=1}^{2}\left|s_{i+1,j}-s_{i,j}\right|<0.001$. If $\sum_{j=1}^{2}\left|s_{i+1,j}-s_{i,j}\right|>0.001$, one of the two fall modes namely a fall backwards and a trip will occurs in the further steps of walking simulation and the corresponding leg

properties of which will not be taken into account for the data analysis. In this section, the dynamic stability of the periodic walking motion is analysed. A periodic motion is stable, if it can return to original state at a given interval after a disturbance. In our study, the human walking motion is treated as a periodic motion in which the stability is investigated at the interval of vertical leg orientation (VLO). The Poincare map is created for the local stability analysis. The local stability is examined on different leg properties and then the change in the initial condition is introduced to evaluate the sensitivity of the dynamic stability to the initial condition. This sensitivity is used to quantify the global stability in term of robustness.

6.4.1 The Poincare map and maximum Floquet multiplier

From the periodic walking solutions at a particular interval of each walking step, the initial (s) and the resulting state variables ($P(s)$) are captured to investigate the return tendency of the state variables. The collection of this capture throughout the consecutive walking steps is called Poincare map (see sub-section 2.4.1 in Chapter 2). This mapping of the state variables from one to the next walking step represents the tendency of the system's state to return to the steady state. If $P(s) = s$, it means that, at a specified interval of each walking step, the resulting state returns to initial state and will always return to this state in the further walking steps. This ideal state leading the system to the origin is so called a fixed point and the returning orbit of which is called the limit cycle. However, the system's state starting close to the fixed point can also converge to steady state. The convergence of the system's state can be analytically examined by constructing the Jacobian matrix around the fixed point to evaluate the gradient of the Poincare map. With our simulation results, the Jacobian matrix can be

determined numerically as in the following scheme (Tedrake, 2004). First, on the periodic walking motion, the fixed point is estimated by the state variables at vertical leg orientation (VLO)that results in the smallest deviation between themselves and those at the consecutive step or $min\ \sum_{j=1}^{2}\left|s_{i+1,j} - s_{i,j}\right|$ when i= number of walking step and j = number of state variable. Then the gradient of the Poincare map around the fixed point or the Jacobian matrix can be created by exploiting the system's state at the vertical leg orientation of all the walking steps (i = 100 steps). The matrix can be written by

$$A = YX^T(XX^T)^{-1} \tag{6.27}$$

when

$$X = \begin{bmatrix} s_{1,1} - s_1^* & \cdots & s_{i-1,1} - s_1^* \\ \vdots & \ddots & \vdots \\ s_{1,j} - s_j^* & \cdots & s_{i-1,j} - s_j^* \end{bmatrix} \tag{6.28}$$

$$Y = \begin{bmatrix} s_{2,1} - s_1^* & \cdots & s_{i,1} - s_1^* \\ \vdots & \ddots & \vdots \\ s_{2,j} - s_j^* & \cdots & s_{i,j} - s_j^* \end{bmatrix} \tag{6.29}$$

$s_{i,j}$ is the j^{th} state variable at i^{th} step and s_j^* is the fixed point of j^{th} state variable. Then the eigenvalues of the Jacobian matrix are evaluated to calculate the rates at which the small perturbations introduced around the fixed point grow (divergence) or decay (convergence) across the consecutive walking steps. These eigenvalues so called Floquet multipliers suggest the stable periodic motion when the magnitude of the greatest value is smaller than one. In this stable periodic motion or stable gait pattern, the smaller the maximum Floquet multiplier is the faster convergence toward the fixed

point is. If the greatest magnitude of the Floquet multipliers is bigger than one while the magnitude of others are smaller than one, the initial condition (s) of this periodic motion is called saddle point. This point can lead the system state back to the origin or away to infinity depending on the selected manifold. The stable manifold encircles all of the stable initial conditions of the dynamic system while the unstable manifold gathers with other unstable initial conditions out of the stable region. Thus, the saddle point can be used to draw the stable manifold, which establishes the boundary of the stable initial conditions (Steven, 1994). Apart from all, the unstable motion is identified when the Floquet multipliers cannot be classified by any of the above conditions. These Floquet multipliers indicate the divergence from the fixed point leading to one of the two fall modes mentioned earlier in this section.

6.4.2 Basin of attraction

As mentioned earlier in section 2.4.1 Chapter2, a basin of attraction is the set of initial conditions leading the system state to the fixed point. It quantifies the robustness or the sensitivity of the orbital stable system to the changes in the initial condition. In this chapter, the basin of attraction is a global stability quantification used to quantify the orbital stability of the periodic walking motions with different dynamic leg properties. For calculating the boundary of the basin of attraction two methods are applied. The first method requires a saddle point to draw the boundary of the stable initial conditions by iterating the stable manifold backwards in time (Shub, 1987; Steven, 1994; Rummel et al., 2010). The second method is applied when the saddle point does not exist or the stable manifold cannot be calculated thoroughly, the fundamental method of steps-to-fall is applied to discretely identify the members in the basin of

attraction (Rummel et al., 2010). In this chapter, by steps-to-fall method, each member in the basin of attraction is selected by a raster scan through the grid of the initial conditions to examine the global stability. From the return map of the 100 walking steps, if the greatest Floquet multiplier of the state variables is less than one, it means the initial condition can lead the system state toward the fixed point and is contained in the basin of attraction. At the boundary of the basin the underlying grid is refined with a higher precision to establish a closed region of the stable initial condition. The area encircled by either method (see Figure 6.9) quantifies the global stability of the periodic walking motion in terms of robustness of the gait pattern provided by individual design of leg property.

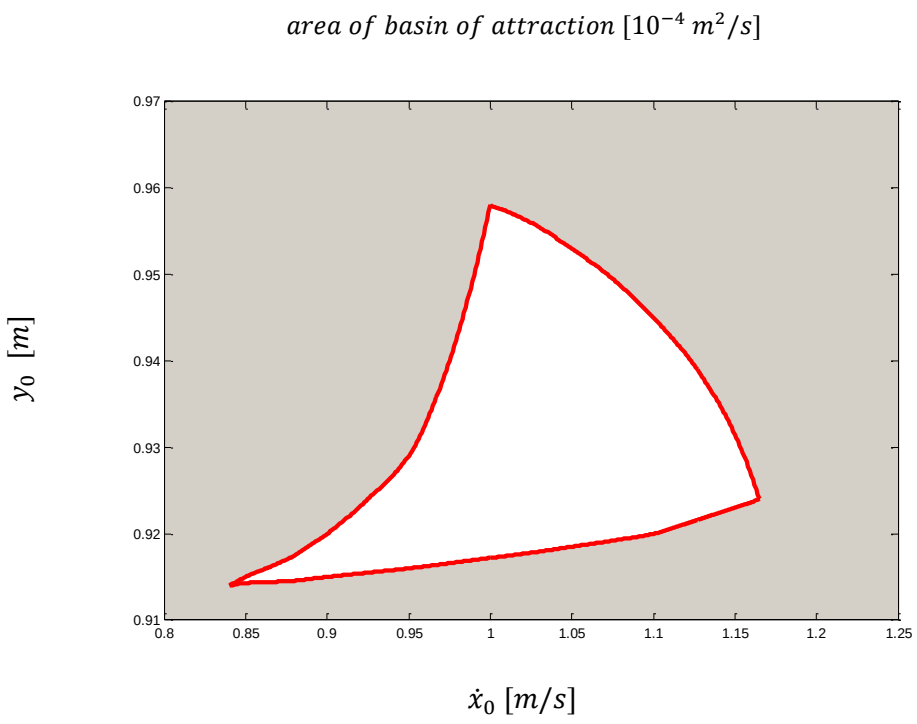

Figure 6.9 Examples of area (white) and region (red) of basin of attraction of human walking motion predicted by CAE model using the linear axial elastic leg properties and initial condition as shown in Table 6.1. The leg properties are obtained from walking measurements of subject no.2 at self-selected low walking speed (dot).

6.4.3 Stable region predicted by linear axial elastic property

The area of the basin of attraction is used to quantify the stability of the walking motions performed by the wide variety combinations of linear axial leg stiffness (k_{lin}^{n}) and touchdown contact angle ($\theta_{td}^{contact}$). The linear axial elastic property and touchdown contact angle ($\theta_{td}^{contact}$) extracted from the measurement data of a representative subject in Chapter 3 is fed into the compliant leg model with axial elastic property (CAE) to examine the global stability estimated by the area of basin of attraction. Only the moving contact condition is examined as the leg properties for fixed contact fails to reproduce periodic walking motion (see sub-section 6.3.4). To examine thoroughly the stable region of axial elastic leg property, the range of linear axial stiffness and touchdown contact angle is extended to the border in which the reproduction of ground reaction force and CoM motion of human walking minimally remain. That is; the RMSE of the vertical ground reaction forces and CoM displacements must be less than the given allowances, which are 130 N, 50 N, 0.6 m and 0.05 m, for the vertical and horizontal ground reaction forces and vertical and horizontal displacements respectively). For all combinations of axial stiffness (k^n) and touchdown contact angle ($\theta_{td}^{contact}$), the rest length (l_0) is fixed at 0.968 meter as it is the nearest value to the extracted rest length, which can reproduce the periodic motion of human walking (see Table 6.1). The axial stiffness is normalised by the body weight and the rest length.

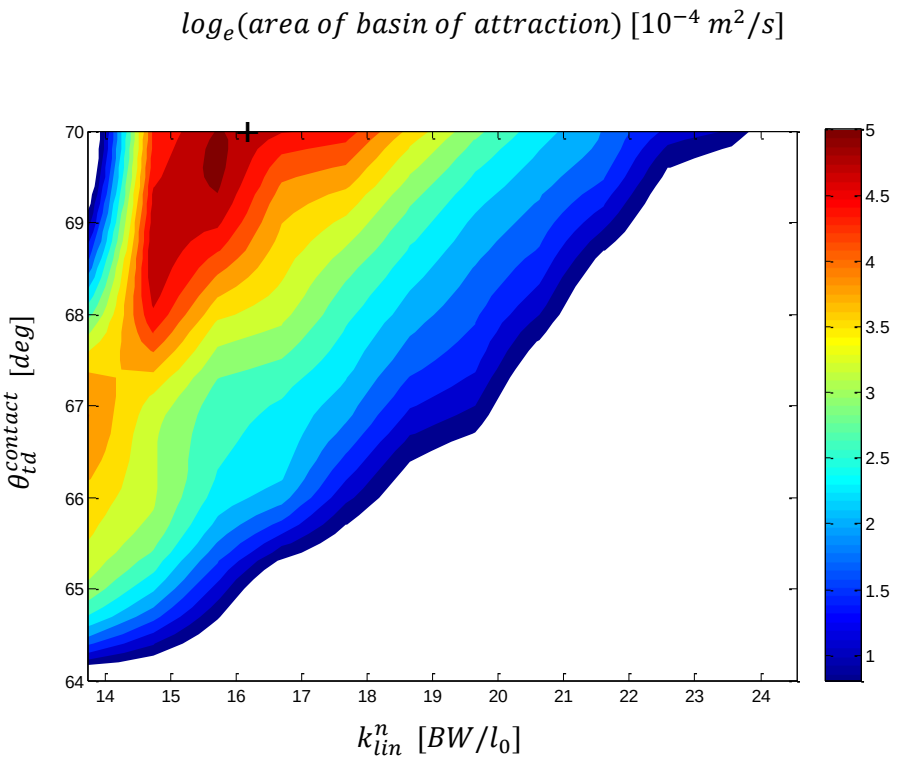

Figure 6.10 The contour plot of the area of basin of attraction of the stable walking motion corresponding to linear axial stiffness (k_{lin}^{n}) and touchdown contact angle ($\theta_{td}^{contact}$) is shown. The extracted linear axial stiffness (k_{lin}^{n}) and touchdown contact angle ($\theta_{td}^{contact}$) as shown in Table 6.1 is marked by green cross (+). The linear axial stiffness (k_{lin}^{n}) is normalised to body weight (BW) and rest length (l_0). The touchdown contact angle ($\theta_{td}^{contact}$) is in degree (deg).

Due to the walking speed limit of walking motion predicted by the compliant leg model with axial elastic property (CAE), the stable region of the linear axial leg properties shown in Figure 6.9 is limited at the maximum walking speed of 1.25 m/s. With the normalised axial stiffness being lower than 15, the area of basin of attraction is maximised at the touchdown contact angle of 67 degree. For the axial stiffness being higher than 15, the area of basin of attraction primarily increases with the bigger touchdown contact angle. The maximum area of basin of attraction is found with the combination of normalised stiffness of 16 and touchdown contact angle of 70 degree. With the nearby combinations, the area of basin of attraction decreases radically. It is interesting that the linear axial stiffness (k_{lin}^{n}) and touchdown contact angle ($\theta_{td}^{contact}$) in

Table 6.1 (normalised axial stiffness of 16.2 and touchdown contact angle of 70 degree) which is the nearest combination to the extracted values that can reproduce periodic motion exist within the region of maximum area of basin of attraction.

6.4.4 Stable region predicted by nonlinear axial elastic property

The similar schemes used in linear axial stiffness are applied to the nonlinear stiffness to examine for the global stability. For all combinations of the nonlinear axial stiffness and touchdown contact angle, the rest length is fixed at 1.0 meter to allow the estimation of basin of attraction based on both linear and nonlinear stiffness. At a particular touchdown contact angle, the basin of attraction of the linear and non-linear stiffness is compared based on the basic linear stiffness ($k^n_{lin,b}$) (see Equation 4.3, Chapter 4) and the stiffness ratio (k^r). The stiffness ratio (k^r) is the ratio between the axial stiffness at the maximum and minimum axial force or $k^r = \frac{k^n_{nln,\,F^n_{max}}}{k^n_{nln,\,F^n_0}}$ (see Figure 6.10). This ratio (k^r) greater and smaller than one indicate soft nonlinear and hard stiffness, respectively. The higher ratio for hard nonlinear stiffness and the lower ratio for soft nonlinear stiffness indicate the stronger nonlinearity. For the linear stiffness, the stiffness ratio (k^r) is equal to one.

Due to the intensive computation needed, the basin of attraction of the linear and non-linear stiffness is estimated in the touchdown contact angle range of 67 $^\circ$ to 70 $^\circ$with 1° increment as this angle range is found to provide large areas of basin of attraction on the linear stiffness in section 6.4.3. The natural log scale is applied to the area of basin of attraction to show the radical change over the different leg stiffness.

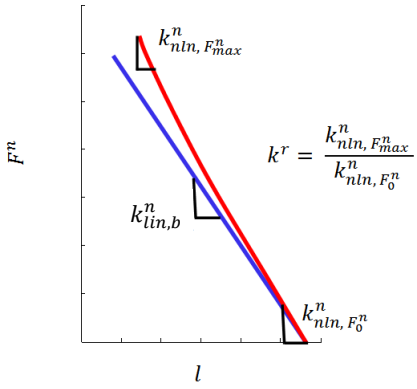

Figure 6.11 The nonlinear axial stiffness in terms of basic linear stiffness ($k^n_{lin,b}$) and the stiffness at the maximum ($k^n_{nln,\,F^n_{max}}$) and minimum axial force ($k^n_{nln,\,F^n_0}$) is shown.

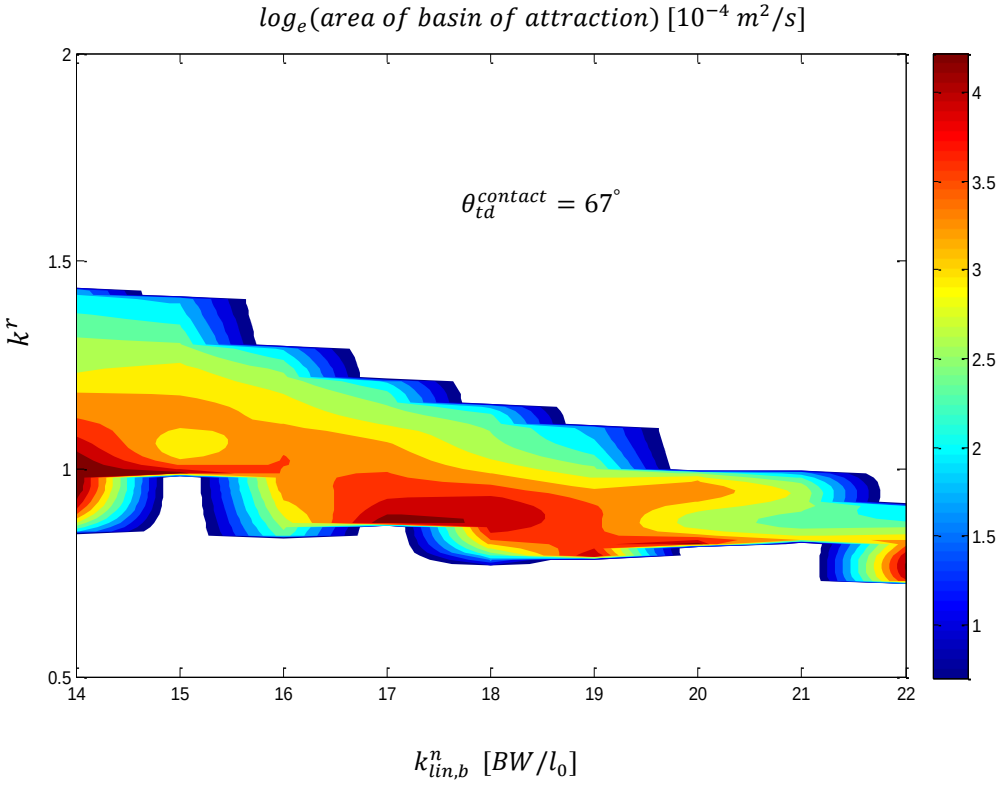

Figure 6.12 The contour plot of the area of basin of attraction of the stable walking motion corresponding to nonlinear axial leg properties at touchdown contact angle ($\theta^{contact}_{td}$) of 67 degree is shown. The area of basin of attraction is shown on the contour line in the unit of $[10^{-4}\ m^2/s]$. The stiffness ratio (k^r) indicates the nonlinearity of stiffness, the hard nonlinear stiffness is indicated by $k^r > 1$, the soft nonlinear stiffness is indicated by $k^r < 1$ and linear stiffness is indicated by $k^r = 1$. The basic linear axial stiffness ($k^n_{lin,b}$) is normalised to the body weight (BW) and rest length (l_0).

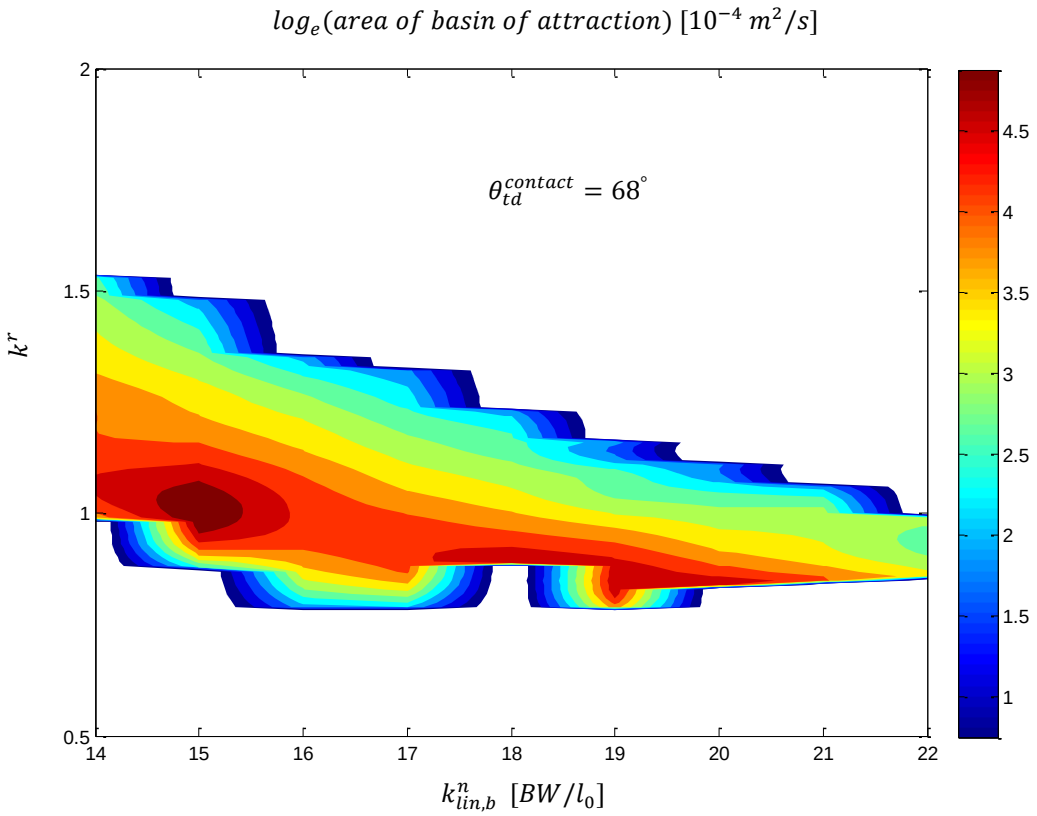

Figure 6.13 The contour plot of the area of basin of attraction of the stable walking motion corresponding to nonlinear axial leg properties at touchdown contact angle ($\theta_{td}^{contact}$) of 68 degree is shown. The area of basin of attraction is shown on the contour line in the unit of $[10^{-4}\ m^2/s]$. The stiffness ratio (k^r) indicates the nonlinearity of stiffness, the hard nonlinear stiffness is indicated by $k^r > 1$, the soft nonlinear stiffness is indicated by $k^r < 1$ and linear stiffness is indicated by $k^r = 1$. The basic linear axial stiffness ($k_{lin,b}^n$) is normalised to the body weight (BW) and unit leg length (l_0).

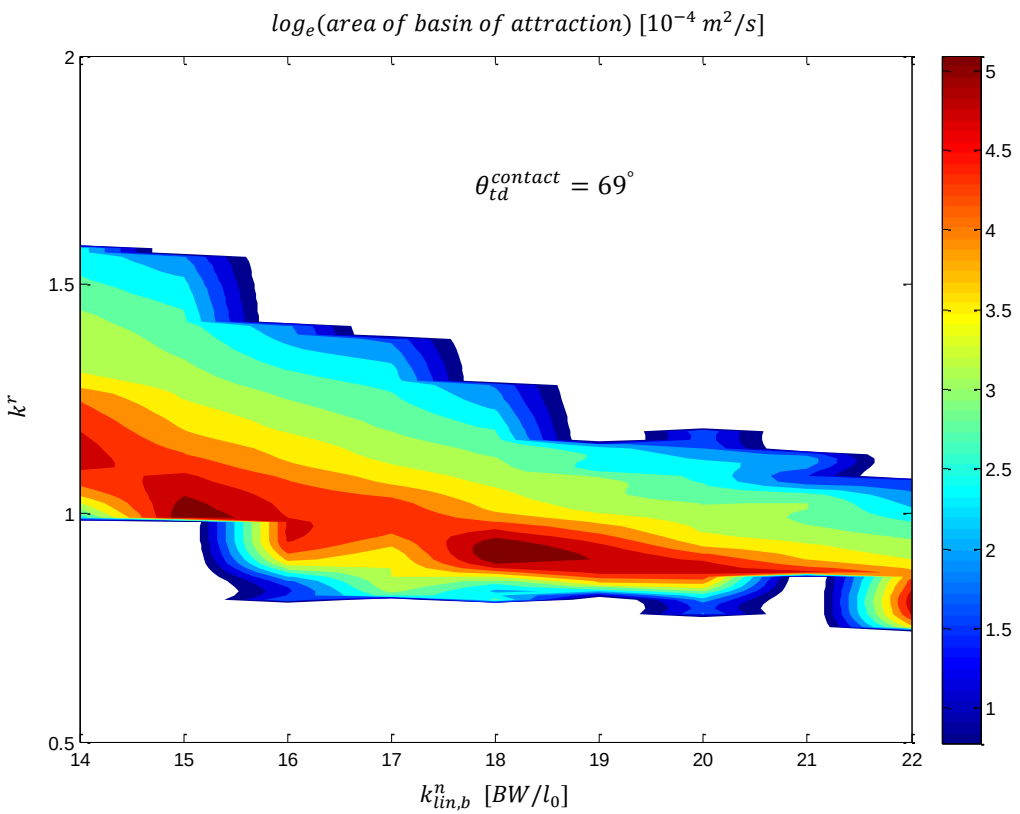

Figure 6.14 The contour plot of the area of basin of attraction of the stable walking motion corresponding to non-linear axial leg properties at touchdown contact angle ($\theta_{td}^{contact}$) of 69 degree is shown. The area of basin of attraction is shown on the contour line in the unit of $[10^{-4}\ m^2/s]$. The stiffness ratio (k^r) indicates the nonlinearity of stiffness, the hard nonlinear stiffness is indicated by $k^r > 1$, the soft nonlinear stiffness is indicated by $k^r < 1$ and linear stiffness is indicated by $k^r = 1$. The basic linear axial stiffness ($k^n_{lin,b}$) is normalised to the body weight (BW) and unit leg length (l_0).

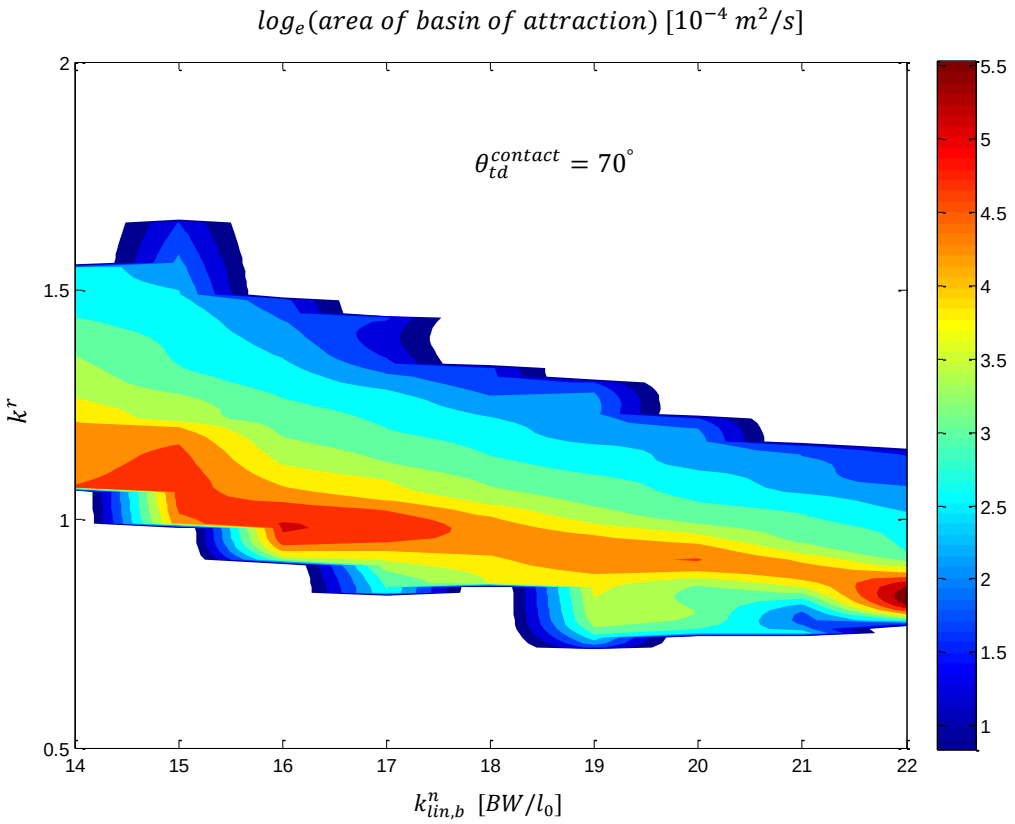

Figure 6.15 The contour plot of the area of basin of attraction of the stable walking motion corresponding to non-linear axial leg properties at touchdown contact angle ($\theta_{td}^{contact}$) of 70 degree is shown. The area of basin of attraction is shown on the contour line in the unit of $[10^{-4}\ m^2/s]$. The stiffness ratio (k^r) indicates the nonlinearity of the stiffness, the hard nonlinear stiffness is indicated by $k^r > 1$, the soft nonlinear stiffness is indicated by $k^r < 1$ and linear stiffness is indicated by $k^r = 1$. The basic linear axial stiffness ($k_{lin,b}^n$) is normalised to the body weight (BW) and unit leg length (l_0).

In Figure 6.11-6.14, the global stability region represented by the existence of the contour of basin of attraction increases with the bigger touchdown contact angle. At touchdown contact angle ($\theta_{td}^{contact}$) of 67 degree, the maximum area of basin of attraction occurs at the normalised linear stiffness of 14 and at the soft nonlinear stiffness with $k_{lin,b}^n$ = 17.5 and k^r = 0.1. At touchdown contact angle ($\theta_{td}^{contact}$) of 68 degree, the maximum area of basin of attraction occurs at the normalised linear stiffness of 15. At touchdown contact angle ($\theta_{td}^{contact}$) of 69 degree, the maximum area of basin of attraction occurs at the normalised linear stiffness of 15.5. Finally, at touchdown contact angle ($\theta_{td}^{contact}$) of 70 degree, the maximum area of basin of

attraction occurs at the normalised linear stiffness of 16.2 and at the soft nonlinear stiffness with k_{lin}^{n} = 22 and k^{r} = 0.2.

For all touchdown contact angles, the global stability region primarily spans over the hard nonlinear stiffness region in which the area of basin of attraction decrease rapidly toward the stiffness ratio (k^{r}) of zero. The stability region of the soft nonlinear stiffness being smaller than that of the hard nonlinear stiffness indicates the higher sensitivity of the soft nonlinear stiffness to the global stability. However, the maximum area of basin of attraction is scattered in this region.

6.4.5 Effects of stiffness change on walking stability

The stable region of nonlinear stiffness in sub-section 6.4.3 showed that the change in the axial stiffness during the gait primarily destabilises the walking motion. These effects of stiffness change are in contrast to the findings in the stability analysis by using the spring leg running model. The soft nonlinear stiffness has been shown to stabilise the spring leg running after perturbation (Karssen and Wisse, 2011) while the hard nonlinear leg stiffness has been shown to stabilise running gait pattern on the occurrence of touchdown impact (Owaki et al., 2006). Since the effects of the nonlinear stiffness on running stability has not been summarised deliberately, we may hypothesise here that, in the stabilisations of compliant leg running the leg stiffness may be considered as the rate of change of the leg force due to the leg compression. For the soft nonlinear stiffness, this rate of change decreases with the increased leg compression. On the introduction of disturbance such as the floor height variation, the motion is disturbed by the increasing of leg compression, but with the decreasing of the

leg force change around the maximum compression, the motion disturbance may be tolerated. For the hard nonlinear stiffness, the rate of change of leg force is minimal at the beginning of leg compression and increases with the higher leg compression. On the introduction of landing impact, the sudden change in the leg force is minimised at the beginning of the leg compression before the leg force increases rapidly around the maximum leg compression. This provides the energy balance during the running cycle and renders to stabilise the running gait pattern.

The change in leg stiffness during gait has been found to stabilise the compliant leg running model. However, such prediction may be more challenging when the stance phase contains both single and double-support as in walking. On the walking with the conservation of system energy, the closed-chain of the whole-body dynamic system during double-support phase constrains the dynamics of the two legs and requires precise energy exchanges to maintain gait cycle. This is underlined by the requirement of proper combination between the axial stiffness (k^n), rest length (l_0) and touchdown contact angle ($\theta_{td}^{contact}$) to stabilise the walking pattern predicted by the compliant leg model with linear axial stiffness as found in (Geyer et al., 2006; Rummel et al., 2010) and supported by our results in sub-section 6.4.3 . With the nonlinear axial stiffness, such proper combination is also required but the change in axial stiffness does not improve the global stability of the walking pattern. This may be affected by the change of strain energy transfer due to the change in axial stiffness, which changes the rate of energy transfers during the walking cycle and results in the improper energy exchanges. However, the global stability of the walking pattern with the external disturbance may be improved by such change in leg stiffness. The change in strain energy transfer in regulating the external disturbance as found in the compliant leg running model may

also benefit in the stabilisation of walking pattern with disturbance. This advantage of the nonlinear stiffness over the linear stiffness on human walking motion requires further investigation.

6.4.6 Stable region predicted by linear axial and tangential elastic leg property

In sub-section 6.3.4, the CATE model operating with linear axial and tangential leg stiffness well predicts the walking speed and vertical ground reaction force but overestimates the vertical displacement of the CoM. This prediction of periodic walking motion is brought into the dynamic stability analysis (see sub-section 6.4.2) to investigate for the effect of rotational elasticity of the virtual leg on the dynamic stability during human walking.

The leg properties for the linear axial and linear tangential elasticity in Table 6.1 are used in the dynamic stability analysis as they are the nearest values to the extracted leg properties, which can reproduce the periodic motion of human walking. The CAE model is used to examine the stability region of the walking motion performed by linear axial stiffness and the CATE model is used to examine the stability region of that affected by the incorporation of linear tangential stiffness. To compare between global stability predicted by these two compliant leg models. The initial velocity angle (θ_0^v) of axial-tangential elastic model is fixed with the measured velocity angle (θ_0^v) of 7 degree (see Table 6.1). Thus, the Poincare map of the two walking systems can be considered from the VLO height (y_0) and VLO horizontal velocity ($\dot{x}_0$) or s_i= $[y_i, \dot{x}_i]$. The global dynamic stability is quantified by the area of basin of attraction or the area of the total set of the initial state variables (s) leading the resultant state variables to the fixed points.

In Figure 6.16, the area of basin of attraction is 62.5 $(10^{-4})\, m^2/s$ for linear axial stiffness and 70.7 $(10^{-4})\, m^2/s$ for the linear axial and tangential stiffness. The range of the VLO height for the stable periodic walking motion is 0.045 meter for linear axial stiffness and 0.056 meter with the incorporation of linear tangential stiffness. Interestingly, the range of VLO horizontal velocity for both leg properties are equivalent at 0.335 meter per second, but by incorporating the linear tangential stiffness this velocity range spans over the range of higher walking speed. By sharing the same linear axial elastic property with that used in the CAE model, the stable walking motion predicted by the CATE model with linear axial and tangential elastic leg property has a wider stable range of VLO height and higher stable range of VLO horizontal velocity. The vertical ground reaction force is underestimated during mid-stance. The stable walking motion predicted by CAE and CATE model shares a small region of basin of attraction of 20.7 $(10^{-4})\, m^2/s$ covering the VLO height (y_i) from 0.92 to 0.946 meter and the VLO horizontal velocity ($\dot{x}_i$) from 0.935 to 1.16 meter per second.

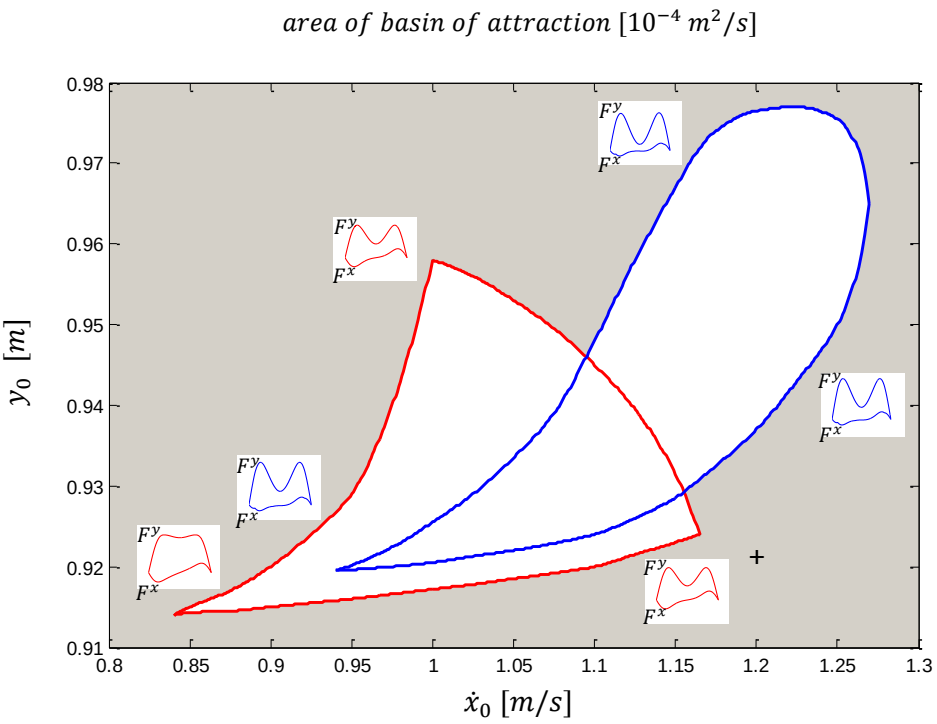

Figure 6.16 The area of basin of attraction (white transparent) of human walking motion generated by the CAE model (red region) and CATE model (blue region) spanned in the state plane (VLO height y_0 and horizontal velocity $\dot{x}_0$) is shown. The leg properties for the linear axial and linear tangential stiffness in Table 6.1 are used. The $F^x - F^y$ icons represent the vertical (F^y) and horizontal (F^x) ground reaction force patterns during the gait predicted by CAE model (red icon) and CATE model (blue icon) using the initial condition nearby each icon. The measured initial condition (+) from Table 6.1 is shown. The leg properties are obtained from walking measurements of subject no.2 at self-selected low walking speed.

6.4.7 Effects of linear tangential stiffness on the dynamic stability of human walking

Quantified by the area of basin of attraction, the incorporation of linear tangential stiffness slightly is found to improve the global stability to the compliant leg model with linear axial elasticity. It enlarges the range of stable VLO height of the CoM and shifts the range of stable VLO horizontal velocity of the CoM closer to the measured velocity (see Table 6.1 and Appendix C).

The enlarged range of stable VLO height and the shifted range of stable VLO horizontal velocity of the CoM may be affected by the incorporation of the angular motion due to the discrete changes in linear tangential stiffness. This angular motion affects on the

span of CoM velocity during the gait in which the horizontal and vertical velocity of the CoM is regulated by the tangential force especially after the mid-stance when the negative tangential force (see Figure6.8) resists the CoM motion and therefore, increases the velocity span of the gait cycle. This is supported by the prolonged stance duration and the decreased magnitude of horizontal ground reaction force compared to that predicted by the compliant leg model with linear axial elasticity alone (see Figure 6.3). Such velocity regulation during the gait may allow proper coordination between CoM oscillation, double support termination and CoM progression to achieve walking step and consequently, allows the virtual leg operation for the wider range of CoM height and higher range of walking speed.

Although, the stable walking motion predicted by the compliant leg model with linear axial and tangential elasticity underestimates the horizontal ground reaction force and vertical ground reaction force during mid-stance. The predicted range of VLO forward velocity of the CoM and the walking speed is shifted closer to the measured values for the self-selected slow speed. This supports the potential use of the CATE model with fundamental leg properties to quantify the dynamic stability of human walking at self-selected slow speed.

6.5 Discussion

Good quality predictions of human walking motion are provided by the proper combinations of the fundamental leg properties and the initial conditions of the CoM motion with reasonable deviations from the extracted leg properties and the measured

initial conditions. Different components of leg property are proficient in predicting different dynamics of walking motion. For example, the CAE model using linear axial elasticity is proficient in predicting the vertical displacement of the CoM, the CAE model using soft nonlinear axial elasticity is proficient in predicting the horizontal ground reaction force and stance duration and the CATE model using linear axial-tangential stiffness is proficient in predicting the peak magnitude of vertical ground reaction force. However, none of the compliant leg models can effectively predict the total horizontal displacement, the nonlinear leg angle and the leg lengthening after the mid-stance of human walking. These limitations may be due to the axial force- leg length relationship of the elastic leg in which the change of leg force is always accompanied by the change in leg length. The leg shortening after the mid-stance is fundamental mechanics for the compliant leg operated in the conservation of system energy, which underestimates the human leg length during the second half of stance phase. Thus, for the realistic prediction of human walking, the change in elastic property after the mid-stance may be required such that the leg lengthening after mid-stance can be reproduced, and thus the CoM can progress further during late stance.

The asymmetry of the walking motion is reproduced by incorporating the linear tangential stiffness with a trade-off of the underestimated horizontal ground reaction force and vertical ground reaction force during mid-stance. The nonlinear tangential force-leg angle relationship may be required such that the leg angle and thus, the vertical - horizontal force components can be better reproduced. In Chapter 4, a simple relationship between tangential force and leg angle was studied. However, based on the minimum RMSE fitting, the second order Fourier series was found to underestimate the

peak horizontal force. A more deliberate nonlinear relationship between tangential force and leg angle may be required.

The quality of the human walking prediction using simple walking models is also influenced by the definitions of the leg property. The leg property has been found to vary with the definition of the leg force and displacement (Coleman et al., 2012). In Chapter 3, we already discussed the direction and decomposition of the total ground reaction force and suggested that, the axial stiffness may be overestimated by transferring the total ground reaction force to apply along the virtual leg. The human walking prediction using the CAE model based on such leg property definition (Lipferth et al., 2012) provided good quality prediction of the magnitude of vertical and horizontal ground reaction force and vertical displacement of the CoM. However, the stance duration was predicted at nearly half of the measured value and more importantly, the human walking prediction is limited to the walking speed of 1.04 m/s. This is in contrast to our predictions using the CAE and CATE model based on decomposed leg forces. The vertical ground reaction force is underestimated by the CAE model based on decomposed leg forces, but it is well predicted when the tangential elasticity is taken into account in the CATE model. By both compliant leg models operating with our leg property definitions, the stance duration is well predicted, and the walking speed is limited to 1.25 m/s. These controversies underline the influences of leg property definitions and the complexity of leg operation in human walking prediction.

Based on the periodic motion predicted by the fundamental leg properties extracted from human walking measurement, the dynamic stability was quantified, and the effect of the different leg properties on the global dynamic stability were analysed. Although,

with the axial elastic properties alone (CAE model), the extracted leg properties cannot produce the periodic walking motion. The nearest neighbours of the extracted rest length (l_0), axial stiffness (k_{lin}^n) and touchdown contact angle ($\theta_{td}^{contact}$) that can produce periodic motion are located in the region of maximum stable walking. This implies that, during walking, the mechanical property of the human leg may be adjusted for the maximal stability.

The deterioration of global stability with the higher axial stiffness and smaller touchdown contact angle is found. This is in contrast to the finding by (Rummel et al., 2010) in which bigger touchdown contact angle limits the stable initial conditions. Such relationship is valid only when the system energy of the walking motion is coupled with the leg stiffness. At particular leg stiffness, the system energy is fixed and thus, the initial height (y_0) and initial velocity of the CoM ($\dot{x}_0, \dot{y}_0$) are coupled based on the conserved system energy. In such motion system, the bigger touchdown contact angle ($\theta_{td}^{contact}$) increases the CoM height at touchdown (y^{td}) and limits the range of initial height of the CoM (y_0), the initial velocity of the CoM ($\dot{x}_0, \dot{y}_0$) and thus the possibility of stable initial conditions.

However, in the dynamic stability quantification of this chapter, the system energy is uncoupled from all leg properties and allowed to vary to reproduce periodic walking motion for each combination of dynamic leg properties. That is; all possibilities of the initial height (y_0) and initial velocity of CoM ($\dot{x}_0, \dot{y}_0$) were examined to quantify the dynamic stability performed by each combination of leg properties. In our walking motion system, the higher CoM height at touchdown (y^{td}) may decrease the possibility of stable initial height (y_0) but does not necessarily decrease the dynamic stability as the system energy is allowed to vary independently to reproduce periodic walking

motion. The deterioration of walking stability with the smaller touchdown contact angle and higher axial stiffness indicates that the late touchdown timing and the stiff leg may decrease stability of human walking.

The change in axial stiffness primarily decreases the global stability compared to that performed by constant axial stiffness. Unlike the running motion with external disturbance predicted by complaint leg model with nonlinear leg stiffness, the walking motion on conserved system energy requires proper energy exchanges to maintain stable gait pattern (Geyer et al., 2006; Rummel et al., 2010). This requirement seems to be challenged by the change in axial stiffness in which the rate of change of strain energy regulated by the nonlinearity of leg stiffness limits the proper energy exchanges with other forms of mechanical energy. This is reflected by the lower number of initial conditions that can lead the proper gravitational and kinetic energy exchange toward the stable walking motion. However, the further investigation on the human walking with external perturbation may reveal benefits of the nonlinear stiffness in the gait pattern stabilisation.

With the higher complexity of leg properties, the incorporation of linear tangential elasticity improves the global stability of periodic walking motion. With a fixed velocity (θ_0^v), linear tangential stiffness enlarges the range of stable initial height of the CoM (y_0), and shifts the range of stable initial horizontal velocity of the CoM ($\dot{x}_0$) close to the measured range of the human walking at self-selected low speed. The regulation of CoM velocity span provided by tangential elasticity plays a major role in shifting the effective range of walking prediction and stability quantification close to the measured range at self-selected slow speed of human walking. The underestimated horizontal ground reaction force and vertical ground reaction force during mid-stance performed by the

linear axial and tangential stiffness are one the major draw backs limiting the prediction of walking at higher speed. This may be improved by the coordination between axial and tangential stiffness. The change of the axial elasticity after the mid-stance incorporating with the nonlinearity of tangential elasticity is suggested for the more accurate and wider speed range of human walking prediction. Further investigation on the wider variety combination of axial and tangential leg properties may be required to provide the entire stable region in human walking range. The axial and tangential leg properties are crucial leg properties in the prediction and dynamic stability quantification of human walking. The linear elastic leg properties limit the prediction and dynamic stability quantification to the slow speed of human walking.

Chapter 7 Human Walking Prediction and Dynamic Stability Analysis based on the Posture - Dependent Leg Property

7.1 Introduction

In Chapter 6, the linear axial and tangential elasticity of the virtual leg operating on the conserved system energy were found to predict the human walking motion only at low speed. In addition, the fundamental leg shortening after the mid-stance described by the single valued force-length relationship of the linear and non-linear elasticity of the virtual leg was found to underestimate the CoM progression during the gait. The change of the axial elasticity after the mid-stance incorporating with the nonlinearity of tangential elasticity on the non-conservative energy of virtual leg operation was suggested to increase the range of human walking prediction and dynamic stability quantification.

In this chapter, the posture-dependent leg property extracted from the human walking measurement as presented in Chapter 5 are used to allow the non-conservation of system energy during the gait cycle. Modified from the linear axial-tangential elastic leg model in Chapter 6, the posture-dependent elastic leg model is proposed to examine the validity region of the posture-dependent leg property in human walking prediction. The dynamic walking stability is quantified and the potential use of the modified axial-

tangential elastic leg model as a walking template to quantify the dynamic stability of walking motion is investigated.

7.2 Background

The variation of system energy managed by a time-dependent leg property during the gait has been found to stabilise the biped machine walking after perturbations (Seipel and Holmes, 2007; Schmitt and Clark, 2009). This energy management during locomotion was adopted from the self-stabilisation dynamics performed by the embedded mechanism in insect running leg (Schmitt and Holmes, 2000a; Schmitt and Holmes, 2000b; Schmitt et al., 2002; Schmitt and Holmes, 2003). With the limitation of sensory feedback during the high speed running, the frequency-independent damping and the anticipated leg lengthening called the pre-flex have been revealed as two of the major designed mechanisms rendering in energy absorption and production to stabilise the insect running over rough terrain (Dudek and Full, 2006). The system energy management can be simply examined during insect and biped robot locomotion. A huge challenge in such examination during human locomotion is the measurement of strain energy. The measurement of force and displacement of the muscles and tendons in human leg would be required and the strained energy stored in and returned from soft tissue structures may be significant in some duration of the gait (Rose and Gamble, 2006). Alternatively, this measurement may be conducted by considering the entire human leg as a spring in which the relationships between leg length, leg angle and resultant leg forces define the total strain energy of the walking system. By this way, the variation of the system energy can be examined and the effects on dynamic stability during human walking can be investigated.

In Chapter 5 and 6, in corresponding to the strain energy, we presented the force-displacement relationships of the virtual leg operation based on the conservation of system energy during human walking motion. This fundamental elasticity renders in human walking prediction and dynamic stability quantification in terms of orbital stability. However, the changes in force –displacement relationships found during the second half of the measured gait drew our attention as it supports the previous studies of system energy variation contributing in dynamic stability of locomotion. Thus, in Chapter 5, we addressed the changes in force –displacement relationships by extracting the posture-dependent leg properties from the human walking measurement to capture the variation of leg property that allows energy variation. These posture-dependent leg properties require the examination of the validity region in human walking prediction such that the dynamic stability analysis can be performed on the human walking prediction. As a consequence, the effect of posture-dependent elastic leg property on the human walking motion and the dynamic stability can be investigated. The differences between the dynamic stability of conservative and non-conservative system can also be investigated.

7.3 Human walking prediction based on posture-dependent leg properties

In Chapter 5, the systematic changes of the posture-dependent leg properties with walking speed showed the potential use as a leg property template to represent human walking at different speed. However, based only on the minimum RMSE fitting, the combinations of these leg properties may not reproduce human walking motion. To provide the validity region of these leg parameters, the implementation in the human walking model is required.

7.3.1 A posture-dependent elastic leg model (PDE)

In this chapter, a posture-dependent elastic leg model (PDE) is proposed. In this model, the axial and tangential properties of the virtual leg are regulated by walking posture index, which is defined by the leg angle of the ipsilateral leg, the leg which starts the considered gait cycle introduced in Chapter5. The posture-dependent leg properties comprising linear axial stiffness ($k_{q,lin}^{n}$), variable force-free leg length ($l_{0,q}$), variable tangential stiffness (k_q^t) and force-free leg angle ($\theta_{0,q}$) extracted from human walking motion require axial-tangential elastic leg model which allows variability of force-displacement relationships. In this section, the posture-dependent elastic leg model (PDE) is proposed to take account of the posture-dependent variation of leg properties.

The equations of motion of the whole-body centre of mass are extended from those in the compliant leg model with axial and tangential elastic property (CATE) by introducing the leg property variations and the difference of leg length at the phase transitions. The equations of motion of the whole-body CoM motion during the walking motion expressed by the posture-dependent elastic leg model (PDE) can be written as

$$m\ddot{x} = \tilde{P}x + \tilde{R}y \tag{7.1}$$

$$m\ddot{y} = \tilde{P}y - \tilde{R}x - mg \tag{7.2}$$

for the initial single support phase,

$$m\ddot{x} = \tilde{P}x - \tilde{Q}(d - x) + (\tilde{R} + \tilde{S})y \tag{7.3}$$

$$m\ddot{y} = (\tilde{P} + \tilde{Q})y - \tilde{R}x + \tilde{S}(d - x) - mg \tag{7.4}$$

for the double support phase and

$$m\ddot{x} = -\tilde{Q}(d - x) + \tilde{S}y \tag{7.5}$$

$$m\ddot{y} = \tilde{Q}y + \tilde{S}(d - x) - mg \tag{7.6}$$

for the final single support phase.

when

$$\tilde{P} = k_{q,lin}^{n} \frac{(l_{0,q} - l^{trail})}{l^{trial}} \tag{7.7}$$

$$\tilde{Q} = k_{q,lin}^{n} \frac{(l_{0,q} - l^{lead})}{l^{lead}} \tag{7.8}$$

$$\tilde{R} = k_{q}^{t} \frac{(\theta_{0,q} - \theta^{trail})}{(l^{trial})^2} \tag{7.9}$$

$$\tilde{S} = k_{q}^{t} \frac{(\theta_{0,q} - \theta^{lead})}{(l^{lead})^2} \tag{7.10}$$

The linear axial ($k_{q,lin}^{n}$), posture-dependent tangential stiffness (k_{q}^{t}), posture-dependent force-free leg length ($l_{0,q}$) and the force-free leg angle ($\theta_{0,q}$) as presented in Equation 5.1 – 5.11, Chapter 5 are used in Equation 7.1-7.12. Similar to the compliant leg model with axial and tangential elastic property (CATE), the leg length (l) and leg angle (θ) during the walking motion are expressed by

$$l^{trail} = \sqrt{x^2 + y^2} \tag{7.11}$$

$$l^{lead} = \sqrt{(d - x)^2 + y^2} \tag{7.12}$$

$$\theta^{trail} = tan^{-1} \frac{x}{y} \tag{7.13}$$

$$\theta^{lead} = tan^{-1} \frac{d - x}{y} \tag{7.14}$$

x is the horizontal distance between the CoM and the contact point. Here, the realistic criteria for the walking phase transitions are introduced. Due to the fact that the leg length at touchdown and take-off are not necessarily equivalent, the transition from single to double support is defined to occur when

$$y = l^{td} \, sin(\theta_{td}^{contact}). \tag{7.15}$$

and the transition from double to single support is identified when

$$F_y^{trail} = 0. \tag{7.16}$$

l^{td} is the leg length at touchdown . The touchdown contact angle ($\theta_{td}^{contact}$) is the angle between horizontal and the virtual leg at touchdown instant. m is the body mass, g is gravitational acceleration and d is the step length defined by the distance between the contact point of leading and trailing leg (see Figure 7.1). The force equations of this model can be found in Appendix B.

This forward dynamic model begins with the initial condition defining either symmetrical or asymmetrical walking motion

$$x(0) = x, \quad \dot{x}(0) = \dot{x}_i,$$
$$y(0) = y_i, \quad \dot{y}(0) = \dot{x}_i \, tan(\theta_0^v). \tag{7.15}$$

when i is the step number. During human walking, the vertical leg orientation (VLO) can occur before, after or at the apex of the CoM motion in which $tan^{-1}(\frac{\dot{y}_i}{\dot{x}_i}) = \theta_0^v$ represents the direction of the total velocity of the CoM (see Figure 7.1). Hence the initial condition can be expressed only by the CoM height (y_0) and the velocity angle (θ_0^v) in terms of $\dot{x}_0$ and $\dot{y}_0$ of for the asymmetric gait. Accordingly, the state variables (s) can be expressed by s_i= $[y_i, \theta_i^v]$ and the periodic gait pattern is identified using a similar method as introduced in Chapter5.

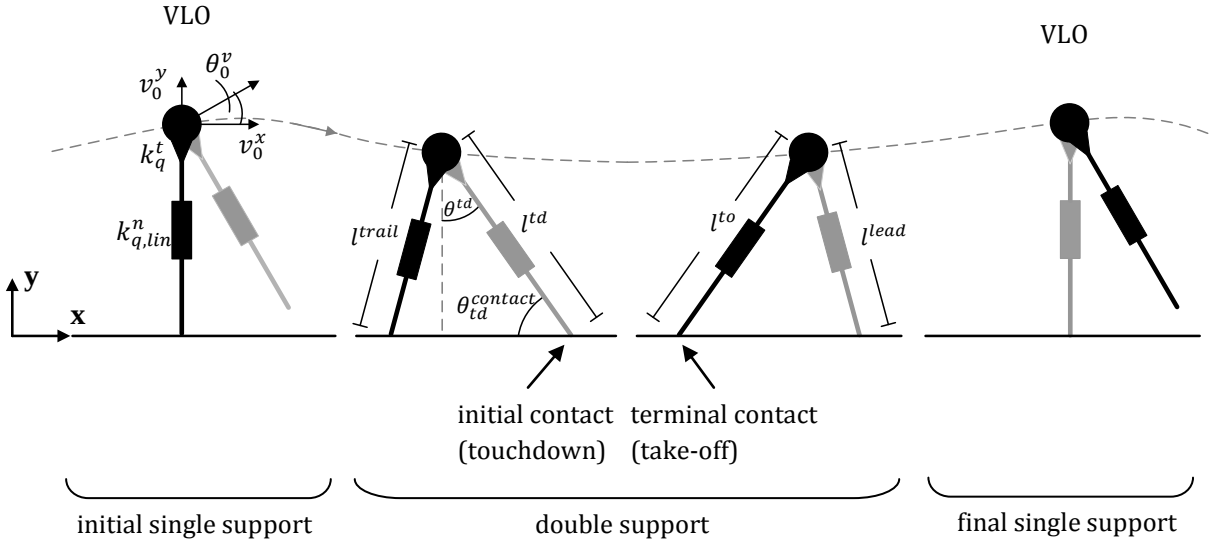

Figure 7.1 A posture-dependent elastic leg model (PDE) for human walking prediction. A walking step begins with the initial single support at vertical leg orientation (VLO) of the trailing leg, enters the double support phase at the touchdown instant (td) of the leading leg and finally, enters the final single support phase at the take-off instant (to) of the trailing leg before terminating the simulation walking step at the consecutive vertical leg orientation (VLO).

7.3.2 Human walking simulation and mechanical energy calculation

The posture-dependent leg property and the initial condition of walking motion from each individual subject are fed into the posture-dependent elastic leg model. It was found that none of the combinations of the extracted leg properties and measured initial

conditions can generate a periodic walking motion. It is probably because the nonlinear relationships between the posture-dependent leg force and displacement requires accurate leg length and leg angle to create a proper fraction of axial and tangential forces (see Equation 5.1-5.11) and thus to achieve a walking cycle . To obtain the periodic walking motion, the initial condition comprising the height (y_0), vertical and horizontal velocity ($\dot{x}_0, \dot{y}_0$) of the CoM at vertical leg orientation is allowed to penetrate around 90-110 % of the measured values while the posture-dependent leg properties are maintained at the extracted values. In this way, the validity region of human walking prediction based on the extracted posture-dependent leg properties can be examined. The initial condition parameter search was conducted to find the nearest values to that of the measured initial condition, which can reproduce periodic walking motion. Each parameter is examined at 1% increment above and below the measured value, respectively. The search gives priority to the height (y_0), the vertical and horizontal velocity ($\dot{x}_0, \dot{y}_0$) of the CoM at vertical leg orientation, respectively.

Another challenge of the human walking prediction is the variation of the system energy due to the non-conservative relationships of axial force-leg length and tangential force-leg angle before and after the mid-stance. These realistic relationships may provide a better prediction of human walking by using a simple walking model but the variation of system energy may limit the repetition of walking motion. By using the posture-dependent elastic leg model (PDE), the system energy of human walking is calculated as

$$E^s = E^k + E^g + E^e \tag{7.16}$$

when

$$E^k = \frac{1}{2}m(\dot{x}^2 + \dot{y}^2) \tag{7.17}$$

$$E^g = mgy \tag{7.18}$$

The elastic potential energy can be calculated by

$$E^e = \frac{1}{2}\left(k^n_{q,lin}(\, l^*_0 - l)^2 + \, k^t_q \, (\theta^*_0 - \theta)^2\right) \tag{7.19}$$

during the single support phase, and by

$$E^e = \frac{1}{2}(k^n_{q,lin}((\, l^*_0 - l^{lead})^2 + \, \left(\, l^*_0 - l^{trail}\right)^2 \,) + k^t_q \, (\, (\theta^*_0 - \theta^{lead})^2 + \, (\theta^*_0 - \theta^{trail})^2)) \tag{7.20}$$

during the double support phase.

E^s, E^k, E^g and E^e are system, kinetic, gravitational potential and strain energy ,respectively. In Chapter 5, the posture-dependent leg properties were introduced to represent the non-conservative force-displacement relationships and non-conserved elastic energy (Equation 7.19 and section 5.4 Chapter 5). This non-conserved elastic energy as a part of the energy exchanges during the walking gait may challenge the returning to original level of the system energy after a gait cycle (see Equation 7.16). Since the returning to steady state of state variables ($y_0, \dot{x_0}$ and $\dot{y_0}$) contained in Equation 7.17 and 7.18 defines the periodic motion. The returning to the original level of the corresponding kinetic (Equation 7.17) and gravitational potential energy (Equation 7.18) may be required. However, the mechanical energy exchanges regulated by the non-conservation of strain energy may limit the returning of those energies and, therefore, limit the generation of periodic walking motion. To gain insight into this

effect of posture-dependent leg properties on periodic walking motion, the energy management during the walking cycle needs to be investigated.

7.3.3 Human walking prediction results and energy management during walking motion

It was found that, with a given deviation from the extracted and measured value (see sub-section 7.3.2), none of the posture-dependent leg property and initial condition can generate the motion of hundred walking steps. The posture-dependent leg properties extracted in moving contact condition fail to generate even a single cycle of human walking motion. The simulations showed that the nonlinearity of leg angle during the early and late stance extracted from the measurement data in moving contact condition cannot be reproduced by the posture-dependent elastic leg model (PDE). In the nonlinear relationships between the forces and displacements of the virtual leg, the forces are highly sensitive to the change in leg angle (see Equation 5.1-5.11, Chapter 5). Therefore, the nonlinear leg angel may be required to achieve a periodic walking motion on moving contact. However, in fixed contact condition, a proper combination of initial condition and posture-dependent leg properties were found to be able to generate some walking cycles. At different walking speeds, the periodic walking motions maximally achieve 3-4 walking steps or 1-2 gait cycles. The corresponding leg properties and the initial condition with smallest deviations from measured values of a representative subject are listed in Table 7.1.

Table 7.1 The combinations of posture-dependent leg properties and the initial conditions that can generate periodic walking motion by using posture-dependent elastic leg model (PDE). The leg parameter set is predicted from the walking measurements of subject no.2 at each self-selected walking speed.

		Slow ($\bar{v}^x$ = 1.2 m/s)		Normal ($\bar{v}^x$ = 1.54 m/s)		Fast ($\bar{v}^x$ = 1.78 m/s)	
		model	measured	model	measured	model	measured
Linear stiffness ($k^n_{q,lin}$)	(kN/m)	4.86	4.86	4.48	4.48	5.12	5.12
Peak amplitude of force –free leg length variation (A^l_0)	(m)	0.073	0.073	0.101	0.101	0.108	0.108
Touchdown leg length (l^{td})	(m)	1.035	1.035	1.044	1.044	1.065	1.065
Excursion length ($l^{to} - l^{td}$) or (d^l)	(m)	0.033	0.033	0.047	0.047	0.048	0.048
Total dynamic stiffness on hardening elastic profile ($z^{t,fixed}_{q,hard}$)	(kN·m/rad)	0.29	0.29	0.26	0.26	0.23	0.23
Total dynamic stiffness on softening elastic profile ($z^{t,fixed}_{q,soft}$)	(kN·m/rad)	0.14	0.14	0.15	0.15	0.17	0.17
Force-free contact angle 90°- (θ^*_0)	(deg)	82.4	82.4	82.4	82.4	82.1	82.1
Touchdown contact angle 90°- (θ^{td})	(deg)	61.3	61.3	60.3	60.3	58.1	58.1
m	(kg)	69	69	69	69	69	69
$\dot{x}_0$	(m/s)	1.2	1.2	1.51	1.54	1.71	1.72
y_0	(m)	0.934	0.921	0.936	0.922	0.928	0.924
θ^v_0	(deg)	6.9	6.9	5.7	5.7	5.6	5.6

By maintaining all the posture-dependent leg properties, the initial conditions within 2% deviation from the measured values were found to achieve at least three consecutive vertical leg orientations. The walking predictions can be achieved at low, normal and high speeds of human walking. The predicted CoM displacement, ground reaction force, leg length and leg angle are shown in Figure 7.2 – 7.5.

The horizontal and vertical ground reaction forces are well predicted for all walking speeds (RMSE are 15.6 -19.5 and 24.6-31.1 for horizontal and vertical ground reaction force, respectively. The horizontal displacement of the CoM is well predicted (RMSE = 0.11-0.16) while the peak magnitude of the vertical displacement is generally overestimated (RMSE = 0.013-0.02). The leg length and leg lengthening after mid-stance is well predicted with an underestimated leg shortening during the early stance (RMSE, l = 0.061-0.073). For all walking speeds, the linear leg angle and stance duration are well predicted (RMSE, θ = 0.06-0.09).

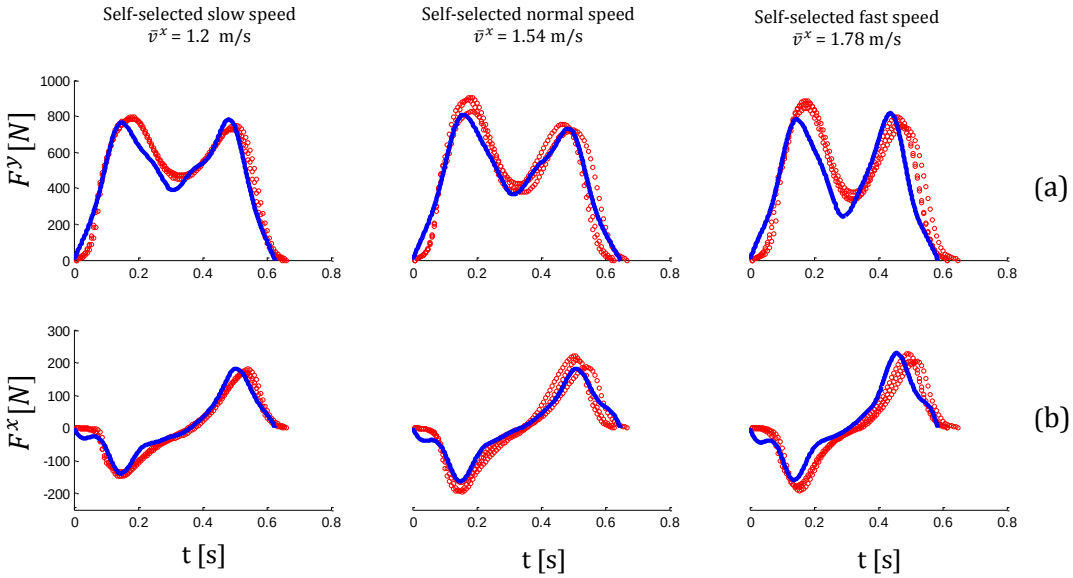

RMSE, $F^y[N]$	24.6	29.5	31.1
RMSE, $F^x[N]$	17.4	15.9	19.5

Figure 7.2 The predicted vertical (a) and horizontal (b) ground reaction force by posture-dependent leg model (solid line) as shown in Table 7.1 compared to the measured ground reaction force at self-selected low, normal and high walking speeds (dot). The data set is obtained from three good trials of the walking measurements of subject no.2 at each self-selected walking speed. The root-mean square errors (RMSE) determined by the difference between the measured and predicted ground reaction forces (F^y, F^x) are given for each walking speed.

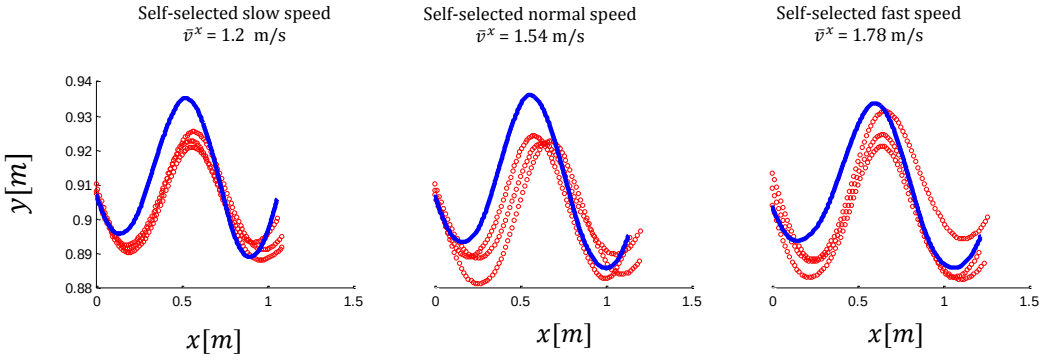

RMSE, $y[m]$	0.11	0.15	0.16
RMSE, $x[m]$	0.016	0.02	0.013

Figure 7.3 The predicted CoM displacement (x, y) between two consecutive touchdowns generated by the posture-dependent leg model (solid line) as shown in Table 7.1 compared to the measured CoM displacement (x, y) at self-selected low, normal and high walking speeds (dot). The data set is obtained from three good trials of the walking measurements of subject no.2 at each self-selected walking speed. The root-mean square errors (RMSE) determined by the difference between the measured and predicted displacment of the CoM (x, y) are given for each walking speed.

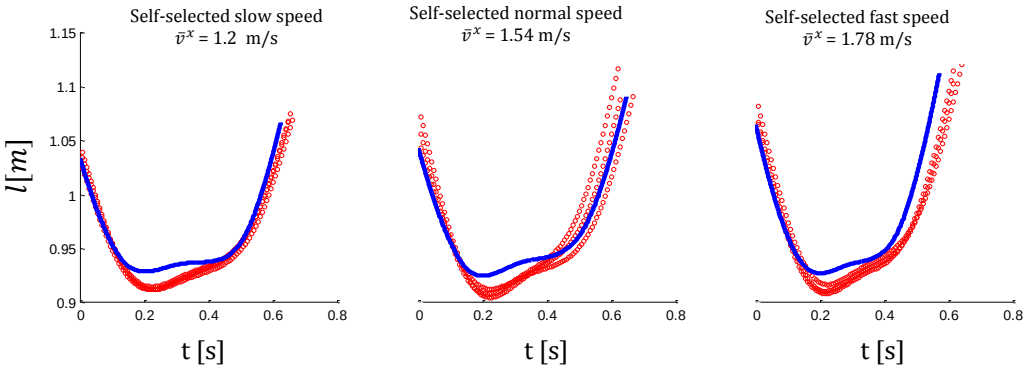

RMSE, $l[m]$	0.065	0.061	0.073

Figure 7.4 The predicted leg length (l) during the contact (t) by the dependent leg model (solid line) as shown in Table 7.1 compared to the measured leg length at self-selected low, normal and high walking speeds (dot). The data set is obtained from three good trials of the walking measurements of subject no.2 at each self-selected walking speed. The root-mean square errors (RMSE) determined by the difference between the measured and predicted leg length (l) are given for each walking speed.

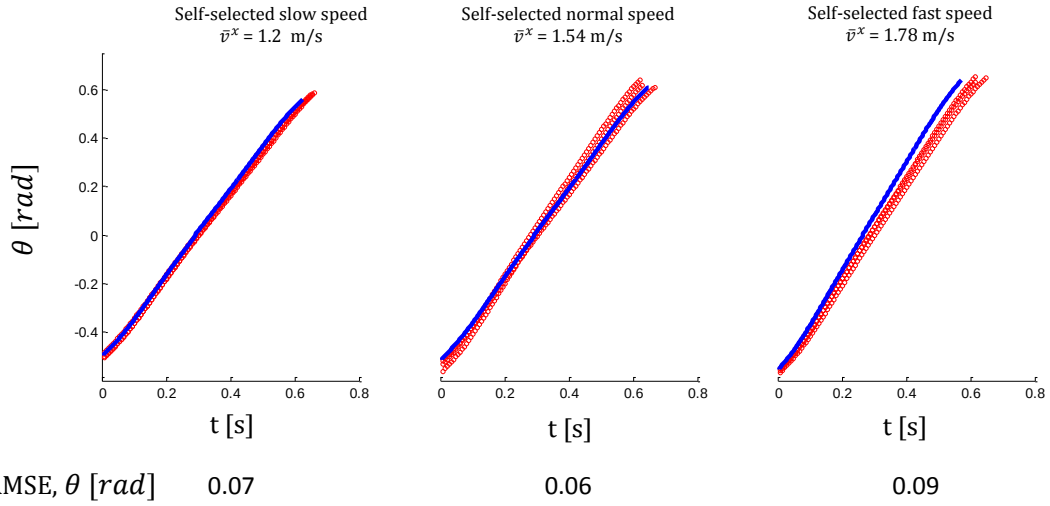

Figure 7.5 The predicted leg angle (θ) during the contact (t) by the posture-dependent leg model (solid line) as shown in Table 7.1 compared with the measured leg angle at self-selected low, normal and high walking speed (dot). The data set is obtained from three good trials of the walking measurements of subject no.2 at each self-selected walking speed. The root-mean square errors (RMSE) determined by the difference between the measured and predicted leg length (θ) are given for each walking speed.

Although all the posture-dependent leg property parameters are maintained, the deviation of the initial condition from the measured values results in some deviations of the force-displacement relationships from the measurement (see Figure 7.6 and 7.7). The simulation results showed that at all walking speeds, the axial force- length relationship is reproduced with the underestimation of the leg length and axial force at the maximum leg shortening (RMSE = 28.4-32.5). However, the tangential force-leg angle relationship is well reproduced (RMSE = 22.4-24.1).

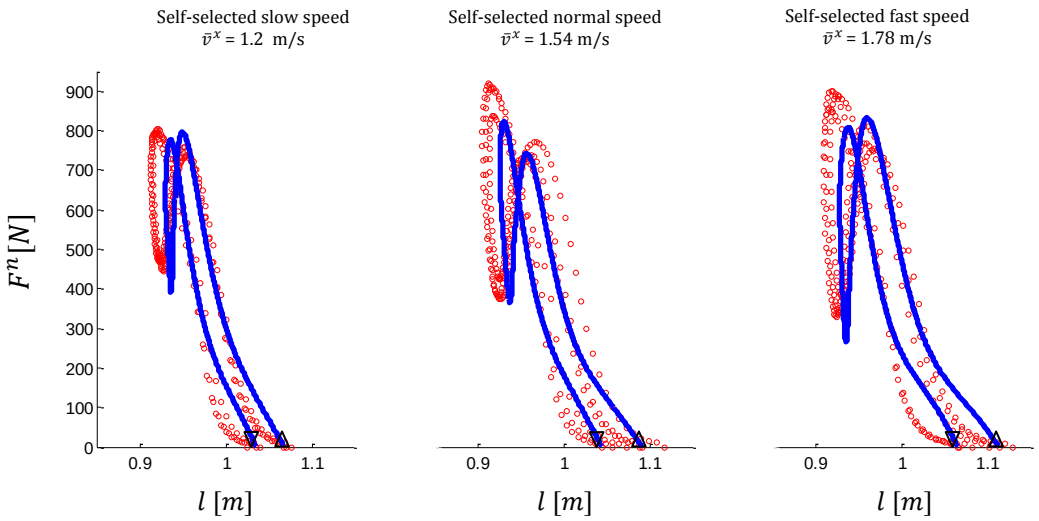

RMSE, $F^n[N]$	28.4	31.2	32.5

Figure 7.6 The reproduced axial force-leg length relationship by posture-dependent leg properties (solid line) as shown in Table 7.1 compared to the measured axial force-leg length relationship (dot) at self-selected low, normal and high speed. The data set is obtained from three good trials of the walking measurements of subject no.2 at each self-selected walking speed. The root-mean square errors (RMSE) determined by the difference between the measured and predicted axial force (F^n) are given for each walking speed.

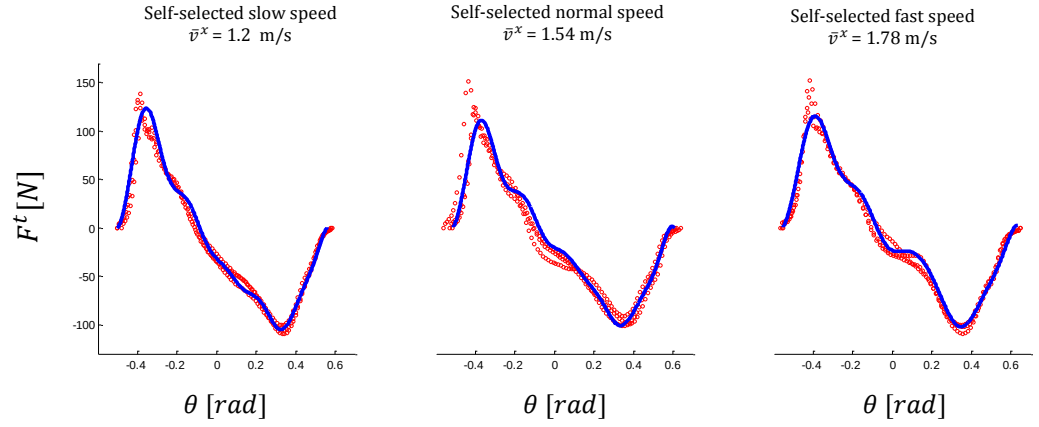

RMSE, $F^t[N]$	22.4	23.8	24.1

Figure 7.7 The reproduced tangential force-leg angle relationship by the posture dependent leg model(solid line) as shown in Table 7.1 compared to the measured tangential force-leg angle relationship (dot) at self-selected low, normal and high speed. The data set is obtained from three good trials of the walking measurements of subject no.2 at each self-selected walking speed. The root-mean square errors (RMSE) determined by the difference between the measured and predicted tangential force (F^t) are given for each walking speed.

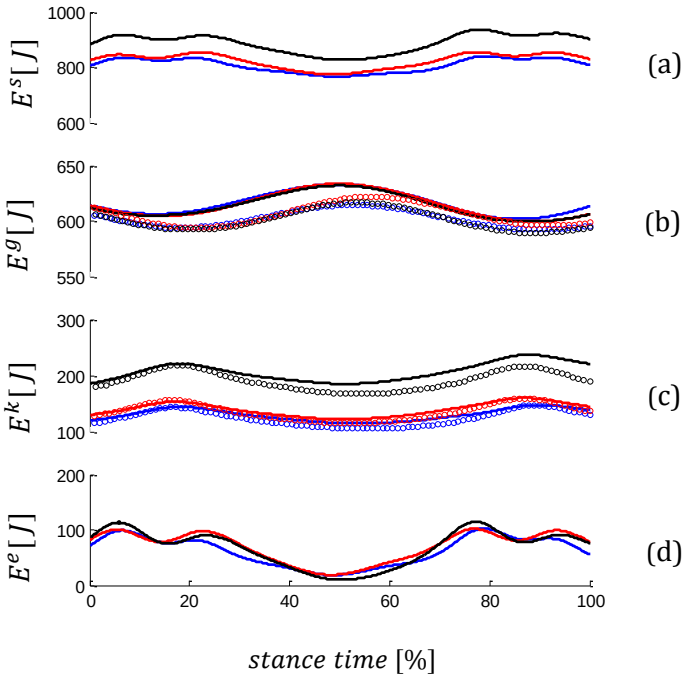

RMSE	Slow	Normal	Fast
$E^g[J]$	22	26	31
$E^k[J]$	15.4	12.5	36

Figure 7.8 The mechanical energies including gravitational potential (b), kinetic (c) and strain energy (d) and the total energy (a) from touchdown to toe-off of the gait cycle at self-selected low (blue), normal (red) and high speed (black) predicted by PDE model as shown in Table 7.1 compared to the measured gravitational potential and strain energy at each walking speed (dot). The data set is obtained from three good trials of the walking measurements of subject no.2 at self-selected low walking speed. The root-mean square errors (RMSE) determined by the difference between the measured and predicted mechanical energies (E^g, E^k) are given for each walking speed.

In Figure 7.8, the energy variation is predicted throughout the stance phase. Beginning with the double-support phase at touchdown of the leading leg, the system energy fluctuates before reducing to the minimum at the mid-stance. The kinematic and elastic energies are also minimised while the gravitational potential energy is maximised at the mid-stance. After the mid-stance the system continue the single support phase before changing to double-support phase with fluctuating energy. At take-off, the system energy for all walking speeds tends to return to the same level as that at the touchdown.

The kinematic energy changes progressively while the gravitational potential and strain energy change very slightly with the change of walking speed.

7.3.4 Effects of non-conserved system energy on human walking prediction.

In Chapter 5, the conserved strain energy of the virtual leg operation limited the human walking prediction to the low walking speed and thus, the non-conserved strain energy of the virtual leg operation was suggested for the wider prediction range of human walking motion. This was supported by the walking prediction results in sub-section 7.3.3. The non-conserved strain energy predicted by the posture-dependent elastic leg model (PDE) extends the effective range of human walking motion to the normal and high walk speed (see Figure 7.2-7.7), compared to that predicted by CAE and CATE model. Better predictions of ground reaction forces, CoM elevation and progression are also achieved (see Figure 7.9 and 7.10). In terms of periodic motion, none of the combination of the initial condition and the posture-dependent leg property extracted from the measurement data based on the non-conservation of system energy can generate a hundred step of human walking. On contrary, the proper combinations of initial condition and linear axial and tangential elastic leg properties extracted from conserved system energy basis were found to be able to generate such periodic motion (see sub-section 6.3.4 and 6.4.5 in Chapter 6). To gain insight into the effect of system energy on the periodicity of the human walking, the mechanical energy in the stance phase of the virtual leg operation on conserved and non-conserved system energy is investigated. The comparison is shown in Figure 7.11. For the virtual leg operation on conserved system energy, none of the mechanical energies is in phase with other forms of the mechanical energy. However, for the virtual leg operation on non-conserved

system energy, the elastic and kinetic are quite in phase while the gravitational potential energy is quite out of phase with other forms of mechanical energy. Such energy exchanges may require precise combination of leg properties and initial condition for the proper coordination of elastic, gravitational and kinetic energy to achieve a gait cycle.

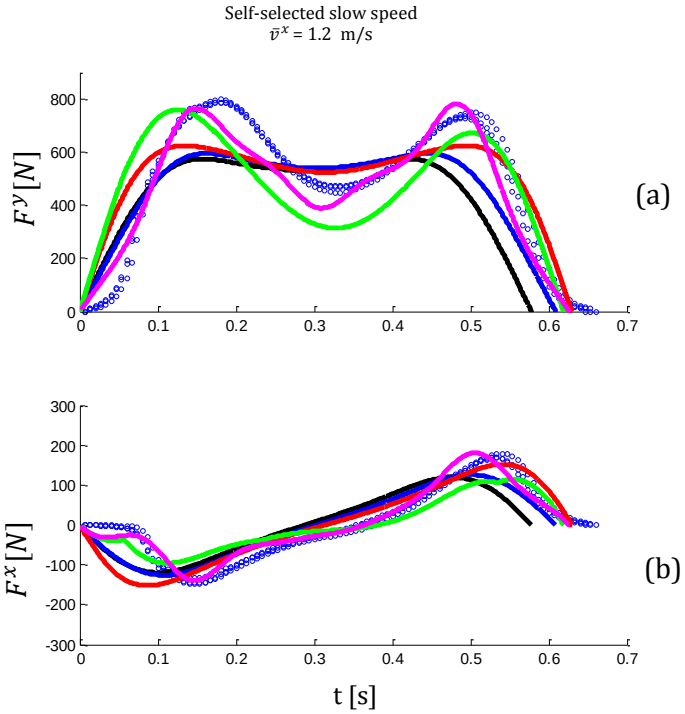

RMSE	Linear axial	Nonlinear axial (hard)	Nonlinear axial (soft)	Linear axial- tangential	Posture-dependent
$F^y[N]$	124	88.4	60.2	46.4	24.6
$F^x[N]$	41.6	33.6	23.8	30.4	17.4

Figure 7.9 The vertical (a) and horizontal (b) ground reaction forces predicted by the linear axial and tangential elastic leg model (red) as shown in Table 6.1 in Chapter 6 and the posture-dependent leg model (blue) as shown in Table 7.1 compared to the measured ground reaction forces at self-selected low speed (dot). The data set is obtained from three good trials of the walking measurements of subject no.2 at self-selected low walking speed. The root-mean square errors (RMSE) determined by the difference between the measured and predicted ground reaction forces (F^y, F^x) are given for the walking at self-selected slow speed.

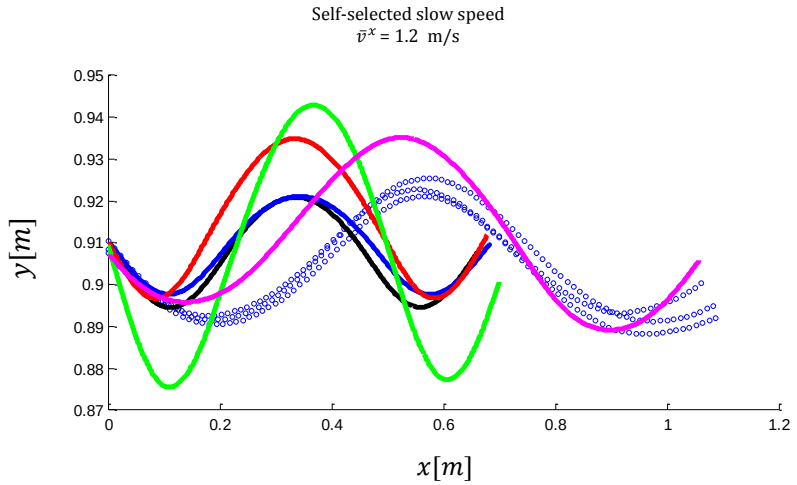

RMSE	Linear axial	Nonlinear axial (hard)	Nonlinear axial (soft)	Linear axial- tangential	Posture-dependent
$y[m]$	0.03	0.024	0.028	0.038	0.16
$x[m]$	0.52	0.48	0.44	0.4	0.11

Figure 7.10 The predicted CoM displacement (x, y) between two consecutive touchdowns by the linear axial-tangential elastic leg model (red) in Table 6.1 of Chapter 6 and by the posture-dependent leg model (blue) as shown in Table 7.1 compared to the measured CoM displacement (x, y) at self-selected low speed (dot). The data set is obtained from three good trials of the walking measurements of subject no.2 at self-selected low speed. The root-mean square errors (RMSE) determined by the difference between the measured and predicted displacements of the CoM (y, x) are given for the walking at self-selected slow speed.

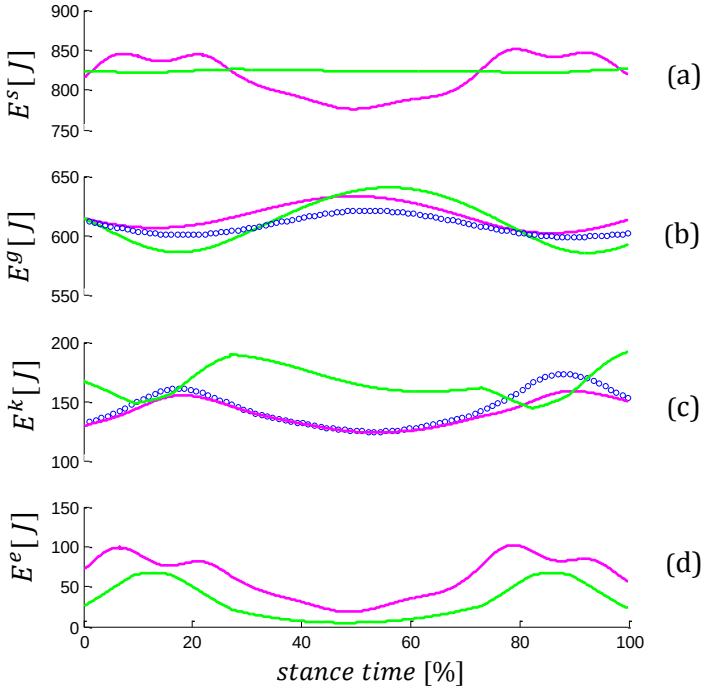

RMSE	Linear axial- tangential	Posture-dependent
$E^g[J]$	31.5	22.0
$E^k[J]$	42.2	15.4

Figure 7.11 The predicted mechanical energies including gravitational potential (b), kinetic (c) and strain energy (d) and the system energy (a) during the stance phase of human walking at low speed by CATE model operating with constant system energy (magenta) and PDE model operating with variable system energy (green) compared to the mean of the measured mechanical energies (E^g, E^k) at self-selected low speed (dot). The data set is obtained from three good trials of the walking measurements of subject no.2 at self-selected low speed. The root-mean square errors (RMSE) determined by the difference between the measured and predicted mechanical energies (E^g, E^k) are given.

7.4 Dynamic stability analysis

In the previous section, it was found that the periodic walking motion predicted by the posture-dependent leg properties is limited to 2 gait cycles. After this limit, the model will produce one of the two fall modes namely, a fall backward and a trip. Based only on the prediction of a couple of gait cycle, the limit cycle cannot be estimated and thus, it is not possible to examine the orbital stability. This limits the use of posture-dependent elastic leg model (PDE) to quantify the dynamic stability of the human walking when it

is treated as periodic motion. The last two orbits before fall mode of the simulated gait cycles at each walking speed are shown in Figure 7.12

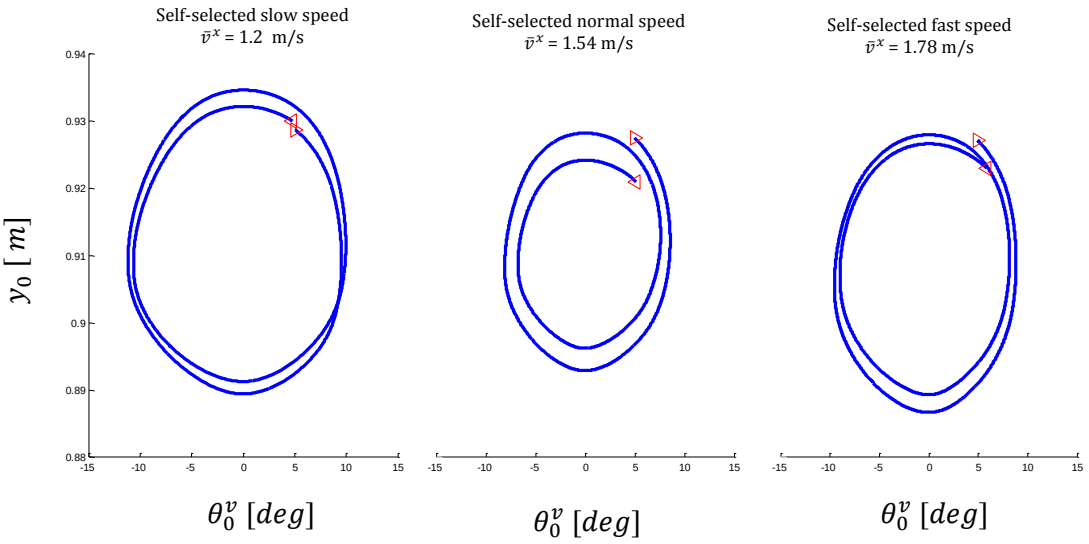

Figure 7.12 The orbits of state variables (y_0, θ_0^v) of the last three vertical leg orientations (VLO) of the periodic walking motion at low, normal and high speed generated by PDE model with leg property in Table 7.1. The initial VLO is represented by (▷) and the last VLO is represented by (◁).

7.5 Discussion

The validity region of posture-dependent leg property for human walking prediction was examined by using the posture-dependent elastic leg model (PDE) operating on non-conserved system energy. The variation of system energy during the gait was represented by the posture-dependent variation of the force-free leg length ($l_{0,q}$) and the tangential leg stiffness (k_q^t) extracted from the measurement data. With the variations of these leg properties, the explicit resources of energy absorption and production are not required, and the simplicity of the walking model can be maintained.

Compared to CATE model using linear elastic leg properties, the posture-dependent elastic leg model with posture-dependent elastic leg properties (PDE) has larger validity region of human walking prediction, which ranges from low to high speed of human walking motion. This may be a benefit of the changes in force-length relationship after the mid-stance due to the variation of system energy. Based on the posture-dependent variation of force-free leg length, the leg lengthening along with the increase of axial force was predicted after mid-stance. This improves the prediction accuracy of the ground reaction forces, CoM displacement and leg length and leg angle to the CATE model operating on conserved system energy. A better reproduction of the tangential force-leg angle relationship was also found. This supports the posture-dependent variation of the tangential stiffness in representing the nonlinear changes of the tangential stiffness from touchdown to toe-off. Only the axial force and leg shortening at the maximum leg shortening is underestimated. This may be due to the adjusted initial condition to achieve walking cycles.

The energy variation challenges the reproduction of periodic walking motion by using the posture-dependent elastic leg model (PDE). The coordination of mechanical energy exchanges found in the energy management during the stance phase may require a proper combination of the initial condition and the posture-dependent leg properties to generate the periodic walking motion and make the stable walking motion. Only a couple of gait cycles were predicted before the fall mode occurs in the further steps. This is consistent with the findings in the bipedal robot with actuated force-free leg length (Schmitt and Clark, 2009). A fine tuning of the change in force-free leg length throughout the stance is required to produce partial asymptotical stable gaits or the gait at the edge of orbital stability. The variation of system energy in this bipedal robot was

designed for the stabilisation of biped running over rough terrain in which the variation of CoM velocity at the Poincare section was required to get over the energetic perturbation. For the stability of gait pattern, the use of touchdown angle variation was suggested (Schmitt and Clark, 2009) to adjust the CoM velocity at the Poincare section. However, as mentioned earlier in Chapter 5, our measurement on the change of touchdown angle is limited to only two consecutive touchdowns. This is insufficient to investigate the significant changes of touchdown angle between consecutive steps. Further development on dynamic stability quantification may need to introduce the energetic perturbation to the walking simulation to investigate for the rate of recovery by using the gait sensitivity norm (Hobbelen and Wisse, 2007)(see sub-section 2.4.1 Chapter 2).

The posture-dependent leg properties improves the validity region and quality of human walking prediction while introduces aperiodic walking motion as a consequence of the variation of state variable at the end of walking steps. This aperiodic motion may represent a daily-life walking in which the stochastic variation of system energy is anticipated to overcome the uneven walking surface, touchdown impact and take-off impact (Byl and Tedrake, 2009). Such walking system may require further study to analyse the stochastic stability or metastability in which the dynamic stability is quantified on the transient dynamic system (Talkner et al., 1987; Bovier, 2004; Bovier, 2000; Weber, 2006).

Chapter 8 Conclusions and Future work

8.1 Conclusions

The objective of this thesis is to develop and validate computational framework based on mathematical models for the prediction and dynamic stability quantification of human walking motion, and to use this computational framework to analyse the effect of mechanical property of the human leg on dynamic stability of the walking motion. From the walking measurements, the extracted mechanical property of the human leg was used to predict the walking motion, which was then be used in dynamic stability analysis. The aim of the research work of this thesis is to provide a computational framework for dynamic stability analysis of human walking that is practical for clinical uses and can differentiate the dynamic stability of individuals. The research work described in this thesis includes three major parts, extraction of mechanical leg properties from gait measurements, development of simple models for human walking prediction and experimental validation, and dynamic stability quantification of human walking using the models.

In Chapter4, fundamental leg properties were extracted by fitting single valued functions of the axial force- leg length and tangential force-leg angle onto the measurement data, which both of linear and nonlinear elastic property are considered. Using a minimum root-mean-square fitting, the fundamental leg properties comprising

axial stiffness, rest leg length, tangential stiffness and force-free leg angles for the walking at different speeds and on different contact conditions were presented.

It was found that the axial and tangential stiffness obtained in the moving contact condition are higher than that obtained in the fixed contact condition, which is consistent with the previous research (Bullimore and Burn, 2006; Whittington and Thelen, 2009). For the linear elastic property, the axial and tangential leg properties obtained are independent of walking speed change for both contact conditions. For the non-linear elastic property, only hard nonlinear elasticity can fit the axial force-leg length relationship but with an overestimation of maximum axial force. The tangential force during early and late stance was underestimated by the Fourier series representation of the tangential force-leg angle relationship. A lower linear axial stiffness and a longer rest length were found, compared to a previous study on treadmill walking with an assumption that the total ground reaction force applies along the leg (Lipfert et al., 2012). The tangential force-leg angle relationship generated by the tangential leg property agrees well with a hip torque profile that stabilises the human walking motion represented by spring-mass model with hip joint and torso (Maus et al., 2010).

In Chapter 5, the posture-dependent variation of leg properties allows for the fitting of non-conservative force-displacement relationships onto the gait measurement data. Under both contact conditions, the axial property parameters comprising the linear axial stiffness and posture-dependent force-free leg length were extracted from axial force-leg length relationship. The tangential property parameters comprising the force-free leg angle and posture-dependent tangential stiffness were extracted from

tangential force-leg angle relationship. The results showed that the linear axial stiffness is independent of walking speed for both contact conditions. However, the other posture-dependent leg property parameters are dependent on walking speed but with different tendencies.

In Chapter 6, the fundamental leg properties were implemented into simple walking models operated with constant system energy in Chapter 5. In this thesis, the compliant leg model with axial elastic leg property (CAE) was used to examine the effect of both linear and nonlinear axial elastic properties on symmetrical walking motion. The complaint leg model with axial-tangential elastic leg property (CATE) was used to examine the effect of linear axial and tangential elastic leg properties on asymmetrical walking motion in which the velocity angle was introduced to represent the vertical leg orientation before or after the apex of the CoM position.

It was found that, for both models, the leg length at touchdown and take-off are equivalent. Using the reasonably adjusted leg property parameters based on measurement data and initial conditions, the model based on fundamental leg properties in moving contact condition generated periodic motion of human walking only in the low speed range of 1.01 – 1.25 m/s. However, the model based on fundamental leg properties in fixed contact condition underestimated the maximum axial force, which results in a failure of gait cycle. The hard spring stiffness that reproduces periodic walking motion is lower than that extracted from the measurement. Interestingly, the soft spring stiffness, which cannot be extracted by the minimum RMSE fitting, can generate periodic walking motions.

Using the compliant leg model with axial elastic property alone (CAE), the vertical-horizontal ground reaction force and the stance duration was better predicted by the non-linear elasticity than by the linear elasticity. The CoM horizontal displacement and the leg length after the mid-stance were underestimated by both linear and non-linear axial elasticity. By using the compliant leg model with axial and tangential elasticity (CATE), the asymmetry of walking motion was represented. The peak magnitude of vertical ground reaction force and the stance duration were better predicted by the CATE model than by the CAE model while the underestimation of horizontal ground reaction force, horizontal displacement of the CoM and the leg length after mid-stance still persisted.

Also in Chapter 6, the dynamic stability of the periodic walking motions was quantified in terms of orbital stability. The greatest Floquet multiplier of walking motions on different leg properties was calculated to identify the initial condition leading the walking motion to steady state. The global stability in terms of robustness was quantified by the area of basin of attraction containing all of those initial conditions. It was found that, using the CAE model with linear elasticity, the global stability improves with a bigger touchdown contact angle. Interestingly, the maximum region of global stability was close to the linear axial stiffness and touchdown contact angle value extracted from the measurement data of walking at self-selected low speed. On the effect of nonlinearity of leg stiffness, the global stability of periodic walking motion decreases rapidly with the stronger nonlinearity of leg stiffness. It is in contrast to the findings in running robots with perturbation where the hard spring absorbs the touchdown impact and the soft spring resists the energy disturbance due to the change in floor height. This suggests the different contributions that the leg properties have on

different type of stability. A proper combination of linear elastic leg property may be required to stabilise gait pattern while the nonlinearity of leg stiffness may be required to stabilise gait cycle after perturbation.

With the incorporation of the tangential elasticity, the global stability improves slightly with a wider range of stable initial CoM height and the shifting of the stable initial horizontal velocity closer to the measured horizontal velocity. The stable region of the walking motion predicted by CATE model is also limited by the underestimation of vertical ground reaction force at mid-stance. To improve the prediction of vertical ground reaction force, the change of leg property from linear to nonlinear property after mid-stance was suggested to decrease the leg shortening and thus increase the CoM progression while reproducing the second peak of vertical and horizontal ground reaction force. The incorporation of the proper nonlinear tangential elasticity was also suggested to improve the reproduction of vertical and horizontal ground reaction force especially during mid-stance.

In Chapter 7, the posture-dependent leg properties were implemented into a simple walking model operated with non-constant system energy. The posture-dependent elastic leg model (PDE) was used to examine the stable region of human walking prediction based on posture-dependent leg properties. The human walking motions were predicted from low to high speed (1.12 – 1.8 m/s) by the PDE model with posture-dependent leg properties extracted from the fixed contact condition. The force-displacement relationship represented by this model showed that a change in leg length and leg angle is not necessarily accompanied by a change in leg force and vice versa. The leg lengthening after mid-stance, the CoM progression, the stance duration and the

magnitude of the vertical and horizontal ground reactions were better predicted compared to the results of the linear axial-tangential elastic leg model.

Also in Chapter 7, the mechanical energies in terms of strain, gravitational potential, kinetic and total energy were calculated to investigate the effect of energy management provided by posture-dependent leg properties on dynamic stability of human walking. The variation of state variables $(y_0, \dot{x}_0, \dot{y}_0)$ at the end of walking steps was found. It was also found that the mechanical energy profiles of this non-conservative system are quite different from those of conservative system that is orbital stable. These differences may affect on the orbital stability of the non-conservative system as the state variables $(y_0, \dot{x}_0, \dot{y}_0)$, which is used to consider the periodic motion, are parts of the variables in the mechanical energies. Thus, the return of mechanical energy after a walking step as found in the conservative system is required to generate the periodic motion. The model based on extracted posture-dependent leg properties reproduced only 1-2 gait cycles before falling over. This makes the identification of orbital stability impossible where a large number of repetitive walking motion is required. A similar phenomenon was also observed in biped running machine with a posture-dependent force-free leg length when a sharp tuning of leg properties were required to maintain the walking motion at the edge of orbital stability (Schmitt and Clark, 2009). The incorporation of the change in leg touchdown angle from one to the next step was suggested for the orbital stability quantification. However, the fluctuation of system energy was found to stabilise the biped machine with posture-dependent force-free leg length when running over rough terrain. This effect of system energy fluctuation on dynamic stability requires further investigation.

In summary, the proposed simple walking models showed potentials in human walking prediction as required in the reproduction of periodic walking motion for the quantification of orbital stability. The dynamic stability analysis using different leg properties provides guidance about the fundamental leg properties required for stable walking motion and the effects of leg property variation on the dynamic stability of human walking. A proper leg definition allows more realistic leg properties to be extracted from the measurement data and a more accurate prediction of the human walking motion. The dynamic stability analysis is more reliable when the dynamic stability is quantified on the accurate prediction of human walking and the wide variety of human leg properties.

8.2 A computational framework for the motion prediction and dynamic stability analysis of human walking

Based on the work in this thesis, a computational framework for the motion prediction and dynamic stability analysis of human walking motion is proposed. The framework involves the combined use of human gait measurements in leg properties extraction and the simple computational models to generate the periodic walking motion to allow the dynamic stability quantification of the gait pattern. The aim of the computational framework is to provide a predictive simulation template for use in the studies of dynamic stability on the subject-specific measurement base.

A schematic diagram of the computational framework is illustrated in Figure 8.1. The initial conditions ($y_0, \dot{x}_0, \dot{y}_0$) and mechanical leg properties (k^n, l_0 and k^t, θ_0) extracted from force-displacement ($F^n - l, F^t - \theta$) relationships of human walking

measurements are the inputs for the simple computational models to predict human walking motion ($F^x, F^y, x, y, l, \theta$). In the parameter region that predicts human walking motion, the reproduction of periodic walking motion was examined. If no solution exists in the region of extracted leg properties and measured initial conditions, some refinement is allowed within a small range away from the measured values. In this way, the periodic walking motion can be recreated by using the simple walking models operating in the established parameter region. Then, dynamic stability of the periodic walking motion is quantified by using a method for global stability analysis in terms of robustness. Finally, the dynamic stability of human walking motion with a wide variety of mechanical leg properties is obtained to better understand the leg property requirement to maintain walking stability.

The core of this computational framework is the simple walking models which allow for a wide variety of mechanical leg properties and virtual leg operations to be examined for human walking prediction. This flexible platform for human walking prediction could gain the insight into the effect of the mechanical property of human leg on the dynamic stability during walking.

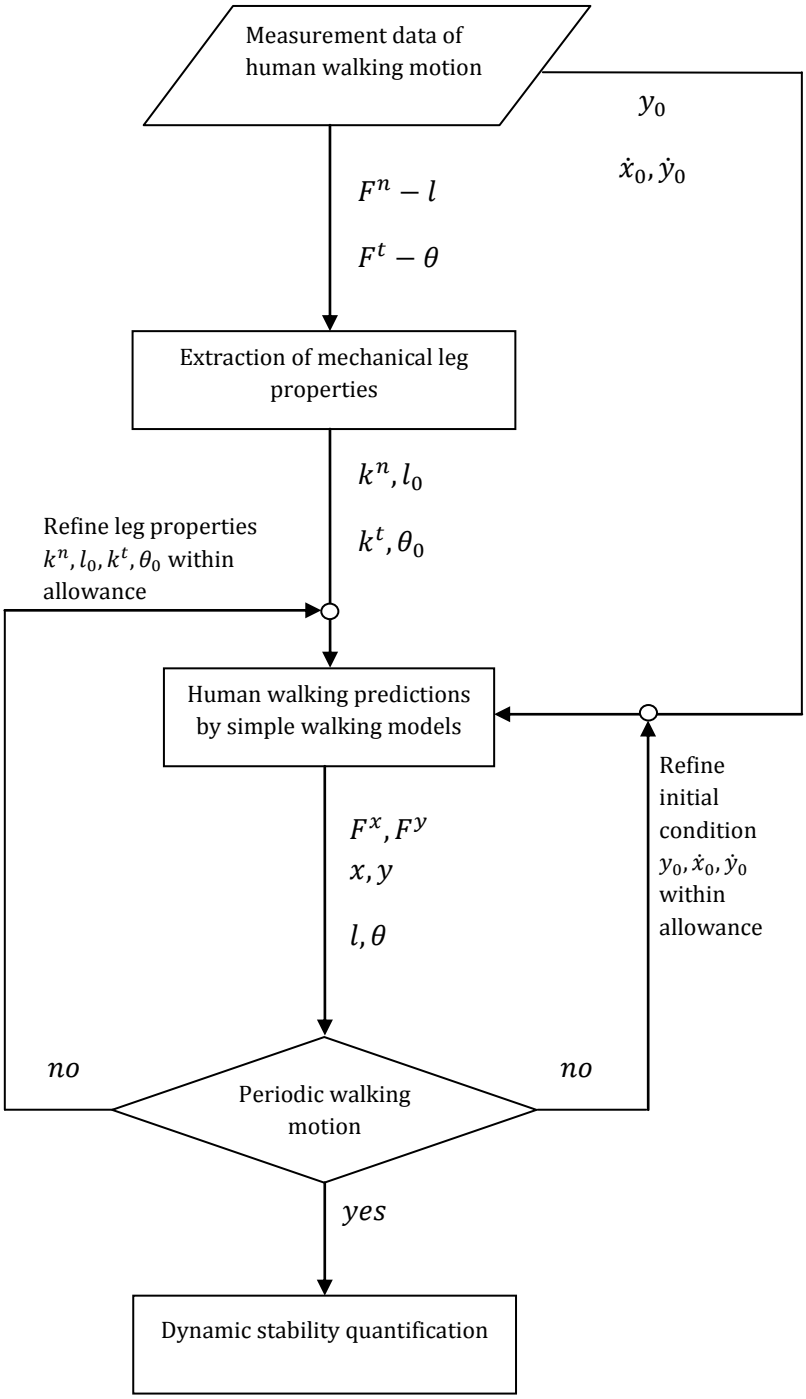

Figure 8.1 Schematic diagram of the computational framework for the motion prediction and dynamic stability analysis of human walking

8.3 Original contributions arising from this work

In this thesis, many original works have been conducted to provide insight into the effects of leg properties on the stability of human walking. First of all, a large measurement database of human walking motion was created. It contains walking measurement data of 8 subjects on 3 self-selected walking speeds, which 10 trials were recorded at each walking speed. The whole-body centre of mass motion and the leg dynamics were calculated from the kinetic and kinematic measurement data. These calculations require only the kinetic-kinematic measurement data at the beginning of the walking step and kinetic data from the force plates during the walking step.

And then, the mechanical property of the human leg was extracted from the measurement database. A leg property definition was adopted from a previous study (Lipfert et. al, 2012), and three different leg property definitions were proposed to extract mechanical property from different mechanical functions that human leg may perform during walking. These leg property definitions comprise linear axial elastic leg property, nonlinear axial elastic leg property, linear axial-tangential elastic leg property and posture-dependent elastic leg property. The effects of walking speed and foot-ground contact condition comprising fixed and moving contact conditions on the leg property were investigated in each extraction. These leg property definitions and investigations are different from a previous study in which only the linear axial elastic property was extracted, and the moving location of foot-ground contact was only investigated.

And then, the linear axial elastic leg property that allows for maximum global stability of the walking motion was predicted by using a compliant leg model with axial elastic property (CAE). The decrease of global stability with the stronger nonlinear leg stiffness

was also predicted by the same model. A compliant leg model with axial and tangential elastic property (CATE) was developed to examine the dynamic stability of human walking with axial and tangential elastic leg property. The CATE model predicts that the maximum speed for stable walking motion is increased by the incorporation of linear tangential elasticity. However, the dynamic stability quantification using CAE and CATE model is limited to the low speed walking (1.01 – 1.25 m/s) only.

Posture-dependent elastic leg model (PDE) was developed to examine the dynamic stability of human walking with posture-dependent elastic leg property. By this model operating with variable system energy, the motions of the leg and the centre of mass were better predicted than by axial-tangential elastic leg model operating with constant system energy. By using PDE model, the effective range of human walking prediction is enlarged to 1.12 -1.8 m/s. This PDE model represents the variation of the CoM velocity at the end of walking steps, which restricts the orbital stability of walking motion.

Finally, by using this flexible computational framework for the dynamic stability analysis, the effect of mechanical property of the leg on the dynamic stability of human walking was presented. In this computational framework, the deliberate leg property definitions can provide insight into the wide variety of the human leg property. To obtain the mechanical property of the human leg, only the measurement data of the ground reaction force during the walking motion and that of the centre of mass motion at the beginning of step is required. The simple models of human walking are flexible to the input parameters extracted from different conditions of human walking, and can predict the accurate motion of the centre of mass (CoM), which are the only motion required for dynamic stability quantification.

In summary, only the motion data of the CoM and the leg is required in this computational framework for the dynamic stability analysis of human walking. The minimal requirements from the human walking measurement to the dynamic stability quantification make this computational framework be flexible and practical for the clinical applications including the dynamic stability diagnostic in pathologic walking conditions. The further improvement in the leg property definition and the simple model will help to provide insight into the subject-specific leg property, which can then allow the differentiation between the dynamic stability of walking motion of individuals.

8.4 Future work

The accuracy of human walking measurement data affects directly on the extracted leg properties. For example, the data of the whole-body centre of mass motion during over ground and treadmill walking provide different range of leg properties. The whole-body centre of mass motion calculated by ground reaction force integration requires a good initial condition from the kinetic and kinematic measurements. Starting the ground reaction force records from standing still may assure low signal drift, but this may not be applicable for the measurement of over ground walking with subject-selected speeds as a very long walking track, a large number of force plates and a large volume of measurement will be required. Also, this may not be replaceable by the measurement on treadmill walking as these two types of measurement generally provide different ground reaction force profiles (AlGheshyan, 2012, Dierick et al., 2004; Schablowski and Gerner, 2006; White et al., 1998). An alternative calculation may be adopted from (Maus et al., 2011) where kinetic and kinematic records on standing still beginning are not required. By this way, although the calculation of centre of mass motion is more

complicated than the convention (Cavagna et al., 1983), the accurate whole-body CoM motion prediction can be provided.

The definition of the mechanical property

The definition of the mechanical property of the human leg may be improved to represent the explicit energy fluctuation, for example, the energy absorption and injection provided by the variation of leg properties. However, it has been found that the relationship between axial force, leg length and leg length change during the gait cycle is singular. In other word, the same combination between leg length and leg length change is responsible to more than one value of axial force. (Boonpratatong and Ren, 2011a; Boonpratatong and Ren, 2011b). This phenomenon occurring during the mid stance may be a consequence of the multi-configurable ankle joint (Boonpratatong and Ren, 2010). This indicates that a constant stiffness incorporating with a constant viscous damping coefficient cannot be used to represent such singular function of leg force, leg length and leg length change. Further investigation on alternative terms to represent the energy fluctuation may be required.

The effect of foot-ground contact on walking stability

The effect of foot-ground contact on walking stability may need further investigation. The human walking model with foot segment may be required. A walking model with roller feet has been used to predict the centre of pressure during human walking motion (Whittington and Thelen, 2009). However, the rolling of whole-body centre of mass on such moving contact is still quite different from that on foot-ground contact during

human walking motion. Since the ankle joint has been found to perform different functions during the first and the second half of stance (Boonpratatong and Ren, 2010). The multi-configuration of the ankle joint may be required to illustrate whole-body centre of mass motion on the moving foot-ground contact during human walking motion. Therefore, for the foot segment, the phase dependent rollover model of the foot (Ren et al., 2008; Ren et al., 2010) may be needed. The investigation into these effects may reveal the explicit dynamics of force-free leg length during human walking motion.

The incorporation of variable leg touchdown

To improve the orbital stability quantification of human walking motion using posture-dependent leg property model, the incorporation of variable leg touchdown angle between walking steps may be required. The measurement set-up, leg property definition and human walking modelling need to be improved, accordingly. In human walking measurement, a longer walking track with more surface mounted force plates is required to capture the variation of leg touchdown angle between walking steps. The mechanical leg property definition needs to be modified accordingly to include the relationship between variable leg touchdown angle and other leg properties. The human walking model needs to be accordingly modified to accommodate this relationship over walking steps. The variation of the other leg properties between walking steps may also be captured by this improvement, which would provide the better prediction of human walking motion and, therefore, more realistic dynamic stability prediction.

The variable system energy as the anticipation of disturbance

To gain better insight into the orbital stability of human walking motion by using posture-depending leg properties, the variable system energy as the anticipation of disturbance may be investigated. To achieve that, some perturbations need to be introduced to the walking simulations, which a proper method for orbital stability quantification on the perturbed walking motion i.e. gait sensitivity norm may be required (Hobbelen and Wisse, 2007).

Generalisation of the mechanical property

Lastly, more experimental studies are needed to generalise the mechanical property of human leg and improve the validations of human walking prediction. These two factors are very crucial to the reliability of the dynamic stability analysis of human walking on the effect of mechanical leg properties. How stable is the walking of an individual human? This question needs further experimental investigations and computational studies. The high complexity of human walking model may not be the solution for a better prediction of human walking. The extraction of the crucial leg properties based on the available human walking measurements and the flexibility of model parameters may be a major key to differentiate the walking motion of one from the other, which can be further used to differentiate the dynamic stability of individuals.

Appendix A – Anatomical landmarks used in 3D gait measurement

(Ren et al., 2005)

Anatomical landmark	Description	Property
Head		
VERT	Vertex, the most cranial point of the head	bony
RTMJ	Right temporomandibular joint	bony
LTMJ	Left temporomandibular joint	bony
Trunk		
PXIP	Xiphoid process	bony
IJUG	Jugular notch	bony
C7SP	Spinous process C7	bony
T8SP	Spinous process T8	bony
Pelvis		
RASIS	Right anterior superior spine	bony
LASIS	Left anterior superior spine	bony
RPSIS	Right posterior superior spine	bony
LPSIS	Left posterior superior spine	bony
Right humerus		
RMHU	Right medial humeral epicondyle	bony
RLHU	Right lateral humeral epicondyle	bony
GJCR	Right glenohumeral joint centre	virtual
Right forearm		
RRSY	Right radial styloid	bony
RUSY	Right ulnar styloid	bony
EJCR	Right elbow joint centre	virtual
Left humerus		
LMHU	Left medial humeral epicondyle	bony

LLHU	Left lateral humeral epicondyle	bony
GJCL	Left glenohumeral joint centre	virtual
Left forearm		
LRSY	Left radial styloid	Bony
LUSY	Left ulnar styloid	Bony
EJCL	Left elbow joint centre	Virtual
Right femur		
RLEP	Right lateral epicondyle	Bony
RMEP	Right medial epicondyle	Bony
HJCR	Right hip joint centre	Virtual
Right shank		
RHFB	Right apex of fibula head	Bony
RTTB	Right tibial tuberosity	Bony
RMML	Right medial malleolus	Bony
RLML	Right lateral malleolus	Bony
Right foot		
CAR	Upper ridge of the calcaneous	Bony
FMR	Dorsal aspect of first metatarsal head	Bony
SMR	Dorsal aspect of second metatarsal head	Bony
VMR	Dorsal aspect of fifth metatarsal head	Bony
Left femur		
LLEP	Left lateral epicondyle	Bony
LMEP	Left medial epicondyle	Bony
HJCL	Left hip joint centre	Virtual
Left shank		
LHFB	Left apex of fibula head	Bony
LTTB	Left tibial tuberosity	Bony

LMML	Left medial malleolus	Bony
LLML	Left lateral malleolus	Bony
Left foot		
CAR	Upper ridge of the calcaneous	Bony
FMR	Dorsal aspect of first metatarsal head	Bony
SMR	Dorsal aspect of second metatarsal head	Bony
VMR	Dorsal aspect of fifth metatarsal head	Bony

Appendix B – Force equations

Chapter 6

6.1A Compliant leg model with axial elastic property (CAE)

$$m\ddot{x} = F^{n,trail}\frac{x}{l^{trail}} \tag{6.1A}$$

$$m\ddot{y} = F^{n,trail}\frac{y}{l^{trail}} - mg, \tag{6.2A}$$

for the initial single support phase.

$$m\ddot{x} = F^{n,trail}\frac{x}{l^{trail}} - F^{n,lead}\frac{(d-x)}{l^{lead}} \tag{6.3A}$$

$$m\ddot{y} = F^{n,trail}\frac{y}{l^{trail}} + F^{n,lead}\frac{y}{l^{lead}} - mg, \tag{6.4A}$$

for the double support phase and

$$m\ddot{x} = -F^{n,lead}\frac{d-x}{l^{lead}} \tag{6.5A}$$

$$m\ddot{y} = F^{n,lead}\frac{y}{l^{lead}} - mg\ , \tag{6.6A}$$

for the final single support phase, where

$$l^{trail} = \sqrt{x^2 + y^2}, \tag{6.9}$$

$$l^{lead} = \sqrt{(d-x)^2 + y^2}. \tag{6.10}$$

Ground reaction forces

$$F_{CAE}^{x,trail} = F^{n,trail}\frac{x}{l^{trail}} \tag{A6.1}$$

$$F_{CAE}^{y,trail} = F^{n,trail}\frac{y}{l^{trail}} \tag{A6.2}$$

$$F_{CAE}^{x,lead} = -F^{n,lead}\frac{d-x}{l^{lead}} \tag{A6.3}$$

$$F_{CAE}^{y,lead} = F^{n,lead}\frac{y}{l^{lead}} \tag{A6.4}$$

6.2A Compliant leg model with axial and tangential elastic property (CATE)

$$m\ddot{x} = F^{n,trail}\frac{x}{l^{trail}} + F^{t,trail}\frac{y}{l^{trail}} \tag{6.14A}$$

$$m\ddot{y} = F^{n,trail}\frac{y}{l^{trail}} + F^{t,trail}\frac{x}{l^{trail}} - mg, \tag{6.15A}$$

for the initial single support phase.

$$m\ddot{x} = F^{n,trail}\frac{x}{l^{trail}} - F^{n,lead}\frac{(d-x)}{l^{lead}} + F^{t,trail}\frac{y}{l^{trail}} + F^{t,lead}\frac{y}{l^{lead}} \tag{6.16A}$$

$$m\ddot{y} = F^{n,trail}\frac{y}{l^{trail}} + F^{n,lead}\frac{y}{l^{lead}} - mg, \tag{6.17A}$$

for the double support phase and

$$m\ddot{x} = -F^{n,lead}\frac{d-x}{l^{lead}} + F^{t,lead}\frac{y}{l^{lead}} \tag{6.18A}$$

$$m\ddot{y} = F^{n,lead}\frac{y}{l^{lead}} + F^{t,lead}\frac{d-x}{l^{lead}} - mg\ , \tag{6.19A}$$

for the final single support phase.

6.3A Ground reaction forces

$$F_{CATE}^{x,trail} = F^{n,trail}\frac{x}{l^{trail}} + F^{t,trail}\frac{y}{l^{trail}} \quad \text{(A6.5)}$$

$$F_{CATE}^{y,trail} = F^{n,trail}\frac{y}{l^{trail}} + F^{t,trail}\frac{x}{l^{trail}} \quad \text{(A6.6)}$$

$$F_{CATE}^{x,lead} = -F^{n,lead}\frac{d-x}{l^{lead}} + F^{t,lead}\frac{y}{l^{lead}} \quad \text{(A6.7)}$$

$$F_{CATE}^{y,lead} = F^{n,lead}\frac{y}{l^{lead}} + F^{t,lead}\frac{d-x}{l^{lead}} \quad \text{(A6.8)}$$

Chapter 7

7.1A Posture-dependent elastic leg model (PDE)

For the PDE model, the equations of motion in terms of force are similar to those for the CATE model. The only difference is leg property variations (see Equation 5.1 – 5.11) and the difference conditions for phase transitions (see Equation 7.15-7.16).

Appendix C – Averaged CoM motion at vertical leg orientation

Table C1 The averaged CoM motion comprising forward velocity (v^x) , height (y) and velocity head (θ^v) at vertical leg orientation of individual subject

Subject	Slow			Normal			Fast		
	v^x	y	θ^v	v^x	y	θ^v	v^x	y	θ^v
No.1	1.146	0.916	5.2	1.433	0.914	4.5	1.629	0.915	4.4
No.2	1.23	0.921	6.9	1.54	0.922	5.7	1.72	0.924	5.6
No.3	1.21	0.854	7.2	1.425	0.841	5.9	1.648	0.851	5.5
No.4	1.24	0.904	5.1	1.372	0.886	4.8	1.619	0.889	4.6
No.5	1.3	0.938	7.1	1.422	0.937	5.6	1.633	0.94	5.5
No.6	1.252	0.941	6.3	1.404	0.938	5.7	1.653	0.94	5.7
No.7	1.128	0.911	4.9	1.52	0.908	4.1	1.614	0.91	4.4
No.8	1.147	0.915	7.1	1.46	0.914	5.9	1.616	0.913	5.7

Appendix D – Some source code for the core work

Chapter 3

3.1D. Calculation of the CoM motion

```
global whole_body_CM
global y_ref
global touch_down_frame end_frame01 start_frame02 start_frame03 end_frame03
global forceVerticalTot forceHxTot forceVertical03_vir forceHx03_vir
global start_frame01  end_frame02
global new_DoS2SS_vel_CMy new_DoS2SS_pos_CMy new_DoS2SS_vel_CMx
new_DoS2SS_pos_CMx

frame_rate = 150; %capturing frame rate (frame/sec)


%exclude NaN data
%%%%%%%%%%%%%%%%%%%%%%
start_frame01 = 53;

end_frame01 = 143;

start_frame02 = 118;

end_frame02 = 207;

overlap = NaN(start_frame02 - start_frame01,1);

touch_down_frame = start_frame02-start_frame01;%started from start_frame01

m = 69;
%%%%%%%%%%%%%%%%%%%%%%
g = 9.81;

accyTotal = zeros(end_frame01-start_frame02,1);
accxTotal = zeros(end_frame01-start_frame02,1);
accx_on_1st = zeros(end_frame01-start_frame02,1);
accx_on_2nd = zeros(end_frame01-start_frame02,1);
accy_on_1st = zeros(end_frame01-start_frame02,1);
accy_on_2nd = zeros(end_frame01-start_frame02,1);
new_DoS2SS_vel_CMx = zeros(end_frame01-start_frame02,1);
new_DoS2SS_vel_CMy = zeros(end_frame01-start_frame02,1);
new_DoS2SS_pos_CMx = zeros(end_frame01-start_frame02,1);
new_DoS2SS_pos_CMy = zeros(end_frame01-start_frame02,1);


forceVertical03_temp = zeros(size(forceVertical01

%force03 imitates force01 and force04 imitates force02
%but start_frame03 can be adjusted as measurement data of force03's timing
is not available
start_frame03 = start_frame02+(2)+(start_frame02 - start_frame01);
```

```
end_frame03 = start_frame03+ (end_frame01 - start_frame01);

%zero force frame included @b4 and @after contact
forceVertical03_temp(start_frame03:end_frame03) =
forceVertical01(start_frame01:end_frame01);

%start 1st frame together with forceVertical01
forceVertical03_vir = forceVertical03_temp;


forceVertical00_temp = zeros(size(forceVertical02));

start_frame00 = start_frame01;

end_frame00 = start_frame01 + (end_frame02 - start_frame03);

forceVertical00_temp(start_frame00-2:end_frame00) =
forceVertical02(start_frame03-2:end_frame02
forceVertical00_vir = forceVertical00_temp ;

if length(forceVertical01)< length(forceVertical03_vir)
extend_size = length(forceVertical03_vir)-length(forceVertical01);
forceVertical01(length(forceVertical01)+1:length(forceVertical03_vir))=zero
s(extend_size,1);
forceVertical02(length(forceVertical02)+1:length(forceVertical03_vir))=zero
s(extend_size,1);
forceVertical00_vir(length(forceVertical00_vir)+1:length(forceVertical03_vi
r))=zeros(extend_size,1);
end
totalVGRF = forceVertical00_vir + forceVertical01 + forceVertical02 +
forceVertical03_vir;

forceHx03_temp = zeros(size(forceHx01));

forceHx03_temp(start_frame03:end_frame03) =
forceHx01(start_frame01:end_frame01);%zero force frame included @b4 and
@after contact

forceHx03_vir = forceHx03_temp ;%start 1st frame together with
forceVertical01

netGRF03 = sqrt(forceHx03_vir.^2 + forceVertical03_vir.^2) ;

forceHx00_temp = zeros(size(forceHx02));

forceHx00_temp(start_frame00-2:end_frame00) = forceHx02(start_frame03-
2:end_frame02);

forceHx00_vir = forceHx00_temp ;

if length(forceHx01)< length(forceHx03_vir)
extend_size = length(forceHx03_vir)-length(forceHx01);
forceHx01(length(forceHx01)+1:length(forceHx03_vir))=zeros(extend_size,1);
forceHx02(length(forceHx02)+1:length(forceHx03_vir))=zeros(extend_size,1);
forceHx00_vir(length(forceHx00_vir)+1:length(forceHx03_vir))=zeros(extend_s
ize,1);
end
totalHGRF = forceHx00_vir + forceHx01 + forceHx02 + forceHx03_vir ;
```

```
forceVerticalTot = (totalVGRF-m*g)/m; %forceVertical01

forceHxTot = totalHGRF/m;


% whole-body motion on marker base started on forceplate01

new_whole_body_CM_stance = whole_body_CM(start_frame01-
2:length(whole_body_CM),:);% include pos @zeroforce frame and extra frame
for diff

new_y_ref_stance = y_ref*ones(length(new_whole_body_CM_stance),1);

Net_whole_body_CMy_stance = (new_whole_body_CM_stance(:,2)-
new_y_ref_stance);

Net_vel_whole_body_CMy_stance =
frame_rate*[NaN;diff(Net_whole_body_CMy_stance)];% vel:mm/s |include vel
@zeroforce frame

Net_acc_whole_body_CMy_stance =
[NaN;diff(Net_vel_whole_body_CMy_stance)];%mm/s/frame


whole_body_CMx_stance = new_whole_body_CM_stance(:,1);% mm

vel_whole_body_CMx_stance =
frame_rate*[NaN;diff(whole_body_CMx_stance)];%mm/sec

acc_whole_body_CMx_stance =
[NaN;diff(vel_whole_body_CMx_stance)];%mm/sec/frame


DoS2SS_vel_CMx  =
vel_whole_body_CMx_stance(touch_down_frame+1:length(vel_whole_body_CMx_stan
ce),:);%include vel @zeroforce frame

DoS2SS_vel_CMy =
Net_vel_whole_body_CMy_stance(touch_down_frame+1:length(Net_vel_whole_body_
CMy_stance),:);include vel @zeroforce frame


new_DoS2SS_pos_CMy(1)= Net_whole_body_CMy_stance(touch_down_frame+1);%pos
@contact = start frame01-2+touchdown+1 = start frame01+touchdown-1

new_DoS2SS_pos_CMx(1)= whole_body_CMx_stance(touch_down_frame+1);%pos
@contact = start frame01-2+touchdown+1


new_DoS2SS_vel_CMx(1) = DoS2SS_vel_CMx(1);

new_DoS2SS_vel_CMy(1) = DoS2SS_vel_CMy(1);
```

```
%calculate position, velocity and acceleration started from touch down
%position-2, touch down vel-1 and touch down acc-0 of leg02

for n = 1:end_frame02-start_frame02+2 %from leg02 touchdown to end of DS of
replicate leg01 on forceplate03 ;

accyTotal(n) = (10^3/frame_rate)*forceVerticalTot(start_frame02+n-2);

new_DoS2SS_vel_CMy(n+1,:) = new_DoS2SS_vel_CMy(n) + accyTotal(n);%vel@ next
= vel@ forcezero + acc btw forcezero frame and the next

new_DoS2SS_pos_CMy(n+1,:) = new_DoS2SS_pos_CMy(n) +
(1/frame_rate)*new_DoS2SS_vel_CMy(n);

accxTotal(n) = (10^3/frame_rate)*forceHxTot(start_frame02+n-2);%mm/s/frame

new_DoS2SS_vel_CMx(n+1,:) = new_DoS2SS_vel_CMx(n) + accxTotal(n);%

new_DoS2SS_pos_CMx(n+1,:) = new_DoS2SS_pos_CMx(n) +
(1/frame_rate)*new_DoS2SS_vel_CMx(n);


end
```

3.2D Calculation of leg force and length

```
%% leg length for trailing and leading leg during double-single support
%on fixed CoP

global new_DoS2SS_pos_CMx new_DoS2SS_pos_CMy
global new_DoS2SS_vel_CMx new_DoS2SS_vel_CMy
global touch_down_frame
global start_frame01 start_frame02 end_frame01 end_frame02
global touch_down_whole_body_CMx touch_down_whole_body_CMy
global touch_down_vel_whole_body_CMx touch_down_vel_whole_body_CMy
global mean_CoPx01 step_length
global normal_force02
global free_length02  init_legVel02 end_length02
global eff_velocity_actuator02 end_eff_velocity_actuator02
global excursion02 end_excursion02 fCoP_velocity_actuator02

global tangent_force02
global free_angle02 int_diff_ang02
global eff_angV02
global rel_angle02 angle_leg02

frame_rate = 150; %capturing frame rate (frame/sec)


overlap = NaN(start_frame02 - start_frame01,1);

touch_down_frame = start_frame02-start_frame01;%started from start_frame01
%%%%%%%%%%%%%%%%%%%%

%global CoP

new_glob_CoPx01 = glob_CoPx01(start_frame01:end_frame01,:);

new_glob_CoPx02 = glob_CoPx02(start_frame02:end_frame02,:);

new_glob_CoPz01 = glob_CoPz01(start_frame01:end_frame01,:);

new_glob_CoPz02 = glob_CoPz02(start_frame02:end_frame02,:);


%motion of Whole-body CoM
%include the WCoM trajectory at contact(when force=0)and extra WCoM for the
calculation of velocity = diff(whole_body_CM)

%
new_whole_body_CM01 = [extra_new_DoS2SS_pos_CMx(1:end_frame01-
start_frame02+3),extra_new_DoS2SS_pos_CMy(1:end_frame01-
start_frame02+3)];%(mm)

new_whole_body_CM02 = [extra_new_DoS2SS_pos_CMx(1:end_frame02-
start_frame02+3), extra_new_DoS2SS_pos_CMy(1:end_frame02-
start_frame02+3)];%(mm)

new_whole_bodyV_CM01 = [extra_new_DoS2SS_vel_CMx(1:end_frame01-
start_frame02+3),extra_new_DoS2SS_vel_CMy(1:end_frame01-start_frame02+3)];
```

```
new_whole_bodyV_CM02 = [extra_new_DoS2SS_vel_CMx(1:end_frame02-
start_frame02+3),extra_new_DoS2SS_vel_CMy(1:end_frame02-start_frame02+3)];


touch_down_whole_body_CMx = new_DoS2SS_pos_CMx(1,1)
;%new_whole_body_CM01(2,1) ;(mm)

touch_down_whole_body_CMy = new_DoS2SS_pos_CMy(1,1)
;%new_whole_body_CM01(2,2);(mm)


touch_down_vel_whole_body_CMx = new_DoS2SS_vel_CMx(1,1) ;%(mm/sec)

touch_down_vel_whole_body_CMy = new_DoS2SS_vel_CMy(1,1) ;%(mm/sec)


%leg length on fixed CoP

[CoM_CoP_value id_CoP_frame]= min(sqrt((new_glob_CoPx02-
(new_DoS2SS_pos_CMx(1:end-2))).^2));%CoP@vertical leg

CoP_vert_leg02 = new_glob_CoPx02(id_CoP_frame);


mean_CoPx01 = mean(new_glob_CoPx01)*ones(length(new_whole_body_CM01),1);

mean_CoPx02 = CoP_vert_leg02*ones(length(new_whole_body_CM02),1);

mean_CoPz01 = mean(new_glob_CoPz01)*ones(length(new_whole_body_CM01),1);

mean_CoPz02 = mean(new_glob_CoPz02)*ones(length(new_whole_body_CM02),1);


%step length and leg length

step_length = mean_CoPx02(1) - mean_CoPx01(1);


extra_length_fCoP01 = sqrt((new_whole_body_CM01(:,1)- mean_CoPx01).^2 +
(new_whole_body_CM01(:,2)).^2);

extra_length_fCoP02 = sqrt((new_whole_body_CM02(:,1)- mean_CoPx02).^2 +
(new_whole_body_CM02(:,2)).^2);

length_fCoP01 = extra_length_fCoP01(1:length(new_whole_body_CM01));

length_fCoP02 = extra_length_fCoP02(1:length(new_whole_body_CM02));

min_length_fCoP02 = min(length_fCoP02);

max_length_fCoP02 = max(length_fCoP02);

free_length02 = length_fCoP02(1);

end_length02 = length_fCoP02(end);
```

```
excursion02 = length_fCoP02 - free_length02;% excursion starts @ zeroforce
frame

end_excursion02 = length_fCoP02 - end_length02;% excursion starts @
zeroforce frame

%%

% lengthening-shortening vel

delx_new_whole_body_CM01 = new_whole_body_CM01(:,1)-
mean_CoPx01(1);%displacement from reference

delx_new_whole_body_CM02 = new_whole_body_CM02(:,1)-
mean_CoPx01(1);%displacement from reference

fCoP_velocity_actuator01 =
(delx_new_whole_body_CM01.*new_whole_bodyV_CM01(:,1) +
new_whole_body_CM01(:,2).*new_whole_bodyV_CM01(:,2))./sqrt(delx_new_whole_b
ody_CM01.^2 + new_whole_body_CM01(:,2).^2);%diff(extra_length_fCoP01));

fCoP_velocity_actuator02 = ((delx_new_whole_body_CM02 -
step_length).*new_whole_bodyV_CM02(:,1) +
new_whole_body_CM02(:,2).*new_whole_bodyV_CM02(:,2))./sqrt((delx_new_whole_
body_CM02 - step_length).^2 +
new_whole_body_CM02(:,2).^2);%(diff(extra_length_fCoP02));

init_legVel02 = fCoP_velocity_actuator02(1) ;

final_legVel02 = fCoP_velocity_actuator02(end) ;

eff_velocity_actuator02 = (fCoP_velocity_actuator02 -
init_legVel02)/init_legVel02 ;

end_eff_velocity_actuator02 = (fCoP_velocity_actuator02 -
final_legVel02)/final_legVel02 ;


%leg angle wrt vertical

extra_angle_leg01 =  atan((new_whole_body_CM01(:,1)-
mean_CoPx01)./(new_whole_body_CM01(:,2)));%opposite to model angle

extra_angle_leg02 =  atan((new_whole_body_CM02(:,1)-
mean_CoPx02)./(new_whole_body_CM02(:,2)));%opposite to model angle

angle_leg01 = extra_angle_leg01(1:length(new_whole_body_CM01));

angle_leg02 = extra_angle_leg02(1:length(new_whole_body_CM02));

angle_leg02_degree = angle_leg02 *180/pi;


min_angle_leg02 = min(angle_leg02);

max_angle_leg02 = max(angle_leg02);
```

```
%%%%%%%%%%%%%%%%%%%%%%%%%%%%%%%%

free_angle02 = angle_leg02(1);

rel_angle02 = angle_leg02 - free_angle02;


%speed of leg angle

diff_angle_leg01 = (new_whole_bodyV_CM01(:,1).*new_whole_body_CM01(:,2)+
delx_new_whole_body_CM01.*new_whole_bodyV_CM01(:,2))./(delx_new_whole_body_
CM01.^2+new_whole_body_CM01(:,2).^2);%diff(extra_angle_leg01);

diff_angle_leg02 = -(new_whole_bodyV_CM02(:,2).*(delx_new_whole_body_CM02-
step_length)-
new_whole_bodyV_CM02(:,1).*new_whole_body_CM02(:,2))./((delx_new_whole_body
_CM02-
step_length).^2+new_whole_body_CM02(:,2).^2);%diff(extra_angle_leg02);


t_angle01 = (2:1:length(angle_leg01)+1)';%1900:10:1990;

new_t_angle01 = (1:1:length(angle_leg01)+1)';

extra_diff_angle_leg01 =
interp1(t_angle01,angle_leg01,new_t_angle01,'cubic');


t_angle02 = (2:1:length(angle_leg02)+1)';%1900:10:1990;

new_t_angle02 = (1:1:length(angle_leg02)+1)';

extra_diff_angle_leg02 =
interp1(t_angle02,angle_leg02,new_t_angle02,'cubic');


diff_angle_leg01_test = frame_rate*diff(extra_diff_angle_leg01);

diff_angle_leg02_test = frame_rate*diff(extra_diff_angle_leg02);

%%%%%%%%%%%%%%%%%%%%%%%%%%%%%%%%%%%%%%%%

int_diff_ang02 = diff_angle_leg02(1);

eff_angV02 = (diff_angle_leg02 - int_diff_ang02)./int_diff_ang02;


new_net_force02 = net_force02(start_frame02-1:end_frame02+1,:);

new_angle_forceWrtVert02 =
angle_forceWrtVert02(start_frame02:end_frame02,:);


%Include force angle @ zeroforce frame; no force exert, force
%direction must be calculated using extrapolation
```

```
init_slope_new_angle_forceWrtVert02 = diff(new_angle_forceWrtVert02(1:3));

init_new_angle_forceWrtVert02 = new_angle_forceWrtVert02(1)-
(2*init_slope_new_angle_forceWrtVert02(1)-
init_slope_new_angle_forceWrtVert02(2)) ;

fnl_slope_new_angle_forceWrtVert02 =
diff(new_angle_forceWrtVert02((end_frame02-start_frame02-2):(end_frame02-
start_frame02+1)));

fnl_new_angle_forceWrtVert02 = new_angle_forceWrtVert02(end_frame02-
start_frame02+1)+ (2*fnl_slope_new_angle_forceWrtVert02(2)-
fnl_slope_new_angle_forceWrtVert02(1)) ;

new_angle_forceWrtVert02 = [init_new_angle_forceWrtVert02;
new_angle_forceWrtVert02; fnl_new_angle_forceWrtVert02 ] ;


%force decomposition into leg direction

net_force_angle02 = -(angle_leg02  - new_angle_forceWrtVert02);

normal_force02 = new_net_force02.* cos(net_force_angle02);

tangent_force02 = new_net_force02.* sin(net_force_angle02);
```

Chapter 4

4.1D. Curve fitting using root-mean-square errors

4.1.1D Linear fitting of axial force

```
function LeastSqrN = forceLinear_whole(coeff)

global normal_force_fCoP_meas_collect
global nForce_model
global leg_length_fCoP_meas_collect

k_linear = coeff(1);
l0 = coeff(2);

nForce_model = k_linear*0.001*(l0 - leg_length_fCoP_meas_collect) ;


diff_force = nForce_model - normal_force_fCoP_meas_collect;

LeastSqrN = norm(diff_force)/sqrt(length(diff_force));
```

4.1.2D Linear fitting of tangential force

```
function LeastSqrT_Linear = forceLinear_angleT5th02(var)

global angle_leg_fCoP_meas_collect tangent_force_fCoP_meas_collect
global tForce_model op_k op_angle

angle_leg02 = angle_leg_fCoP_meas_collect ;
init_angle02 = min(angle_leg02);
final_angle02 = max(angle_leg02);
angle_period = final_angle02-init_angle02;

k1 = var(1);
a_re01 = var(2);
a_F0 = var(3);
k3 = var(4);
a_re02 = var(5);

%-----partI
angle_re01 = init_angle02 + a_re01*angle_period ;

tForce_model = k1*(angle_leg02 - init_angle02).*(angle_leg02 <=
angle_re01);

%-----partII
Ft_re1 = k1*(angle_re01 - init_angle02);
angle_F0 = init_angle02 + a_F0*angle_period ;

k2 = (0 - Ft_re1)/(angle_F0 - angle_re01);

tForce_model = tForce_model + (angle_leg02 > angle_re01 & angle_leg02 <=
angle_F0).* (k2*(angle_leg02 - angle_F0));

%-----partIII
angle_re02 = init_angle02 + a_re02*angle_period ;

tForce_model = tForce_model + (angle_leg02 > angle_F0 & angle_leg02 <=
angle_re02).* (k3*(angle_leg02 - angle_F0));

%-----partIV
Ft_re3 = k3*(angle_re02 - angle_F0);

k4 = (0 - Ft_re3)/(final_angle02 - angle_re02 );

tForce_model = tForce_model + (angle_leg02 > angle_re02 & angle_leg02 <=
final_angle02).* (k4*(angle_leg02 - angle_re02)+ Ft_re3);

op_k = [k1;k2;k3;k4];
op_angle = [init_angle02;angle_re01;angle_F0;angle_re02;final_angle02];

%----- RMSE
diff_force = tForce_model - tangent_force_fCoP_meas_collect;

LeastSqrT_Linear = norm(diff_force)/sqrt(length(diff_force));
```

4.1.3D Nonlinear fitting of axial force

```
function LeastSqrN = forceBnln4_whole(coeff)

global normal_force_fCoP_meas_collect
global nForce_model nForce_model_ln
global leg_length_fCoP_meas_collect
global k_linear n k_linear_fit l0_fit


k_linear = coeff(1);
a0 = coeff(2);
b0 = coeff(3);
l0 = coeff(4);


k_Bnln = k_linear*(1 + a0*exp(b0*n)*(0.001*l0 -
0.001*leg_length_fCoP_meas_collect).^n-1);

nForce_model = k_Bnln *0.001.*(l0 - leg_length_fCoP_meas_collect);

nForce_model_ln = k_linear *0.001.*(l0 - leg_length_fCoP_meas_collect);

diff_force = nForce_model - normal_force_fCoP_meas_collect;

LeastSqrN = norm(diff_force)/sqrt(length(diff_force));
```

4.1.4D Nonlinear fitting of tangential force

```
function LeastSqrT = forceSeries_T2th02(coeff)

% y = a0 + a1 * cos(pi*x/period) + b1 * sin(pi*x/period) + a2 *
cos(2*pi*x/period)+ b2 * sin(2*pi*x/period);
global tangent_force_fCoP_meas_collect
global Q_period init_angle02
global tForce_model angle_leg_fCoP_meas_collect LeastSqrT_test

rel_angle_fCoP02 = angle_leg_fCoP_meas_collect - init_angle02;

a1L = coeff(1);
b1L = coeff(2);
a2L = coeff(3);
b2L = coeff(4);


l1_term = a1L * (cos(2*pi*rel_angle_fCoP02/Q_period)-1)+ b1L *
sin(2*pi*rel_angle_fCoP02/Q_period);
l2_term = a2L * (cos(2*2*pi*rel_angle_fCoP02/Q_period)-1)+ b2L *
sin(2*2*pi*rel_angle_fCoP02/Q_period);

% stiffness = (l1_term + l2_term);
% tForce_model = stiffness.*(rel_angle_fCoP02/Q_period) ;
tForce_model = l1_term + l2_term;

diff_force = tForce_model - tangent_force_fCoP_meas_collect;

LeastSqrT_test =
sum(diff_force);%.^2/length(diff_force);%sqrt((sum(diff_force).^2))/length(
diff_force);
LeastSqrT = norm(diff_force)/sqrt(length(diff_force));
```

Chapter 5

5.1D. Parametric fitting of axial force

```
function LeastSqrN = forceSeries_l0fq_kq_r_mean_N5th02(coeff)

global mean_normal_force_fCoP_meas_collect
global nForce_model_l0
global mean_leg_length_fCoP_meas_collect mean_angle_leg_fCoP_meas_collect
global free_length02 end_length02
global elastic_term  posture excursion02_l0 fl0 fl0_rate
global stiffness testSqrN

init_angle = mean_angle_leg_fCoP_meas_collect(1);

final_angle = mean_angle_leg_fCoP_meas_collect(end);

posture = (mean_angle_leg_fCoP_meas_collect- init_angle)/(final_angle-
init_angle);

free_length02 = mean_leg_length_fCoP_meas_collect(1);

end_length02 = mean_leg_length_fCoP_meas_collect(end);

a1L = coeff(1);
b1L = coeff(2);
a2L = coeff(3);
b2L = coeff(4);
a3L = coeff(5);
b3L = coeff(6);
a4L = coeff(7);
b4L = coeff(8);
a5L = coeff(9);
b5L = coeff(10);
stiffness = coeff(11);

l1_term = a1L * (cos(2*pi*posture)-1)+ b1L * sin(2*pi*posture);
l2_term = a2L * (cos(2*2*pi*posture)-1)+ b2L * sin(2*2*pi*posture);
l3_term = a3L * (cos(2*3*pi*posture)-1)+ b3L * sin(2*3*pi*posture);
l4_term = a4L * (cos(2*4*pi*posture)-1)+ b4L * sin(2*4*pi*posture);
l5_term = a5L * (cos(2*5*pi*posture)-1)+ b5L * sin(2*5*pi*posture);

nln_term = l1_term + l2_term + l3_term + l4_term + l5_term;

fl0_rate = end_length02 - free_length02;

fl0 = free_length02 + fl0_rate *(posture + nln_term);
excursion02_l0 = fl0 - mean_leg_length_fCoP_meas_collect;

elastic_term = stiffness.* 0.001.*excursion02_l0;
nForce_model_l0 = elastic_term;

diff_force = nForce_model_l0 - mean_normal_force_fCoP_meas_collect;
testSqrN = sqrt(sum(diff_force)^2)/length(diff_force);

LeastSqrN = norm(diff_force)/sqrt(length(diff_force));
```

5.2D. Parametric fitting of tangential force

```
function LeastSqrT = forceSeries_angleT5th02(coeff)

global tangent_force02
global tForce_model
global rel_angle02
global Q_period

a1Q = coeff(1);
b1Q = coeff(2);

a2Q = coeff(3);
b2Q = coeff(4);

a3Q = coeff(5);
b3Q = coeff(6);

a4Q = coeff(7);
b4Q = coeff(8);

a5Q = coeff(9);
b5Q = coeff(10);

q1_term = a1Q * (cos(2*pi*rel_angle02/Q_period)-1)+ b1Q *
sin(2*pi*rel_angle02/Q_period);
q2_term = a2Q * (cos(2*2*pi*rel_angle02/Q_period)-1)+ b2Q *
sin(2*2*pi*rel_angle02/Q_period);
q3_term = a3Q * (cos(2*3*pi*rel_angle02/Q_period)-1)+ b3Q *
sin(2*3*pi*rel_angle02/Q_period);
q4_term = a4Q * (cos(2*4*pi*rel_angle02/Q_period)-1)+ b4Q *
sin(2*4*pi*rel_angle02/Q_period);
q5_term = a5Q * (cos(2*5*pi*rel_angle02/Q_period)-1)+ b5Q *
sin(2*5*pi*rel_angle02/Q_period);

tForce_model =  q1_term + q2_term + q3_term + q4_term + q5_term ;

diff_force = tForce_model - tangent_force02;

LeastSqrT = norm(diff_force)/sqrt(length(diff_force));
```

Chapter 6

6.1D. Human walking prediction using compliant leg model with axial elastic leg property (CAE)

6.1.1D CAE model with linear elastic leg property

```
%Simulation of each initial condition with a combination of CoM
%height,linear leg stiffness,touch down angle and system energy
%Fixed point = [y; atan(dy/dx)]
%__
global k l0 mass stepLength g x_int_sing01 step_sizeSS step_sizeDS
step_sizeSS2
%------------------------------------------------------------
k = 12000;%N/m
design_touch_down_angle = 67 * pi/180;%rad
vx_int_sing01 = 1.53;%m/s
%------------------------------------------------------------
l0 = 1;%m
mass = 80;%kg
g = 9.81;% m/s2
k_dimless = k*l0/(mass*g);

%%

x_int_sing01 = 0.0; %m

y_int_sing01 = 0.98 ;%m

vy_int_sing01 = 0;

delta_spring_length = l0 - y_int_sing01 ; % apex height at vertical leg
only

y_touch = l0*sin(design_touch_down_angle);

sys_E = 0.5*mass*(vx_int_sing01^2 + vy_int_sing01^2)+ mass*g*y_int_sing01 +
0.5*k*(delta_spring_length)^2;



int_sing01 = [x_int_sing01 vx_int_sing01 y_int_sing01 vy_int_sing01];

x_new_cycle = [];

delxHx_new_cycle = [];

init_del_xs = [];

norm_D_Ic = [];

for cycle = 1:100
step_sizeSS = 0.0001;
res_SS = 2000 ;
```

```
end_spanSS = res_SS * step_sizeSS ;
time_spanSS = 0:step_sizeSS:end_spanSS; %max = 1 millisec

[ts1,xs] =
ode113(@spring_leg_single01,time_spanSS,int_sing01(cycle,:),[],cycle);

int_sing01_abs(cycle,:) = [xs(1,1)-
int_sing01(cycle,1),int_sing01(cycle,2:4)];

int_V_state(cycle) = int_sing01(cycle,2);

map_point(cycle,:) = [int_sing01(cycle,3),int_V_state(cycle)];


for count01 = 1:res_SS

del_xs(count01,:) = xs(count01,1)-int_sing01(cycle,1);


l_trail01_SS(cycle,count01) = sqrt(del_xs(count01,:)^2+xs(count01,3)^2);

angle_trail01_SS(cycle,count01) =
atan(del_xs(count01,:)/xs(count01,3));%wrt vertical

lead_angle(cycle,count01) = asin(xs(count01,3)/l0);%virtual angle when lead
leg leaning to touched

lead_angle_degree(cycle,count01) = lead_angle(cycle,count01)*180/pi;

pSS(count01,:) =  k*(l0/sqrt(del_xs(count01,:) ^2+xs(count01,3)^2)-1);

GRF_SSx(count01,:) = (pSS(count01,:).*del_xs(count01,:)) ;

GRF_SSy(count01,:) = (pSS(count01,:)*xs(count01,3));

check_hight(cycle,count01) = xs(count01,3)- y_touch;

    if ((check_hight(cycle,count01) <= 0.00004) &&
(check_hight(cycle,count01) >= -0.00004))

    touch_down_angle(cycle) = lead_angle(cycle,count01) ;

    touch_down_angle_degree(cycle) = lead_angle_degree(cycle,count01);

    touch_down_timeSS(cycle) = count01;

    end

end

%%
l_trail01_touch(cycle) = sqrt((xs(touch_down_timeSS(cycle),1)-
x_int_sing01(cycle))^2+xs(touch_down_timeSS(cycle),3)^2);
trial_angle(cycle) =
asin(xs(touch_down_timeSS(cycle),3)/l_trail01_touch(cycle));
trial_angle_degree(cycle) = trial_angle(cycle) * 180 / pi ;
```

```
stepLength(cycle) = l0*cos(touch_down_angle(cycle))+
l_trail01_touch(cycle)*cos(trial_angle(cycle));

x_int_db(cycle) = xs(touch_down_timeSS(cycle),1);
vx_int_db(cycle) = xs(touch_down_timeSS(cycle),2);
y_int_db(cycle) = xs(touch_down_timeSS(cycle),3);
vy_int_db(cycle) =xs(touch_down_timeSS(cycle),4);
int_db(cycle,:) = [x_int_db(cycle) vx_int_db(cycle) y_int_db(cycle)
vy_int_db(cycle) ];

step_sizeDS =  step_sizeSS;
res_DS = 2000 ;
end_spanDS = res_DS * step_sizeDS ;
time_spanDS = 0:step_sizeDS:end_spanDS;

[td,xd] = ode113(@spring_double,time_spanDS,int_db(cycle,:),[],cycle);

for count02 = 1:res_DS

del_xd(count02,:) = xd(count02,1)-int_sing01(cycle,1);

l_trail01_leave(cycle,count02) = sqrt(del_xd(count02,:)^2+
xd(count02,3)^2);

angle_trail01_leave(cycle,count02) = atan(del_xd(count02,:)/xd(count02,3));

pDS(count02,:) = k*(l0/sqrt(del_xd(count02,:)^2+xd(count02,3)^2)-1);

qDS(count02,:) = k*(l0/sqrt((stepLength(cycle)-
del_xd(count02,:))^2+xd(count02,3)^2)-1);

GRF_DSx_1(count02,cycle) = (- qDS(count02,:)*(stepLength(cycle)-
del_xd(count02,:)));

GRF_DSy_1(count02,cycle) = (qDS(count02,:)*xd(count02,3));

GRF_DSx(count02,:) = (pDS(count02,:)*del_xd(count02,:) );

GRF_DSy(count02,:) = (pDS(count02,:)*xd(count02,3));

l_lead02_DS(cycle,count02) = sqrt((stepLength(cycle)-
del_xd(count02,:))^2+xd(count02,3)^2) ;

angle_lead02_DS(cycle,count02) = atan((stepLength(cycle)-
del_xd(count02,:))/xd(count02,3)) ;%wrt vertical


check_length(cycle,count02) = l0 - l_trail01_leave(cycle,count02) ;

    if (check_length(cycle,count02) <= 0.00005 &&
(check_length(cycle,count02) >= -0.00005))

    l_trail01_take_off(cycle) = l_trail01_leave(cycle,count02);

    take_off(cycle) = count02;

    end
```

```
end


%%
x_int_sing02(cycle) = xd(take_off(cycle),1);
vx_int_sing02(cycle) = xd(take_off(cycle),2);
y_int_sing02(cycle) = xd(take_off(cycle),3);
vy_int_sing02(cycle) =xd(take_off(cycle),4);
int_sing02(cycle,:) = [x_int_sing02(cycle) vx_int_sing02(cycle)
y_int_sing02(cycle) vy_int_sing02(cycle) ];

l_trail01_start_SS2 = sqrt((xd(take_off(cycle),1)-x_int_sing01(cycle))^2+
xd(take_off(cycle),3)^2);

step_sizeSS2 =  step_sizeDS;

res_SS2 = 2000 ;

end_spanSS2 = res_SS2 * step_sizeSS2 ;

time_spanSS02 = 0:step_sizeSS2:end_spanSS2;

[ts2,xs2] =
ode113(@spring_leg_single02,time_spanSS02,int_sing02(cycle,:),[],cycle);
 [maxValue(cycle) maxIndex(cycle)] = max(xs2(:,3));

for count03 = 1:res_SS2

del_xs2(count03,:) = xs2(count03,1)-int_sing01(cycle,1);

qS2(count03,:) = k*(l0/sqrt((stepLength(cycle)- del_xs2(count03,:))^2+
xs2(count03,3)^2)-1);

lead_legAngle_SS2(cycle,count03) = atan(xs2(count03,3)/(stepLength(cycle)-
del_xs2(count03,:)));

angle_lead02_SS2(cycle,count03) = atan((stepLength(cycle)-
del_xs2(count03,:))/xs2(count03,3));%wrt vertical

GRF_SS2x(count03,cycle) = (-qS2(count03,:)*(stepLength(cycle)-
del_xs2(count03,:)));

GRF_SS2y(count03,cycle) = (qS2(count03,:)* xs2(count03,3));

lead_forceAngle_SS2(count03,:) =
atan(GRF_SS2y(count03,:)/GRF_SS2x(count03,:));

l_lead02_SS2(cycle,count03) = sqrt((stepLength(cycle)-
del_xs2(count03,:))^2+ xs2(count03,3)^2) ;

check_hight02(cycle,count03) = int_sing01(cycle,3)- xs2(count03,3);

check_angle(cycle,count03) =   0.5*pi - lead_legAngle_SS2(cycle,count03);

V_state(count03,:) = xs2(count03,2);
diff_V_state(cycle,count03) = int_V_state(cycle)- V_state(count03,:);
```

```
diff_y_state(cycle,count03) = int_sing01(cycle,3)- xs2(count03,3);

check_state(cycle,count03) = norm([diff_y_state(cycle,count03);
diff_V_state(cycle,count03)]);

    if count03== maxIndex(cycle)

         max_height(cycle) = xs2(maxIndex(cycle),3);
         if check_state(cycle,count03) <= 0.001;

          endSS02(cycle) = count03 ;

          end_check_state(cycle) = check_state(cycle,count03);

          disp(['achieved cycle',num2str(cycle)])

        end

    end
end


x_cycle{cycle} =
{xs(1:touch_down_timeSS(cycle),:);xd(1:take_off(cycle),:);xs2(1:endSS02(cyc
le),:)};

delxHx_cycle{cycle} =
{del_xs(1:touch_down_timeSS(cycle),:);del_xd(1:take_off(cycle),:);del_xs2(1
:endSS02(cycle),:)};

x_new_cycle =  [x_new_cycle;x_cycle{cycle}];

delxHx_new_cycle = [delxHx_new_cycle;delxHx_cycle{cycle}];

int_sing01(cycle+1,:) = xs2(endSS02(cycle),:);

int_sing01_rel(cycle+1,:) = [xs2(endSS02(cycle),1)-
int_sing01(cycle,1),xs2(endSS02(cycle),2:4)];

x_int_sing01(cycle+1) = int_sing01(cycle+1,1);

init_del_xs = [init_del_xs;del_xs2(endSS02(cycle),:)];

y_int_sing01(cycle+1) = int_sing01(cycle+1,3);



end

%return map and Floquet multipliers

             D_map_point = diff(map_point);
             norm_map_point = [];
             for map_row = 1:length(D_map_point)
             norm_map_point =
[norm_map_point;norm(D_map_point(map_row,:))];
```

```
            end
            [val_min_norm Id_lim_cycle]= min(norm_map_point);

GRF_x = [GRF_DSx_1(1:take_off(cycle-1),cycle-1);GRF_SS2x(1:endSS02(cycle-
1),cycle-
1);GRF_SSx(1:touch_down_timeSS(cycle),:);GRF_DSx(1:take_off(cycle),:)];

GRF_y = [GRF_DSy_1(1:take_off(cycle-1),cycle-1);GRF_SS2y(1:endSS02(cycle-
1),cycle-
1);GRF_SSy(1:touch_down_timeSS(cycle),:);GRF_DSy(1:take_off(cycle),:)];

GRF_net = sqrt(GRF_x.^2+ GRF_y.^2);

legLength = [l_lead02_DS(cycle-1,1:take_off(cycle-1))';l_lead02_SS2(cycle-
1,1:endSS02(cycle-
1))';l_trail01_SS(cycle,1:touch_down_timeSS(cycle))';l_trail01_leave(cycle,
1:take_off(cycle))'];


sumGRF_DSx = GRF_DSx_1(:,cycle) + GRF_DSx ;

sumGRF_DSx_step = GRF_DSx_1(1:take_off(cycle),cycle) +
GRF_DSx(1:take_off(cycle),:) ;


sumGRF_DSy = GRF_DSy_1(:,cycle) + GRF_DSy ;

sumGRF_DSy_step = GRF_DSy_1(1:take_off(cycle),cycle) +
GRF_DSy(1:take_off(cycle),:) ;


netGRF_SS = sqrt(GRF_SSx.^2 + GRF_SSy.^2);

netGRF_SS_step = sqrt(GRF_SSx(1:touch_down_timeSS(cycle),:).^2 +
GRF_SSy(1:touch_down_timeSS(cycle),:).^2);

netGRF_DS = sqrt(sumGRF_DSx.^2 + sumGRF_DSy.^2);

netGRF_DS_step = sqrt(sumGRF_DSx(1:take_off(cycle),:).^2 +
sumGRF_DSy(1:take_off(cycle),:).^2);

netGRF_SS02 = sqrt(GRF_SS2x(:,cycle).^2 + GRF_SS2y(:,cycle).^2);

netGRF_SS02_step = sqrt(GRF_SS2x(1:endSS02(cycle-1),cycle-1).^2 +
GRF_SS2y(1:endSS02(cycle-1),cycle-1).^2);


netGRF_step = [netGRF_SS_step;netGRF_DS_step;netGRF_SS02_step];
DnetGRF_step = diff(netGRF_step);
sumDnetGRF_step = sum(DnetGRF_step);


phase = length(x_new_cycle);

for count_phase = 1:phase
   length_x_new_cycle(count_phase) = length(x_new_cycle{count_phase});
```

```
end

sum_length = sum(length_x_new_cycle) ;

renew_x_new_cycle = zeros(sum_length,4);

renew_delxHx_new_cycle = zeros(sum_length,1);

leg_length_cycle = zeros(sum_length,1);

count_x_new_cycle = 1;

%obtain CoM motion from cell array to matrix

for count_phase = 1:phase

    %for count_x_new_cycle = 1: sum_length

        for count_x_inphase = 1:length(x_new_cycle{count_phase})

            renew_x_new_cycle(count_x_new_cycle,:) =
x_new_cycle{count_phase}(count_x_inphase,:);

            renew_delxHx_new_cycle(count_x_new_cycle,:) =
delxHx_new_cycle{count_phase}(count_x_inphase,:);

            leg_length_cycle(count_x_new_cycle,:) =
sqrt(renew_delxHx_new_cycle(count_x_new_cycle,:).^2+
renew_x_new_cycle(count_x_new_cycle,3).^2);

            count_x_new_cycle = count_x_new_cycle + 1 ;


        end


end

diff_leg_length_cycle =
(1/step_sizeSS)*[diff(leg_length_cycle(1:2,:));diff(leg_length_cycle)];

%%
%Distance btw apex point and 45 degree line

fixed_point = map_point(Id_lim_cycle,:);

% %
fit_first = [];
fit_next = [];

[row_IC col_IC]= size(map_point);

for count04 = 1:col_IC

fit_first = [fit_first; map_point(1:end-1,count04)' - fixed_point(count04)'
];
```

```
fit_next = [fit_next; map_point(2:end,count04)' - fixed_point(count04)' ];

end

Jmatrix = (fit_next * fit_first')*pinv(fit_first*fit_first');


FQmult = abs(eig(Jmatrix));
max_FQmult = max(FQmult);
min_FQmult = min(FQmult);


    if (max_FQmult < 1)

    disp(['k                              |  ',num2str(k)])
    disp(['angle                          |
',num2str(design_touch_down_angle*180/pi)])
    disp(['cycle                          |  ',num2str(cycle)])
    disp(['fixed point                    |  ',num2str(fixed_point)])
    disp(['y0                             |  ',num2str(y_int_sing01(1))])
    disp(['y transition                   |  ',num2str(y_touch)])
    disp(['Stable Floquet multiplier      |  ',num2str(max_FQmult)])

    elseif (max_FQmult > 1 && min_FQmult < 1)

    disp(['k                              |  ',num2str(k)])
    disp(['angle                          |
',num2str(design_touch_down_angle*180/pi)])
    disp(['cycle                          |  ',num2str(cycle)])
    disp(['fixed point                    |  ',num2str(fixed_point)])
    disp(['y0                             |  ',num2str(y_int_sing01(1))])
    disp(['y transition                   |  ',num2str(y_touch)])
    disp(['Saddle Floquet multiplier      |  ',num2str(max_FQmult)])

    else

    disp(['k                              |  ',num2str(k)])
    disp(['angle                          |
',num2str(design_touch_down_angle*180/pi)])
    disp(['cycle                          |  ',num2str(cycle)])
    disp(['fixed point                    |  ',num2str(fixed_point)])
    disp(['y0                             |  ',num2str(y_int_sing01(1))])
    disp(['y transition                   |  ',num2str(y_touch)])
    disp(['Unstable Floquet multiplier     |  ',num2str(max_FQmult)])

    end
```

6.1.2D CAE model with nonlinear elastic leg property

```
%Simulation of each initial condition with a combination of CoM
%height,non-linear(hard) leg stiffness,touch down angle and system energy
%Fixed point = [y; atan(dy/dx)]
%__

global k design_touch_down_angle sys_E a0 b0 a1 b1 n l0 mass stepLength g
x_int_sing01 step_sizeSS step_sizeDS step_sizeSS2
%-----------------------------------------------------------
k = 10000;%N/m
design_touch_down_angle = 69.5* pi/180;%rad
b0 = 1.2 ;
sys_E = 676;
%-----------------------------------------------------------
a0 = k ;
a1 = 0 ;
b1 = 1 ;
n = 3;

l0 = 0.972;%m
mass = 69;%kg
g = 9.81;% m/s2
k_dimless = k*l0/(mass*g);

touch_down_timeSS =[];
take_off = [];
endSS02 = [];
bound = 0;
%%

x_int_sing01 = 0.0 ; %m

y_int_sing01 = 0.921;%m

delta_spring_length = l0 - y_int_sing01 ; % apex height at vertical leg
only

y_touch = l0*sin(design_touch_down_angle);

k_non = a0*exp(b0*n)*delta_spring_length^(a1+b1*n-1);

k_hard = k + k_non ;

vx_int_sing01 = sqrt(2*sys_E/mass - 2*g*y_int_sing01 -
(k_hard*delta_spring_length^2)/mass);

vy_int_sing01 = 0;

int_sing01 = [x_int_sing01 vx_int_sing01 y_int_sing01 vy_int_sing01];

x_new_cycle = [];

delxHx_new_cycle = [];

init_del_xs = [];

norm_D_Ic = [];
```

```
set_cycle = 50;

for cycle = 1:set_cycle


step_sizeSS = 0.0001;
res_SS = 2000 ;
end_spanSS = res_SS * step_sizeSS ;
time_spanSS = 0:step_sizeSS:end_spanSS; %max = 1 millisec

[ts1,xs] =
ode113(@spring_basic_nln_single01,time_spanSS,int_sing01(cycle,:),[],cycle)
;

int_sing01_abs(cycle,:) = [xs(1,1)-
int_sing01(cycle,1),int_sing01(cycle,2:4)];

int_tanV_state(cycle) = atan(int_sing01(cycle,4)/int_sing01(cycle,2));

map_point(cycle,:) =
[int_sing01(cycle,3),atan(int_sing01(cycle,4)/int_sing01(cycle,2))];

for count01 = 1:res_SS

del_xs(count01,:) = xs(count01,1)-int_sing01(cycle,1);


l_trail01_SS(cycle,count01) = sqrt(del_xs(count01,:)^2+xs(count01,3)^2);

angle_trail01_SS(cycle,count01) =
atan(del_xs(count01,:)/xs(count01,3));%wrt vertical

lead_angle(cycle,count01) = asin(xs(count01,3)/l0);%virtual angle when lead
leg leaning to touched

lead_angle_degree(cycle,count01) = lead_angle(cycle,count01)*180/pi;

k_hard01(cycle,count01) = k + a0* exp(b0*n)*(l0- sqrt(del_xs(count01,:) ^2+
xs(count01,3)^2))^(a1+b1*n-1);


pSS(count01,:) =  k_hard01(cycle,count01)*(l0/sqrt(del_xs(count01,:)
^2+xs(count01,3)^2)-1);

GRF_SSx(count01,:) = (pSS(count01,:)*del_xs(count01,:)) ;

GRF_SSy(count01,:) = (pSS(count01,:)*xs(count01,3));

kinetic_E_SS(cycle,count01) = 0.5*mass*(xs(count01,2)^2+xs(count01,4)^2);

potential_E_SS(cycle,count01) = mass*g*xs(count01,3);

elastic_E_SS(cycle,count01) =
0.5*k_hard01(cycle,count01)*(l_trail01_SS(cycle,count01)-l0)^2;

check_energy_SS(cycle,count01) = kinetic_E_SS(cycle,count01) +
potential_E_SS(cycle,count01) + elastic_E_SS(cycle,count01) ;
```

```
 check_hight(cycle,count01) = xs(count01,3)- y_touch;

    if ((check_hight(cycle,count01) <= 0.00004) &&
(check_hight(cycle,count01) >= -0.00004))

    touch_down_angle(cycle) = lead_angle(cycle,count01) ;

    touch_down_angle_degree(cycle) = lead_angle_degree(cycle,count01);

    touch_down_timeSS(cycle) = count01;

    end

end

%%
l_trail01_touch(cycle) = sqrt((xs(touch_down_timeSS(cycle),1)-
x_int_sing01(cycle))^2+xs(touch_down_timeSS(cycle),3)^2);
trial_angle(cycle) =
asin(xs(touch_down_timeSS(cycle),3)/l_trail01_touch(cycle));
trial_angle_degree(cycle) = trial_angle(cycle) * 180 / pi ;
stepLength(cycle) = l0*cos(touch_down_angle(cycle))+
l_trail01_touch(cycle)*cos(trial_angle(cycle));

x_int_db(cycle) = xs(touch_down_timeSS(cycle),1);
vx_int_db(cycle) = xs(touch_down_timeSS(cycle),2);
y_int_db(cycle) = xs(touch_down_timeSS(cycle),3);
vy_int_db(cycle) =xs(touch_down_timeSS(cycle),4);
int_db(cycle,:) = [x_int_db(cycle) vx_int_db(cycle) y_int_db(cycle)
vy_int_db(cycle) ];

step_sizeDS =  step_sizeSS;
res_DS = 2000 ;
end_spanDS = res_DS * step_sizeDS ;
time_spanDS = 0:step_sizeDS:end_spanDS;

[td,xd] =
ode113(@spring_basic_nln_double,time_spanDS,int_db(cycle,:),[],cycle);

for count02 = 1:res_DS

del_xd(count02,:) = xd(count02,1)-int_sing01(cycle,1);

l_trail01_leave(cycle,count02) = sqrt(del_xd(count02,:)^2+
xd(count02,3)^2);

angle_trail01_leave(cycle,count02) = atan(del_xd(count02,:)/xd(count02,3));

k_hard_Dp(cycle,count02) = k + a0 * exp(b0*n)*(l0-
sqrt(del_xd(count02,:)^2+xd(count02,3)^2))^(a1+b1*n-1);

k_hard_Dq(cycle,count02) = k + a0 * exp(b0*n)*(l0- sqrt((stepLength(cycle)-
del_xd(count02,:))^2 + xd(count02,3)^2))^(a1+b1*n-1);

pDS(count02,:) =
k_hard_Dp(cycle,count02)*(l0/sqrt(del_xd(count02,:)^2+xd(count02,3)^2)-1);
```

```
qDS(count02,:) = k_hard_Dq(cycle,count02)*(l0/sqrt((stepLength(cycle)-
del_xd(count02,:))^2+xd(count02,3)^2)-1);

GRF_DSx_1(count02,cycle) = (- qDS(count02,:)*(stepLength(cycle)-
del_xd(count02,:)));

GRF_DSy_1(count02,cycle) = (qDS(count02,:)*xd(count02,3));

GRF_DSx(count02,:) = (pDS(count02,:)*del_xd(count02,:) );

GRF_DSy(count02,:) = (pDS(count02,:)*xd(count02,3));

kinetic_E_DS(cycle,count02) = 0.5*mass*(xd(count02,2)^2+xd(count02,4)^2);

potential_E_DS(cycle,count02) = mass*g*xd(count02,3);

l_lead02_DS(cycle,count02) = sqrt((stepLength(cycle)-
del_xd(count02,:))^2+xd(count02,3)^2) ;

angle_lead02_DS(cycle,count02) = -atan((stepLength(cycle)-
del_xd(count02,:))/xd(count02,3)) ;%wrt vertical


elastic_E_DS(cycle,count02) =
0.5*k_hard_Dp(cycle,count02)*(l_trail01_leave(cycle,count02)-l0)^2 +
0.5*k_hard_Dq(cycle,count02)*(l_lead02_DS(cycle,count02)-l0)^2 ;

check_energy_DS(cycle,count02) = kinetic_E_DS(cycle,count02) +
potential_E_DS(cycle,count02) + elastic_E_DS(cycle,count02) ;

check_length(cycle,count02) = l0 - l_trail01_leave(cycle,count02) ;

    if (check_length(cycle,count02) <= 0.00005 &&
(check_length(cycle,count02) >= -0.00005))

    l_trail01_take_off(cycle) = l_trail01_leave(cycle,count02);

    take_off(cycle) = count02;

    end

end


x_int_sing02(cycle) = xd(take_off(cycle),1);
vx_int_sing02(cycle) = xd(take_off(cycle),2);
y_int_sing02(cycle) = xd(take_off(cycle),3);
vy_int_sing02(cycle) =xd(take_off(cycle),4);
int_sing02(cycle,:) = [x_int_sing02(cycle) vx_int_sing02(cycle)
y_int_sing02(cycle) vy_int_sing02(cycle) ];

l_trail01_start_SS2 = sqrt((xd(take_off(cycle),1)-x_int_sing01(cycle))^2+
xd(take_off(cycle),3)^2);

step_sizeSS2 =  step_sizeDS;

res_SS2 = 2000 ;
```

```
end_spanSS2 = res_SS2 * step_sizeSS2 ;

time_spanSS02 = 0:step_sizeSS2:end_spanSS2;

[ts2,xs2] =
ode113(@spring_basic_nln_single02,time_spanSS02,int_sing02(cycle,:),[],cycl
e);

 [maxValue(cycle) maxIndex(cycle)] = max(xs2(:,3));

for count03 = 1:res_SS2

del_xs2(count03,:) = xs2(count03,1)-int_sing01(cycle,1);

k_hard02(cycle,count03) = k + a0 * exp(b0*n)*(l0- sqrt((stepLength(cycle)-
del_xs2(count03,:))^2+ xs2(count03,3)^2))^(a1+b1*n-1);

qS2(count03,:) = k_hard02(cycle,count03)*(l0/sqrt((stepLength(cycle)-
del_xs2(count03,:))^2+ xs2(count03,3)^2)-1);

lead_legAngle_SS2(count03,:) = atan(xs2(count03,3)/(stepLength(cycle)-
del_xs2(count03,:)));

angle_lead02_SS2(cycle,count03) = -atan((stepLength(cycle)-
del_xs2(count03,:))/xs2(count03,3));%wrt vertical

GRF_SS2x(count03,cycle) = (-qS2(count03,:)*(stepLength(cycle)-
del_xs2(count03,:)));

GRF_SS2y(count03,cycle) = (qS2(count03,:)* xs2(count03,3));

lead_forceAngle_SS2(count03,:) =
atan(GRF_SS2y(count03,cycle)/GRF_SS2x(count03,cycle));

kinetic_E_SS2(cycle,count03) =
0.5*mass*(xs2(count03,2)^2+xs2(count03,4)^2);

potential_E_SS2(cycle,count03) = mass*g*xs2(count03,3);

l_lead02_SS2(cycle,count03) = sqrt((stepLength(cycle)-
del_xs2(count03,:))^2+ xs2(count03,3)^2) ;

elastic_E_SS2(cycle,count03) =
0.5*k_hard02(cycle,count03)*(l_lead02_SS2(cycle,count03)-l0)^2 ;

check_energy_SS2(cycle,count03) = kinetic_E_SS2(cycle,count03) +
potential_E_SS2(cycle,count03) + elastic_E_SS2(cycle,count03) ;

check_hight02(cycle,count03) = int_sing01(cycle,3)- xs2(count03,3);

tanV_state(count03,:) = atan(xs2(count03,4)/xs2(count03,2));

diff_y_state(cycle,count03) = int_sing01(cycle,3)- xs2(count03,3);

diff_tanV_state(cycle,count03) = int_tanV_state(cycle)-
tanV_state(count03,:);
```

```
check_state(cycle,count03) = norm([diff_y_state(cycle,count03);
diff_tanV_state(cycle,count03)]);

    if count03== maxIndex(cycle)

         max_height(cycle) = xs2(maxIndex(cycle),3);
         if check_state(cycle,count03) <= 0.01;

          endSS02(cycle) = count03 ;

          end_check_state(cycle) = check_state(cycle,count03);

          disp(['achieved cycle',num2str(cycle)])

        end

    end
end

x_cycle{cycle} =
{xs(1:touch_down_timeSS(cycle),:);xd(1:take_off(cycle),:);xs2(1:endSS02(cyc
le),:)};

delxHx_cycle{cycle} =
{del_xs(1:touch_down_timeSS(cycle),:);del_xd(1:take_off(cycle),:);del_xs2(1
:endSS02(cycle),:)};

x_new_cycle = [x_new_cycle;x_cycle{cycle}];

delxHx_new_cycle = [delxHx_new_cycle;delxHx_cycle{cycle}];

int_sing01(cycle+1,:) = xs2(endSS02(cycle),:);

int_sing01_rel(cycle+1,:) = [xs2(endSS02(cycle),1)-
int_sing01(cycle,1),xs2(endSS02(cycle),2:4)];

x_int_sing01(cycle+1) = int_sing01(cycle+1,1);

init_del_xs = [init_del_xs;del_xs2(endSS02(cycle),:)];

y_int_sing01(cycle+1) = int_sing01(cycle+1,3);


end

      %Return map and Floquet multiplier

             D_map_point = diff(map_point);
             norm_map_point = [];
             for map_row = 1:length(D_map_point)
             norm_map_point =
[norm_map_point;norm(D_map_point(map_row,:))];
             end
             [val_min_norm Id_lim_cycle]= min(norm_map_point);
```

```
k_hard = [k_hard_Dq(cycle-1,1:take_off(cycle-1)),k_hard02(cycle-
1,1:endSS02(cycle-1)),k_hard01(cycle,1:touch_down_timeSS(cycle)),
k_hard_Dp(cycle,1:take_off(cycle))];

k_hard_max = max(k_hard);

k_rel_hard = k_hard_max /min(k_hard);

GRF_x = [GRF_DSx_1(1:take_off(cycle-1),cycle-1);GRF_SS2x(1:endSS02(cycle-
1),cycle-
1);GRF_SSx(1:touch_down_timeSS(cycle),:);GRF_DSx(1:take_off(cycle),:)];

GRF_y = [GRF_DSy_1(1:take_off(cycle-1),cycle-1);GRF_SS2y(1:endSS02(cycle-
1),cycle-
1);GRF_SSy(1:touch_down_timeSS(cycle),:);GRF_DSy(1:take_off(cycle),:)];

GRF_net = sqrt(GRF_x.^2+ GRF_y.^2);

legLength = [l_lead02_DS(cycle-1,1:take_off(cycle-1))';l_lead02_SS2(cycle-
1,1:endSS02(cycle-
1))';l_trail01_SS(cycle,1:touch_down_timeSS(cycle))';l_trail01_leave(cycle,
1:take_off(cycle))'];

legAngle = [angle_lead02_DS(cycle-1,1:take_off(cycle-
1))';angle_lead02_SS2(cycle-1,1:endSS02(cycle-
1))';angle_trail01_SS(cycle,1:touch_down_timeSS(cycle))';angle_trail01_leav
e(cycle,1:take_off(cycle))'];


sumGRF_DSx = GRF_DSx_1(:,cycle) + GRF_DSx ;

sumGRF_DSx_step = GRF_DSx_1(1:take_off(cycle),cycle) +
GRF_DSx(1:take_off(cycle),:) ;


sumGRF_DSy = GRF_DSy_1(:,cycle) + GRF_DSy ;

sumGRF_DSy_step = GRF_DSy_1(1:take_off(cycle),cycle) +
GRF_DSy(1:take_off(cycle),:) ;


netGRF_SS = sqrt(GRF_SSx.^2 + GRF_SSy.^2);

netGRF_SS_step = sqrt(GRF_SSx(1:touch_down_timeSS(cycle),:).^2 +
GRF_SSy(1:touch_down_timeSS(cycle),:).^2);

netGRF_DS = sqrt(sumGRF_DSx.^2 + sumGRF_DSy.^2);

netGRF_DS_step = sqrt(sumGRF_DSx(1:take_off(cycle),:).^2 +
sumGRF_DSy(1:take_off(cycle),:).^2);

netGRF_SS02 = sqrt(GRF_SS2x(:,cycle).^2 + GRF_SS2y(:,cycle).^2);

netGRF_SS02_step = sqrt(GRF_SS2x(1:endSS02(cycle-1),cycle-1).^2 +
GRF_SS2y(1:endSS02(cycle-1),cycle-1).^2);
```

```
netGRF_step = [netGRF_SS_step;netGRF_DS_step;netGRF_SS02_step];
DnetGRF_step = diff(netGRF_step);
sumDnetGRF_step = sum(DnetGRF_step);



phase = length(x_new_cycle);

for count_phase = 1:phase

   length_x_new_cycle(count_phase) = length(x_new_cycle{count_phase});

end

sum_length = sum(length_x_new_cycle) ;

renew_x_new_cycle = zeros(sum_length,4);

renew_delxHx_new_cycle = zeros(sum_length,1);

leg_length_cycle = zeros(sum_length,1);

count_x_new_cycle = 1;

%obtain CoM motion from cell array to matrix

for count_phase = 1:phase

        for count_x_inphase = 1:length(x_new_cycle{count_phase})

            renew_x_new_cycle(count_x_new_cycle,:) =
x_new_cycle{count_phase}(count_x_inphase,:);

            renew_delxHx_new_cycle(count_x_new_cycle,:) =
delxHx_new_cycle{count_phase}(count_x_inphase,:);

            leg_length_cycle(count_x_new_cycle,:) =
sqrt(renew_delxHx_new_cycle(count_x_new_cycle,:).^2+
renew_x_new_cycle(count_x_new_cycle,3).^2);

            count_x_new_cycle = count_x_new_cycle + 1 ;

        end


end

diff_leg_length_cycle =
(1/step_sizeSS)*[diff(leg_length_cycle(1:2,:));diff(leg_length_cycle)];

%%
%Distance btw apex point and 45 degree line

fixed_point = map_point(Id_lim_cycle,:);
```

```
fit_first = [];
fit_next = [];

[row_IC col_IC]= size(map_point);

for count04 = 1:col_IC

fit_first = [fit_first; map_point(1:end-1,count04)' - fixed_point(count04)'
];
fit_next = [fit_next; map_point(2:end,count04)' - fixed_point(count04)' ];

end

Jmatrix = (fit_next * fit_first')*pinv(fit_first*fit_first');


FQmult = abs(eig(Jmatrix));
max_FQmult = max(FQmult);
min_FQmult = min(FQmult);

    if (max_FQmult < 1)

    disp(['k                              |  ',num2str(k)])
    disp(['angle                          |
',num2str(design_touch_down_angle*180/pi)])
    disp(['cycle                          |  ',num2str(cycle)])
    disp(['fixed point                    |  ',num2str(fixed_point)])
    disp(['y0                             |  ',num2str(y_int_sing01(1))])
    disp(['y transition                   |  ',num2str(y_touch)])
    disp(['Stable Floquet multiplier      |  ',num2str(max_FQmult)])

    elseif (max_FQmult > 1 && min_FQmult < 1)

    disp(['k                              |  ',num2str(k)])
    disp(['angle                          |
',num2str(design_touch_down_angle*180/pi)])
    disp(['cycle                          |  ',num2str(cycle)])
    disp(['fixed point                    |  ',num2str(fixed_point)])
    disp(['y0                             |  ',num2str(y_int_sing01(1))])
    disp(['y transition                   |  ',num2str(y_touch)])
    disp(['Saddle Floquet multiplier      |  ',num2str(max_FQmult)])

    else

    disp(['k                              |  ',num2str(k)])
    disp(['angle                          |
',num2str(design_touch_down_angle*180/pi)])
    disp(['cycle                          |  ',num2str(cycle)])
    disp(['fixed point                    |  ',num2str(fixed_point)])
    disp(['y0                             |  ',num2str(y_int_sing01(1))])
    disp(['y transition                   |  ',num2str(y_touch)])
    disp(['Unstable Floquet multiplier     |  ',num2str(max_FQmult)])

    end
```

6.2D. Human walking prediction using compliant leg model with axial and tangential elastic leg property (CATE)

6.2.1D CATE model with linear elastic leg property

```
%%
global k l0 kt_SS angH0_SS kt_DS angH0_DS mass stepLength g x_int_sing01
step_sizeSS step_sizeDS step_sizeSS2
global a_re01 a_F0 a_re02 kt1 kt3
global init_angle02 final_angle02

%-------------------------------------------------------------
k = 10976;%N/m
kt3 = -220;

init_angle02 = -0.37;
design_touch_down_angle = 0.5*pi - abs(init_angle02);%horizontal angle
marks td timing, big angle = early td
final_angle02 = 0.41;
%-------------------------------------------------------------
l0 = 0.972;%m

a_re01 =  0.075;
a_F0 = 0.39;
a_re02 = 0.9;

kt1= (1.07)*-kt3*(final_angle02-(init_angle02 + a_F0*(final_angle02-
init_angle02)))*(a_re02-a_F0)/(a_F0*(final_angle02-init_angle02)*a_re01);
mass = 69;%kg
g = 9.81;% m/s2

%%

toggle_check = 0;

x_int_sing01 = 0.0; %m

y_int_sing01 = 0.935;%m

delta_spring_length = l0 - y_int_sing01; % apex height at vertical leg only

y_touch = l0*sin(design_touch_down_angle);


vx_int_sing01 = 1.15;
vel_angle = 7*pi/180;
vy_int_sing01 = vx_int_sing01*tan(vel_angle);

int_sing01 = [x_int_sing01 vx_int_sing01 y_int_sing01 vy_int_sing01];

x_new_cycle = [];

delxHx_new_cycle = [];
```

```
init_del_xs = [];

norm_D_state = [];

for cycle = 1:3

step_sizeSS = 0.0001;
res_SS = 3000 ;
end_spanSS = res_SS * step_sizeSS ;
time_spanSS = 0:step_sizeSS:end_spanSS; %max = 1 millisec

[ts1,xs] =
ode113(@spring_leg_newNT_single_asym01,time_spanSS,int_sing01(cycle,:),[],c
ycle);

int_sing01_abs(cycle,:) = [xs(1,1)-
int_sing01(cycle,1),int_sing01(cycle,2:4)];

for count01 = 1:res_SS

del_xs(count01,:) = xs(count01,1)-int_sing01(cycle,1);

l_trail01_SS(cycle,count01) = sqrt(del_xs(count01,:)^2+xs(count01,3)^2);

angle_trail01_SS(cycle,count01) =
atan(del_xs(count01,:)/xs(count01,3));%wrt vertical

angleH_trail01_SS(cycle,count01) =
atan(xs(count01,3)/del_xs(count01,:));%wrt horizontal

lead_angle(cycle,count01) = asin(xs(count01,3)/l0);%virtual angle when lead
leg leaning to touched wrt horizontal

lead_angle_degree(cycle,count01) = lead_angle(cycle,count01)*180/pi;

nForce_model_SS(count01,cycle) =  k*(l0-l_trail01_SS(cycle,count01));

Fnx_SS(count01,:)= nForce_model_SS(count01,cycle)*
del_xs(count01,:)/l_trail01_SS(cycle,count01);

Fny_SS(count01,:)= nForce_model_SS(count01,cycle)*
xs(count01,3)/l_trail01_SS(cycle,count01);


%%%%%%%%%%

angle_period = final_angle02-init_angle02;
        %-----partI

        angle_re01 = init_angle02 + a_re01*angle_period ;

        tForce_model_SS(count01,cycle) =
kt1*(angle_trail01_SS(cycle,count01) -
init_angle02).*(angle_trail01_SS(cycle,count01) <= angle_re01);

        %-----partII
```

```
        Ft_re1 = kt1*(angle_re01 - init_angle02);
        angle_F0 = init_angle02 + a_F0*angle_period ;

        kt2 = (0 - Ft_re1)/(angle_F0 - angle_re01);

        tForce_model_SS(count01,cycle) = tForce_model_SS(count01,cycle) +
(angle_trail01_SS(cycle,count01) > angle_re01 &
angle_trail01_SS(cycle,count01) <= angle_F0).*
(kt2*(angle_trail01_SS(cycle,count01) - angle_F0));

        %-----partIII
        angle_re02 = init_angle02 + a_re02*angle_period ;

        tForce_model_SS(count01,cycle) = tForce_model_SS(count01,cycle) +
(angle_trail01_SS(cycle,count01) > angle_F0 &
angle_trail01_SS(cycle,count01) <= angle_re02).*
(kt3*(angle_trail01_SS(cycle,count01) - angle_F0));

        %-----partIV
        Ft_re3 = kt3*(angle_re02 - angle_F0);

        kt4 = (0 - Ft_re3)/(final_angle02 - angle_re02 );

        tForce_model_SS(count01,cycle) = tForce_model_SS(count01,cycle) +
(angle_trail01_SS(cycle,count01) > angle_re02 &
angle_trail01_SS(cycle,count01) <= final_angle02).*
(kt4*(angle_trail01_SS(cycle,count01) - angle_re02)+ Ft_re3);

Ftx_SS(count01,:)= tForce_model_SS(count01,cycle)*
xs(count01,3)/l_trail01_SS(cycle,count01);

Fty_SS(count01,:)= -tForce_model_SS(count01,cycle)*
del_xs(count01,:)/l_trail01_SS(cycle,count01);

%%%%%%%%%%

GRF_SSx(count01,:) = Fnx_SS(count01,:) + Ftx_SS(count01,:);

GRF_SSy(count01,:) = Fny_SS(count01,:)+ Fty_SS(count01,:);


check_hight(cycle,count01) = xs(count01,3)- y_touch;

    if ((check_hight(cycle,count01) <= 0.0001) &&
(check_hight(cycle,count01) >= -0.0001))

    touch_down_angle(cycle) = lead_angle(cycle,count01) ;

    touch_down_angle_degree(cycle) = lead_angle_degree(cycle,count01);

    touch_down_timeSS(cycle) = count01;

    end

end

%%
```

```
l_trail01_touch(cycle) = sqrt((xs(touch_down_timeSS(cycle),1)-
x_int_sing01(cycle))^2+xs(touch_down_timeSS(cycle),3)^2);
trail_angle(cycle) =
asin(xs(touch_down_timeSS(cycle),3)/l_trail01_touch(cycle));
trail_angle_degree(cycle) = trail_angle(cycle) * 180 / pi ;
stepLength(cycle) = l0*cos(touch_down_angle(cycle))+
l_trail01_touch(cycle)*cos(trail_angle(cycle));

x_int_db(cycle) = xs(touch_down_timeSS(cycle),1);
vx_int_db(cycle) = xs(touch_down_timeSS(cycle),2);
y_int_db(cycle) = xs(touch_down_timeSS(cycle),3);
vy_int_db(cycle) =xs(touch_down_timeSS(cycle),4);
int_db(cycle,:) = [x_int_db(cycle) vx_int_db(cycle) y_int_db(cycle)
vy_int_db(cycle) ];

step_sizeDS =  step_sizeSS;
res_DS = 3000 ;
end_spanDS = res_DS * step_sizeDS ;
time_spanDS = 0:step_sizeDS:end_spanDS;

kt_DS = kt_SS*(angH0_SS - trail_angle(cycle))/(angH0_DS -
trail_angle(cycle));

[td,xd] =
ode113(@spring_leg_newNT_double_asym,time_spanDS,int_db(cycle,:),[],cycle);

for count02 = 1:res_DS

del_xd(count02,:) = xd(count02,1)-int_sing01(cycle,1);

l_trail01_leave(cycle,count02) = sqrt(del_xd(count02,:)^2+
xd(count02,3)^2);

l_lead02_DS(cycle,count02) = sqrt((stepLength(cycle)-
del_xd(count02,:))^2+xd(count02,3)^2) ;

angle_trail01_leave(cycle,count02) =
atan(del_xd(count02,:)/xd(count02,3));%wrt vertical

angleH_trail01_leave(cycle,count02) =
atan(xd(count02,3)/del_xd(count02,:));

angle_lead02_DS(cycle,count02) = - atan((stepLength(cycle)-
del_xd(count02,:))/xd(count02,3)) ;%wrt vertical

angleH_lead02_DS(cycle,count02) = atan(xd(count02,3)/(stepLength(cycle)-
del_xd(count02,:))) ;

nForce_model_trail(count02,cycle) =  k*(l0 -
l_trail01_leave(cycle,count02));

nForce_model_lead(count02,cycle) =  k*(l0 - l_lead02_DS(cycle,count02));

Fnx_DS_lead(count02,cycle) = -
(nForce_model_lead(count02,cycle)*(stepLength(cycle)-
del_xd(count02,:))/l_lead02_DS(cycle,count02)) ;
```

```
Fny_DS_lead(count02,cycle) =
(nForce_model_lead(count02,cycle)*xd(count02,3)/l_lead02_DS(cycle,count02))
;

Fnx_DS(count02,:) =
(nForce_model_trail(count02,cycle)*del_xd(count02,:)/l_trail01_leave(cycle,
count02)) ;

Fny_DS(count02,:) =
(nForce_model_trail(count02,cycle)*xd(count02,3)/l_trail01_leave(cycle,coun
t02));



%%%%%%%%%%%%%%%%%%%%%%%%%%%%%%%%
        %-----part I

        tForce_model_lead(count02,cycle) =
kt1*(angle_lead02_DS(cycle,count02) -
init_angle02).*(angle_lead02_DS(cycle,count02) <= angle_re01);

        %-----part II

        tForce_model_lead(count02,cycle) = tForce_model_lead(count02,cycle)
+ (angle_lead02_DS(cycle,count02) > angle_re01 &
angle_lead02_DS(cycle,count02) <= angle_F0).*
(kt2*(angle_lead02_DS(cycle,count02) - angle_F0));

        %-----part III

        tForce_model_trail(count02,cycle) =
(angle_trail01_leave(cycle,count02) > angle_F0 &
angle_trail01_leave(cycle,count02)<= angle_re02).*
(kt3*(angle_trail01_leave(cycle,count02) - angle_F0));


        %-----partIV

        tForce_model_trail(count02,cycle) =
tForce_model_trail(count02,cycle) + (angle_trail01_leave(cycle,count02) >
angle_re02 & angle_trail01_leave(cycle,count02) <= final_angle02).*
(kt4*(angle_trail01_leave(cycle,count02) - angle_re02)+ Ft_re3);


%%%%%%%%%%

Ftx_DS_lead(count02,cycle)=
tForce_model_lead(count02,cycle)*xd(count02,3)/l_lead02_DS(cycle,count02);

Fty_DS_lead(count02,cycle)=
tForce_model_lead(count02,cycle)*(stepLength(cycle)-
del_xd(count02,:))/l_lead02_DS(cycle,count02);


Ftx_DS(count02,:)= tForce_model_trail(count02,cycle)*
xd(count02,3)/l_trail01_leave(cycle,count02);
```

```
Fty_DS(count02,:)= -tForce_model_trail(count02,cycle)*
del_xd(count02,:)/l_trail01_leave(cycle,count02) ;

%%%%%%%%%%%%%%%%%%%%%%%%%%%%%%%

GRF_DSx_lead(count02,cycle) = Fnx_DS_lead(count02,cycle) +
Ftx_DS_lead(count02,cycle);

GRF_DSy_lead(count02,cycle) = Fny_DS_lead(count02,cycle)+
Fty_DS_lead(count02,cycle);

GRF_DSx(count02,:) = Fnx_DS(count02,:)+ Ftx_DS (count02,:) ;

GRF_DSy(count02,:) = Fny_DS(count02,:)+ Fty_DS(count02,:);


GRF_DSx_sum(count02,cycle) = GRF_DSx_lead(count02,cycle)+
GRF_DSx(count02,:);

GRF_DSy_sum(count02,cycle) = GRF_DSy_lead(count02,cycle)+
GRF_DSy(count02,:);


check_length(cycle,count02) = l0 - l_trail01_leave(cycle,count02) ;

    if (check_length(cycle,count02) <= 0.0001 &&
(check_length(cycle,count02) >= -0.0001))

    l_trail01_take_off(cycle) = l_trail01_leave(cycle,count02);

    take_off(cycle) = count02;

    end

end


%%
x_int_sing02(cycle) = xd(take_off(cycle),1);
vx_int_sing02(cycle) = xd(take_off(cycle),2);
y_int_sing02(cycle) = xd(take_off(cycle),3);
vy_int_sing02(cycle) =xd(take_off(cycle),4);
int_sing02(cycle,:) = [x_int_sing02(cycle) vx_int_sing02(cycle)
y_int_sing02(cycle) vy_int_sing02(cycle) ];

l_trail01_start_SS2 = sqrt((xd(take_off(cycle),1)-x_int_sing01(cycle))^2+
xd(take_off(cycle),3)^2);

step_sizeSS2 =  step_sizeDS;

res_SS2 = 4000 ;

end_spanSS2 = res_SS2 * step_sizeSS2 ;

time_spanSS02 = 0:step_sizeSS2:end_spanSS2;

toggle_check = 0 ;
```

```
 [ts2,xs2] =
ode113(@spring_leg_newNT_single_asym02,time_spanSS02,int_sing02(cycle,:),[]
,cycle);
 [maxValue(cycle) maxIndex(cycle)] = max(xs2(:,3));

for count03 = 1:res_SS2

del_xs2(count03,:) = xs2(count03,1)-int_sing01(cycle,1);

l_lead02_SS2(cycle,count03) = sqrt((stepLength(cycle)-
del_xs2(count03,:))^2+ xs2(count03,3)^2) ;

angleH_lead02_SS2(cycle,count03) = atan(xs2(count03,3)/(stepLength(cycle)-
del_xs2(count03,:)));

angle_lead02_SS2(cycle,count03) = -atan((stepLength(cycle)-
del_xs2(count03,:))/xs2(count03,3));%wrt vertical

nForce_model_SS2(count03,cycle) = k*(l0 - l_lead02_SS2(cycle,count03));

Fnx_SS2(count03,cycle) = -nForce_model_SS2(count03,cycle)*
(stepLength(cycle)- del_xs2(count03,:))/l_lead02_SS2(cycle,count03);

Fny_SS2(count03,cycle) = nForce_model_SS2(count03,cycle)*
xs2(count03,3)/l_lead02_SS2(cycle,count03);

%%%%%%%%%%%%%%%%%%%%%%%%%%%%%%%%%%%%

        %-----part I

        tForce_model_SS2(count03,cycle) =
kt1*(angle_lead02_SS2(cycle,count03) -
init_angle02).*(angle_lead02_SS2(cycle,count03) <= angle_re01);

        %-----part II

        tForce_model_SS2(count03,cycle) = tForce_model_SS2(count03,cycle) +
(angle_lead02_SS2(cycle,count03) > angle_re01 &
angle_lead02_SS2(cycle,count03) <= angle_F0).*
(kt2*(angle_lead02_SS2(cycle,count03) - angle_F0));

        %-----part III

        tForce_model_SS2(count03,cycle) = tForce_model_SS2(count03,cycle)
+(angle_lead02_SS2(cycle,count03) > angle_F0 &
angle_lead02_SS2(cycle,count03)<= angle_re02).*
(kt3*(angle_lead02_SS2(cycle,count03) - angle_F0));



Ftx_SS2(count03,cycle)= tForce_model_SS2(count03,cycle)*
xs2(count03,3)/l_lead02_SS2(cycle,count03);

Fty_SS2(count03,cycle)= tForce_model_SS2(count03,cycle)*
(stepLength(cycle)- del_xs2(count03,:))/l_lead02_SS2(cycle,count03);

%%%%%%%%%%%%%%%%%%%%%%%%%%%%%%%%%%%%
```

```
GRF_SS2x(count03,cycle) = Fnx_SS2(count03,cycle)+ Ftx_SS2(count03,cycle);

GRF_SS2y(count03,cycle) = Fny_SS2(count03,cycle)+ Fty_SS2(count03,cycle);

lead_forceAngle_SS2(count03,:) =
atan(GRF_SS2y(count03,:)/GRF_SS2x(count03,:));

check_hight02(cycle,count03) = int_sing01(cycle,3)- xs2(count03,3);

check_angle(cycle,count03) =   angle_lead02_SS2(cycle,count03);

angle_head(cycle,count03) = atan(xs2(count03,4)/xs2(count03,2));

temp_state_end(count03,:)= [xs2(count03,2),angle_head(cycle,count03)];

temp_state_org(count03,:) =
[int_sing01(cycle,2),atan(int_sing01(cycle,4)/int_sing01(cycle,2))];

check_state(cycle,count03) = norm(temp_state_org(count03,:)-
temp_state_end(count03,:));


       if ((check_angle(cycle,count03) <= 0.001) &&
(check_angle(cycle,count03) >= -0.001))

           if toggle_check == 0

           upright_time (cycle)= count03;

           upright_state(cycle) = check_state(cycle,count03);

           upright_height(cycle) = xs2(count03,3);

           toggle_check = 1;


            if check_state(cycle,count03) <= 0.15;


            state_end(cycle,:)=[xs2(count03,2),angle_head(cycle,count03)];

            state_org(cycle,:) =
[int_sing01(cycle,2),atan(int_sing01(cycle,4)/int_sing01(cycle,2))];

            endSS02(cycle) = count03 ;

            end_check_state(cycle) = check_state(cycle,count03);

            disp(['achieved cycle',num2str(cycle)])

            end

%              toggle_check = 0 ;

           end
```

```
       end

   end
toggle_check = 0 ;

x_cycle{cycle} =
{xs(1:touch_down_timeSS(cycle),:);xd(1:take_off(cycle),:);xs2(1:endSS02(cyc
le),:)};

delxHx_cycle{cycle} =
{del_xs(1:touch_down_timeSS(cycle),:);del_xd(1:take_off(cycle),:);del_xs2(1
:endSS02(cycle),:)};

x_new_cycle =  [x_new_cycle;x_cycle{cycle}];

delxHx_new_cycle = [delxHx_new_cycle;delxHx_cycle{cycle}];

int_sing01(cycle+1,:) = xs2(endSS02(cycle),:);

state_org(cycle+1,:) = state_end(cycle,:);

int_sing01_abs(cycle+1,:) = [ xs2(endSS02(cycle),1)-
int_sing01(cycle+1,1),int_sing01(cycle+1,2:4)];

x_int_sing01(cycle+1) = int_sing01(cycle+1,1);


init_del_xs = [init_del_xs;del_xs2(endSS02(cycle),:)];

y_int_sing01(cycle+1) = int_sing01(cycle+1,3);


norm_state(cycle,:) = norm(state_org(cycle,:)); %%%

               %%
        if cycle ==1

        figure;

plot(xs(1:touch_down_timeSS(cycle),1),xs(1:touch_down_timeSS(cycle),3),'-
bo','MarkerSize',3)
        hold on
        plot(xd(1:take_off(cycle),1),xd(1:take_off(cycle),3),'-
ro','MarkerSize',3)
        hold on
        plot(xs2(1:endSS02(cycle),1),xs2(1:endSS02(cycle),3),'-
ko','MarkerSize',3)
        grid on
        title('displacement')

        figure;

plot(xs(1:touch_down_timeSS(cycle),2),xs(1:touch_down_timeSS(cycle),4),'-
bo','MarkerSize',3)
        hold on
        plot(xd(1:take_off(cycle),2),xd(1:take_off(cycle),4),'-
ro','MarkerSize',3)
```

```
        hold on
        plot(xs2(1:endSS02(cycle),2),xs2(1:endSS02(cycle),4),'-
ko','MarkerSize',3)
        grid on
        title('velocity')

        end
end

%GRF one leg
GRF_x = [GRF_DSx_lead(1:take_off(cycle-1),cycle-
1);GRF_SS2x(1:endSS02(cycle-1),cycle-
1);GRF_SSx(1:touch_down_timeSS(cycle),:);GRF_DSx(1:take_off(cycle),:)];

GRF_y = [GRF_DSy_lead(1:take_off(cycle-1),cycle-
1);GRF_SS2y(1:endSS02(cycle-1),cycle-
1);GRF_SSy(1:touch_down_timeSS(cycle),:);GRF_DSy(1:take_off(cycle),:)];

GRF_net = sqrt(GRF_x.^2+ GRF_y.^2);


Ft_cycle = [tForce_model_lead(1:take_off(cycle-1),cycle-
1);tForce_model_SS2(1:endSS02(cycle-1),cycle-
1);tForce_model_SS(1:touch_down_timeSS(cycle),cycle);tForce_model_trail(1:t
ake_off(cycle),cycle)];

legLength = [l_lead02_DS(cycle-1,1:take_off(cycle-1))';l_lead02_SS2(cycle-
1,1:endSS02(cycle-
1))';l_trail01_SS(cycle,1:touch_down_timeSS(cycle))';l_trail01_leave(cycle,
1:take_off(cycle))'];

legAngle = [angle_lead02_DS(cycle-1,1:take_off(cycle-
1))';angle_lead02_SS2(cycle-1,1:endSS02(cycle-
1))';angle_trail01_SS(cycle,1:touch_down_timeSS(cycle))';angle_trail01_leav
e(cycle,1:take_off(cycle))'];



%GRF both legs
sumGRF_DSx = GRF_DSx_lead(:,cycle) + GRF_DSx ;

sumGRF_DSx_step = GRF_DSx_lead(1:take_off(cycle),cycle) +
GRF_DSx(1:take_off(cycle),:) ;


sumGRF_DSy = GRF_DSy_lead(:,cycle) + GRF_DSy ;

sumGRF_DSy_step = GRF_DSy_lead(1:take_off(cycle),cycle) +
GRF_DSy(1:take_off(cycle),:) ;


netGRF_SS = sqrt(GRF_SSx.^2 + GRF_SSy.^2);

netGRF_SS_step = sqrt(GRF_SSx(1:touch_down_timeSS(cycle),:).^2 +
GRF_SSy(1:touch_down_timeSS(cycle),:).^2);

netGRF_DS = sqrt(sumGRF_DSx.^2 + sumGRF_DSy.^2);
```

```
netGRF_DS_step = sqrt(sumGRF_DSx(1:take_off(cycle),:).^2 +
sumGRF_DSy(1:take_off(cycle),:).^2);

netGRF_SS02 = sqrt(GRF_SS2x(:,cycle).^2 + GRF_SS2y(:,cycle).^2);

netGRF_SS02_step = sqrt(GRF_SS2x(1:endSS02(cycle-1),cycle-1).^2 +
GRF_SS2y(1:endSS02(cycle-1),cycle-1).^2);


netGRF_step = [netGRF_SS_step;netGRF_DS_step;netGRF_SS02_step];
DnetGRF_step = diff(netGRF_step);
sumDnetGRF_step = sum(DnetGRF_step);


%%return map and Floquet multipliers

phase = length(x_new_cycle);

for count_phase = 1:phase

   length_x_new_cycle(count_phase) = length(x_new_cycle{count_phase});

end

sum_length = sum(length_x_new_cycle) ;

renew_x_new_cycle = zeros(sum_length,4);

renew_delxHx_new_cycle = zeros(sum_length,1);

leg_length_cycle = zeros(sum_length,1);

count_x_new_cycle = 1;

%obtain CoM motion from cell array to matrix

for count_phase = 1:phase

    %for count_x_new_cycle = 1: sum_length

        for count_x_inphase = 1:length(x_new_cycle{count_phase})

            renew_x_new_cycle(count_x_new_cycle,:) =
x_new_cycle{count_phase}(count_x_inphase,:);

            renew_delxHx_new_cycle(count_x_new_cycle,:) =
delxHx_new_cycle{count_phase}(count_x_inphase,:);

            leg_length_cycle(count_x_new_cycle,:) =
sqrt(renew_delxHx_new_cycle(count_x_new_cycle,:).^2+
renew_x_new_cycle(count_x_new_cycle,3).^2);

            count_x_new_cycle = count_x_new_cycle + 1 ;

            %count_x_new_cycle_odd(count_x_new_cycle) =
        end
```

```
    %end

end

diff_leg_length_cycle =
(1/step_sizeSS)*[diff(leg_length_cycle(1:2,:));diff(leg_length_cycle)];

%%
%Distance btw apex point and 45 degree line

actual_state = [norm_state(1:end-1,:), norm_state(2:end,:)];

ref_state = [norm_state(1:end-1,:), norm_state(1:end-1,:)];


D_state = actual_state - ref_state;
norm_D_state = norm(D_state);
[val_min_norm Id_lim_cycle]= min(norm_D_state);


fixed_point = state_org(Id_lim_cycle,:);


fit_first = [];
fit_next = [];


[row_IC col_IC]= size(state_org);

for count04 = 1:col_IC

fit_first = [fit_first; state_org(1:end-1,count04)' - fixed_point(count04)'
];

fit_next = [fit_next; state_org(2:end,count04)' - fixed_point(count04)' ];

end

sqr_fit_first = fit_first*fit_first';

dfit_first = det(fit_first*fit_first');


Jmatrix = (fit_next * fit_first')*pinv(fit_first*fit_first');


FQmult = eig(Jmatrix);
max_FQmult = max(abs(FQmult));

disp(['k                        |  ',num2str(k)])
disp(['angle                    |
',num2str(design_touch_down_angle*180/pi)])
disp(['cycle                    |  ',num2str(cycle)])
disp(['fixed point              |  ',num2str(fixed_point)])
disp(['y0                       |  ',num2str(y_int_sing01(1))])
disp(['y transition             |  ',num2str(y_touch)])
```

```
disp(['Max Floquet multiplier   |  ',num2str(max_FQmult)])
```

Chapter 7

7.1D. Human walking prediction using posture-dependent elastic leg model (PDE)

```
global l0 lf q0 qf fl0 fq0
global angle_leg02 length_fCoP02 tForce_model_q0
global mass stepLength g x_int_sing01 step_sizeSS step_sizeDS step_sizeSS2
global LeastSqrN_l0 LeastSqrT %stiffnessN stiffnessT

mass = 69;%kg
g = 9.81;% m/s2

l0 = length_fCoP02(1);%(m)
lf = length_fCoP02(end);%(m)
q0 = angle_leg02(1);
qf = angle_leg02(end);

[minFt IDminFt] = min(abs(tForce_model_q0(10:end-10)));
fq0 = angle_leg02(10+IDminFt);

y_touch = zeros(1,1);

y_touch(1) = 0.001*l0*cos(q0);

%CoM motion @ vertical leg angle

toggle_check = 0;

x_int_sing01 = 0; %mm

y_int_sing01 = 0.924;%mm

vx_int_sing01 = 1.6;

vy_int_sing01 = 0.17;

vel_angle = atan(vy_int_sing01/vx_int_sing01);

vel_angle_deg = atan(vy_int_sing01/vx_int_sing01)*180/pi;


int_sing01 = [x_int_sing01 vx_int_sing01 y_int_sing01 vy_int_sing01];

x_new_cycle = [];

delxHx_new_cycle = [];

init_del_xs = [];

norm_D_Ic = [];

for cycle = 1:2

step_sizeSS = 0.0001;%max = 1 millisec
res_SS = 2000;
```

```
end_spanSS = res_SS * step_sizeSS ;
time_spanSS = 0:step_sizeSS:end_spanSS; %max = 1 millisec
toggle = 0 ;

[ts1,xs] =
ode113(@nln_legFnfq_NTsingle01,time_spanSS,int_sing01(cycle,:),[],cycle);

int_sing01_abs(cycle,:) = [xs(1,1)-
int_sing01(cycle,1),int_sing01(cycle,2:4)];

    for count01 = 1:res_SS

    del_xs(count01,:) = xs(count01,1)-int_sing01(cycle,1);

    l_trail01_SS(cycle,count01) =
sqrt(del_xs(count01,:)^2+xs(count01,3)^2);

    angle_trail01_SS(cycle,count01) =
atan(del_xs(count01,:)/xs(count01,3));%wrt vertical

    lead_angle_SS(cycle,count01) = asin(xs(count01,3)/(0.001*10));%virtual
angle when lead leg leaning to touch

    lead_angle_SS_degree(cycle,count01) =
lead_angle_SS(cycle,count01)*180/pi;


    sin_angle_trail(cycle,count01) =
del_xs(count01,:)/l_trail01_SS(cycle,count01);

    cos_angle_trail(cycle,count01) =
xs(count01,3)/l_trail01_SS(cycle,count01);

    posture(count01,:) = (angle_trail01_SS(cycle,count01) - q0)/(qf - q0);

    a1L = LeastSqrN_l0(1);
    b1L = LeastSqrN_l0(2);
    a2L = LeastSqrN_l0(3);
    b2L = LeastSqrN_l0(4);
    a3L = LeastSqrN_l0(5);
    b3L = LeastSqrN_l0(6);
    a4L = LeastSqrN_l0(7);
    b4L = LeastSqrN_l0(8);
    a5L = LeastSqrN_l0(9);
    b5L = LeastSqrN_l0(10);
    stiffnessN = LeastSqrN_l0(11);


    l1_term = a1L * (cos(2*pi*posture(count01,:))-1)+ b1L *
sin(2*pi*posture(count01,:));
    l2_term = a2L * (cos(2*2*pi*posture(count01,:))-1)+ b2L *
sin(2*2*pi*posture(count01,:));
    l3_term = a3L * (cos(2*3*pi*posture(count01,:))-1)+ b3L *
sin(2*3*pi*posture(count01,:));
    l4_term = a4L * (cos(2*4*pi*posture(count01,:))-1)+ b4L *
sin(2*4*pi*posture(count01,:));
    l5_term = a5L * (cos(2*5*pi*posture(count01,:))-1)+ b5L *
sin(2*5*pi*posture(count01,:));
```

```
     nln_term = l1_term + l2_term + l3_term + l4_term + l5_term ;

    fl0_rate = lf - l0;
    fl0(cycle,count01) = l0 + fl0_rate*(posture(count01,:) + nln_term);

    excursion02_l0(cycle,count01) = fl0(cycle,count01) -
1000*l_trail01_SS(cycle,count01);

    nForce_angSS(count01,:) = stiffnessN .* 0.001.*
excursion02_l0(cycle,count01);


    Fnx_SS(count01,:)= nForce_angSS(count01,:)*
sin_angle_trail(cycle,count01);

    Fny_SS(count01,:)= nForce_angSS(count01,:)*
cos_angle_trail(cycle,count01);



    rel_angle_q0(cycle,count01) = fq0 - angle_trail01_SS(cycle,count01);

    a1Q = LeastSqrT(1);
    b1Q = LeastSqrT(2);
    a2Q = LeastSqrT(3);
    b2Q = LeastSqrT(4);
    a3Q = LeastSqrT(5);
    b3Q = LeastSqrT(6);
    a4Q = LeastSqrT(7);
    b4Q = LeastSqrT(8);
    a5Q = LeastSqrT(9);
    b5Q = LeastSqrT(10);


    q1_term = a1Q * (cos(2*pi*posture(count01,:))-1)+ b1Q *
sin(2*pi*posture(count01,:));
    q2_term = a2Q * (cos(2*2*pi*posture(count01,:))-1)+ b2Q *
sin(2*2*pi*posture(count01,:));
    q3_term = a3Q * (cos(2*3*pi*posture(count01,:))-1)+ b3Q *
sin(2*3*pi*posture(count01,:));
    q4_term = a4Q * (cos(2*4*pi*posture(count01,:))-1)+ b4Q *
sin(2*4*pi*posture(count01,:));
    q5_term = a5Q * (cos(2*5*pi*posture(count01,:))-1)+ b5Q *
sin(2*5*pi*posture(count01,:));


    stiffnessT(cycle,count01) = q1_term + q2_term + q3_term + q4_term +
q5_term ;

    tForce_kq0SS(cycle,count01) = stiffnessT(cycle,count01) .*
rel_angle_q0(cycle,count01);

    Ftx_SS(count01,:)= tForce_kq0SS(cycle,count01)*
cos_angle_trail(cycle,count01);

    Fty_SS(count01,:)= -tForce_kq0SS(cycle,count01)*
sin_angle_trail(cycle,count01);
```

```
    GRF_SSx(count01,:) =  Fnx_SS(count01,:) + Ftx_SS(count01,:);

    GRF_SSy(count01,:) =  Fny_SS(count01,:) + Fty_SS(count01,:);


    check_hight(cycle,count01) = xs(count01,3)- y_touch;

    check_angle_trail(cycle,count01) = angle_trail01_SS(cycle,count01)-
0.364;%trail leg angle at lead leg td

        if ((check_hight(cycle,count01) <= 0.00005) &&
(check_hight(cycle,count01) >= -0.00005))

            if toggle == 0

            touch_down_timeSS(cycle) = count01;

            touch_down_angle(cycle) =
lead_angle_SS(cycle,touch_down_timeSS(cycle)) ;

            touch_down_angle_degree(cycle) =
lead_angle_SS_degree(cycle,touch_down_timeSS(cycle));

            angle_leg_touch_down(cycle) = 0.5*pi -
touch_down_angle(cycle);%wrt virtical

            angle_trail_leg_touch_down(cycle) =
angle_trail01_SS(cycle,touch_down_timeSS(cycle));%wrt virtical

            end

            toggle = 1;

        end

    end


trail_angle(cycle)= 0.5*pi - angle_trail_leg_touch_down(cycle);
trail_angle_degree(cycle) = trail_angle(cycle) * 180 / pi ;
l_trail01_touch(cycle) = l_trail01_SS(cycle,touch_down_timeSS(cycle));
stepLength(cycle) = 0.001*10*cos(touch_down_angle(cycle))+
l_trail01_touch(cycle)*cos(trail_angle(cycle));

x_int_db(cycle) = xs(touch_down_timeSS(cycle),1);
vx_int_db(cycle) = xs(touch_down_timeSS(cycle),2);
y_int_db(cycle) = xs(touch_down_timeSS(cycle),3);
vy_int_db(cycle) =xs(touch_down_timeSS(cycle),4);
int_db(cycle,:) = [x_int_db(cycle) vx_int_db(cycle) y_int_db(cycle)
vy_int_db(cycle) ];

step_sizeDS =  step_sizeSS;
res_DS = 3000 ;
end_spanDS = res_DS * step_sizeDS ;
time_spanDS = 0:step_sizeDS:end_spanDS;
```

```
[td,xd] =
ode113(@nln_legFnfq_NTdouble,time_spanDS,int_db(cycle,:),[],cycle);

for count02 = 1:res_DS

del_xd(count02,:) = xd(count02,1)-int_sing01(cycle,1);

l_trail01_leave(cycle,count02) = sqrt(del_xd(count02,:)^2+
xd(count02,3)^2);

l_lead02_DS(cycle,count02) = sqrt((stepLength(cycle)-
del_xd(count02,:))^2+xd(count02,3)^2) ;

angle_trail01_leave(cycle,count02) = atan(del_xd(count02,:)/xd(count02,3));

angle_lead02_DS(cycle,count02) = -atan((stepLength(cycle)-
del_xd(count02,:))/xd(count02,3)) ;%wrt vertical


sin_trail_DS(cycle,count02) =
del_xd(count02,:)/l_trail01_leave(cycle,count02);

cos_trail_DS(cycle,count02) = xd(count02,3)/l_trail01_leave(cycle,count02);

sin_lead_DS(cycle,count02) = (stepLength(cycle)-
del_xd(count02,:))/l_lead02_DS(cycle,count02);

cos_lead_DS(cycle,count02) = xd(count02,3)/l_lead02_DS(cycle,count02);



posture_trail(cycle,count02) = (angle_trail01_leave(cycle,count02) -
q0)/(qf-q0);

posture_lead(cycle,count02) = (angle_lead02_DS(cycle,count02) - q0)/(qf-
q0);


    %-------------------------------------------------------------------

    l1_term_trail = a1L * (cos(2*pi*posture_trail(cycle,count02))-1)+ b1L *
sin(2*pi*posture_trail(cycle,count02));
    l2_term_trail = a2L * (cos(2*2*pi*posture_trail(cycle,count02))-1)+ b2L
* sin(2*2*pi*posture_trail(cycle,count02));
    l3_term_trail = a3L * (cos(2*3*pi*posture_trail(cycle,count02))-1)+ b3L
* sin(2*3*pi*posture_trail(cycle,count02));
    l4_term_trail = a4L * (cos(2*4*pi*posture_trail(cycle,count02))-1)+ b4L
* sin(2*4*pi*posture_trail(cycle,count02));
    l5_term_trail = a5L * (cos(2*5*pi*posture_trail(cycle,count02))-1)+ b5L
* sin(2*5*pi*posture_trail(cycle,count02));


    nln_term_trail = l1_term_trail + l2_term_trail + l3_term_trail +
l4_term_trail + l5_term_trail ;

    fl0_trail(cycle,count02) = l0 + fl0_rate*(posture_trail(cycle,count02)
+ nln_term_trail);
```

```
    excursion02_l0_trail(cycle,count02) = fl0_trail(cycle,count02) -
1000*l_trail01_leave(cycle,count02);

    nForce_ang_trail(count02,:) = stiffnessN .* 0.001.*
excursion02_l0_trail(cycle,count02) ;

    Fnx_trail_DS(count02,:)= nForce_ang_trail(count02,:)*
sin_trail_DS(cycle,count02);

    Fny_trail_DS(count02,:)= nForce_ang_trail(count02,:)*
cos_trail_DS(cycle,count02);


    q1_term_trail = a1Q * (cos(2*pi*posture_trail(cycle,count02))-1)+ b1Q *
sin(2*pi*posture_trail(cycle,count02));
    q2_term_trail = a2Q * (cos(2*2*pi*posture_trail(cycle,count02))-1)+ b2Q
* sin(2*2*pi*posture_trail(cycle,count02));
    q3_term_trail = a3Q * (cos(2*3*pi*posture_trail(cycle,count02))-1)+ b3Q
* sin(2*3*pi*posture_trail(cycle,count02));
    q4_term_trail = a4Q * (cos(2*4*pi*posture_trail(cycle,count02))-1)+ b4Q
* sin(2*4*pi*posture_trail(cycle,count02));
    q5_term_trail = a5Q * (cos(2*5*pi*posture_trail(cycle,count02))-1)+ b5Q
* sin(2*5*pi*posture_trail(cycle,count02));


    stiffnessT_trail(cycle,count02) = q1_term_trail + q2_term_trail +
q3_term_trail + q4_term_trail + q5_term_trail ;

    rel_angle_trail(cycle,count02) = fq0 -
angle_trail01_leave(cycle,count02);

    tForce_kq0_trail(cycle,count02) = stiffnessT_trail(cycle,count02) .*
rel_angle_trail(cycle,count02);

    Ftx_trail_DS(count02,:)= tForce_kq0_trail(cycle,count02)*
cos_trail_DS(cycle,count02);

    Fty_trail_DS(count02,:)= -tForce_kq0_trail(cycle,count02)*
sin_trail_DS(cycle,count02);


       %-------------------------------------------------------------------


    l1_term_lead = a1L * (cos(2*pi*posture_lead(cycle,count02))-1)+ b1L *
sin(2*pi*posture_lead(cycle,count02));
    l2_term_lead = a2L * (cos(2*2*pi*posture_lead(cycle,count02))-1)+ b2L *
sin(2*2*pi*posture_lead(cycle,count02));
    l3_term_lead = a3L * (cos(2*3*pi*posture_lead(cycle,count02))-1)+ b3L *
sin(2*3*pi*posture_lead(cycle,count02));
    l4_term_lead = a4L * (cos(2*4*pi*posture_lead(cycle,count02))-1)+ b4L *
sin(2*4*pi*posture_lead(cycle,count02));
    l5_term_lead = a5L * (cos(2*5*pi*posture_lead(cycle,count02))-1)+ b5L *
sin(2*5*pi*posture_lead(cycle,count02));
```

```
    nln_term_lead = l1_term_lead + l2_term_lead + l3_term_lead +
l4_term_lead + l5_term_lead ;

    fl0_lead(cycle,count02) = l0 + fl0_rate*(posture_lead(cycle,count02) +
nln_term_lead);

    excursion02_l0_lead(cycle,count02) = fl0_lead(cycle,count02) -
1000*l_lead02_DS(cycle,count02);

    nForce_ang_lead(cycle,count02) = stiffness .* 0.001.*
excursion02_l0_lead(cycle,count02) ;

    Fnx_lead_DS(count02,:)= -nForce_ang_lead(cycle,count02)*
sin_lead_DS(cycle,count02);

    Fny_lead_DS(count02,:)= nForce_ang_lead(cycle,count02)*
cos_lead_DS(cycle,count02);


    q1_term_lead = a1Q * (cos(2*pi*posture_lead(cycle,count02))-1)+ b1Q *
sin(2*pi*posture_lead(cycle,count02));
    q2_term_lead = a2Q * (cos(2*2*pi*posture_lead(cycle,count02))-1)+ b2Q *
sin(2*2*pi*posture_lead(cycle,count02));
    q3_term_lead = a3Q * (cos(2*3*pi*posture_lead(cycle,count02))-1)+ b3Q *
sin(2*3*pi*posture_lead(cycle,count02));
    q4_term_lead = a4Q * (cos(2*4*pi*posture_lead(cycle,count02))-1)+ b4Q *
sin(2*4*pi*posture_lead(cycle,count02));
    q5_term_lead = a5Q * (cos(2*5*pi*posture_lead(cycle,count02))-1)+ b5Q *
sin(2*5*pi*posture_lead(cycle,count02));


    stiffnessT_lead(cycle,count02) = q1_term_lead + q2_term_lead +
q3_term_lead + q4_term_lead + q5_term_lead ;

    rel_angle_lead(cycle,count02) = fq0 - angle_lead02_DS(cycle,count02);

    tForce_kq0_lead(cycle,count02) = stiffnessT_lead(cycle,count02) .*
rel_angle_lead(cycle,count02);

    Ftx_lead_DS(count02,:)= tForce_kq0_lead(cycle,count02)*
cos_lead_DS(cycle,count02);

    Fty_lead_DS(count02,:)= tForce_kq0_lead(cycle,count02)*
sin_lead_DS(cycle,count02);


GRF_DSx(count02,:) = Fnx_trail_DS(count02,:)+ Ftx_trail_DS(count02,:);%each
leg

GRF_DSx_1(count02,cycle) = Fnx_lead_DS(count02,:)+ Ftx_lead_DS(count02,:) ;


GRF_DSy(count02,:) = Fny_trail_DS(count02,:)+ Fty_trail_DS(count02,:) ;

GRF_DSy_1(count02,cycle) =  Fny_lead_DS(count02,:)+ Fty_lead_DS(count02,:);
```

```
check_length(cycle,count02) = lf - l_trail01_leave(cycle,count02) ;


     if (GRF_DSy(count02,:) <= 1 && (GRF_DSy(count02,:) >= -1))


     l_trail01_take_off(cycle) = l_trail01_leave(cycle,count02);

     take_off(cycle) = count02;

    end

end


%%

x_int_sing02(cycle) = xd(take_off(cycle),1);
vx_int_sing02(cycle) = xd(take_off(cycle),2);
y_int_sing02(cycle) = xd(take_off(cycle),3);
vy_int_sing02(cycle) =xd(take_off(cycle),4);
int_sing02(cycle,:) = [x_int_sing02(cycle) vx_int_sing02(cycle)
y_int_sing02(cycle) vy_int_sing02(cycle) ];

l_trail01_start_SS2 = sqrt((xd(take_off(cycle),1)-x_int_sing01(cycle))^2+
xd(take_off(cycle),3)^2);

step_sizeSS2 =  step_sizeDS;

res_SS2 = 2000 ;

end_spanSS2 = res_SS2 * step_sizeSS2 ;

time_spanSS02 = 0:step_sizeSS2:end_spanSS2;

[ts2,xs2] =
ode113(@nln_legFnfq_NTsingle02,time_spanSS02,int_sing02(cycle,:),[],cycle);
toggle_check = 0;

for count03 = 1:res_SS2

del_xs2(count03,:) = xs2(count03,1)-int_sing01(cycle,1);

l_lead02_SS2(cycle,count03) = sqrt((stepLength(cycle)-
del_xs2(count03,:))^2+ xs2(count03,3)^2) ;

lead_legAngle_SS2(cycle,count03) = atan(xs2(count03,3)/(stepLength(cycle)-
del_xs2(count03,:)));

angle_lead02_SS2(cycle,count03) = - atan((stepLength(cycle) -
del_xs2(count03,:))/xs2(count03,3));%wrt vertical

angle_lead02_SS2_deg(cycle,count03) = (- atan((stepLength(cycle) -
del_xs2(count03,:))/xs2(count03,3)))*180/pi;%wrt vertical

sin_lead_SS2(cycle,count03) = (stepLength(cycle) -
del_xs2(count03,:))/l_lead02_SS2(cycle,count03);
```

```
 cos_lead_SS2(cycle,count03) = xs2(count03,3)/l_lead02_SS2(cycle,count03);

posture_lead_SS2(cycle,count03) = (angle_lead02_SS2(cycle,count03) -
q0)/(qf-q0);


        l1_term_lead_SS2 = a1L *
(cos(2*pi*posture_lead_SS2(cycle,count03))-1)+ b1L *
sin(2*pi*posture_lead_SS2(cycle,count03));
        l2_term_lead_SS2 = a2L *
(cos(2*2*pi*posture_lead_SS2(cycle,count03))-1)+ b2L *
sin(2*2*pi*posture_lead_SS2(cycle,count03));
        l3_term_lead_SS2 = a3L *
(cos(2*3*pi*posture_lead_SS2(cycle,count03))-1)+ b3L *
sin(2*3*pi*posture_lead_SS2(cycle,count03));
        l4_term_lead_SS2 = a4L *
(cos(2*4*pi*posture_lead_SS2(cycle,count03))-1)+ b4L *
sin(2*4*pi*posture_lead_SS2(cycle,count03));
        l5_term_lead_SS2 = a5L *
(cos(2*5*pi*posture_lead_SS2(cycle,count03))-1)+ b5L *
sin(2*5*pi*posture_lead_SS2(cycle,count03));

        nln_term_lead_SS2 = l1_term_lead_SS2 + l2_term_lead_SS2 +
l3_term_lead_SS2 + l4_term_lead_SS2 + l5_term_lead_SS2 ;

        fl0_lead_SS2(cycle,count03) =  l0 +
fl0_rate*(posture_lead_SS2(cycle,count03) + nln_term_lead_SS2);

        excursion02_l0_lead_SS2(cycle,count03) =
fl0_lead_SS2(cycle,count03) - 1000*l_lead02_SS2(cycle,count03);

        nForce_angSS2(cycle,count03) = stiffness *0.001*
excursion02_l0_lead_SS2(cycle,count03);

        Fnx_lead_SS2(count03,:) = -nForce_angSS2(cycle,count03)*
sin_lead_SS2(cycle,count03);

        Fny_lead_SS2(count03,:) = nForce_angSS2(cycle,count03)*
cos_lead_SS2(cycle,count03);



        q1_term_lead_SS2 = a1Q *
(cos(2*pi*posture_lead_SS2(cycle,count03))-1)+ b1Q *
sin(2*pi*posture_lead_SS2(cycle,count03));
        q2_term_lead_SS2 = a2Q *
(cos(2*2*pi*posture_lead_SS2(cycle,count03))-1)+ b2Q *
sin(2*2*pi*posture_lead_SS2(cycle,count03));
        q3_term_lead_SS2 = a3Q *
(cos(2*3*pi*posture_lead_SS2(cycle,count03))-1)+ b3Q *
sin(2*3*pi*posture_lead_SS2(cycle,count03));
        q4_term_lead_SS2 = a4Q *
(cos(2*4*pi*posture_lead_SS2(cycle,count03))-1)+ b4Q *
sin(2*4*pi*posture_lead_SS2(cycle,count03));
        q5_term_lead_SS2 = a5Q *
(cos(2*5*pi*posture_lead_SS2(cycle,count03))-1)+ b5Q *
sin(2*5*pi*posture_lead_SS2(cycle,count03));
```

```
        stiffnessT_leadSS2(cycle,count03) = q1_term_lead_SS2 +
q2_term_lead_SS2 + q3_term_lead_SS2 + q4_term_lead_SS2 + q5_term_lead_SS2 ;

        rel_angle_leadSS2(cycle,count03) = fq0 -
angle_lead02_SS2(cycle,count03);

        tForce_kq0_leadSS2(cycle,count03) =
stiffnessT_leadSS2(cycle,count03) .* rel_angle_leadSS2(cycle,count03);

        Ftx_lead_SS2(count03,:)= tForce_kq0_leadSS2(cycle,count03)*
cos_lead_SS2(cycle,count03);

        Fty_lead_SS2(count03,:)= tForce_kq0_leadSS2(cycle,count03)*
sin_lead_SS2(cycle,count03);



GRF_SS2x(count03,cycle)  = Fnx_lead_SS2(count03,:)+
Ftx_lead_SS2(count03,:);

GRF_SS2y(count03,cycle) = Fny_lead_SS2(count03,:)+ Fty_lead_SS2(count03,:);

lead_forceAngle_SS2(count03,:) =
atan(GRF_SS2y(count03,:)/GRF_SS2x(count03,:));


check_hight02(cycle,count03) = int_sing01(cycle,3)- xs2(count03,3);

check_state(cycle,count03) = norm(int_sing01(cycle,2:4)- xs2(count03,2:4));


check_angle(cycle,count03) = angle_lead02_SS2(cycle,count03);

       if ((check_angle(cycle,count03) <= 0.005) &&
(check_angle(cycle,count03) >= -0.005))

           if toggle_check == 0

           upright_state(cycle) = check_state(cycle,count03);

           upright_height(cycle) = xs2(count03,3);

           toggle_check = 1;


          endSS02(cycle) = count03 ;

          end_check_state(cycle) = check_state(cycle,count03);

          disp(['achieved cycle',num2str(cycle)])

          end

       end
end
```

```
x_cycle{cycle} =
{xs(1:touch_down_timeSS(cycle),:);xd(1:take_off(cycle),:);xs2(1:endSS02(cyc
le),:)};

delxHx_cycle{cycle} =
{del_xs(1:touch_down_timeSS(cycle),:);del_xd(1:take_off(cycle),:);del_xs2(1
:endSS02(cycle),:)};

x_new_cycle =  [x_new_cycle;x_cycle{cycle}];

delxHx_new_cycle = [delxHx_new_cycle;delxHx_cycle{cycle}];

int_sing01(cycle+1,:) = xs2(endSS02(cycle),:);

int_sing01_abs(cycle+1,:) = [ xs2(endSS02(cycle),1)-
int_sing01(cycle+1,1),int_sing01(cycle+1,2:4)];

x_int_sing01(cycle+1) = int_sing01(cycle+1,1);

init_del_xs = [init_del_xs;del_xs2(endSS02(cycle),:)];

y_int_sing01(cycle+1) = int_sing01(cycle+1,3);


            D_int_sing01(cycle,:) = int_sing01_abs(cycle+1,:)-
int_sing01_abs(cycle,:) ;
            norm_D_Ic = [norm_D_Ic; norm(D_int_sing01(cycle,:))];
            [val_min_norm Id_lim_cycle]= min(norm_D_Ic);


end

legLength = [l_lead02_DS(cycle-1,1:take_off(cycle-1))';l_lead02_SS2(cycle-
1,1:endSS02(cycle-
1))';l_trail01_SS(cycle,1:touch_down_timeSS(cycle))';l_trail01_leave(cycle,
1:take_off(cycle))'];

legAngle = [angle_lead02_DS(cycle-1,1:take_off(cycle-
1))';angle_lead02_SS2(cycle-1,1:endSS02(cycle-
1))';angle_trail01_SS(cycle,1:touch_down_timeSS(cycle))';angle_trail01_leav
e(cycle,1:take_off(cycle))'];


fl0_cycle = 0.001*[fl0_lead(cycle-1,1:take_off(cycle-1))';
fl0_lead_SS2(cycle-1,1:endSS02(cycle-1))';
fl0(cycle,1:touch_down_timeSS(cycle))';
fl0_trail(cycle,1:take_off(cycle))'];

nForce = [nForce_ang_lead(cycle-1,1:take_off(cycle-
1))';nForce_angSS2(cycle-1,1:endSS02(cycle-
1))';nForce_angSS(1:touch_down_timeSS(cycle),:);nForce_ang_trail(1:take_off
(cycle),:)];

tForce = [tForce_kq0_lead(cycle-1,1:take_off(cycle-
1))';tForce_kq0_leadSS2(cycle-1,1:endSS02(cycle-
```

```
1))';tForce_kq0SS(cycle,1:touch_down_timeSS(cycle))';tForce_kq0_trail(cycle
,1:take_off(cycle))'];

netForce_test = sqrt(nForce.^2 + tForce.^2);

GRF_x = [GRF_DSx_1(1:take_off(cycle-1),cycle-1);GRF_SS2x(1:endSS02(cycle-
1),cycle-
1);GRF_SSx(1:touch_down_timeSS(cycle),:);GRF_DSx(1:take_off(cycle),:)];

GRF_y = [GRF_DSy_1(1:take_off(cycle-1),cycle-1);GRF_SS2y(1:endSS02(cycle-
1),cycle-
1);GRF_SSy(1:touch_down_timeSS(cycle),:);GRF_DSy(1:take_off(cycle),:)];

GRF_net = sqrt(GRF_x.^2+ GRF_y.^2);


sumGRF_DSx = GRF_DSx_1(:,cycle) + GRF_DSx ;

sumGRF_DSx_step = GRF_DSx_1(1:take_off(cycle),cycle) +
GRF_DSx(1:take_off(cycle),:) ;


sumGRF_DSy = GRF_DSy_1(:,cycle) + GRF_DSy ;

sumGRF_DSy_step = GRF_DSy_1(1:take_off(cycle),cycle) +
GRF_DSy(1:take_off(cycle),:) ;


netGRF_SS = sqrt(GRF_SSx.^2 + GRF_SSy.^2);

netGRF_SS_step = sqrt(GRF_SSx(1:touch_down_timeSS(cycle),:).^2 +
GRF_SSy(1:touch_down_timeSS(cycle),:).^2);

netGRF_DS = sqrt(sumGRF_DSx.^2 + sumGRF_DSy.^2);

netGRF_DS_step = sqrt(sumGRF_DSx(1:take_off(cycle),:).^2 +
sumGRF_DSy(1:take_off(cycle),:).^2);

netGRF_SS02 = sqrt(GRF_SS2x(:,cycle).^2 + GRF_SS2y(:,cycle).^2);

netGRF_SS02_step = sqrt(GRF_SS2x(1:endSS02(cycle-1),cycle-1).^2 +
GRF_SS2y(1:endSS02(cycle-1),cycle-1).^2);


netGRF_step = [netGRF_SS_step;netGRF_DS_step;netGRF_SS02_step];
DnetGRF_step = diff(netGRF_step);
sumDnetGRF_step = sum(DnetGRF_step);


phase = length(x_new_cycle);

for count_phase = 1:phase

   length_x_new_cycle(count_phase) = length(x_new_cycle{count_phase});

end
```

```
 sum_length = sum(length_x_new_cycle) ;

renew_x_new_cycle = zeros(sum_length,4);

renew_delxHx_new_cycle = zeros(sum_length,1);

leg_length_cycle = zeros(sum_length,1);

count_x_new_cycle = 1;

%obtain CoM motion from cell array to matrix

for count_phase = 1:phase


        for count_x_inphase = 1:length(x_new_cycle{count_phase})

            renew_x_new_cycle(count_x_new_cycle,:) =
x_new_cycle{count_phase}(count_x_inphase,:);

            renew_delxHx_new_cycle(count_x_new_cycle,:) =
delxHx_new_cycle{count_phase}(count_x_inphase,:);

            leg_length_cycle(count_x_new_cycle,:) =
sqrt(renew_delxHx_new_cycle(count_x_new_cycle,:).^2+
renew_x_new_cycle(count_x_new_cycle,3).^2);

            count_x_new_cycle = count_x_new_cycle + 1 ;

        end

end

diff_leg_length_cycle =
(1/step_sizeSS)*[diff(leg_length_cycle(1:2,:));diff(leg_length_cycle)];

%%
%Distance btw apex point and 45 degree line

fixed_point = int_sing01_abs(Id_lim_cycle,:);

fit_first = [];
fit_next = [];

[row_IC col_IC]= size(int_sing01_abs);

for count04 = 1:col_IC

fit_first = [fit_first; int_sing01_abs(1:end-1,count04)' -
fixed_point(count04)' ];

fit_next = [fit_next; int_sing01_abs(2:end,count04)' -
fixed_point(count04)' ];

end
```

```
sqr_fit_first = fit_first*fit_first';

dfit_first = det(fit_first*fit_first');

Jmatrix = (fit_next * fit_first')*pinv(fit_first*fit_first');


FQmult = abs(eig(Jmatrix));
max_FQmult = max(FQmult);

disp(['kn(N/m)                    |   ',num2str(stiffnessN)])
disp(['angle(deg)                 |   ',num2str(q0*180/pi)])
disp(['cycle                      |   ',num2str(cycle)])
disp(['l0 rate(m/cycle)           |   ',num2str(0.001*fl0_rate)])
disp(['y0(m)                      |   ',num2str(y_int_sing01(1))])
disp(['y transition(m)            |   ',num2str(y_touch)])
```

References

Alexander, M. R. (1988). Elastic mechanisms in animal movement. Cambridge: Cambridge University Press.

Alexander, R. (1988b). The spring in your step: the role of elastic mechanisms in human running. de Groot, G. Hollander, A. Huijing, P. van Ingen Schenau, G. Biomechanics XI-A. International Series on Biomechnaics. Amsterdam: Free University Press.

Alexander, R. M. (1980). Optimum walking techniques for quadrapeds and bipeds. Journal of Zoology, 192, 97-117.

Alghesheyan, F. (2012). Comparison of ground reaction force in treadmill walking and in overground walking. Master of Science, University of Miami.

Anderson, F. C. & Pandy, M. G. (2001). Dynamic optimization of human walking. Journal of Biomechanical Engineering-Transactions of the Asme, 123.

Bartle, R. (1976). The elements of real analysis, New York, John Wiley & Sons.

Bauby, C. E. & Kuo, A. D. (2000). Active control of lateral balance in human walking. Journal of Biomechanics, 33, 1433-1440.

Bedford, M. & Fowler, W. 1996. Engineering Mechanics: Dynamics, England, Addison Wesley Longman.

Blickhan, R. (1989). The spring mass model for running and hopping. Journal of Biomechanics, 22, 1217-1227.

Blickhan, R., Seyfarth, A., Geyer, H., Grimmer, S., Wagner, H. & Guenther, M. (2007). Intelligence by mechanics. Philosophical Transactions of the Royal Society a-Mathematical Physical and Engineering Sciences, 365.

Blum, Y. Lipfert , S. W. & Seyfarth, A. (2009). Effective leg stiffness in running. Journal of Biomechanics, 42, 2400-2405.

Boonpratatong, A. & Ren, L. (2010). The human ankle-foot complex as a multi-configurable mechanism during the stance phase of walking. Journal of Bionic Engineering, 7, 211-218.

Boonpratatong, A. & Ren, L. (2011a). The Non-Linear Nature of Virtual Human Leg Property during Level Walking. XXIIrd Congress of International Society of Biomechanics, Belgium.

Boonpratatong, A. & Ren, L. (2011b). The non-linear mechanical property of human leg during level walking. 6th North West Biomechanics Research Day. Manchester, UK: Institute for Biomedical Research into Human Movement & Health.

Bovier, A., Eckhoff, M., Gayrard, V. & Klein, M. 2000. Metastability and small eigenvalues in Markov chains. Journal of Physics A: Mathematical and General, **33,** 4.

Brach, J. S., Berlin, J. E., Vanswearingen, J. M., Newman, A. B. & Studenski, S. A. (2005). Too much or too little step width variability is associated with a fall history in older persons who walk at or near normal gait speed. Journal of neuroengineering and rehabilitation, 2, 21-21.

Brach, J. S., Studenski, S. A., Perera, S., Vanswearingen, J. A. & Newman, A. B. (2007). Gait variability and the risk of incident mobility disability in community-dwelling older adults. Journals of Gerontology Series a-Biological Sciences and Medical Sciences, 62, 983-988.

Bruijn, S. (2010). Is stability an unstable concept?: Quantifying dynamic stability of human locomotion. Doctoral, Vrije Universiteit Amsterdam.

Bruijn, S. M., Bregman, D. J. J., Meijer, O. G., Beek, P. J. & Van Dieen, J. H. (2011). The validity of stability measures: A modelling approach. Journal of Biomechanics, 44, 2401-2408.

Bruijn, S. M., Bregman, D. J. J., Meijer, O. G., Beek, P. J. & Van Dieen, J. H. (2012). Maximum Lyapunov exponents as predictors of global gait stability: A modelling approach. Medical Engineering & Physics, 34, 428-436.

Bruijn, S. M., Van Dieen, J. H., Meijer, O. G. & Beek, P. J. (2009). Statistical precision and sensitivity of measures of dynamic gait stability. Journal of Neuroscience Methods, 178, 327-333.

Buchanan, T. S. & Shreeve, D. A. (1996). An evaluation of optimization techniques for the prediction of muscle activation patterns during isometric tasks. Journal of Biomechanical Engineering-Transactions of the Asme, 118, 565-574.

Buchanan, T. S., Lloyd, D. G., Manal, K. & Besier, T. F. (2004). Neuromusculoskeletal modeling: Estimation of muscle forces and joint moments and movements from measurements of neural command. Journal of Applied Biomechanics, 20, 367-395.

Bullimore, S. R. & Burn, J. F. (2006). Consequences of forward translation of the point of force application for the mechanics of running. Journal of Theoretical Biology, 238, 211-219.

Byl, K., and Tedrake, R. 2008. Approximate optimal control of the compass gait on rough terrain. ICRA 2008, IEEE International Conference on Robotics and Automation.

Byl, K. & Tedrake, R. 2009. Metastable Walking Machines. International Journal of Robotics Research, 28, 1040-1064.

Cappozzo, A. (1984). Gait analysis methodology. Human Movement Science, 3, 27-50.

Cappozzo, A., Catani, F., Della Croce, U. & Leardini, A. (1995). Position and orientation in-space of bones during movement - anatomical frame definition and determination. Clinical Biomechanics, 10, 171-178.

Carver, S. G., N. J. Cowan & J. M. Guckenheimer. (2009). Lateral stability of the spring-mass hopper suggests a two-step control strategy for running. Chaos, 19.

Cavagna, G. A. (1975). Force platforms as ergometers. Journal of Applied Physiology, 39, 174-179.

Cavagna, G. A., N. C. Heglund & C. R. Taylor. (1977). Mechanical work in terrestrial locomotion - 2 basic mechanisms for minimizing energy-expenditure. American Journal of Physiology, 233, R243-R261.

Cavagna, G. A., Saibene, F. P. & Margaria, R. (1963). External work in walking. Journal of applied physiology, 18, 1-9.

Cavagna, G. A., Tesio, L., Fuchimoto, T. & Heglund, N. C. (1983). Ergometric evaluation of pathological gait. Journal of Applied Physiology, 55, 607-613.

Cavagna, G. A., Thys, H. & Zamboni, A. (1976). Sources of external work in level walking and running. Journal of Physiology-London, 262, 639-657.

Chevallereau, C., A. Formalsky, B. Perrin & Ieee. (1997). Control of a walking robot with feet following a reference trajectory derived from ballistic motion. In 1997 IEEE International Conference on Robotics and Automation (ICRA97) - Teaming to Make an Impact, 1094-1099. Albuquerque, Nm.

Chevallereau, C., A. Formal'sky, B. Perrin & Ieee. (1998). Low energy cost reference trajectories for a biped robot. In IEEE International Conference on Robotics and Automation, 1398-1404. Katholieke Univ Leuven, Leuven, Belgium.

Coleman, D. R., Cannavan, D., Horne, S. & Blazevich, A. J. (2012). Leg stiffness in human running: Comparison of estimates derived from previously published models to direct kinematic-kinetic measures. Journal of Biomechanics, 45.

Collins, S. H., M. Wisse & A. Ruina. (2001). A three-dimensional passive-dynamic walking robot with two legs and knees. International Journal of Robotics Research, 20, 607-615.

Crowninshield, R. D. & R. A. Brand. (1981). A physiologically based criterion of muscle force prediction in locomotion. Journal of Biomechanics, 14.

Daley, M. A. & A. A. Biewener. (2006). Running over rough terrain reveals limb control for intrinsic stability. Proceedings of the National Academy of Sciences of the United States of America, 103, 15681-15686.

Daley, M. A., Felix, G. & Biewener, A. A. (2007). Running stability is enhanced by a proximo-distal gradient in joint neuromechanical control. Journal of Experimental Biology, 210, 383-394.

De Leva, P. (1996). Adjustments to Zatsiorsky-Seluyanov's segment inertia parameters. Journal of Biomechanics, 29, 1223-1230.

Dierick, F., Penta, M., Renaut, D. & Detrembleur, C. (2004). A force measuring treadmill in clinical gait analysis. Gait & Posture, 20, 299-303.

Dingwell, J. B. & Cusumano, J. P. (2000). Nonlinear time series analysis of normal and pathological human walking. Chaos, 10, 848-863.

Dingwell, J. B. & H. G. Kang. (2007). Difference between local and orbital dynamic stability during human walking. Journal of Biomechanical Engineering-Transactions of the Asme, 129, 586-593.

Dingwell, J. B. & Marin, L. C. (2006). Kinematic variability and local dynamic stability of upper body motions when walking at different speeds. Journal of Biomechanics, 39, 444-452.

Dingwell, J. B., Cusumano, J. P., Cavanagh, P. R. & Sternad, D. (2001). Local dynamic stability versus kinematic variability of continuous overground and treadmill walking. Journal of Biomechanical Engineering-Transactions of the Asme, 123, 27-32.

Dingwell, J. B., Cusumano, J. P., Sternad, D. & Cavanagh, P. R. (2000). Slower speeds in patients with diabetic neuropathy lead to improved local dynamic stability of continuous overground walking. Journal of Biomechanics, 33, 1269-1277.

Dingwell, J. B., Kang Hyun, G. & Marin, L. C. (2007). The effects of sensory loss and walking speed on the orbital dynamic stability of human walking. Journal of Biomechanics, 40, 1723-1730.

Dudek, D. M. & R. J. Full. (2006). Passive mechanical properties of legs from running insects. Journal of Experimental Biology, 209, 1502-1515.

Eyler, A. A., Browson, R. C., Bacak, S. J. & Housemann, R. A. (2003). The epidemiology of walking for physical activity in the United States. Medicine and Science in Sports and Exercise, 35, 1529-1536.

Farley, C. T. & O. Gonzalez. (1996). Leg stiffness and stride frequency in human running. Journal of Biomechanics, 29, 181-186.

Farley, C. T., J. Glasheen & T. A. McMahon. (1993). Running springs - speed and animal size. Journal of Experimental Biology, 185, 71-86.

Frank, A. A. (1970). Approach to dynamic analysis and synthesis of biped locomotion machines. Medical & Biological Engineering, 8, 465-&.

Full, R. J. & D. E. Koditschek. (1999). Templates and anchors: Neuromechanical hypotheses of legged locomotion on land. Journal of Experimental Biology, 202.

Fung, Y. C. (1993). Biomechanics: Mechanical properties of living tissues, New York, Springer-Verlag.

Gamage, S. & Lasenby, J. (2002). New least squares solutions for estimating the average centre of rotation and the axis of rotation. Journal of Biomechanics, 35, 87-93.

Garcia, M., A. Chatterjee, A. Ruina & M. Coleman. (1998). The simplest walking model: Stability, complexity, and scaling. Journal of Biomechanical Engineering-Transactions of the Asme, 120, 281-288.

Geyer, H. (2005). Simple Models of Legged Locomotion based on Compliant Limb Behavior. Dr. phil., Friedrich-Schiller-University Jena.

Geyer, H., A. Seyfarth & R. Blickhan. (2005). Spring-mass running: simple approximate solution and application to gait stability. Journal of Theoretical Biology, 232, 315-328.

Geyer, H., Seyfarth, A. & Blickhan, R. (2006). Compliant leg behaviour explains basic dynamics of walking and running. Proceedings of the Royal Society B-Biological Sciences, 273, 2861-2867.

Glitsch, U. & W. Baumann. (1997). The three-dimensional determination of internal loads in the lower extremity. Journal of Biomechanics, 30.

Goldman, D. I., T. S. Chen, D. M. Dudek & R. J. Full. (2006). Dynamics of rapid vertical climbing in cockroaches reveals a template. Journal of Experimental Biology, 209, 2990-3000.

Goswami, A., B. Espiau & A. Keramane. (1997). Limit cycles in a passive compass gait biped and passivity-mimicking control laws. Autonomous Robots, 4, 273-286.

Goswami, A., B. Espiau, A. Keramane, R. Ieee & S. O. C. Automat. (1996). Limit cycles and their stability in a passive bipedal gait. In 1996 IEEE International Conference on Robotics and Automation, 246-251. Minneapolis, Mn.

Goswami, A., B. Thuilot & B. Espiau. (1998). A study of the passive gait of a compass-like biped robot: Symmetry and chaos. International Journal of Robotics Research, 17, 1282-1301.

Granata, K. P. & Lockhart, T. E. (2008). Dynamic stability differences in fall-prone and healthy adults. Journal of Electromyography and Kinesiology, 18, 172-178.

Guckenheimer, J. & Holmes, P. (1983). Nonlinear oscillations, dynamical systems, and bifurcations of vector fields, ser. Applied mathematical science, New York, Springer.

Gunther, M. & R. Blickhan. (2002). Joint stiffness of the ankle and the knee in running. Journal of Biomechanics, 35, 1459-1474.

Gunther, M., V. Keppler, A. Seyfarth & R. Blickhan. (2004). Human leg design: optimal axial alignment under constraints. Journal of Mathematical Biology, 48, 623-646.

Haken, H., Kelso, J. A. S. & Bunz, H. (1985). A theoretical-model of phase-transitions in human hand movements. Biological Cybernetics, 51, 347-356.

Hartmut, G. (2005). Simple models of legged locomotion based on compliant limb behavior. Dr. phil., Friedrich-Schiller-University Jena.

Hasan, N. A. (1995). Applied nonlinear dynamics : analytical computational and experimental methods, New York NY, Wiley.

Hase, K. & N. Yamazaki. (1998). Computer simulation of the ontogeny of bipedal walking. Anthropological Science, 106, 327-347.

Health and Safety Executive. (2012). Slips, trips and fall from height [Online]. http://www.hse.gov.uk/statistics/causinj/slips-trips-and-falls.pdf: Health and Safety

Heglund, N. C. & G. A. Cavagna. (1985). Efficiency of vertebrate locomotory muscles. Journal of Experimental Biology, 115, 283-292.

Herzog, W. & T. R. Leonard. (1991). Validation of optimization models that estimate the forces exerted by synergistic muscles. Journal of Biomechanics, 24, 31-39.

Hill, A. V. (1938). The heat of shortening and the dynamic constants of muscle. Proceedings of the Royal Society B-Biological Sciences, 126.

Hibbeler, R. (1997). Engineering Mechanics: Dynamics, Singapore, Prentice Hall.

Hobbelen, D. G. E. & M. Wisse. (2007). A disturbance rejection measure for limit cycle walkers: The Gait Sensitivity Norm. Ieee Transactions on Robotics, 23, 1213-1224.

Hof, A. (1990). Effects of muscle elasticity in walking and running. Winter, J. Woo,S. Multiple Muscle Systems. New York: Springer.

Hof, A. L., Gazendam, M. G. J. & Sinke, W. E. (2005). The condition for dynamic stability. Journal of Biomechanics, 38, 1-8.

Hof, A. L., Van Bockel, R. M., Schoppen, T. & Postema, K. (2007). Control of lateral balance in walking - Experimental findings in normal subjects and above-knee amputees. Gait & Posture, 25, 250-258.

Hsu, C. S. (1987). Cell-to-cell mapping; a method of global analysis for nonlinear systems. Applied mathematical sciences. New York: Springer.

Hurmuzlu, Y. & Basdogan, C. (1994). On the measurement of dynamic stability of human locomotion. Journal of Biomechanical Engineering-Transactions of the Asme, 116, 30-36.

Hurmuzlu, Y. & Moskowitz, G. D. (1986). The role of impact in the stability of bipedal locomotion. Dynamics and Stability of Systems: An International Journal, 1, 17.

Hurst, J. W. & A. A. Rizzi. (2008). Series compliance for an efficient running gait - Lessons learned from the electric cable differential leg. Ieee Robotics & Automation Magazine, 15, 42-51.

Hutter, M., C. D. Remy, M. A. Hopflinger, R. Siegwart & Ieee. (2010). SLIP running with an articulated robotic leg. In IEEE/RSJ International Conference on Intelligent Robots and Systems, 4934-4939. Taipei, TAIWAN.

Huxley, A. F. & R. M. Simmons. (1971). Proposed mechanism of force generation in striated muscle. Nature, 233, 533-&.

Huxley, A. F. (1957). Muscle structure and theories of contraction. Progress in Biophysics & Molecular Biology, 7.

Iida, F., J. Rummel & A. Seyfarth. (2007). Bipedal walking and running with compliant legs. Proc. IEEE Int. Conf. on Robotics and Automation, 10, 6.

Inman, V. T. (1966). Human locomotion. Canadian Medical Association Journal, 94, 1047-&.

Inman, V. T., H. J. Ralston & F. Todd. (1994). Human locomotion. In Human Walking, 2-22. Baltimore, MD: Williams & Wilkins.

Kajita, S., F. Kanehiro, K. Kaneko, K. Fujiwara, K. Yokoi, H. Hirukawa, Ieee & I. Ieee. (2002). A realtime pattern generator for biped walking. 2002 Ieee International Conference on Robotics and Automation, Vols I-Iv, Proceedings, 31-37.

Kajita, S., O. Matsumoto, M. Saigo. (2001). Real-time 3D walking pattern generation for a biped robot with telescopic legs. In IEEE International Conference on Robotics and Automation, 2299-2306. Seoul, South Korea.

Kallin, K., Jensen, J., Olsson, L. L., Nyberg, L. & Gustafson, Y. (2004). Why the elderly fall in residential care facilities, and suggested remedies. Journal of Family Practice, 53, 41-52.

Kang, H. G. & Dingwell, J. B. (2008). Effects of walking speed, strength and range of motion on gait stability in healthy older adults. Journal of Biomechanics, 41, 2899-2905.

Kang, H. G. & Dingwell, J. B. (2009). Dynamic stability of superior vs. inferior segments during walking in young and older adults. Gait & Posture, 30, 260-263.

Kantz, H. (2004). Nonlinear time series analysis, Cambridge UK, Cambridge University Press.

Karssen, J. G. D. & M. Wisse. (2011). Running with improved disturbance rejection by using non-linear leg springs. International Journal of Robotics Research, 30, 1585-1595.

Kim, S. & S. Park. (2011). Leg stiffness increases with speed to modulate gait frequency and propulsion energy. Journal of Biomechanics, 44, 1253-1258.

Kivell, T. L. & D. Schmitt. (2009). Independent evolution of knuckle-walking in African apes shows that humans did not evolve from a knuckle-walking ancestor. Proceedings of the National Academy of Sciences of the United States of America, 106, 14241-14246.

Kooij, v. d. 2001. Human balance control in standing and walking. Enschede, The Netherlands.: University of Twente.

Kubow, T. M. & R. J. Full. (1999). The role of the mechanical system in control: a hypothesis of self-stabilization in hexapedal runners. Philosophical Transactions of the Royal Society of London Series B-Biological Sciences, 354, 849-861.

Kukillaya, R. P. & P. J. Holmes. (2007). A hexapedal jointed-leg model for insect locomotion in the horizontal plane. Biological Cybernetics, 97, 379-395.

Kuo, A. D. (1999). Stabilization of lateral motion in passive dynamic walking. International Journal of Robotics Research, 18, 917-930.

Kurz, M. J., Markopoulou, K. & Stergiou, N. (2010). Attractor divergence as a metric for assessing walking balance. Nonlinear Dynamics Psychology and Life Sciences, 14, 151-164.

Leardini, A., Cappozzo, A., Catani, F., Toksvig-Larsen, S., Petitto, A., Sforza, V., Cassanelli, G. & Giannini, S. (1999). Validation of a functional method for the estimation of hip joint centre location. Journal of Biomechanics, 32, 99-103.

Lee, C. R. & Farley, C. T. (1998). Determinants of the center of mass trajectory in human walking and running. Journal of Experimental Biology, 201, 2935-2944.

Lindstedt, S. L., Reich, T. E., Keim, P. & Lastayo, P. C. (2002). Do muscles function as adaptable locomotor springs? Journal of Experimental Biology, 205, 2211-2216.

Lipfert, S. W., Gunther, M., Renjewski, D., Grimmer, S. & Seyfarth, A. (2012). A model-experiment comparison of system dynamics for human walking and running. Journal of Theoretical Biology, 292, 11-17.

Lloyd, D. G. & Buchanan, T. S. (1996). A model of load sharing between muscles and soft tissues at the human knee during static tasks. Journal of Biomechanical Engineering-Transactions of the Asme, 118, 367-376.

Lloyd, D. G. & T. F. Besier. (2003). An EMG-driven musculoskeletal model to estimate muscle forces and knee joint moments in vivo. Journal of Biomechanics, 36.

Lockhart, T. E. & Liu, J. (2008). Differentiating fall-prone and healthy adults using local dynamic stability. Ergonomics, 51, 1860-1872.

Lockhart, T. E., Woldstad, J. C. & Smith, J. L. (2003). Effects of age-related gait changes on the biomechanics of slips and falls. Ergonomics, 46, 1136-1160.

Lovejoy, C. O., G. Suwa, L. Spurlock, B. Asfaw & T. D. White. (2009). The pelvis and femur of ardipithecus ramidus: the emergence of upright walking. Science, 326.

Ludwig, C., S. Grimmer, A. Seyfarth & H. M. Maus. (2012). Multiple-step model-experiment matching allows precise definition of dynamical leg parameters in human running. Journal of Biomechanics, 45.

Maclellan, M. J. & Patla, A. E. (2006). Adaptations of walking pattern on a compliant surface to regulate dynamic stability. Experimental Brain Research, 173, 521-530.

Maki, B. E. (1997). Gait changes in older adults: Predictors of falls or indicators of fear? Journal of the American Geriatrics Society, 45, 313-320.

Maas, A., Martinez, S. & Martin, J. S. 2004. Dynamics and Randomness II, Dodrecht, Kluwer.

Maus, H. M., Lipfert, S. W., Gross, M., Rummel, J. & Seyfarth, A. (2010). Upright human gait did not provide a major mechanical challenge for our ancestors. Nature Communications, 1.

Maus, H.-M., A. Seyfarth & S. Grimmer. (2011). Combining forces and kinematics for calculating consistent centre of mass trajectories. Journal of Experimental Biology, 214.

Mcgeer, T. (1990). Passive dynamic walking. International Journal of Robotics Research, 9, 62-82.

McGhee, R. & M. Kuhner. (1969). On the dynamic stability of legged locomotion systems. in Proc. 3rd Int. Symp. on External Control of Human Extremities. Dubrovnik, Yugoslavia., 13.

McGill, S. M. & R. W. Norman. (1986). Partitioning of the l4-l5 dynamic moment into disk, ligamentous, and muscular components during lifting. Spine, 11, 666-678.

McMahon, T. (1984). Muscles, reflexes and locomotion. Princeton, N.J, USA.

McMahon, T. A. & Cheng, G. C. (1990). The mechanics of running - how does stiffness couple with speed. Journal of Biomechanics, 23, 65-78.

Millard, M., McPhee, J. & Kubica, E. (2012). Foot placement and balance in 3d. Journal of Computational and Nonlinear Dynamics, 7.

Millard, M., Wight, D., McPhee, J., Kubica, E. & Wang, D. (2009). Human foot placement and balance in the sagittal plane. Journal of Biomechanical Engineering-Transactions of the Asme, 131.

Minetti, A. E. & Alexander, R. M. (1997). A theory of metabolic costs for bipedal gaits. Journal of Theoretical Biology, 186, 467-476.

Morasso, P. G. & Schieppati, M. (1999). Can muscle stiffness alone stabilize upright standing? Journal of Neurophysiology, 82.

Moreland, J. D., Richardson, J. A., Goldsmith, C. H. & Clase, C. M. (2004). Muscle weakness and falls in older adults: A systematic review and meta-analysis. Journal of the American Geriatrics Society, 52, 1121-1129.

Morin, J. B., G. Dalleau, H. Kyrolainen, T. Jeannin & A. Belli. (2005). A simple method for measuring stiffness during running. Journal of Applied Biomechanics, 21, 167-180.

Morin, J.-B., P. Samozino & G. Y. Millet. (2011). Changes in running kinematics, kinetics, and spring-mass behavior over a 24-h run. Medicine and Science in Sports and Exercise, 43, 829-836.

Moritz, C. T. & Farley, C. T. (2003). Human hopping on damped surfaces: strategies for adjusting leg mechanics. Proceedings of the Royal Society B-Biological Sciences, 270, 1741-1746.

Nanayakkara, T., Byl, K., Liu, H., Song, X., Villabona,T. 2012. Dominant sources of variability in passive walking. IEEE International Conference on Robotics and Automation (ICRA), 2012.

Nashif, A. D., D. I. G. Jones & J. P. Henderson. (1985). Vibration Damping. New York, Chichester: Wiley.

National Accident Helpline Limited. (2013). Slip and trip claims [Online]. http://www.national-accident-helpline.co.uk/accident-claims/slips-and-trips.html: National Accident Helpline Limited. [Accessed 16 May 2013.

Owaki, D., A. Ishiguro & Ieee. (2006). Enhancing self-stability of a passive dynamic runner by exploiting nonlinearity in the leg elasticity. 2006 SICE-ICASE International Joint Conference, Vols 1-13.

Pandy, M. G. & Anderson, F. C. (2000). Dynamic simulation of human movement using large-scale models of the body. Phonetica, 57, 219-228.

Pandy, M. G. & Berme, N. (1988b). Synthesis of human walking - a planar model for single support. Journal of Biomechanics, 21, 1053-1060.

Pandy, M. G. & N. Berme. (1988a). A numerical-method for simulating the dynamics of human walking. Journal of Biomechanics, 21, 1043-1051.

Pandy, M. G. & T. P. Andriacchi. (2010). Muscle and joint function in human locomotion. In Annual Review of Biomedical Engineering, Vol 12, eds. M. L. Yarmush, J. S. Duncan & M. L. Gray, 401-433.

Pandy, M. G. (2001). Computer modeling and simulation of human movement. Annual Review of Biomedical Engineering, 3, 245-273.

Pandy, M. G., F. C. Anderson & D. G. Hull. (1992). A parameter optimization approach for the optimal-control of large-scale musculoskeletal systems. Journal of Biomechanical Engineering-Transactions of the Asme, 114.

Parker, T. S. & Chua, L. O. (1989). Practical numerical algorithms for chaotic system, New York, Springer.

Pavol, M. J., Owings, T. M., Foley, K. T. & Grabiner, M. D. (2002). Influence of lower extremity strength of healthy older adults on the outcome of an induced trip. Journal of the American Geriatrics Society, 50, 256-262.

Pijnappels, M., Van Der Burg, J. C. E., Reeves, N. D. & Van Dieen, J. H. (2008). Identification of elderly fallers by muscle strength measures. European Journal of Applied Physiology, 102, 585-592.

Pollock, C. M. & Shadwick, R. E. (1994). Allometry of muscle, tendon, and elastic energy-storage capacity in mammals. American Journal of Physiology, 266, R1022-R1031.

Popovic, M. B., Goswami, A. & Herr, H. (2005). Ground reference points in legged locomotion: Definitions, biological trajectories and control implications. International Journal of Robotics Research, 24, 1013-1032.

Pratt, J., Carff, J., Drakunov, S., Goswami, A. & Ieee. (2006). Capture point: A step toward humanoid push recovery. 6th IEEE/RAS International Conference on Humanoid Robots, 2006 Dec 04-06 2006 Genoa, ITALY. 200-207.

Pratt, J., Chew, C. M., Torres, A., Dilworth, P. & Pratt, G. (2001). Virtual model control: An intuitive approach for bipedal locomotion. International Journal of Robotics Research, 20, 129-143.

Purslow, P. P. (2002). The structure and functional significance of variations in the connective tissue within muscle. Comparative Biochemistry and Physiology a-Molecular and Integrative Physiology, 133, 947-966.

Raibert, M. (1986). Legged robots that balance. Cambridge, Massachusetts: MIT Press.

Ren, L., Howard, D., Ren, L., Nester, C. & Tian, L. (2010). A generic analytical foot rollover model for predicting translational ankle kinematics in gait simulation studies. Journal of Biomechanics, 43, 194-202.

Ren, L., Howard, D., Ren, L.-Q., Nester, C. & Tian, L.-M. (2008). A Phase-Dependent Hypothesis for Locomotor Functions of Human Foot Complex. Journal of Bionic Engineering, 5, 175-180.

Ren, L., R. K. Jones & D. Howard. (2005). Dynamic analysis of load carriage biomechanics during level walking. Journal of Biomechanics, 38, 853-863.

Ren, L., R. K. Jones & D. Howard. (2007). Predictive modelling of human walking over a complete gait cycle. Journal of Biomechanics, 40, 1567-1574.

Ren, L., R. K. Jones & D. Howard. (2008). Whole body inverse dynamics over a complete gait cycle based only on measured kinematics. Journal of Biomechanics, 41, 2750-2759.

Riese, S. & A. Seyfarth. (2012). Stance leg control: variation of leg parameters supports stable hopping. Bioinspiration & Biomimetics, 7.

Roberts, T. J. & E. Azizi. (2011). Flexible mechanisms: the diverse roles of biological springs in vertebrate movement. Journal of Experimental Biology, 214, 353-361.

Roos, P. E. & Dingwell, J. B. (2011). Influence of simulated neuromuscular noise on the dynamic stability and fall risk of a 3D dynamic walking model. Journal of Biomechanics, 44, 1514-1520.

Rose, J. & Gamble, J. (2006). Human walking, Philadelphia, USA, Lippincott Williams & Wilkins.

Rosenstein, M. T., Collins, J. J. & De Luca, C. J. (1993). A practical method for calculating largest lyapunov exponents from small data sets. Physica D-Nonlinear Phenomena, 65, 117-134.

Rostami, M. & G. Bessonnet. (2001a). Sagittal gait of a biped robot during the single support phase. Part 1: passive motion. Robotica, 19, 163-176.

Rostami, M. & G. Bessonnet. (2001b). Sagittal gait of a biped robot during the single support phase. Part 2: optimal motion. Robotica, 19, 241-253.

Rummel, J. & A. Seyfarth. (2008). Stable running with segmented legs. International Journal of Robotics Research, 27, 919-934.

Rummel, J., Y. Blum, H. M. Maus, C. Rode, A. Seyfarth. (2010). Stable and robust walking with compliant legs. In IEEE International Conference on Robotics and Automation (ICRA), 5250-5255.

Saunders, J., V. T. Inman & H. D. Eberhart. (1953). The major determinants in normal and pathological gait. Journal of Bone and Joint Surgery-American Volume, 35-A, 543-558.

Schablowski, A. & Gerner, H. J. (2006). Comparison of two measures of dynamic stability during treadmill walking. Fast Motions in Biomechanics and Robotics: Optimization and Feedback Control, 340, 345-360.

Schmitt, J. & J. Clark. (2009). Modeling posture-dependent leg actuation in sagittal plane locomotion. Bioinspiration & Biomimetics, 4.

Schmitt, J. & P. Holmes. (2000a). Mechanical models for insect locomotion: dynamics and stability in the horizontal plane - II. Application. Biological Cybernetics, 83, 517-527.

Schmitt, J. & P. Holmes. (2000b). Mechanical models for insect locomotion: dynamics and stability in the horizontal plane I. Theory. Biological Cybernetics, 83, 501-515.

Schmitt, J. & P. Holmes. (2003). Mechanical models for insect locomotion: active muscles and energy losses. Biological Cybernetics, 89, 43-55.

Schmitt, J. (2006). A simple stabilizing control for sagittal plane locomotion. Journal of Computational and Nonlinear Dynamics, 1.

Schmitt, J., M. Garcia, R. C. Razo, P. Holmes & R. J. Full. (2002). Dynamics and stability of legged locomotion in the horizontal plane: a test case using insects. Biological Cybernetics, 86, 343-353.

Schwab, A. L. & Wisse, M. (2001). Basin of attraction of the simplest walking model. International Conference on Noise and Vibration (2001), 21363, 22.

Seipel, J. & P. Holmes. (2007). A simple model for clock-actuated legged locomotion. Regular & Chaotic Dynamics, 12, 502-520.

Seipel, J. E., P. J. Holmes & R. J. Full. (2004). Dynamics and stability of insect locomotion: a hexapedal model for horizontal plane motions. Biological Cybernetics, 91, 76-90.

Seyfarth, A. (2000). Elastically operating legs-strategies and construction principles. PhD, Friedrich-Schiller-University Jena.

Seyfarth, A., Geyer, H. & Heff, H. (2003). Swing-leg retraction: a simple control model for stable running. Journal of Experimental Biology, 206, 2547-2555.

Seyfarth, A., Geyer, H., Blickhan, R., Lipfert, S., Rummel, J., Minekawa, Y. & Iida, F. (2006). Running and walking with compliant legs. In: DIEHL, M. & MOMBAUR, K. (eds.) Fast Motions in Biomechanics and Robotics: Optimization and Feedback Control.

Seyfarth, A., Geyer, H., Gunther, M. & Blickhan, R. (2002). A movement criterion for running. Journal of Biomechanics, 35, 649-655.

Seyfarth, A., M. Gunther & R. Blickhan. (2001). Stable operation of an elastic three-segment leg. Biological Cybernetics, 84, 365-382.

Shub, M. (1987). Global stability of dynamical system, New York, Springer-Verlag.

Siegler, S., Seliktar, R. & Hyman, W. (1982). Simulation of human gait with the aid of a simple mechanical model. Journal of Biomechanics, 15, 415-425.

Simpson, M. E., Serdula, M., Galuska, D. A., Gillespie, C., Donehoo, R., Macera, C. & Mack, K. (2003). Walking trends among US adults - The Behavioral Risk Factor Surveillance System, 1987-2000. American Journal of Preventive Medicine, 25, 95-100.

Sponberg, S. & R. J. Full. (2008) Neuromechanical response of musculo-skeletal structures in cockroaches during rapid running on rough terrain. Journal of Experimental Biology, 211, 433-446.

Srinivasan, M. & Ruina, A. (2006). Computer optimization of a minimal biped model discovers walking and running. Nature, 439, 72-75.

Stergiou, N. & Decker, L. M. (2011). Human movement variability, nonlinear dynamics, and pathology: Is there a connection? Human Movement Science, 30, 869-888.

Steven, S. H. (1994). Nonlinear Dynamics and Chaos: With Applications to Physics, Biology, Chemistry and Engineering, Cambridge, MA, USA, Perseus Books Publishing.

Su, J. L.-S. & Dingwell, J. B. (2007). Dynamic stability of passive dynamic walking on an irregular surface. Journal of Biomechanical Engineering-Transactions of the Asme, 129, 802-810.

Taga, G. (1994). Emergence of bipedal locomotion through entrainment among the neuro-musculo-skeletal system and the environment. Physica D, 75, 190-208.

Taga, G. (1995a). A model of the neuro-musculo-skeletal system for human locomotion .1. emergence of basic gait. Biological Cybernetics, 73, 97-111.

Taga, G. (1995b). A model of the neuro-musculo-skeletal system for human locomotion .2. real-time adaptability under various constraints. Biological Cybernetics, 73, 113-121.

Taga, G., Y. Yamaguchi & H. Shimizu. (1991). Self-organized control of bipedal locomotion by neural oscillators in unpredictable environment. Biological Cybernetics, 65, 147-159.

Talkner, P., Hanggi, P., Friedkin, E. & Trautman, D. 1987. Discrete dynamics and metastability: Mean first passage times and escape rates. Journal of Statistical Physics, 48**,** 17.

Tedrake, R. L. (2004). Applied optimal control for dynamically stable legged locomotion. *PhD Thesis*, Massachusetts Institute of Technology.

Tesio, L., Rota, V., Chessa, C. & Perucca, L. (2010). The 3D path of body centre of mass during adult human walking on force treadmill. Journal of Biomechanics, 43, 938-944.

Thelen, D. G., A. B. Schultz, S. D. Fassois & J. A. Ashtonmiller. (1994). Identification of dynamic myoelectric signal-to-force models during isometric lumbar muscle contractions. Journal of Biomechanics, 27, 907-919.

Thorpe, S. K. S., R. L. Holder & R. H. Crompton. (2007). Origin of human bipedalism as an adaptation for locomotion on flexible branches. Science, 316, 1328-1331.

Tinetti, M. E., Doucette, J. T. & Claus, E. B. (1995). The contribution of predisposing and situational risk-factors to serious fall injuries. Journal of the American Geriatrics Society, 43, 1207-1213.

Townsend, M. A. (1985). Biped gait stabilization via foot placement. Journal of Biomechanics, 18, 21-38.

Van der Kooij, H. (2001). Human balance control in standing and walking. Enschede, The Netherlands.: University of Twente.

Van Emmerik, R. E. A. & Van Wegen, E. E. H. (2002). On the functional aspects of variability in postural control. Exercise and Sport Sciences Reviews, 30, 177-183.

Vanderhelm, F. C. T. & Pronk, G. M. (1995). 3-Dimensional recording and description of motions of the shoulder mechanism. Journal of Biomechanical Engineering-Transactions of the Asme, 117, 27-40.

Vaughan, C. (1999). Biomechanics of human gait: An Electronic Bibliography. Cape Town: Kiboho Publishers.

Vaughan, C., B. Davis & C. O' Connor. (1999). Dynamics of human gait. Cape Town: Kinoho Publishers.

Verdaasdonk, B. W., H. F. J. M. Koopman & F. C. T. van der Helm. (2009). Energy efficient walking with central pattern generators: from passive dynamic walking to biologically inspired control. Biological Cybernetics, 101, 49-61.

Vukobrat. M & Juricic, D. (1969). Contribution to synthesis of biped gait. Ieee Transactions on Biomedical Engineering, BM16, 1-&.

Weber, M., Kube, S., Walter, L. & Deuflhard, P. 2006. Stable computation of probability densities for metastable dynamical systems. Technical Report ZIB-Report 06-39, Konrad-Zuse-Zentrum fur Informationstechnik Berlin.

Wainwright, A. S., D. W. Biggs, J. D. Curry & J. M. Gosline. (1976). Mechanical design in organism. London: Edward Arnold Limited.

White, S. C., Yack, H. J., Tucker, C. A. & Lin, H. Y. (1998). Comparison of vertical ground reaction forces during overground and treadmill walking. Medicine and Science in Sports and Exercise, 30, 1537-1542.

Whittington, B. R. & D. G. Thelen. (2009). A Simple Mass-Spring Model With Roller Feet Can Induce the Ground Reactions Observed in Human Walking. Journal of Biomechanical Engineering-Transactions of the Asme, 131.

Wight, D. L., Kubica, E. G. & Wang, D. W. L. (2008). Introduction of the foot placement estimator: a dynamic measure of balance for bipedal robotics. Journal of Computational and Nonlinear Dynamics, 3.

Wisse, M. (2004). Essentials of dynamic walking; analysis and design of two-legged robots. doctoral thesis, TU Delft, Delft University of Technology.

Wisse, M., A. L. Schwab & F. C. T. van der Helm. (2004). Passive dynamic walking model with upper body. Robotica, 22, 681-688.

Wisse, M., D. G. E. Hobbelen, R. J. J. Rotteveel, S. O. Anderson, G. J. Zeglin & Ieee. (2006). Ankle springs instead of arc-shaped feet for passive dynamic walkers. 2006 6th IEEE-RAS International Conference on Humanoid Robots, Vols 1 and 2, 110-116.

Wisse, M., Schwab, A. L., Van Der Linde, R. Q. & Van Der Helm, F. C. T. (2005). How to keep from falling forward: Elementary swing leg action for passive dynamic walkers. Ieee Transactions on Robotics, 21, 393-401.

Yamazaki, N., K. Hase, N. Ogihara & N. Hayamizu. (1996). Biomechanical analysis of the development of human bipedal walking by a neuro-musculo-skeletal model. Folia Primatologica, 66, 253-271.

Zajac, F. E., R. R. Neptune & S. A. Kautz. (2002). Biomechanics and muscle coordination of human walking - Part I: Introduction to concepts, power transfer, dynamics and simulations. Gait & Posture, 16, 215-232.

Zajac, F. E., R. R. Neptune & S. A. Kautz. (2003). Biomechanics and muscle coordination of human walking Part II: Lessons from dynamical simulations and clinical implications. Gait & Posture, 17, 1-17.